

THÈSE

En vue de l'obtention du

DOCTORAT DE L'UNIVERSITÉ DE TOULOUSE

Délivré par *Institut National Polytechnique de Toulouse*
Discipline ou spécialité : *Dynamique des Fluides*

Présentée et soutenue par *Hossein Fadaei*
Le *04/12/2009*

Titre : *Etude de la récupération de bruts lourds en réservoir carbonaté fracturé par le procédé de combustion in situ*

JURY

Arian Kamp, Ingénieur de Recherche, CHLOE, (membre)
Bernard Corre, Ingénieur de Recherche, Total S.A., (membre)
Gerald Debenest, Maître de Conférences, IMFT, (co-directeur)
Gérard Renard, Ingénieur de Recherche, IFP, (membre)
Henri Bertin, Directeur de Recherche CNRS, TREFLE-ENSAM, (rapporteur)
Hans Bruining, Professeur des Universités, Delft University, (rapporteur)
Michel Quintard, Directeur de Recherche CNRS, IMFT, (directeur)
Syilvian Salvador, Professeur, EMAC, (membre)

Ecole doctorale : *Mécanique, Energétique, Génie civil, Procédés*
Unité de recherche : *Institut de Mécanique des Fluides de Toulouse*
Directeur(s) de Thèse : *Michel Quintard*

Acknowledgements

I would like to thank my advisers, Prof. Michel Quintard, Dr. Gerald Debenest and Dr. Arjan Kamp for their help during this work.
Special thank to Total S.A. for sponsoring my PhD study in France also for providing financial support of the experimental part of the thesis done at Stanford University.
I would also like to thank Dr. Louis Castanier and Dr. Anthony Kovscek of Stanford University for their valuable contributions to the experimental study.

Table of contents

Abstract **vi**

Résume des chapitres en français **vii**

CHAPTER 1. INTRODUCTION 1

1.1 Methodology 2

1.1.1 Small scale challenges and the feasibility of the ISC 2
1.1.2 Large scale challenges, the upscaling method 4
1.1.3 Presenting the chapters 6

CHAPTER 2. COMBUSTION IN HETEROGENEOUS POROUS MEDIA 9

2.1 Combustion processes in homogeneous porous media 9

2.1.1 Typical observations of combustion in a homogeneous porous medium 9

2.2 In situ combustion (ISC) in an oil reservoir 11

2.2.1 Types of in situ combustion processes 12
2.2.2 Chemical changes of crude oil due to temperature increase 13
2.2.3 Advantages of the ISC 16
2.2.4 Disadvantages of the ISC 16
2.2.5 Physical changes of crud oil due to temperature increase 17
2.2.6 How the ISC process works? 19

2.3 In situ combustion in fractured reservoirs 23

2.3.1 Laboratory works and simulation 23
2.3.2 Pilot or field test results 26
2.3.3 Summary 26

2.4 Fractured reservoirs modeling challenges 26

2.4.1 Hierarchical length scale in a typical fractured reservoir 27
2.4.2 Idealized representation of the fractured reservoir 29
2.4.3 Simplified geometry 30
2.4.4 Fluid flow modeling in fractured reservoirs 30
2.4.5 Two-equation models 35
2.4.6 Summary 39

CHAPTER 3. NUMERICAL STUDY OF THE PROPAGATION OF A COMBUSTION FRONT IN A FRACTURED SYSTEM 43

3.1 Validation of the simulator 43

3.1.1 Mathematical model of the combustion process in porous media 43
3.1.2 Validation case: One and two dimensional diffusion tests 45
3.1.3 Validation case: One dimensional solid-gas combustion test 47
3.1.4 Crude oil combustion in a non-fractured core 49
3.1.5 Comparison of simulation results with Kumar's experiment 51
3.1.6 Summary 54

3.2 Simulation of oil combustion in a fractured core 54

3.2.1 Simulation model 54
3.2.2 Typical combustion of crude oil in fractured core (base-case) 56
3.2.3 Extinction/propagation condition 58
3.2.4 Analysis based on dimensionless numbers 63
3.2.5 Horizontal configuration 66
3.2.6 Oil production mechanisms 67
3.2.7 Shape of the coke zone 70
3.2.8 Summary 71

3.3 Simulation of ISC process in a single matrix block 71

3.3.1 Temperature 72
3.3.2 Coke zone 75
3.3.3 Oil saturation 76
3.3.4 Combustion front velocity 77
3.3.5 Water saturation and steam plateau 78
3.3.6 Oil upgrading 79
3.3.7 Oil production 80
3.3.8 Summary 81

3.4 Multi-block simulation 82

3.4.1 Temperature profile 83
3.4.2 Fluid saturations 84
3.4.3 Coke zone 85
3.4.4 Oil production 86
3.4.5 Average temperature and mole fraction 86
3.4.6 Horizontal and vertical extension of the temperature 89
3.4.7 Summary 91

CHAPTER 4. EXPERIMENTAL ANALYSIS OF ISC IN FRACTURED CARBONATES 92

4.1 Material and methods 92

4.1.1 Experimental set up 92
4.1.2 Oil-sand mixture preparation 95
4.1.3 Consolidated core saturation 95

4.2 Combustion tube experiments 96

4.2.1 Combustion in a non-consolidated porous medium 97
4.2.2 Combustion in a consolidated porous medium 101

4.3 Kinetic cell experiments 107

4.3.1 Kinetics in a non-consolidated medium 107
4.3.2 Kinetics in a consolidated medium 109

4.4 Numerical simulation 112

4.4.1 Kinetic cell simulation 112
4.4.2 Combustion tube simulation 114
4.4.3 Summary 117

CHAPTER 5. CONCLUSIONS AND PERSPECTIVES 118

5.1 Conclusions 118

5.2 Perspectives 120

APPENDIXES 124

A. Combustion in fractured core 125

A.1 Effect of oxygen diffusion coefficient on ISC 125
A.2 Effect of matrix permeability on ISC 128

B. Upscaling of the solid-gas combustion using the volume averaging method 132

B.1 Introduction 132
B.2 Solid-gas combustion in fractured porous medium 133

References 139

Table of figures

Figure 2.1. One dimensional smoldering model. 10
Figure 2.2. Reaction leading (left) and reaction trailing (right) structures. 11
Figure 2.3. In situ combustion process (Sarathi 1999). 12
Figure 2.4. Typical oxygen consumption curve in ISC process (Sarathi 1999). 14
Figure 2.5. General classification of crude oil (Audibert et al. 1991). 15
Figure 2.6. Comparison of long distance (conventional methods) and short distance (THAI and SAGD) processes for heavy oil recovery (Greaves 2006). 17
Figure 2.7. Diagram of forward in situ combustion (Castanier et al. 2003). 20
Figure 2.8. Comparison of steam and combustion fronts (top, Wolf lake oil and bottom, Nielburg crude). 21
Figure 2.9. Schulte and De Vries experimental setup (Schulte and De Vries, 1985). 24
Figure 2.10. An example of upscaling strategy (Delaplace et al. 2006). 25
Figure 2.11. Heterogeneous structure of the fractured reservoir at different scales. 27
Figure 2.12. Simplified representation of the heterogeneity in fractured reservoir at different scales. 28
Figure 2.13. Basic idealized models of a fractured matrix. 29
Figure 2.14. Simplified representation of the fracture and matrix in our study. 30
Figure 2.15. Experimental system used by Zinn et al. (2004, see Golfier et al. 2007). 34
Figure 2.16. Empirical categorization of one or two-equation model based on Péclet number. 34
Figure 2.17. Pore scale description of the combustion process. 35
Figure 3.1. Oxygen mole fraction vs. time at 0.03m from the inlet, grid size effect. 46
Figure 3.2. Oxygen mole fraction vs. time at 0.03m from the sides, grid size effect. 47
Figure 3.3. Schematic of one dimensional solid-gas combustion model. 47
Figure 3.4. 1-D solid-gas combustion front velocity, simulation and analytical solution. 49
Figure 3.5. Cumulative oil and water production, comparison of simulation and experiment. 51
Figure 3.6. Peak temperature along the core length, simulation and experimental results. 52
Figure 3.7. Peak temperature and coke concentration along the core (12 block). 52
Figure 3.8. Simulation result for 24 block, comparison with Kumar's results. 53
Figure 3.9. Comparison of the coke content for 12, 24 and 48-block cases. 54
Figure 3.10. Schematic of the fractured core model. 55
Figure 3.11. Cumulative oil and water production under ISC (base case). 56
Figure 3.12. Temperature profiles at the core center during ISC (base-case). 57
Figure 3.13. Coke concentration profiles at the core center during ISC (base-case). 57
Figure 3.14. Oil production vs. oxygen diffusion and matrix permeability. 59
Figure 3.15. Temperature and oil saturation in first row [K0.1, D0.1] and [K0.1, D0.02]. 60
Figure 3.16. Temperature and saturation profiles for different points in the Table (3.7). 61
Figure 3.17. Temperature and saturation profiles for [K0.1, D0.02] and [K0.02, D0.02]. 62
Figure 3.18. Temperature and saturation profiles for [K0.01, D0.01] and [K0.002, D0.01]. 62
Figure 3.19. Rate of reacted oxygen vs. time. 65
Figure 3.20. Mass of oil produced in fractured and non-fractured cores. 67
Figure 3.21. Cumulative oil production in horizontal and vertical configurations. 68
Figure 3.22. Oil saturation and oil phase velocity vectors in vertical and horizontal configurations. 69
Figure 3.23. Schematic of the system under ISC and electrical heating. 69
Figure 3.24. Oil production via in situ combustion and electrical heaters. 70
Figure 3.25. Shape of the coke phase when permeability or oxygen diffusion is varying. 70
Figure 3.26. Schematic of a model used for single block simulation. 71
Figure 3.27. Temperature along the block diagonal at different times for K=1270 md. 72
Figure 3.28. Temperature profile and gas phase velocity vectors (left), temperature profile and oil phase velocity vectors (right). 74
Figure 3.29. Coke concentration along the diagonal of the simulation domain for different times for K=1270 md. 76
Figure 3.30. Oil saturation along the block diagonal at different times for K=1270 md. 77

Figure 3.31. Combustion front velocity based on the oil saturation profile. 77
Figure 3.32. Water saturation evolution with time (K=1270 md). 78
Figure 3.33. Cumulative volume of heavy oil produced as a fraction of initial volume, both measured at standard condition. 80
Figure 3.34. Cumulative oil production at standard condition for different matrix permeability. 80
Figure 3.35. Oil saturation during ISC in a single matrix block (K =1270 md). 81
Figure 3.36. Schematic of the multi-block model. 83
Figure 3.37. Temperature (°C) profile for different simulation time. 84
Figure 3.38. Oil saturation profile for different simulation time. 84
Figure 3.39. Water saturation profile for different simulation time. 85
Figure 3.40. Coke concentration (grmol/m^3) profile for different simulation time. 85
Figure 3.41. Oil production rate and the cumulative oil produced at standard condition. 86
Figure 3.42. Average temperature in matrix blocks and corresponding fractures. 87
Figure 3.43. Average light oil mole fraction in matrix blocks and corresponding fractures. 88
Figure 3.44. Average light oil mole fraction in matrix blocks and corresponding fractures (cont.). 89
Figure 3.45. Temperature profiles in the horizontal direction. 90
Figure 3.46. Temperature profiles in the vertical direction. 90
Figure 4.1. Schematic of the experimental setup (taken from Castanier and Brigham 2003). 93
Figure 4.2. Combustion tube image, left: in horizontal position with electrical heater attached to the far end, right: in the vertical position. 94
Figure 4.3. Kinetic cell image with the heating coil at the bottom. 94
Figure 4.4. Core holder image (left) and a schematic of the coreholder (right). 96
Figure 4.5. Combustion tube composition, run 1. 97
Figure 4.6. Gases profile at the exit of the combustion tube, run 1. 98
Figure 4.7. Temperature profile along the core centre, run 1. 99
Figure 4.8. Composition of the combustion tube, non-consolidated heterogeneous experiment (run 6). 99
Figure 4.9. Gases profile at the exit of the combustion tube, run 6. 100
Figure 4.10. Temperature profile along the core centre, run 1. 101
Figure 4.11. Composition of the combustion tube, consolidated experiment (run 2). 101
Figure 4.12. Gas analyzer results (top) and temperature profile along the core centre (bottom) for run 2. 103
Figure 4.13. Post run image of run 2. 103
Figure 4.14. Gas analyzer results (top) and temperature profile along the core (bottom) for run 3. 104
Figure 4.15. Gas analyzer results (top) and temperature profile along the core (bottom) for run 4. 105
Figure 4.16. Gas analyzer results (top) and temperature profile along the core (bottom) for run 5. 106
Figure 4.17. Kinetic cell results for homogeneous mixture (base case). 108
Figure 4.18. Temperature of the kinetic cell. 108
Figure 4.19. Kinetic cell results for the oil-carbonate mixture. 109
Figure 4.20. Kinetic cell composition in the consolidated core experiment. 110
Figure 4.21. Kinetic cell results for consolidated core. 110
Figure 4.22. Kinetic cell composition in the core pieces experiment. 111
Figure 4.23. Kinetic cell results for core pieces. 111
Figure 4.24. Kinetic cell simulation model and some important model parameters. 113
Figure 4.25. Oxygen volume fraction in the homogeneous kinetic cell. 113
Figure 4.26. Combustion tube simulation model and some important model parameters. 115
Figure 4.27. Temperature versus distance; Top: normal air, Bottom: enriched air. 115
Figure 4.28. Coke profile at time = 3.5 hr; left: normal air, right: enriched air. 116
Figure 4.29. Oxygen profile at time = 3.5 hr; left: normal air, right: enriched air. 116
Figure 5.1. Schematic of the Darcy scale model (top) and the unit cell (bottom). 122
Figure 5.2. Dimensionless temperature vs. distance (Damköhler =0.3). 123
Figure 5.3. Dimensionless temperature vs. distance (Damköhler =30). 123
Figure B.1. Averaging volume and the position vectors (taken from Quintard and Whitaker 1993). 132
Figure B.2. How the multiplier term changes with temperature. 136

Table of tables

Table 2.1. Combustion zone thickness and air flux reported in literature. 22
Table 2.2. Experimental parameters of Greaves et al. (1991) and Schulte and De Vries (1985). 24
Table 3.1. Characteristics of the one and two dimensional diffusion simulation model. 45
Table 3.2, Characteristics of the one dimensional combustion model. 47
Table 3.3. Simulation input data. 50
Table 3.4. Reaction kinetic model and parameters. 50
Table 3.5. Simulation input data. 55
Table 3.6. Simulation model dimensions. 55
Table 3.7. Extinction/ propagation diagram on x-y plane. 59
Table 3.8. Values for Pe_g and Pe_o for different points on Table (3.7). 64
Table 3.9. Extinction/ Propagation diagram for horizontal configuration (red: propagation, blue: extinction. 67
Table 3.10. Parameters of multi-block simulation model. 82
Table 4.1. Composition of the porous medium in the kinetic cell. 95
Table 4.2. Experimental condition for tube runs. 97
Table 4.3. Composition of the porous media in the kinetic cell. 107
Table 4.4. Reaction scheme used in kinetic cell simulation 112
Table 5.1. Model parameters. 121
Table B.1. Parameters for estimation of the reaction term . 135

Abstract

The aim of the present work is to study the in situ combustion (ISC) process at inter-well scale in a fractured reservoir. Due to the complexity associated with the ISC process, highly heterogeneous nature of the fractured reservoirs and some unsuccessful attempts in the past to put the process into practice, the subject of ISC in fractured systems has been receiving little interest and there are still many essential open questions in this area. It is very challenging to answer the question whether the ISC process could be applied in a heavy oil fractured reservoir or not. And if the answer is positive, what is (are) the dominant oil recovery mechanism(s) and finally, how can we model and simulate this process, at least, at inter-well scale.

This work tries to give answers to some of these questions. In this regard, we followed a step by step procedure. In the first step, general literature concerning the combustion process in porous media and particularly that related to the combustion process in an oil reservoir was reviewed. Some other references about the modeling of fracture reservoirs were also reviewed. This led us to distinguish some of the main challenges in this area and define a methodology for the rest of the work. Based on this methodology, the first target was to understand and to characterize the behavior of a combustion front at small (Darcy) scale. The second target was to apply the knowledge of the first part to propose a suitable model for ISC at larger scale. To this end, a commercial thermal reservoir simulator (STARS) was used. The simulator was validated for both simple process for which an analytical solution is available and for a more complex process where the laboratory results are on hand. Then, after the validation part, the numerical tool has been used to widely investigate the conditions where a reaction front can propagate in a fractured core. This allowed us to understand some of the leading mechanisms (oxygen diffusion coefficient for extinction/ propagation of combustion front and matrix permeability for oil production). Some other numerical studies provided us with some understanding about the most important mechanism(s) of oil production.

Thereafter, some single block simulations were done to investigate the two-dimensional behavior of the ISC process, based on which the underlying process was found to be diffusion dominated both for heat and mass transfers. These results also helped us to distinguish the characteristic length scale of some important parameters (temperature, coke concentration, combustion front, etc.) which can give useful information about the large scale model.

After that, an experimental part has been performed to find propagation conditions of ISC at laboratory scale. This was done by varying both the operational conditions (flowrate, pressure and oxygen concentration) and the characteristics of the fractured system (aperture, surface area, permeability). This permitted us to find that in some suitable conditions there is a possibility to generate a combustion front in a fractured system containing heavy oil.

To give an idea about the modeling of the process at larger scale, some fine grid simulations are also performed using a multi-block model. By analyzing the results of this model some guidelines are proposed for the large scale model. At the end, a short discussion about the upscaling of an easy system (solid-gas combustion using an Arrhenius law as a function for the mass sink term in a conductive system) is presented based on an upscaling using the volume averaging method.

Résume des chapitres en français

Chapitre 1.

Ce chapitre présente l'introduction, la méthodologie et les chapitres suivants de ce manuscrit. L'objectif du travail de thèse est d'étudier le processus de combustion dans un milieu poreux très hétérogène à grande échelle. Plus précisément, nous somme intéressés à la simulation du procédé de combustion in situ (CIS) dans un réservoir carbonaté fracturé.

Le procédé de combustion en milieu poreux a fait l'objet d'un grand intérêt en raison de ses vastes applications dans différents domaines:

1. Environnement en ce qui concerne l'étude des incendies de forêts ou de l'incinération de déchets.
2. Production de matériaux synthétiques (à la base des métaux ou de céramiques).
3. Brûleurs poreux (combustion basse richesse).
4. Régénération de lits catalytiques dans les raffineries et de nombreuses autres applications.

L'idée de cette thèse, est d'étudier la physique du processus de combustion dans un système fracturé à l'échelle de Darcy et d'identifier les possibilités et pistes existantes pour passer à l'échelle du réservoir en employant une architecture de puits particulière à base de drains horizontaux, stabilisée par la gravité. Nous avons fait ceci en deux temps.

Tout d'abord, nous avons identifié les processus à la base de la combustion in situ en réservoir. Contrairement à d'autres méthodes de récupération thermique dans lesquelles une source extérieure de chaleur (eau chaude ou vapeur) est fournie dans le réservoir afin de mobiliser l'huile, dans la CIS, le réservoir doit fournir cette énergie lui-même. Il est donc indispensable que le processus de combustion soit autonome à différentes échelles (le pore, la carotte et le réservoir). La propagation de ce processus dépend de divers paramètres (hétérogénéité du réservoir, caractéristiques de huile, conditions opérationnelles, etc.), dont les rôles ne sont pas complètement cernés, même à petite échelle.

En ce qui concerne la production d'huile, différents mécanismes sont présentés et leurs importances dépendent de divers paramètres difficiles à bien identifier.

Pour ce faire, nous avons utilisé un outil de simulation réservoir qui est adapté pour étudier le processus. Après avoir validé le code de transport réactif, nous avons effectué des simulations afin d'étudier le phénomène de CIS dans une carotte fracturée, initialement saturée en huile, eau et gaz. En particulier, la propagation du front de combustion et les mécanismes de récupération du pétrole sont finement étudiés et caractérisés.

Ensuite, une partie expérimentale a été effectuée afin de vérifier que des conditions stables de propagation à l'échelle du laboratoire existaient. Cela a été fait en faisant varier les paramètres opérationnels (pression, concentration en oxygène, etc.) et les caractéristiques du milieu (ouverture de fracture, surface, perméabilité). Ceci permet de constater que dans certaines conditions, le front de combustion peut se propager. Ces résultats sont ensuite confrontés avec des résultats de simulation numérique où le même comportement qualitatif est retrouvé.

Dans l'industrie pétrolière, la prédiction de taux de récupération du pétrole et du gaz a une importance cruciale. Cela se fait généralement en utilisant des outils numériques. La simulation type réservoirs peut s'avérer très coûteuse si l'on décide d'effectuer une simulation avec un maillage fin. C'est pourquoi nous avons travaillé sur la mise à l'échelle réservoir pour identifier quels types de modèles seraient utilisables.
Ainsi, nous avons réalisé une analyse détaillée du processus de combustion pour un bloc puis pour plusieurs blocs, et ce, en deux dimensions.

L'analyse des résultats a été faite en faisant les estimations des moyennes des grandeurs sur chaque bloc et fractures. Quelques éléments de réponse sont ainsi donnés.
In fine, une étude de mise à l'échelle d'un système simple (combustion de solide-gaz dans un système fracturé avec un terme réactif de type Arrhenius) avec la méthode de prise de moyenne est réalisée.

Chapitre 2

Dans ce chapitre, on fait l'état de l'art et l'analyse de la bibliographie des processus de combustion dans les milieux poreux et fracturés.

En premier lieu, la combustion d'un système simple (solide-gaz) dans un milieu homogène et notamment les travaux de Schult (1996) sont présentés. Deux types de comportements sont caractérisés en fonction de le vitesse du front de combustion par rapport à la disponibilité d'oxygène, à savoir les systèmes type « reaction leading » (la réaction avance plus vite que le front thermique) ou « reaction trailing » (la réaction avance moins vite que par moins vite que le front thermique).

Par la suite, la combustion d'une huile dans un réservoir pétrolier est abordée. Un schéma typique de production par combustion in situ dans un réservoir est détaillé. Différents types de processus de combustion qui ont été mis en pratique par l'industrie pétrolière sont mentionnés ainsi que leurs avantages et inconvénients.

Puis, on aborde le problème de la réactivité de l'huile et des effets des réactions chimiques sur le processus. On distingue majoritairement deux types de réactions :

1. Les réactions a basse température, qui réduisent la viscosité d'huile et qui sont appelées LTO (Low Temperature Oxidation) et
2. Les réactions a haute température HTO (High Temperature Oxidation), qui sont réellement les réactions de combustion.

La compréhension du fonctionnement de la combustion en réservoir est toujours le sujet d'études importantes. Ce système est très complexe et les pistes d'étude concernent les réactions de craquages qui jouent un rôle très important sur l'upgrading d'huile, mais aussi sur les effets importants de la vapeur d'eau sur les propriétés de l'huile produite. On peut aussi mentionner les effets des carbonates sur la combustion qui jouent un rôle sur les plans thermique (puits de chaleur), chimique (modification de la réactivité) mais aussi sur le transport par modification du squelette carbonaté.

Une autre partie de ce chapitre concerne les diverses études de combustion dans un système fracturé. Ce système semble être piloté, en ce qui concerne la combustion, par la diffusion d'oxygène. La production d'huile, quant à elle, semble être gouvernée par l'expansion et

l'évaporation de l'huile. Néanmoins, on peut insister sur le fait que ces systèmes sont très durs à allumer et que la combustion ne se propage que difficilement, ceci étant du aux forts contrastes de perméabilité existant entre matrices et fractures.

Dans ce contexte peu favorable, nous avons essayé de dégager des pistes d'étude et de proposer des réponses. Par exemple une question à laquelle il nous faut nous intéresser est le schéma réactif et son utilisation en milieu fortement hétérogène. Est-ce que la réponse d'une cellule cinétique faite en milieu homogène est suffisante pour déterminer un schéma réactif en milieu fracturé ?

Dans la deuxième partie de ce chapitre nous abordons l'aspect modélisation de ce processus a l'échelle de réservoir, dans un système fracturé. Au début, la complexité géométrique de ce type de réservoirs est mentionnée et un modèle simplifié (type « sugar box ») est introduit.

Ensuite, la problématique de la modélisation d'écoulement de fluides dans les systèmes fracturés est présentée. Dans le domaine pétrolier, il s'agit de modèles à une ou deux équations, les transferts entre matrice et fracture étant définis par des termes d'échange classiques.
Nous avons également présenté la méthode de prise de moyenne volumique et son utilisation dans l'hypothèse d'équilibre local. Mais la plupart des cas traités par cette méthode sont moins complexes que des problèmes de combustion générant des fronts raides et dont le terme de réaction est dépendant d'une fonction type Arrhenius.

Chapitre 3.

Dans ce chapitre, nous présentons les résultats des simulations numériques. Comme nous l'avons mentionné précédemment, un simulateur commercial de réservoir a été utilisé dans cette étude.

Dans la première partie de ce chapitre, nous présentons les équations du modèle, à savoir, équations de conservation de masse, de quantité de mouvement et de transport. Ce sont des équations moyennées à l'échelle de Darcy qui ont fait l'objet de simplifications.
Ce logiciel est basé sur l'hypothèse de l'équilibre local. Il considère, pour chaque maille, une seule température pour toutes les phases. Les réactions de craquage et de combustion sont de type Arrhenius. Il est admis que la loi de Darcy généralisée est valide.
Ce logiciel peut traiter quatre phases : l'eau, le gaz, et l'huile sont mobiles et peuvent contenir plusieurs composants et la phase solide est immobile. La phase solide contient le coke et la partie inerte. Le coke se forme lors des réactions de craquage et peut réagir avec l'oxygène dans la réaction de combustion à haute température.

Avant de faire les simulations de système fracturé, nous avons validé le simulateur. Dans un premier temps, les résultats de simulation de diffusion d'oxygène en une et deux dimensions sont comparés avec des solutions analytiques. Ensuite, nous avons comparé la simulation de la combustion d'un système simple (solide-gaz) avec la solution analytique publiée dans la littérature. Les résultats montrent que l'outil numérique est capable de traiter ces problèmes. Puis, une simulation de combustion d'huile dans un système non-fracturé a été comparée avec les résultats expérimentaux qui ont été publiés par Kumar (1987). Il s'agit d'une combustion d'huile relativement légère (26 °API) dans une carotte non-consolidée. On rappelle ici que

nous sommes intéressés par la simulation d'un processus de combustion qui est stabilisé par la gravité. Dans ce type de processus (qui est connu comme « top-to-down injection » dans le domaine pétrolier), l'air est injecté en haut du système et l'huile est produite par le bas.

La phase huile contient deux composants (un lourd et un léger). Le composant lourd peut se dissocier à cause de la chaleur et produire le composant léger et le coke. Les composants lourd et léger ainsi que le coke peuvent réagir avec l'oxygène à haute température et produire de l'eau et du dioxyde de carbone. Les saturations initiales ainsi que les perméabilités relatives sont les mêmes que celles présentées par Kumar.
Nous avons comparé le taux de production d'huile et d'eau ainsi que la température maximale au centre du système avec les données d'expérience. Les résultats indiquent un bon accord entre les simulations et les données de laboratoire. Une étude de sensibilité au maillage a montré que les résultats (i.e., la température) sont dépendants de la finesse de la grille.
A ce stade, nous avons conclu que notre outil numérique est suffisamment robuste afin d'étudier le problème de combustion dans un système fracturé.

Dans l'étape suivante, le problème de la combustion dans un système fracturé à l'échelle du laboratoire est présenté. Les simulations ont été réalisées en simple milieu. La même géométrie que le cas précédent est utilisée.
Dans cette partie, notre but est, (1) d'identifier les conditions d'extinction/propagation de la combustion et, (2) de comprendre les mécanismes de production d'huile dans une situation où le front de combustion peut se propager.
Pour cela, l'outil numérique a été largement utilisé pour étudier les conditions dans lesquelles un front de réaction peut se propager. Il est montré également que l'effet thermique et la gravité jouent un rôle important sur la production d'huile.
Nous avons essayé d'expliquer le comportement du système, en analysant les champs de température, de saturation et de concentration en coke mais aussi en estimant des nombres adimensionnels caractéristiques.

Pour étudier le comportement bidimensionnel du processus de combustion, plusieurs simulations ont été réalisées à l'échelle d'un bloc matriciel. Ce bloc mesure de 0.5 m de profondeur et 1.0 m de largeur. Les résultats de ces simulations montrent que les processus de transferts de chaleur et de masse (i.e., l'oxygène) dans le bloc sont pilotés par la diffusion. Dans ce processus multi-fronts, la taille caractéristique de certains processus varie avec l'avancée du front de combustion (i.e largeur de front, épaisseur de front thermique). Ceci est un point important qui doit être considéré pour la mise à échelle.

La production d'huile indique que le plupart de la production se fait lors de la deuxième moitié du temps de processus. C'est un point intéressant car contraire aux résultats publiés dans les revues sur la production d'huile dans une carotte fracturée qui montrent que ceci se fait majoritairement lors de la première moitié du processus. La différence peut être due à la non prise en compte du caractère multidimensionnel du processus de combustion dans un bloc.

Dans la dernière partie, nous avons étudié la combustion dans un système fracturé à plusieurs blocs. L'allumage est fait dans le premier bloc en haut à gauche du réservoir, et la production d'huile est faite par le bas. Comme nous l'avons vu précédemment pour un bloc, le front de combustion avance moins vite que le front de saturation d'huile. Différents fronts peuvent coexister dont les tailles caractéristiques varient avec le temps. A cause de la présence de fractures, la vapeur d'eau se trouve en haut du domaine au lieu d'être en aval du front de

combustion. Ce phénomène peut éventuellement influencer la répartition de l'huile dans les blocs. Néanmoins, les pressions capillaires des systèmes eau/huile et huile/gaz sont considérées comme étant nulles ce qui peut influencer nos résultat et leurs interprétations.

Pour le passage à la grande échelle, la différence des moyennes des grandeurs dans la matrice et la fracture peut être un indicateur important. Par exemple, si la température moyennée dans la matrice n'est pas très différente de celle de fracture, et si les gradients sont faibles, nous pouvons représenter la température dans la matrice et la fracture avec une seule équation à la grande échelle. En revanche, si la différence est importante et/ou si les gradients sont forts, nous devons représenter la température dans la matrice et la fracture avec deux équations différentes (modèle type non-équilibre local). Nous avons donc estimé les moyennes de température et de fraction molaire des composants légers afin de trouver quel modèle pouvait répondre à la grande échelle. Ces résultats indiquent que la température pourrait certainement être représentée par un modèle à une équation mais que les fractions molaires ne pourraient l'être que par un modèle non équilibre local.

Chapitre 4.

Ce chapitre présente les résultats expérimentaux. Ces expériences ont été menées afin de vérifier les résultats de simulation et d'apporter une meilleure compréhension du processus de combustion dans un milieu fracturé. Plus précisément, nous nous sommes attachés à déterminer les conditions dans lesquelles un front de combustion peut se propager dans un système fortement hétérogène.
Comme nous l'avons mentionné précédemment, nous n'avons trouvé que deux travaux expérimentaux relativement détaillés correspondants à ce processus. Les deux cas correspondent à une combustion à l'échelle d'une carotte et où le front de combustion a pu se propager; l'évaporation et l'expansion sont mentionnées comme étant les mécanismes importants relativement à la production d'huile. Ces deux études ont été faites avec une pression de tube qui est relativement basse (pression variant de 4 à 17 bars).
Deux autres références concernent une expérience de combustion à l'échelle d'une carotte, où le front de combustion n'a pas pu se propager. Celles-ci ont été faites à basse pression (entre 1 et 7 bars). Les auteurs ont indiqué que le contraste important de perméabilité entre la matrice et la fracture favorise le passage de l'air par la fracture, sans entrer dans la matrice.
Ceci nous a donc contraint à vérifier ces résultats contradictoires et à réaliser cette partie expérimentale.
Dans ce travail, la combustion dans un tube et la cinétique des réactions d'une huile dans une cellule cinétique ont été étudiées. Le but du test dans un tube est de comprendre le comportement de la combustion dans le milieu poreux, notamment en ce qui concerne la température, les saturations des fluides et la vitesse du front de combustion. L'étude de cellule cinétique est faite afin de déterminer les paramètres des réactions de craquage et de combustion.
Nous avons réalisé les tests de combustion dans le tube pour les milieux consolidés et non-consolidés. Un mélange du sable, d'eau et d'huile (Wilmington, 15 °API) a été préparé afin de réaliser les essais du milieu non-consolidé. Pour caractériser le comportement de l'huile, le premier test a été effectué dans un système non-consolidé et homogène. Les résultats de ce test ont montré une combustion à haute température (450 °C) avec un avancement stable de front de combustion. Le « plateau de la vapeur » a bien été détecté à travers les courbes de température. Les résultats des analyses de gaz ont indiqué une élution faible d'oxygène et un

taux de CO_2 stable ce qui est en accord avec l'observation des courbes de température. Cet essai a été considéré comme cas de référence.
La combustion dans un milieu non-consolidé et hétérogène a été étudié en mettant le mélange de sable et huile au centre du tube (un cylindre de 6 cm de diamètre) et les sables grossiers autour. Les résultats de ce cas montrent que le front de combustion peut se propager dans ce système, mais avec un taux de production d'oxygène plus élevé et la température maximale mois élevée que dans le cas de référence.
Ensuite, nous avons réalisé des tests de combustion dans le milieu consolidé. Un dispositif expérimental a été préparé pour imposer les saturations initiales dans la carotte consolidée. Ce dispositif possède un fluide de confinement qui nous permet une injection stable d'huile visqueuse. Plusieurs étapes sont nécessaires pour obtenir les saturations initiales en huile et en eau dans la carotte (mettre sous vide, connexion au réservoir d'eau, injection d'eau et injection d'huile).
Ensuite vient l'allumage de la carotte consolidée. Nous avons commencé par un cas où différents types d'hétérogénéités, caractérisées par leurs tailles, ont été introduites dans le tube afin de vérifier l'effet de ces hétérogénéités sur la propagation du front de combustion. Le front s'est propagé dans les hétérogénéités de petites tailles (5 cm) mais il ne s'est pas propagé dans les hétérogénéités de grandes tailles (20 cm). La présence du « plateau de la vapeur » est aussi moins visible par rapport au cas de référence.
Dans un autre cas, une carotte consolidée, initialement saturée en eau et en huile a été mise dans le tube. La différence entre le diamètre du tube et de la carotte de 0.5 cm a permis une ouverture qui a joué le rôle d'une fracture autour de la matrice qu'est la carotte.
Le front de combustion n'a pas pu se propager dans ce système. Après un allumage réussi, la température à la proximité du collier chauffant a diminué et le taux de production de CO_2 à la sortie de l'analyseur de gaz a brutalement chuté.
Nous avons réalisé plusieurs tests afin d'améliorer les conditions de propagation du front de combustion dans un milieu consolidé fracturé, mais finalement dans des conditions opératoires avec de l'air normal, aucune n'a permis la propagation. Malgré tout, la surface spécifique de la fracture et la pression dans le tube sont des paramètres influençant ce processus et ceci a été caractérisé et montré par le biais de ces tests.
Par contre, la combustion dans un milieu consolidé fracturé avec de l'air enrichi conduit à la propagation du front de combustion. Ces résultats montrent que la concentration d'oxygène est très importante et qu'en augmenter la disponibilité permet le maintien du front.
Dans l'étude de cellule cinétique, nous avons abordé l'effet de la présence du carbonate et du milieu consolidé sur la cinétique des réactions. Un essai de cinétique d'un milieu non consolidé et homogène a été effectué afin d'avoir la caractéristique cinétique de l'huile dans un cas de référence. Les résultats d'analyseur de gaz ont montré deux pics pour la fraction volumique de CO_2 qui représente un comportement typique de combustion (réaction HTO et LTO).
Un test avec un milieu consolidé a montré que ceci peut influencer la cinétique des réactions en regroupant les deux pics initiaux en un seul.
Dans le cas où le sable dans le mélange de sable-huile a été remplacé par le carbonate, une modification de cinétique a été observée et ceci indique qu'il faut prendre en compte la présence des carbonates dans l'étude cinétique afin de ne pas biaiser la réponse finale.

Conclusion

Nous rappelons que l'objectif du travail de thèse était d'étudier le processus de combustion dans un milieu poreux très hétérogène à grande échelle. Plus précisément, nous avons étudié la physique du processus de combustion dans un système fracturé à l'échelle de Darcy et essayé d'identifier les possibilités pour passer à l'échelle du réservoir.

Tout d'abord, un état de l'art et l'analyse de la bibliographie des processus de combustion dans les milieux poreux et fracturés ont été présenté. L'analyse nous a permis d'identifier quelques questions essentielles, comme par exemple, les effets des réactions de craquage ou de la vapeur d'eau sur les propriétés de l'huile produite et la présence de carbonate sur la combustion. Une des autres questions importantes est : «est-ce que la réponse d'une cellule cinétique faite en milieu homogène est suffisante pour déterminer un schéma réactif en milieu fracturé ? ». Les études de combustion dans un système fracturé indiquent que les conditions de propagation ne sont pas complètement connues.
En ce qui concerne l'aspect modélisation de ce processus à l'échelle du réservoir, la définition des termes d'échange dans les modèles à 2 équations reste un des problèmes d'importance.

Dans ce travail, nous avons utilisé un outil de simulation réservoir qui est adapté pour étudier le processus. Avant de faire les simulations de système fracturé, nous avons validé le simulateur. Les résultats montrent que l'outil numérique est capable de traiter ces problèmes.
Les simulations à l'échelle de la carotte, ont permis de comprendre les mécanismes moteurs (coefficient de diffusion de l'oxygène pour l'extinction/propagation de la combustion et la perméabilité de matrice sur la production de pétrole). Il est montré également que l'effet thermique et la gravité jouent un rôle important sur la production d'huile.

L'étude du comportement bidimensionnel du processus de combustion a montré que les processus de transferts de chaleur et de masse (i.e., l'oxygène) dans le bloc sont pilotés par la diffusion. Dans ce processus multi-fronts, la taille caractéristique de certains processus varie avec l'avancée du front de combustion (i.e largeur de front, épaisseur de front thermique). Ceci est un point important qui doit être considéré pour la mise à échelle.

Les simulations sur plusieurs blocs indiquent que différents fronts peuvent coexister dont les tailles caractéristiques varient avec le temps. A cause de la présence de fractures, la vapeur d'eau migre vers le haut du domaine au lieu d'être en aval du front de combustion. Les calculs des moyennes de paramètres indiquent que la température pourrait certainement être représentée par un modèle à une équation mais que les fractions molaires ne pourraient l'être que par un modèle non équilibre local.

L'étude expérimentale de la combustion dans un milieu non-consolidé et homogène montre une combustion à haute température, faible élution d'oxygène et un avancement stable du front de combustion. Les résultats de combustion dans un système non-consolidé et hétérogène montrent que le front de combustion peut se propager dans ce système, mais avec un taux de production d'oxygène plus élevé et une température maximale mois élevée que dans le cas non consolidé. La combustion dans une carotte fracturée ne s'est produite qu'avec de l'air enrichi.
L'étude de combustion dans un cellule cinétique a montré que la présence du carbonate et du milieu consolidé peut affecter la cinétique des réactions.

Chapter 1. Introduction

The aim of the present work is to study the combustion process in a highly heterogeneous porous medium. More precisely, the heterogeneous porous medium here is a fractured oil reservoir and the combustion process applied to such reservoirs is called in situ combustion (ISC). The idea is to study the underlying physics of the combustion process in fractured systems on one hand, and on the other hand, to identify the upscaling challenges when one is willing to simulate the ISC process at reservoir scale. To do so, some numerical and experimental works are done. The followings are the main works done in our research:

- In order to determine the stability condition of the ISC process and find out the mechanism(s) of oil recovery at laboratory scale, some numerical simulations are done at this scale.
- Some ISC laboratory experiments are conducted to validate numerical results and to give better understanding of the process in a fractured core.
- The numerical study of this process is also done at single and multiple block scales to observe the two dimensional behavior, mainly the evolution of different parameters (temperature, oil water and gas saturations etc.) during the ISC process.
- Based on these observations and some theoretical analysis, some guidelines are presented for the upscaling of this process to large-scale systems in a simplified case.

The combustion process in porous media has been the subject of great interest because of its vast applications in different areas: the environmental applications such as forest fire or waste incineration and cigarette burning, production of new materials like synthesized porous media based on metals or ceramics, porous burners in which a mixture of a fuel and an oxidizer burns, regeneration of some catalytic beds in the refineries and many other applications (Sarathi 1999, Ohlemiller 1985 and Oliviera and Kaviani 2001).
One of the specific applications of this process is in the hydrocarbon recovery. The common point in all of these applications is (i) the presence of homogeneous and/or heterogeneous combustion reactions and (ii) in most applications the porous medium is not homogeneous.
Most of the above mentioned problems are some how less complex than heavy oil combustion in a heterogeneous porous medium. This is either due to the simpler physics of the problem or milder heterogeneity of the porous medium under consideration. For example, in a typical filtration combustion there are essentially three phases, gas, solid fuel and solid porous matrix, while in a crude oil combustion there are at least three mobile phases (oil, water and gas) and two immobile phases (solid fuel and solid porous matrix). In addition to that, in the majority of these applications, the solid part of the porous medium could be considered as inert regarding the chemical reactions. But in the case of carbonate oil reservoirs, the porous matrix also may participate in the chemical reaction (Bagci and Shamsul 1999, Boris 1997, Sanders and Gallagher 2002, Kharrat et al. 2007) through de-carbonization reactions. When the porous system is highly heterogeneous, the characteristic time of the changes that take place in one part of the system is not of the same order of the magnitude as the changes that take place in the other part. This may hinder one to be able to treat the problem using only one equation to represent both parts of the system. In such a situation, one of the possible solutions is to consider an equation for each part and the relation between two equations is made using some extra (exchange) terms. This can add more difficulty to the modeling and simulation tasks.

Another important issue related to fractured systems is the early breakthrough of the injected fluid. This phenomenon is more important in the ISC process because of security concerns associated with oxygen breakthrough. It is possible to reduce the risk by applying a process so called top-down injection in which a gravity stabilized combustion front may develop. In the present work this type of ISC process is studied.

1.1 Methodology

1.1.1 Small scale challenges and the feasibility of ISC

In the first part, some of the main challenges of the ISC process application in petroleum reservoirs are addressed. Unlike other thermal recovery methods in which an external heat source (hot water or steam) is supplied to the reservoir to mobilize the oil, in ISC the reservoir should provide this energy by itself. Hence it is necessary to obtain a self sustained combustion in the reservoir at different scales (pore, core and inter-well). The sustainability of this process in turn depends on different parameters (reservoir heterogeneity, oil characteristic, operating condition, etc.), the roles of which are not fully understood and are still under investigation even at small scale (Awoleke 2007, Castanier and Brigham 2003, Fassihi et al. 1994, Okamoto and Bourbiaux 2005, Mailybaev et al. 2009 and Moore et al. 1998).

Different deriving forces may take part in the oil recovery via ISC such as steam distillation, viscosity reduction, evaporation, oil expansion and gas drive. The importance of each of these mechanisms may depend on different parameters and it is not known *a priori*. Fine grid simulation in which most of these mechanisms are taken into account in the mathematical model, can help us to distinguish the most important one(s).

The presence of different phases and components in crude oil combustion leads to a complex problem in terms of transport characteristics and chemistry. This is especially the case in fractured reservoirs where heterogeneity of the porous media adds more complexity to the problem. Due to some early unsuccessful experiences, the application of air injection methods was abandoned in these reservoirs and since then not enough effort has been done to better understand the problem. However, some laboratory and simulation results showed that the ISC in fractured reservoir is feasible and some researchers have mentioned that these unsuccessful stories could be partly due to lack of our knowledge about the behavior of in situ combustion in these highly heterogeneous systems (Schulte and de Vries 1985, Greaves et al. 1991, Sarathi 1999 and Tabasinejad et al. 2006).

First step

The purpose of our study in a first step is to determine the conditions (reservoir heterogeneity, crude oil characteristics and operational conditions) under which the combustion front can propagate through a fractured system. Here, the scale of our problem is Darcy-scale where a porous matrix surrounded by fractures is considered (figure 1.1). The injected air into the fracture, in presence of enough heat, reacts either with the oil in the fracture or with the oil in the matrix after that oxygen has diffused in the matrix. When the combustion process starts, different phases may develop and combustion fronts will move along the system.

Initially, we may use the thermal reservoir simulation tools which are available to study the process. Using these tools, we will be able to perform very fine scale simulation (small spatial and temporal discretization) based on one equation models, i.e., assuming local equilibrium as will be discussed in the manuscript, also incorporating the maximum process complexity available in the simulator. Before applying this methodology, the underlying mathematical model of the tools under consideration should be understood. In the next step, reliability of the tools should be verified in a suitable manner. The validation could be done, firstly, for

some simple cases where the exact mathematical solution is available and, secondly, based on the available experimental data in the literature.
After the validation step we will conduct simulations to study the behavior of a fractured core, initially saturated with oil, water and gas under in situ combustion process. In particular, the sustainability of the combustion front and the oil recovery mechanism are studied.
Further, the simulation results will help us to design an experimental protocol where the combustion process will be studied in a real world. The results obtained from these experiments will not only provide us with the answer of feasibility of the ISC process but also make it possible to verify the reliability of our numerical tool. This has a great importance when one is thinking of the ISC feasibility and recovery prediction at pilot or field scales. Few experimental works are found in the literature (Greaves et al. 1991, Schulte and de Vries 1985 and Awoleke 2007) and most of them were done in the 80's or the years before, when it seems that the equipments were not enough powerful to properly control the experimental conditions (i.e., temperature control and heat losses). It is necessary to conduct some more precise experiments that enable us to answer the above mentioned question.
Finally, using all these tools it may be possible to propose a range of feasibility for ISC processes at the Darcy-scale.

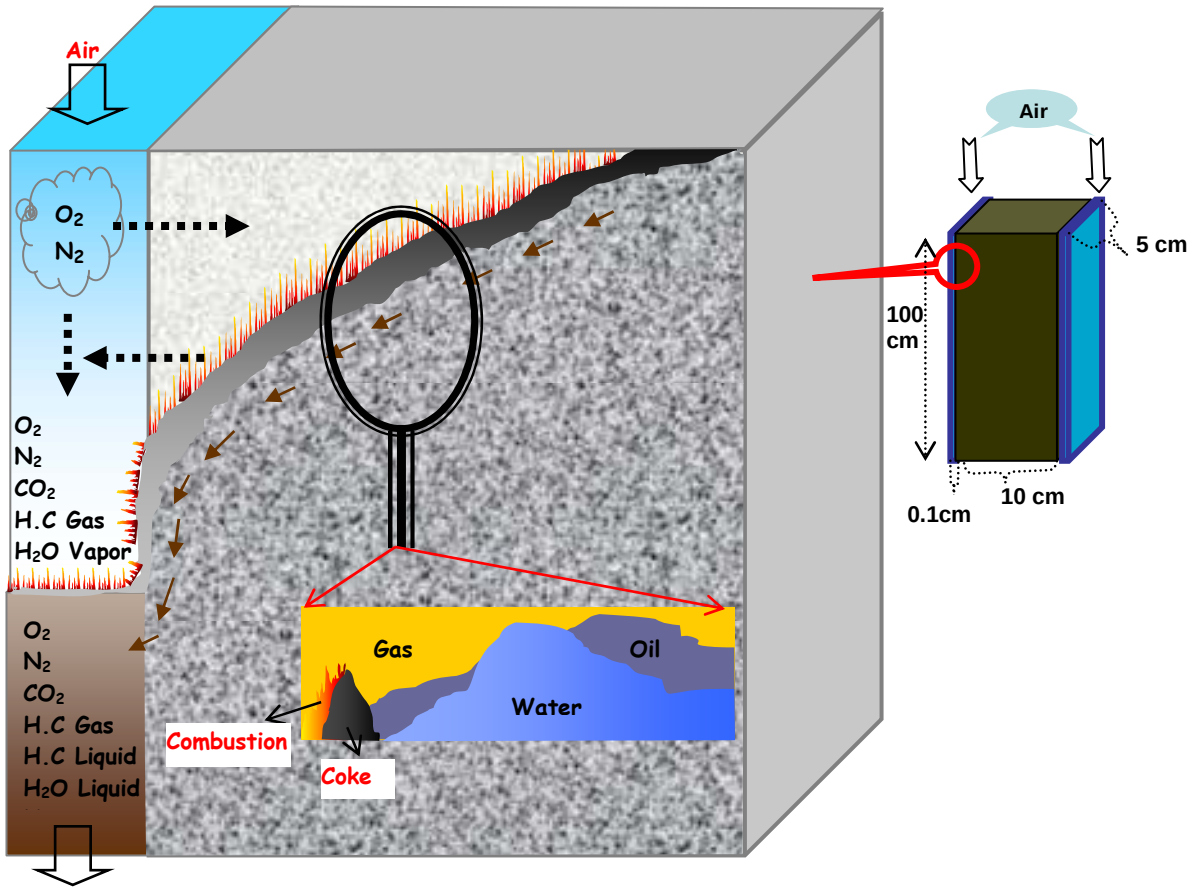


Figure 1.1. The schematic of in situ combustion process in fractured reservoirs based on the present knowledge.

1.1.2 Large scale challenges, the upscaling method

In petroleum industry, as far as the recovery methods are concerned, the prediction of oil and gas production rate has a crucial importance. This prediction is usually done using numerical simulators. Simulation of petroleum reservoirs could be very costly if one decides to perform a simulation task with small discretization in space and time. Thus, to have simulation results in a reasonable time we are obliged to use some large scale discretization.
On the other hand, many enhanced oil recovery processes operate locally, over a length scale which is much less than the inter-well distances. The physical mechanisms which govern these processes act at very short distances, even over few centimeters in in situ combustion. Even if the physics is properly represented in the simulator, the numerical errors due to large discretization may mask the physics. The numerical error arises from the spatial and temporal discretization of the governing equations. While, thanks to the advances in numerical methods, one can minimize those errors, they cannot be fully avoided.
In enhanced oil recovery processes, simulation errors are not only due to small temporal and spatial scales of the process but also to the highly non-linear physics of these processes. This is the case in in situ combustion of heavy oils, for example, where the chemical reaction is strongly coupled with the temperature. Small numerical errors can quickly become coupled and magnified with the non linearity of the process. As a consequence, it may be difficult to interpret the simulation results.
In naturally fractured reservoir, one is confronted with highly heterogeneous porous media. To simulate the behavior of such a complex object, one needs to simplify in a first step the geometry and, in a second step, the underlying physics. While many researchers have devoted their time to study these reservoirs (Van Golf-Racht 1982, Barenblatt et al. 1960, Warren and Root 1963 and Quintard and Whitaker 1998), the subject is still open to research even for simple processes like water injection . Using one or two-equation models, constant or variable exchange terms between fracture and porous matrix are still under investigation.
Thus, considering the above mentioned challenges, simulation of a fractured reservoir in which a combustion process is being applied at a large-scale (larger than Darcy-scale), is a complicated job. One should think of an upscaling procedure in which a non-linear nature of the combustion reaction that acts at small distances should be respected, on one hand, and, on the other hand, the exchange terms between fracture and matrix should be defined considering non steady-state undergoing changes in the fracture.

Second step

According to the upscaling literature, to perform an upscaling step, one needs to know the behavior of the system at the small-scale (the scale lower than the upscaled one). In this study we are interested to find an upscaled model at the inter-well scale.
To this end, we need to perform a detailed analysis of the combustion process at Darcy-scale to decide about the suitable model for upscaling (one equation, two equation or mixed model). Part of the material necessary for this analysis will be provided in the “first step” which is mentioned earlier (core scale). Some other fine grid simulations are done also at a single block scale. Single block simulations enable us to identify the two dimensional behavior of ISC and the relative scale of different parameters compared to the block size; Some important ones are: the size and the shape of the combustion front in the porous matrix and its relative position to that of the fracture, the characteristics of different fluid saturations (relative position and extent), the shape and the size of the fuel zone, how different parameters are changing in the fracture with respect to time and space, etc.

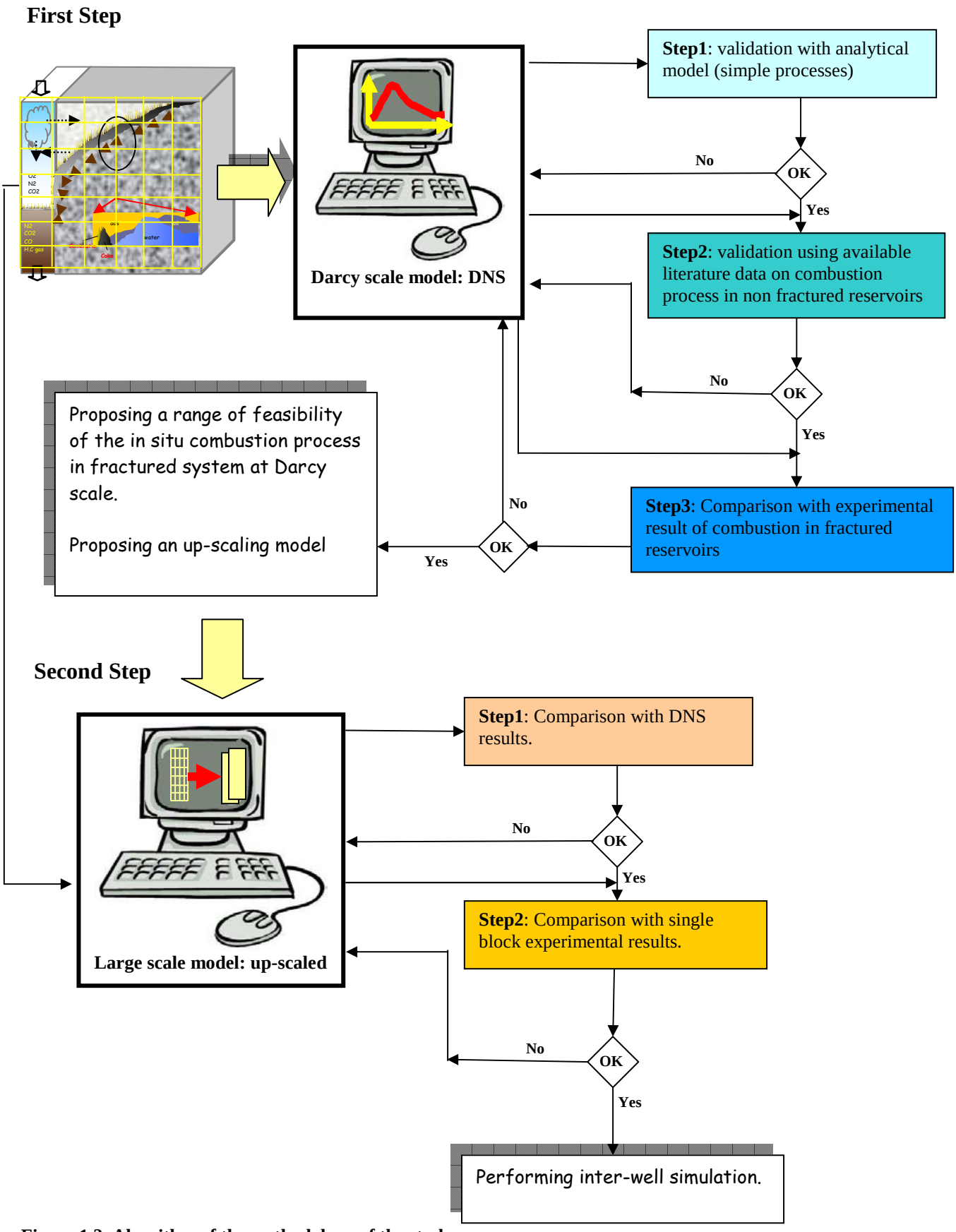


Figure 1.2. Algorithm of the methodology of the study.

Usually, in the upscaled model, some effective parameters are defined. The validity of these effective parameters is assessed by comparing the small scale model results with the upscaled model.
Further validation could be achieved if real world data were available. To this end, only simulation of ISC at a multiple block scale using single porosity, fine grid simulation is done. The algorithm of the above mentioned methodology consists of two main steps as shown in the figure (1.2).

1.1.3 Presenting the chapters

Considering the main objectives of this study and the methodology at hand to fulfill these objectives, here the next chapters of the manuscript are briefly presented.
The combustion process in a homogeneous porous medium is discussed in more details in chapter 2. In particular, the in situ combustion process to hydrocarbon production is reviewed. Based on this literature, the underlying physics of the ISC process is reviewed and, in particular, the presence of different driving mechanisms for oil production, possible physico-chemical changes of hydrocarbons in the presence of a ISC front or the combustion products (steam, hot gases, etc.) are mentioned. A review of the kinetics of crude oil oxidation reactions in presence of porous media, which is essential to understand the behavior of the combustion process in porous media, is also introduced.
In the following part of this chapter, a literature review of the combustion process in heterogeneous systems is introduced. However, few cases were found and even less cases were found in which the problem of crude oil combustion has been treated.

Numerical study of the propagation of a combustion front in a fractured system is presented in chapter 3. The governing equations for heat, mass and momentum transfer are introduced in a general form which could be found in a typical commercial reservoir simulator. In the first part, simulation results of this process at Darcy scale are presented. Before doing the simulation, the numerical tool was validated. The validation was done by comparing the simulation results with the solution of the problem for simple cases (i.e., one and two dimensional diffusion and one dimensional diffusion driven solid-gas combustion) for which analytical solutions exist. After having validated the simulator, the simulation of a combustion process in a fracture core was performed. The simulator input data are taken from the work done by Kumar (1987). The main goal of these simulations is, on one hand, to identify the condition under which a high temperature combustion front can propagate in a fractured system and, on the other hand, to determine the oil production mechanism(s) under a sustained combustion process.
In the next step, some other simulations were done at a single block scale. The importance of these simulations is that one can distinguish the relative extension of the profile of different parameters in the matrix block. The governing mechanism of oxygen delivery to the combustion front and the oil production is analyzed.
In the last step of the simulation work, the application of ISC at a multiple block scale is simulated to study the behavior of this process at larger scale and the possible interference between different blocks and also to propose some guidelines for the upscaling of the process.

In order to validate the simulation results and also to have better understanding of the practical challenges of the ISC process, we realized laboratory experiments at Stanford University School of Earth Science in collaboration with Energy Resources Engineering department. We did this work under the supervision of Dr. Anthony Kovscek and Dr. Louis Castanier and we deeply appreciate their collaboration.
Two different types of experiments were conducted: kinetic cell and combustion tube. The kinetic cell experiment is used generally to determine the kinetic parameters of the reactions

taking place during the combustion process. The combustion tube experiment is designed to study the behavior of combustion processes (i.e. oil production, heat and mass transfer, relative position of different fronts) at a scale which is normally larger than the kinetic cell scale. These experiments were done at core scale using a heavy oil. Only two examples of laboratory work were found in the literature (Schulte and de Vries 1985, Greaves et al. 1991). Both of these works were done more than 20 years ago. Technical limitations may have affected the accuracy of results. In the present study, we managed to overcome part of those technical difficulties in order to have more reliable results. This issue is discussed in this chapter. The main finding of these experiments is that, having a sustained combustion front in fractured systems is much more challenging than that in homogeneous porous media. It seems that, due to the large permeability contrast between the matrix and fracture, oxygen penetration into the porous matrix and eventually feeding the combustion front is limited. Under this condition and especially in low operating pressure condition, injection of normal air into the fracture reservoir may lead to the extinction of the ISC front. Our observations show that a sustainable combustion is achievable if the oxygen flux from fractures into the matrix is large enough.
In the kinetic cell experiment, the effect of the carbonate presence in the porous matrix is studied. Results show that it can significantly modify the kinetics of reactions in the ISC process. Kinetic cell experiments are usually done using a non-consolidated porous medium. In our case, the presences of highly conductive fractures adjacent to the matrix cause most of the injected air to flow through the fractures and some gas to flow through the matrix because of diffusion. We thought that this may have an effect on the combustion reaction inside the matrix. That is why some experiments were done using a consolidated porous medium in the kinetic cell. The free passage of air around this consolidated core mimics the matrix fracture situation. Results show that both LTO and HTO reaction kinetics are affected.
In the next step, experimental results are confronted with numerical simulations designed using the experimental condition both for the kinetic cell and the combustion tube. These simulations reproduce qualitatively the results obtained in the experiments.

The final target of this work is to simulate the combustion process at reservoir scale. To do so, as mentioned earlier, there are basically two possibilities: either using a one equation model and performing fine grid simulation or using one or two equation models and performing an upscaled simulation. The first approach in not feasible considering geological scales of a typical reservoir on one hand (requires large number of nodes in fine grid simulation) and, on the other hand, the complexity associated with the ISC process by itself (solving non-linear and coupled equations which is time costly). The second approach is however less time consuming and computationally feasible but it has its own complications. Any upscaling process calls for the representation of some upscaled parameters in the governing equations and in the case of two-equation models a representation also needed for the so called exchanged term between the two equations (or two domains). The volume averaging method (VA) is used as an upscaling approach in this study. Doing the upscaling of ISC process in its complete form (presence of five phases and multi-component) by the VA method is currently to much a challenge, thus a simplified form of the ISC process is studied: the combustion of solid-gas in a porous medium.
In chapter 5, after presenting the conclusions, an upscaling approach using the VA method is presented as the perspective for future studies. The mathematical formulation of the upscaling process using the VA method is presented based on which the effective parameters as well as the matrix fracture exchange terms are derived for the upscaled equations. The simulation results of fine grid simulation and the upscaled ones are compared.

Notations (chapter 2)

$A_{\pi\theta}$	Interface between two phases, (m^2)
a	Inclusion length scale, (m)
$a_v h$	Exchange coefficient, (J/m^3.s.K)
b	
b_1	Constants
b_2	
b_3	
C_P	Heat capacity, (J/mol.°C)
C_π	Concentration in the phase π
c	Compressibility, (1/Pa)
$D_{\pi i}$	Pore scale diffusion coefficient, (m^2/sec)
$D^*_{\pi\pi}$	large scale diffusion coefficient (m^2/sec)
$D^*_{\pi\pi,mix}$	large scale diffusion coefficient in mixed model, (m^2/sec)
D^*_π	Darcy scale effective diffusion coefficient, (m^2/sec)
K_π	Permeability, (m^2)
K	Absolute permeability, (m^2)
k_{rw}	Water relative permeability
$k_{\pi\theta}$	Volume weighted thermal conductivity, (W/m.°C)
L	Large scale length, (m)
l	Small scale length, (m)
$n_{\pi\theta}$	The normal vector at the interface
P_π	Darcy scale pressure, (Pa)
$\overline{P}_\pi$	Average pressure, (Pa)
$\overline{S}_w$	Average water saturation
S_w	Water saturation
T_π	Phase temperature, (°C)
T	Darcy scale temperature, (°C)
ΔT	Temperature difference, °C
V	Total volume, (m^3)
V_π	Phase volume, (m^3)

Greek symbols

α	General shape factor, ($1/m^2$)
α^*	Effective mass transfer coefficient (1/s)
α_h	Hydraulic diffusivity
σ_s	Saturation shape factor
σ_p	Pressure shape factor
π, θ	Phase indicators
ε	Porosity
ϕ	Volume fraction
μ	Viscosity, (Pa.s)
$\langle\rangle$	Average property
$\langle\rangle^\pi$	Intrinsic average property
$\sim$	Deviation term
Pe	Péclet number

Chapter 2. Combustion in heterogeneous porous media

In this chapter, a review of combustion processes in a homogeneous porous medium is presented, then a literature review on the problem of combustion in a petroleum reservoir is introduced and, finally, the combustion process in a heterogeneous porous medium is reviewed.

2.1 Combustion processes in homogeneous porous media

As mentioned briefly in the previous chapter, combustion in a porous medium has been a subject of interest in different domains. The porous medium could be inert, catalytic or contains some fuels. It may be homogeneous or heterogeneous at different scales. The fluid that occupies the porous part may have different physical and chemical properties. The delivery of the oxidizer to the combustion front could be governed by convective and/or diffusive flow. The chemical reaction by itself may be only combustion or some pyrolysis and cracking of molecules may occur before the combustion. The geometric scale of the problem could be also different, while the scale of a porous burner is about few centimeters, combustion can take place in a few meters long rode of wood.
All these different situations result in different conditions for the combustion process. Generally speaking, combustion in porous media is known as filtration combustion, where delivery of reactants through the pores to the reaction site is an important aspect of the combustion process *(*Matowsky et al. 2001). Smoldering and SHS (self-propagating high-temperature synthesis) are two important categories of the filtration combustion.
As defined by Ohlemiller (1985) “Smoldering is a slow, low-temperature, flameless form of combustion, sustained by the heat evolved when oxygen directly attacks the surface of a condensed-phase fuel”. Smoldering of a porous carbonaceous rod is normally controlled by two main parameters: availability of oxygen to the combustion front and heat losses from it. The velocity of the combustion front into the carbonaceous fuel after the ignition by an external heat source and the peak temperature are two indicators of the sustenance of combustion. It is a transient process, which is controlled by a combination of endothermic and exothermic chemical reactions in the pyrolysis and combustion zones, diffusion of oxygen to the combustion zone, diffusion of reaction products away from the sources, and heat transfer as well.

2.1.1 Typical observations of combustion in a homogeneous porous medium

In a pioneering work Aldushin and Seplyarskii (1977) studied the one dimensional combustion wave propagation in a porous medium. Based on the asymptotic method, they determined the structure of the solution. Many other researchers have been involved in the development of this method, most of their works are based on the macroscopic approach for presenting the transport equations. The work of Ohlemiller (1985), Schult et al. (1996) and Oliviera and Kaviani (2001) are some important references.
Here a brief review of Schult et al. (1996) is presented in which an analytical solution is proposed for one dimensional combustion in a porous medium. The basic assumptions are the same as those considered by other researchers who have been trying to develop an analytical solution for this problem. Figure (2.1) shows the schematic of the model. The porous medium is a cylinder isolated from the surrounding except at the ends. The combustion wave starts from one end and moves toward the other end in the same direction as the injected gas

(forward combustion) or in the opposite direction (reverse combustion). Here we are dealing with the forward combustion.

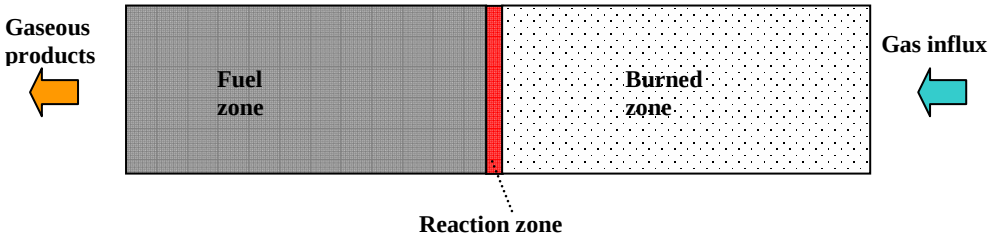


Figure 2.1. One dimensional smoldering model.

Following are the basic characteristics and assumptions of Schult et al.'s (1996) model; the porous medium consists of the inert solid phase, solid fuel and the porous space initially filled with the inert gas. Only one equation describes the complex chemistry of smoldering. In this reaction the solid fuel reacts with the oxygen and produces solid and gaseous products and generates heat. Local thermal equilibrium exists between the gas phase and the inert solid (i.e., the phases averaged temperatures are equal). Radiation is neglected in the heat transfer equation. The solid phase is stationary and non deformable. Fick's law describes the diffusion of oxidizer through the gas with constant oxygen diffusion coefficient. Density of the gas phase is considered to be much smaller than that of the solid phase. The sample is considered to be highly porous so that the characteristic length-scale of the pressure variations is much larger than that for temperature variations. In other words, the flow resistance through the porous sample is small thus the pressure is essentially constant. Inlet gas phase velocity is considerably higher than the combustion front velocity. Reaction rate is considered to be of Arrhenius type which depends on the oxygen and the solid fuel concentrations. Large activation energy is assumed, which induces a very thin reaction zone. Heat transfer rate is very fast compared to the smoldering rate. The sample is sufficiently long so that end effects are negligible.

The asymptotic method was used to describe smolder combustion and different structures were observed. A so-called reaction leading structure (figure 2.2) occurs when the velocity of the combustion front exceeds that of the heat transfer layer, while a so called reaction trailing structure (figure 2.2) is obtained when the combustion front is slower than the heat transfer front. It is indicated that the analytical solution provides qualitative theoretical description of various experimental observations both for reaction trailing and reaction leading structures (Schult et al. 1996). Each structure has two interior layers: region of rapid variation in temperature separated by a longer region in which the temperature is essentially constant (figure 2.2). The first layer is due to the heat release by combustion and the second is due to heat transfer between solid and gas phase. In both structures the temperature profile exhibits three zones in which the temperature is constant. The temperature in the combustion zone is high and this zone is surrounded by two cooler regions. Two transition layers, in which the temperature changes rapidly, connect these two lower temperature regions to the combustion zone.

A simple one step reaction model was considered:

$$\textit{Solid reactant} + \textit{Oxygen} \longrightarrow \textit{Solid Product} + \textit{Gaseous Product} + \textit{Heat}$$

Many smolder reaction schemes have two steps. The solid fuel decomposes through endothermic pyrolysis, producing solid char and gaseous products. The char then oxidizes, usually in a highly exothermic reaction in which it is converted to gaseous product and ash.

The endothermic pyrolysis reaction is thought to have little impact on the structure of the solution. Schult et al. (1996) believe that the presented reaction scheme is the rate limiting step in a more complex reaction scheme and is a good approximation for many smoldering processes.
It is found that the solutions in forced forward smolder show a superadiabatic burning temperature for both reaction leading and trailing structures. Superadiabatic temperatures are achieved because the energy released in the reaction remains in the region between the two adjacent low temperature layers.

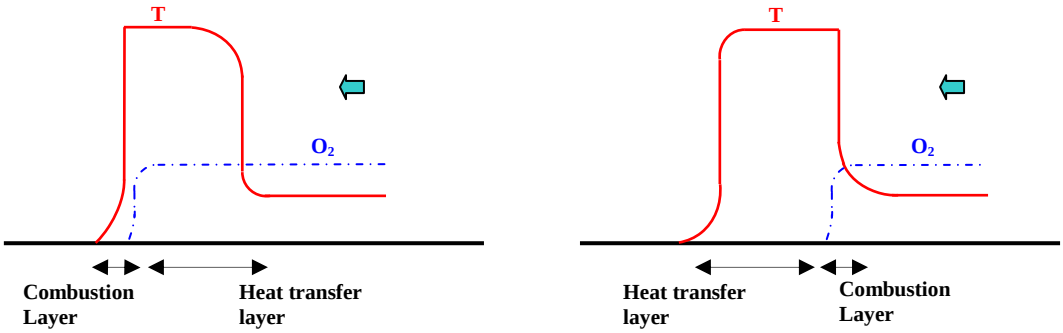


Figure 2.2. Reaction leading (left) and reaction trailing (right) structures.

The influence of oxygen availability was studied for both leading and trailing structures. In the reaction leading structure when the system is under the stoichiometric control (low oxygen supply compared to the reaction rate) the combustion propagation speed is proportional to the oxygen concentration. The same behavior was observed for the trailing structure under stoichiometric control. But, when the system is under kinetic control (high oxygen supply compared to the reaction rate) the combustion propagation speed is determined by the reaction rate, while this was not the case for the trailing structure where it is found that the incoming oxygen affects the smolder velocity and the burning temperature.
The simplified combustion process reviewed in the above case is different from the oil combustion in a petroleum reservoir. Some aspects of this difference come from the multiphase nature of the reservoir thus much more complicated reaction chemistry, fluid flow, as well as the phase behavior, are expected. There is also another important difference if one considers the case of fractured systems where, due to the lower permeability of the matrix block, most of the transfers between matrix and fracture seem to be under diffusion control. Under this condition the combustion process is also expected to be diffusion driven. A review of diffusion driven smoldering is presented in chapter 3 and the available analytical solution is used as a validation test for our numerical tool.

2.2 In situ combustion (ISC) in an oil reservoir

In situ combustion is a gas injection process as shown in figure (2.3), in which the injected gas (air) is chemically reactive with oil in the reservoir. The combustion reactions resulting from injected air, produce sufficient amount of energy to heat the reservoir content (rock+ fluids) and to sustain the combustion process. It pushes also the heated fluids toward the production well. Historically, air injection goes back to the 1900's. In situ combustion of reservoir crude probably occurred in the air injection projects carried out in south-eastern Ohio during the early time of this century. In a warm air injection into the formation to tackle the paraffin deposition problem, the possible occurrence of combustion process was mentioned (Sarathi 1999). It is also called fire-flooding as the fire front moves toward the

producer. The method is one of the earliest enhanced oil recovery methods. Despite the fact that it is a very efficient thermal recovery, due to the high associated risk, it has not found wide spread acceptance.

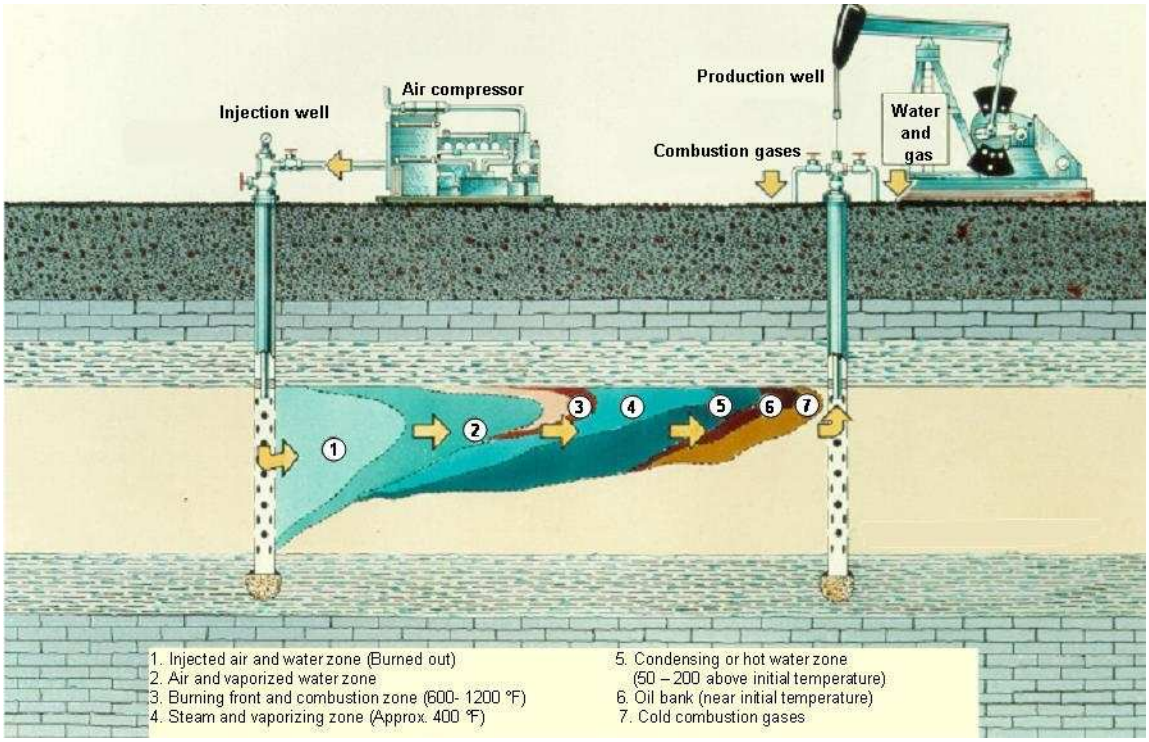


Figure 2.3. In situ combustion process (Sarathi 1999).

However, analysis of the successful projects indicates that the process is applicable to a wide range of reservoirs and the chances of failure can be minimized by careful selection of the reservoir and adopting low risk engineering practice. Some authors believe that the operational problems associated with fire-flooding are not more severe than those existing in other recovery techniques (Sarathi 1999).

2.2.1 Types of in situ combustion processes

Dry forward Combustion

In this process, air is first injected by an injection well, and then, the oil in the formation is ignited. Ignition is usually done using downhole gas burners, electric heaters or a hot fluid such as steam. In some cases, auto ignition of the in situ crude occurs (Vossoughi et al. 2005). After ignition, the combustion front is sustained by a continuous flow of air. This combustion is like smoldering and no flame is appearing underground. As the burning front moves away from the injection well, several zones develop in the reservoir between the injector and producer (figure 2.3). These zones are the result of heat and mass transport and the chemical reactions that occur in a forward in situ combustion process (Prats 1982, Sarathi 1999).

Wet forward Combustion

In the dry forward combustion process, most of the heat generated during burning is left behind the burning front and is not used for oil displacement. The injected air, on its way from the injection well to the combustion front, can not capture this heat due to low heat capacity. Water has higher heat capacity so, if it is injected together with air, much of the heat stored in the burned sand can be recovered and transported forward. Injection of water

simultaneously or intermittently with air is commonly known as wet combustion. The ratio of the injected water rate to the air rate influences the rate of burning front advance and the oil displacement behavior.
The injected water absorbs heat from the burned zone, vaporizes into steam, passes through the combustion front and releases the heat as it condenses in the cooler sections of the reservoir. Thus, the growths of the steam and water banks ahead of the burning front are accelerated, resulting in faster heat movement and oil displacement. The size of these banks and the rate of oil recovery are dependent upon the amount of water injected (Sarathi 1999, Prats 1982).

Reverse Combustion

In this method the combustion zone is initiated in the production well and moves toward the injection. The injected air travels through the reservoir until it contacts the combustion zone. The basic concept in reverse combustion is that the major portion of the heat remains between the production well and the oil when it is mobilized. Reservoir heating ahead of the combustion front is mainly by conduction as there is no oil flow in the direction of front propagation. This process is not well understood and despite of demonstration in laboratory no field application was reported for that (Sarathi 1999, Prats 1982).

Other processes

Few other processes have been developed based on dry or wet combustion aiming to increase the efficiency of ISC. Limited field application of these processes has been reported. (Sarathi 1999).

- Reverse combustion
- Cyclic dry combustion.
- Cyclic wet combustion.
- Steam chamber process.
- Oxygen recycled produced gas process.
- COSH (Combustion Override Split production Horizontal well process)

2.2.2 Chemical changes of crude oil due to temperature increase

In the ISC, the injected air reacts with crude oil in the reservoir. The extent and nature of these chemical reactions, as well as the heating effects they induce, depend on the characteristics of the oil-matrix system. The reservoir rock minerals and the clay contents of the reservoir are known to influence the fuel formation reactions and their subsequent combustion. The thermal alteration of the crude oil could be categorized in two main phenomena (Audibert et al. 1991).

- Pyrolysis: cracking, dehydration and condensation.
- Oxidation: low and high temperature oxidation.

While cracking may result in break down of large molecules that in turn make the oil lighter, the low temperature oxidation generally produces viscous oxygenated compounds. Many reactions may occur as the temperature develops during ISC but, to have a generalized scheme of the undergoing chemical changes, three types of reactions are usually considered corresponding to three ranges of temperature occurring in combustion processes (Islam et al. 1991).
a) Low temperature oxidation (LTO)
b) Intermediate temperature, fuel (coke) formation reactions
c) High temperature oxidation (HTO) or combustion of the solid hydrocarbon residue (coke)
However different reactions schemes have been used in the literature for different cases and, even with one single reaction scheme, good history match of laboratory data was achieved. To

model the kinetics of the in situ combustion, reactions are considered to be of Arrhenius type (Akin et al. 2000, Le Thiez et al. 1990).

LTO reactions

LTO is the reaction between the oxygen and hydrocarbons in which partially oxygenated compounds and little or no carbon oxides and water are produced. Oxygenated hydrocarbons are carboxylic acids, aldehydes, ketones, alcohols, and hydroperoxides (Burger et al. 1984). These are heterogeneous (gas/liquid) reactions that may occur even at low reservoir temperature. These are caused by the dissolution of oxygen in the crude and result in complex reactions whose nature is not completely understood (Audibert et al. 1991). Generally oxygen uptake reactions that occur at temperature lower than 350°C are considered as LTO reactions although this temperature range may vary for different crudes. Reactions above this temperature are intermediate and HTO reactions. It has been shown that the LTO reaction increases the amount of fuel available for combustion and causes a substantial decline in recoverable oil from the distillation and cracking zones (Sarathi 1999).
In a typical oxygen uptake curve, low temperature oxidation is characterized with a negative temperature gradient (figure 2.4).

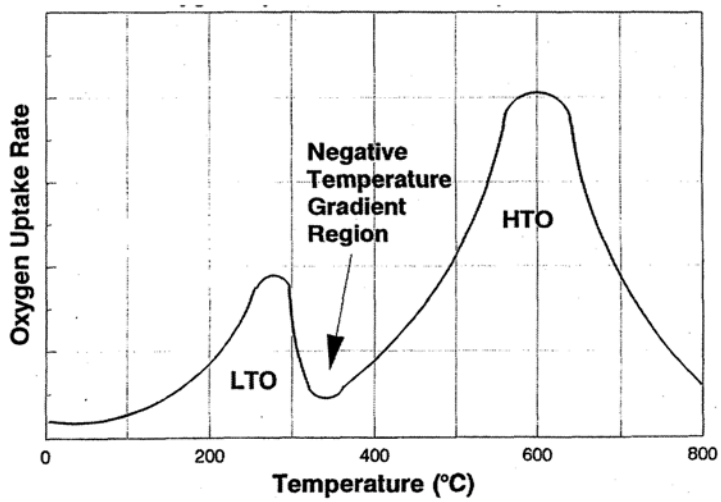


Figure 2.4. Typical oxygen consumption curve in ISC process (Sarathi 1999).

LTO dramatically affects the mobility of heavier cruds (i.e., those with high asphaltenes and resin contents). For these oils, LTO increases both the viscosity and density. Thus, conditions that promote LTO reactions must be minimized during the in situ combustion of heavy oils (Sarathi 1999).

Medium temperature reactions

Medium temperature fuel formation reactions involve cracking/pyrolysis of hydrocarbons, which leads to the formation of coke (a heavy carbon rich, low volatility hydrocarbon fraction) and these are generally endothermic reactions.
Laboratory pyrolysis studies on heavy crude oils indicate that the pyrolysis of crude oil in porous media goes through three overlapping stages: distillation, visbreaking, and coking. During distillation, the oil loses most of its light gravity and part of its medium gravity fractions. At higher temperatures (200-280°C), mild cracking of the oil (visbreaking) occurs in which the hydrocarbon loses small side groups and hydrogen atoms to form less branched compounds, that are more stable and less viscous. At still higher temperatures (above 280°C), the oil remaining in the porous medium cracks into a volatile fraction and a non volatile

carbon rich residue often referred to as “coke”. Coke is defined as the toluene insoluble fraction of oil and generally contains 80-90% carbon and 3–9% hydrogen (Audibert et al. 1991, Sarathi 1999). Both visbreaking and cracking reactions produce hydrogen gas and some light hydrocarbons in the gas phase (Hallam et al. 1985). It is observed that distillation of crude oil at low temperatures plays an important role in shaping the nature and extent of the cracking and coke formation reactions (Sarathi 1999).

HTO reactions

High temperature combustion reactions are heterogeneous reactions, in which the oxygen in the gas phase reacts with unoxidized oil, fuel and the oxygenated compounds to give carbon oxides and water. HTO occur at temperatures above 350°C and the heat released from these reactions sustains the combustion front propagation. As these reactions are gas-solid heterogeneous reactions, different transport phenomena could be present in high temperature combustion (Sarathi 1999). Oxygen diffuses from the bulk gas phase to the fuel surface where it is absorbed to this surface and reacts with the fuel. In the next step, the combustion products will be desorbed away from the reaction sites and finally diffuse into the bulk gas stream.
The overall combustion process will be controlled by the step, which is slower than the others. In general, chemical reactions are much faster than the diffusional processes. Therefore, the overall combustion rate is likely to be diffusion controlled (Sarathi 1999). The issue whether the chemical reaction rate or the oxygen diffusion rate controls the combustion process is under debate. Some investigators believe that the experiments are conducted under ideal situations in which the convective oxygen transport may mask the influence of diffusion on the combustion reactions in the reservoir. At high air fluxes the reaction is rate controlled and at low air fluxes the reaction is diffusion limited (Fassihi et al. 1984).

SARA based reaction models

Another way to represent the chemical reaction is based on SARA components of the crude oil. Figure (2.5) shows a general classification of the crude oil. In this way crude oil is considered to have the following chemical groups:

S: Saturates
A: Aromatics
R: Resins
A: Asphaltenes

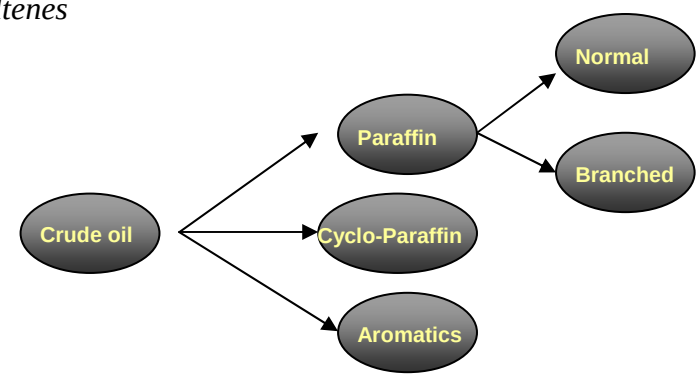


Figure 2.5. General classification of crude oil (Audibert et al. 1991).

Some authors have used the SARA representation of the crude in the study of in situ combustion. The reason is that there are some evidences that each SARA fraction oxidizes at a different rate and that, perhaps, different reactions can be distinguished. They have argued that this method can model the kinetics of reactions more accurately (Freitag and Exelby 2006, Bagci et al. 2002).

Effect of non-hydrocarbon materials

The most common non hydrocarbon materials found in the crude oil are non metallic (oxygen, nitrogen and sulfur derivatives) and metallic (iron, vanadium, aluminum, magnesium, nickel). Presence of the derivatives of sulfur in high temperature environment can produce corrosive components, which are harmful for the production lines and downstream facilities. Effect of minerals, which are present in the reservoir, could be either on rock composition modification or on reaction kinetics (Sarathi 1999).

2.2.3 Advantages of the ISC

The following advantages are mentioned in the literature (Sarathi 1999, Prats 1982) for ISC process.

1. Air is cheap and available everywhere.
2. Heat is produced in situ so, from a thermal point of view, it is the most efficient oil recovery process.
3. It can be applied in both light oil and heavy oil reservoirs.
4. Recovery efficiency is better than for other oil recovery processes.
5. The process can be implemented after waterflood and steamflood processes.
6. It can be applied in reservoirs where waterflood and/or steamflood are not effective.
7. Combustion projects permit the use of wider well spacing and can result in higher ultimate oil recovery in comparison to steamflood.
8. For thin reservoirs where steam injection has less efficiency, ISC could be more attractive.

2.2.4 Disadvantages of the ISC

Researchers have discovered that many operators of unsuccessful projects (i.e., in Canada) did not inject enough air into the wells for the process to function properly. Another significant finding was that the reaction temperature must be at least 350°C to efficiently mobilize the oil and reduce the problem of low-temperature oxidation reactions (Moore et al. 1998). The following drawbacks are mentioned in the literature (Sarathi 1999, Prats 1982):

1. Air compression and the maintenance of the compressors are costly.
2. Combustion is more attractive for thin reservoirs where steam injection has less efficiency.
3. Operational problems associated with combustion are more complex than for steam injection due to higher operation risk (oxygen breakthrough, low injectivity, high corrosion in production lines).
4. Planning and design of a combustion project is more complex and expensive compared to steam injection as it requires detailed kinetic analysis of combustion of crude oil.
5. Simulation of combustion is more time consuming and may not have enough accuracy without small discretization in time and space.

Moore et al. (1998) indicated that the key to success in operating an ISC process is to operate it in a high temperature oxidation (HTO) mode in order to sustain vigorous propagating combustion. According to the ISC Handbook (Sarathi 1999) at the end of 1997 there were 20 active ISC project worldwide which are producing more than 28900 bbl per day. In USA, at this time, 8 projects were active among which 6 projects were implemented in deep light oil and the rest in shallow heavy oil reservoirs (Prats 1982). Greaves (2006) reported that more than 130 pilots and development projects were active during the 1970s and 80s but ISC fell-out of favor. He believes that it could be partly explained by the characteristics of the long distance displacement process (figure 2.6). Conventional ISC is operating as a long-distance displacement process, using vertical wells. Although the inter-well distances are generally

not very large, 100-200m, severe gas override and advective instabilities usually happen, unless the reservoir geology is especially favorable.
Early gas breakthrough can occur, leading to an early cessation of operation, as occurred in some of the earlier projects. This 'bad experience' is considered as a drawback of the ISC process. When we apply long-distance processes (figure 2.6), fluids tend to accumulate downstream of the displacement front. For the ISC process, this can reduce the gas permeability, leading to reduction of air injectivity and eventual loss of high temperature combustion activity, causing the process to become locked in a low temperature oxidation (LTO) mode, from which it is almost impossible to recover.
To overcome the problems associated with long distance displacement a so called THAI – Toe-to Heel Air Injection was developed. It is able to operate as a short-distance displacement process (figure 2.6). Thus, the mobilized oil only has to be displaced a few meters into the horizontal producer below, rather than 100s of meters in conventional long-distance displacement.

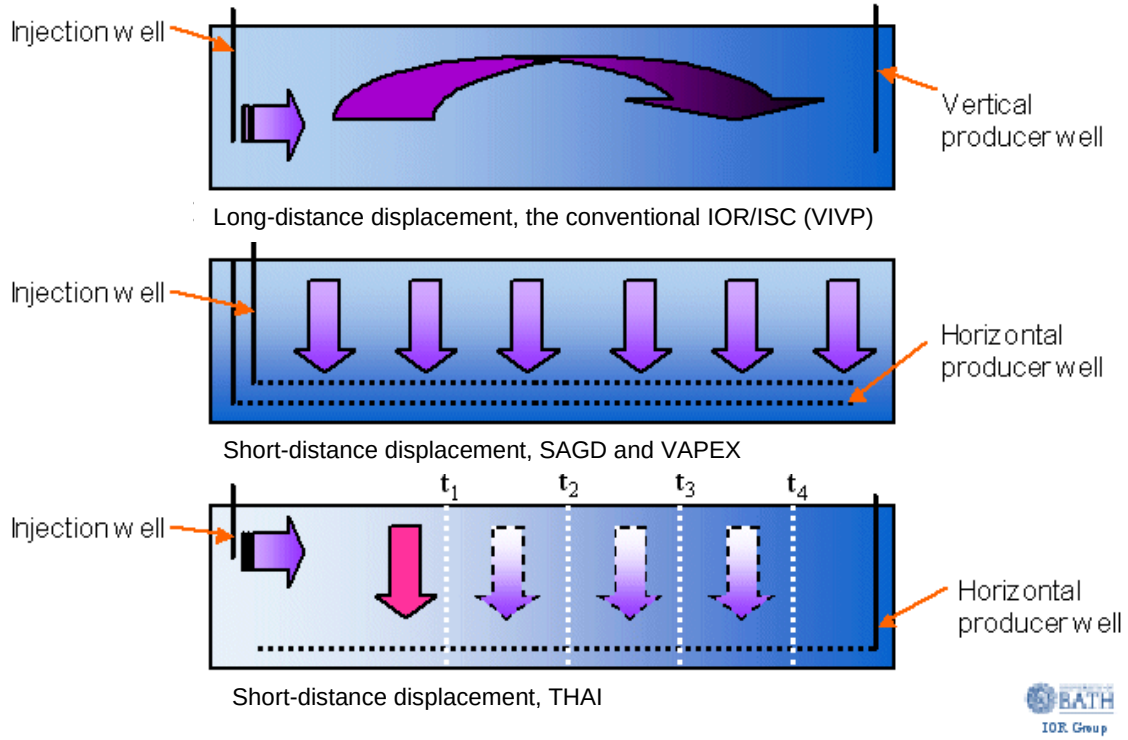


Figure 2.6. Comparison of long distance (conventional methods) and short distance (THAI and SAGD) processes for heavy oil recovery (Greaves 2006).

2.2.5 Physical changes of crude oil due to temperature increase

We will cover this part by a review of two books written about the thermal methods in heavy oil recovery (Burger et al. 1984, Butler 1998). The aim is to have a general sense about the influence of temperature on the oil physical properties. A thorough understanding of course needs more detailed analysis and there are still several open areas for research on this subject.

Dynamic Viscosity of gas and liquid

According to kinetic theory of gases for ideal gas, viscosity is independent of pressure and it is proportional to the square root of the absolute temperature.

$$\mu = b \times \sqrt{T} \tag{2-1}$$

But for real gases, viscosity increases with pressure and increases more rapidly than the square root of the temperature.

$$\mu = b \times \sqrt[n]{T} \tag{2-2}$$

in which *n* is a constant.
Liquid viscosity decreases exponentially with temperature. The Andrade's equation can be used for the calculation:

$$\mu = b \times e^{d/T} \tag{2-3}$$

b and d are the coefficients.
It is important to mention that dissolution of some gases in hydrocarbon can reduce the viscosity. This dissolution will cause the phenomenon which is called the *swelling* effect. This effect will be more pronounced for heavy oils. It is very important to calculate the viscosity accurately as it has direct relation to the calculation of oil phase velocity.

Surface tension and contact angle

Interfacial surface tension of the fluids and the wettability of the rock will change with temperature. Oil-water surface tension decreases as temperature increases. This is the same if we measure the contact angle of oil-water system on a glass or quartz meaning that the wettability to water increases with increase of temperature.

Relative permeability

According to the experiments on two phase flow, it is known that irreducible water saturation increases with increase of temperature while residual oil saturation decreases. This is in favor of recovery efficiency. One reason for this variation of irreducible and residual saturation is the effect of temperature on the mobility ratio and especially on the viscosity ratio (μ_{oil} / μ_{water}). Variation of the ratio of relative permeability does not show a general behavior. One can observe the variation of this ratio with temperature but it is not possible to generalize prediction of the changes.

Heat capacity

Generally the heat capacity of the solids, liquids and gases increases with temperature and pressure has a minor influence on it. For ideal gas it is independent of pressure. The following equation is often used:

$$C_p = b_1 + b_2 T + b_3 T^2 \tag{2-4}$$

b_1, b_2 and b_3 are the constant coefficients and C_P is the heat capacity in (J/kg.°C).

Thermal conductivity

Gas thermal conductivity increases with temperature and it has weak dependency to pressure while for liquids it decreases as temperature increases. Natural rocks are porous materials so the thermal conductivity of rocks depends on the properties of the solid matrix and the fluid inside the pore space. Generally the thermal conductivity of the solids deceases as temperature increases.

Thermal expansion

For ideal gases, the thermal expansion coefficient is proportional to $\frac{1}{T}$ and, for hydrocarbons, it is on the order of 10^{-3}(1/K) and for water it is 2×10^{-4}(1/K). For the solid phase, it has a

smaller value compared to that of liquid and gas and it is on the order of 3.8×10^{-5}(1/K). That is why the increase of temperature leads to the expulsion of oil from the solid matrix.

2.2.6 How the ISC process works?

ISC incorporates all of the main displacement mechanisms found in other enhanced oil recovery schemes: steam, hot water, immiscible gas, and miscible solvent drives (Greaves 2006). Castanier and Brigham (2003) defined different zones for the ISC process according to the temperature and consequently the fluids saturations (figure 2.7). The lower portion of this figure shows the temperature distribution and the upper portion shows fluid saturation from injection well to producer. This figure is an idealized representation of a forward combustion process and developed based on linear combustion tube experiments.
Starting from the injector seven zones can be defined:

A) The burned zone mostly filled with air which may contain a small amount of unburned residual organic solid. Temperature is less than the next zone, which is the combustion zone.
B) Combustion front: is very thin (several centimeters) HTO reactions occur in this part. It is the zone with highest temperature. In this zone the H/C ratio is 1 to 2. This fuel is the heaviest part of the oil.
C) and D, the cracking and vaporization zone is downstream of the front. Oil in this zone is the residual oil left behind the steam plateau. Due to high temperature front, light ends are vaporized and transported further, the heavy ends pyrolyse, resulting in hydrocarbon gases and solid fuel.
E) The steam plateau is the next downstream; most of the oil is displaced ahead of the steam front. Depending on the temperature the original oil may undergo a mild cracking often named visbreaking.
F) At the end of the steam plateau is the water bank.
G) The oil bank is the next. This zone contains most of the oil displaced from the upstream including the light ends resulted from the cracking.
H) The last zone is the original reservoir oil. Gas saturation is slightly higher due to the high mobility of the combustion gases. The production mechanism in this part is mainly gas drive.

The important point of this zoning is that, here, it is considered that light hydrocarbons can pass all along the steam plateau to be added to the oil phase ahead of this plateau. So any changes in oil properties is the result of LTO reactions that takes place in the cracking zone, and the steam distillation. It also considers that the oil saturation in the cracking zone is low.

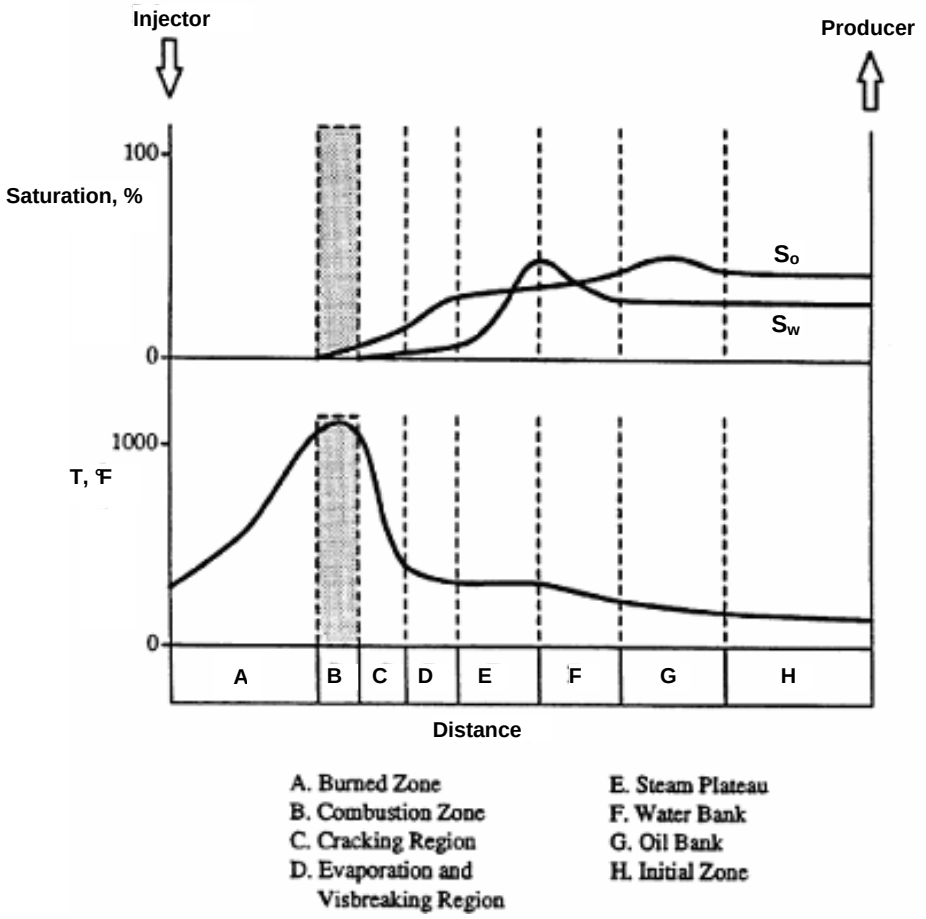


Figure 2.7. Diagram of forward in situ combustion (Castanier et al. 2003).

In another work, Freitag and Exelby (2006) conducted some experiments in order to distinguish the effect of the combustion and steam fronts (figure 2.8). They reported that, opposite to common belief, before steam breakthrough, the properties of the produced oil are much more influenced by steam distillation than by cracking reactions. While the combustion front mobilizes a substantial amount of oil, almost all of it remains behind the steam front. This oil has properties that differ significantly of that of the original oil.

Another interesting finding is that the contribution of the steam distillation to oil recovery before steam breakthrough was small. Examining the post-run tube they observed a significant amount of oil saturation left behind the steam front and near the combustion front. Increasing the recovery due to combustion front effect is much more pronounced for the heavier oil (79% higher than for steam gas recovery of Wolf Lake oil). Figure (2.8) shows a typical oil saturation in ISC process after steam breakthrough and the same curve for the steam-gas injection as presented by Freitag and Exelby (2006).

The residual oil after steam gas injection was 20%; the oil saturation in combustion test after steam breakthrough was also high (50%) which means that a strong oil bank exists ahead of the combustion front.

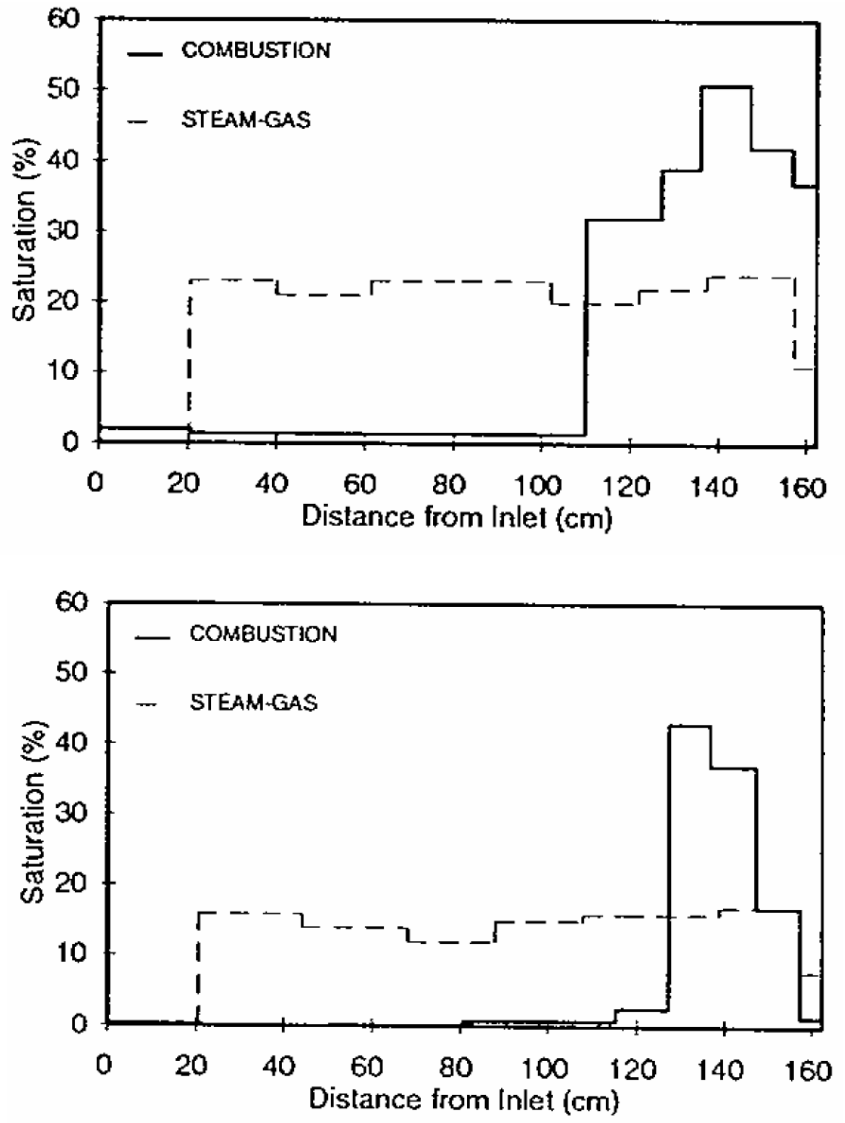


Figure 2.8. Comparison of steam and combustion fronts (top, Wolf lake oil and bottom, Nielburg crude).

From this paper one can conclude that the position of the main oil bank in a ISC process depends on the oil properties. In lighter oils, where the efficiency of the steam drive is high, the major oil banks remains ahead of the water bank, while this is not the case for the heavy oil where strong oil bank exists behind the water bank.

Greaves and Xia (2000) mentioned that the high temperature front created by combustion plays a major role in heavy oil recovery. The distillation performance of Wolf Lake oil and the residual oil after steam-gas flooding both were strong evidence that, if there was no thermal cracking taking place in the oil layer, much higher residual oil content would be expected in the unburned sand pack. Furthermore, in both the dry and wet 3-D combustion experiments, it was found that the volume of clean burned sand pack represents only about 38% to 43% of the total volume of the sand pack. Since the oil recovery was very high at 85% OOIP, this strongly indicates that the high temperature front created by in situ combustion plays a major part in the displacement of the heavy oil. A narrow mobile oil zone created ahead of the combustion front was observed which causes thermal upgrading of the heavy oil.

Kumar and Garon (1991) indicated that the issue of fuel formation during ISC is under debate. For example, many studies have assumed that the fuel for combustion in high

temperature-oxidation (HTO) reactions is formed primarily through thermal cracking reactions of crude oil constituents. Evidence exists, however, that thermal cracking alone may not be sufficient to deposit fuel and that LTO processes are also important in this process.
Sarathi (1999) considered the same zones as Castanier and Brigham (2003) except that the evaporation and the steam plateau zones are squeezed in the condensing steam zone.
Bagci and Shamsul (1999) in a study of different zone thicknesses in the ISC process considered the same zoning as Sarathi (1999) and Castanier and Brigham (2003). The concept of a combustion zone where fuel is deposited and consumed has been studied extensively. One approach for measuring the combustion zone thickness was to stop the combustion tube experiment and analyze the residual coked material. It is found that most of the coked material was deposited in a narrow band about 25.4 mm thick (Bagci 1998). In a dynamic approach Bousaid and Ramey (1968) tried to determine the combustion zone from a probe placed inside the combustion tube which gives an instantaneous measure of the fuel burning rate and temperature distribution. As the front passed the probe, the test results indicated that efficient combustion was limited to an interval of about 20 mm wide. A summary of the combustion zone thickness reported in literature is presented in Table (2.1).
In a study of the Cold Lake bitumen kinetics, Mamora et al. (1993) observed high combustion temperatures when clay or fine sands were present. These particles reduced the permeability of the sand pack and also provided a large reaction surface area. Consequently, the residual oil saturation and, hence the fuel concentration increased, which resulted in high temperature combustion. All of the injected oxygen reacted in the combustion zone.

Table 2.1. Combustion zone thickness and air flux reported in literature.

Kumar and Garon (1991)	25	1.7×10^{-3}
Thomas et al. (1979)	127 >	-
Fassihi et al. 1984	89	-
Bagci (1998)	80 (dry), 50(wet)	6×10^{-3}
Berry (1968)	25,4	-
Bousaid (1968)	20	-
Martins (2008)	10>	-

Thus, hydrocarbons ahead of the combustion front did not undergo low-temperature oxidation. The atomic H/C ratios which were similar to those of the original crude were another proof for that. It was considered that distillation was the main mechanism for fuel deposition.
In contrast, low-temperature oxidation was obtained in a combustion tube run in which the sample matrix contained only 20-30 mesh sand. Ignition was not obtained due to the low fuel concentration, and the oxygenated hydrocarbon fuel, which was detected in elemental analysis after the run, showed that a substantial amount of oxygen had moved ahead of the combustion zone. Based on this observation Mamora et al. (1993) proposed a new oxidation reaction model which describes the physics of oxidation reactions better than the previous models. These findings led them to conclude that oxidation reactions in kinetic and combustion tube experiments are different because of the different types of fuel deposited. They suggest that a new experimental technique should be developed to obtain kinetic parameters of fuel reactions encountered in combustion tube experiments or in field operations.

Effect of carbonate matrix

Calcium carbonate ($CaCO_3$) is the main component of carbonate reservoirs. However, in dolomite reservoirs magnesium carbonate is also present. Both of these components are subjected to chemical decomposition when temperature rises, which is the case in the combustion process. The general form of this decomposition is:

$$CaCO_3(s) \xrightarrow{Heat} CaO(s) + CO_2 \qquad \textbf{(2-5)}$$

This thermal decomposition has been the subject of many researches (Boris 1997, Sanders and Gallagher 2002). However, in the case of in situ combustion in oil reservoirs, there is a lack of information on whether temperature will modify the carbonate matrix or not. Bagci and Shamsul (1999) observed an excess production of carbon dioxide during in situ combustion of a Turkish carbonate reservoir. Initially they argued that the high CO_2 production may result from the decomposition of carbonate minerals. However, X-ray diffraction analysis of original limestone and burned limestone showed no change in $CaCO_3$ and $CaMg(CO_3)_2$ amounts. Thus they supposed that the increase in CO_2 production was due to the conversion of CO to CO_2 in presence of steam at high temperatures.
Study of the in situ combustion of an Iranian fractured carbonate reservoir showed that this process is feasible at laboratory scale. It was observed both in combustion tube test and TGA/DST analysis that there is no risk of carbonate rock decomposition during high temperature combustion (Kharrat et al. 2007).

2.3 In situ combustion in fractured reservoirs

The simple schematic of a typical ISC process in fractured system is shown in the first chapter. As indicated there, the injected air passes mainly though the fractures and, under a favorable condition a combustion front may develop in the matrix as well as in the fracture and the hydrocarbons (liquid and/or gas) are produce via the fracture and/ or the matrix. In this part, first, we review the work in the literature on the ISC in fractured systems and, then, some large scale modeling challenges are addressed. The combustion process by itself is a complex process and when applied in fractured reservoir it becomes more complex.

2.3.1 Laboratory works and simulation

Schulte and de Vries (1985) studied ISC in a fractured core at laboratory scale. They simulated the fracture as a narrow pathway adjacent to the core situated vertically in a core holder in a combustion tube experiment (figure 2.9). The main characteristics of this setup are presented in Table (2.2). In this experiment, they observed that the process was governed by diffusion of oxygen into the matrix. The main oil production mechanisms were found to be thermal expansion and evaporation. From numerical simulation and analytical modeling they concluded that the process is feasible for fractured reservoirs. To prevent oxygen breakthrough, injection rate should be limited (determined by fracture spacing) and to sustain the front propagation a minimum injection rate is necessary based on heat losses. A cone shape front was observed after cutting the core sample. The front inside the sample lags behind that in the fracture because it takes some time for the oxygen to diffuse to the canter. From combustion front velocity and air flow, it is calculated that 15% of the oil was burned. The same experimental configuration was applied by Greaves et al. (1991) but their combustion tube had larger diameter and was longer (table 2.2). They also criticized Schulte and De Vries's work by saying that the extensive heat losses made their results non realistic. In their experiments, core surface temperature profiles exhibit a broad and flat characteristic, rather than the more accentuated peaks obtained by Schulte and de Vries. Although they

(Schulte and de Vries) employed higher oil saturation, the peak temperature was significantly lower. In the work by Greaves et al. (1991) the combustion front is barely advancing during the early time of the experiment (first few hours) while this was not the case in Schulte and de Vries work. Like other experiment the cone shape front was observed with a length of approximately 0.17 m.

The length of this cone shape boundary increased at higher peak temperatures. The effect of oxygen enrichment was not clear and a range of oil recovery of 58~80% was measured. The highest recovery achieved by air combustion and more than 75% of the recovery achieved in the first half of all experiments. Very significant upgrading was obtained with the oxygen enriched cases. In normal combustion tests the extent of cracking is higher than for combustion in fractured media.

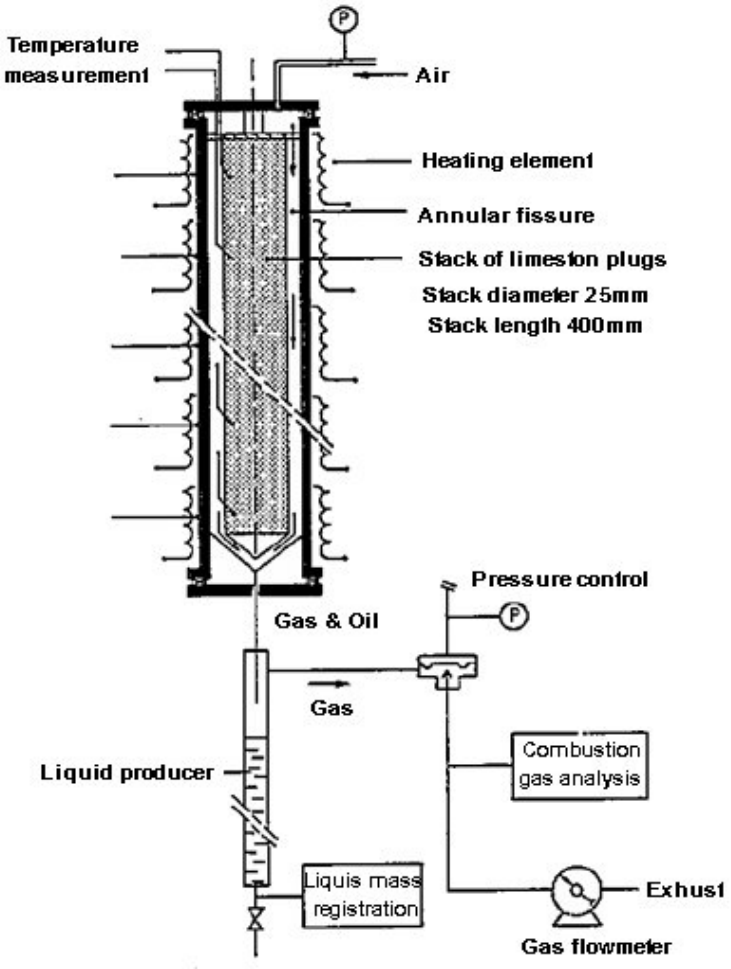


Figure 2.9. Schulte and De Vries experimental setup (Schulte and De Vries, 1985).

Table 2.2. Experimental parameters of Greaves et al. (1991) and Schulte and De Vries (1985).

Parameter	*D (cm)*	*L (cm)*	*Tube thickness (mm)*	*Fracture width (mm)*	*air flow (m^3/hr)*	*air flux (m^3/m^2hr)*	*front speed (m/hr)*	*Peak T (℃)*	*S_{wi} (%)*	*ΔL (cm)*
Schulte	2.5	43.2		1	0.017	29.9	0.01	600	0.0	40*
Greaves	6.6	76	1.5	1~2	0.036	10.52	0.037	750	34	34

* : Simulation, D: Core diameter, L: Core length, ΔL : Coke zone length

In another study done by Miller et al. (1983) using a fractured core, 33% of the initial oil in place was produced as a result of the combustion process while 45% was used for fuel. The combustion experiment with the fracture, which was propped with glass beads, was not successful. The authors believe that the air flow in this case passed through the fracture and was not supplied to the combustion front. Some works were done at Stanford University on in situ combustion in a fractured reservoir (Awoleke 2007). Two types of heterogeneous porous media were used to investigate the effect of heterogeneity on the ISC process. It was observed that the combustion front was not hindered by small scale (average 2.5 cm) heterogeneity while it was not sustained in the case of large scale (67 cm) heterogeneity.
Simulation of in situ combustion of light oil (26°API) in a fractured core was done by Tabasinejad et al. (2006). Their results show that the combustion front propagated successfully in the tube and high oil recovery (>80%) was achieved although it was lower for a conventional combustion process. The peak temperature in the fractured system was also lower than for the non fractured core. Air injection into a light oil fractured reservoir was studied by Delaplace et al. (2006) using a reservoir simulator. They performed a fine grid simulation at core scale where they found that the oxygen diffusion into the matrix and the thermodynamic exchanges between the gas in fracture and matrix oil are controlled by the matrix-fracture exchange. Further, they proposed a strategy for the upscaling of the process using a dual porosity model (figure 2.10).
Akkutlu and Yortsos (2000) studied the effect of the heterogeneity on the propagation of the combustion front in a porous medium containing two different layers using an analytical model. In this study, there was no mass transfer between the two layers. It was shown that there is a critical value for the permeability-thickness ratio of the two layers, below which two fronts are fully separated and above which two fronts are cohered. Coupling of two fronts could lead to a lower temperature in the faster front which then may privilege the LTO reaction in this layer. Separation of the two fronts may lead to early breakthrough.

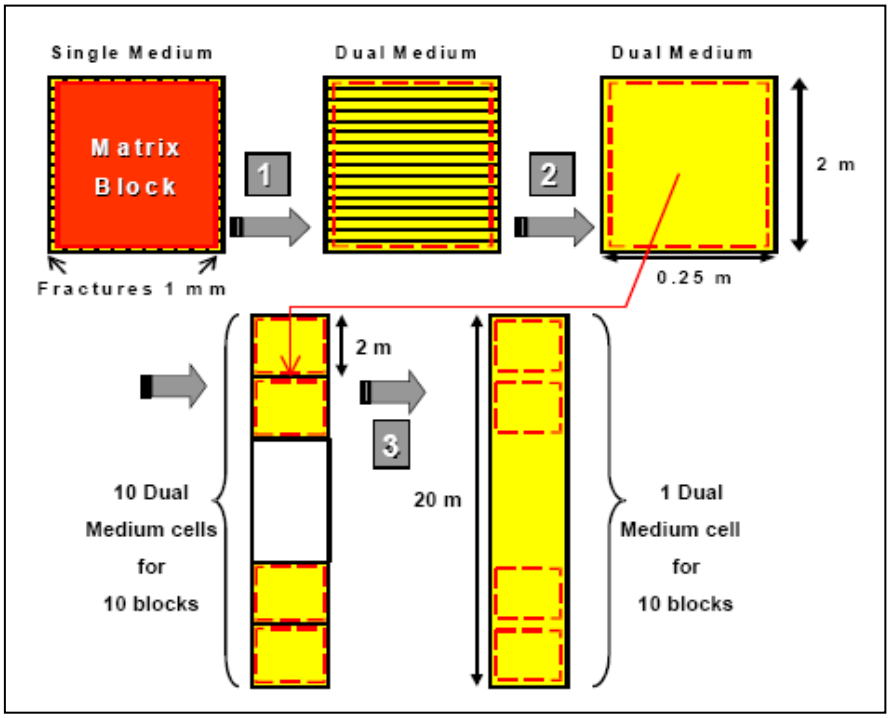


Figure 2.10. An example of upscaling strategy (Delaplace et al. 2006).

2.3.2 Pilot or field test results

Craig and Parrish (1974) reported some ISC pilot tests in a carbonate fractured reservoir in southwest Oklahoma. They concluded that severe heterogeneity (including high-permeability streaks, reservoir scale fractures, directional permeability and zones of low oil content) can lead to poor combustion efficiency and result in producing well problems. Based on that, they emphasize the need for detailed analysis of reservoir non-uniformities before starting a combustion project. They also believed that, for a low porosity reservoir (where the ratio of pore to rock volume is small), application of thermal recovery like ISC is not feasible simply because there is not sufficient energy to heat up the matrix.

2.3.3 Summary

At the end of this part, a brief summary is presented in the following:

- Based on the reservoir and oil properties, the condition under which the combustion process in a fractured system is sustained is not fully understood.
- Under a sustained propagation of combustion front, the recovery mechanisms are considered to be the evaporation and expansion. In case of the light oil it is shown that the thermodynamic exchanges are also important. In high temperature other mechanisms like gas drive may play a role and their contribution has not been fully distinguished.
- There is a question whether we can use the reaction schemes which are developed and used in homogenous system for a highly heterogeneous media like fractured reservoir. The hypothesis of three types of reactions we have mentioned before are made when the ISC is consider in a homogenous kinetic cell. We have not found yet a work on this subject for a kinetic cell which is heterogeneous.
- Regarding the modeling of the process at reservoir scale, to our knowledge, very little references are found in the literature.

2.4 Fractured reservoirs modeling challenges

Transport phenomena in heterogeneous porous media have been receiving a great attention in many domains ranging from environmental science to chemical and petroleum engineering. Dealing with heterogeneous porous media one is confronted with the presence of heterogeneity at different scales; from pore, core (packed bed column), pilot (inter-well) to field scale (Whitaker 1999).

With regard to transport phenomena, in some processes, this multi-scale heterogeneous system may behave in a so-called non-ideal manner which results in an anomalous behavior at large scale (i.e., non-Fickian response in case of solute transport, Quintard and Whitaker 1995, 1996, Ahmadi et al. 2007, Cherblanc et al. 2007 and Golfier et al. 2007). In this study, we are dealing with a specific type of heterogeneous porous media called fractured reservoir in petroleum notion and fissured medium in general porous media literature. In this class of material, most of the fluid in place is in the porous matrix, which is embedded with fractures network. A small fraction of the fluid is in the fractures, which have a far greater permeability than the matrix. It is important to note that, in general, fracture and fissures are different from the modeling point of view: a fracture is considered as a porous structure with high permeability for which one can consider the well-known Darcy equation at local scale, while fissure could be treated as a thin channel with almost hundred percent porosity for which Navier-Stokes equation could be applied even at Darcy scale (Quintard and Whitaker 1998). In our study we will consider the first definition and in the rest of the text we will use the “fracture” notion.

We are interested in the modeling of the combustion process of heavy oil in fractured reservoirs at the pilot scale. By pilot we mean the scale larger than the Darcy scale but still

smaller than the large scale (field scale) and which is usually used for the modeling of processes between two wells.
In reservoirs with a great number of fractures, simulation of this process at field scale would only be practical using dual medium models, i.e., they are the only models reproducing some observed tendencies (Debenest and Quintard 2008) while being acceptable in terms of computing requirements. However, validated dual medium models do not exist for in situ combustion. In particular, the write-up of the matrix-fracture exchange terms is unknown.
To introduce a suitable mathematical model, we attempted to distinguish the geometrical and process characteristics, which will lead to understanding different scales associated with this problem. This knowledge is the primary need to construct a large scale mathematical model. Based on this brief introduction the rest of this part is organized in the following manner: first the geological characteristics of the fractured reservoirs will be reviewed. Then, modeling challenges of transport phenomena in a combustion process applied in fractured reservoirs are addressed.

2.4.1 Hierarchical length scale in a typical fractured reservoir

In a typical petroleum fractured reservoir, one can observe the fractures at different scales larger than pore scale. Presence of fractures could be either due to structural or tectonic reasons. Based on that, also based on the observation at different scales (i.e., seismic, outcrop, well log, well test, and core analysis) one can find fractures at all these different scales (Estebenet et al. 2001). Figure (2.11) shows the heterogeneous structure of a fractured reservoir at different scales.

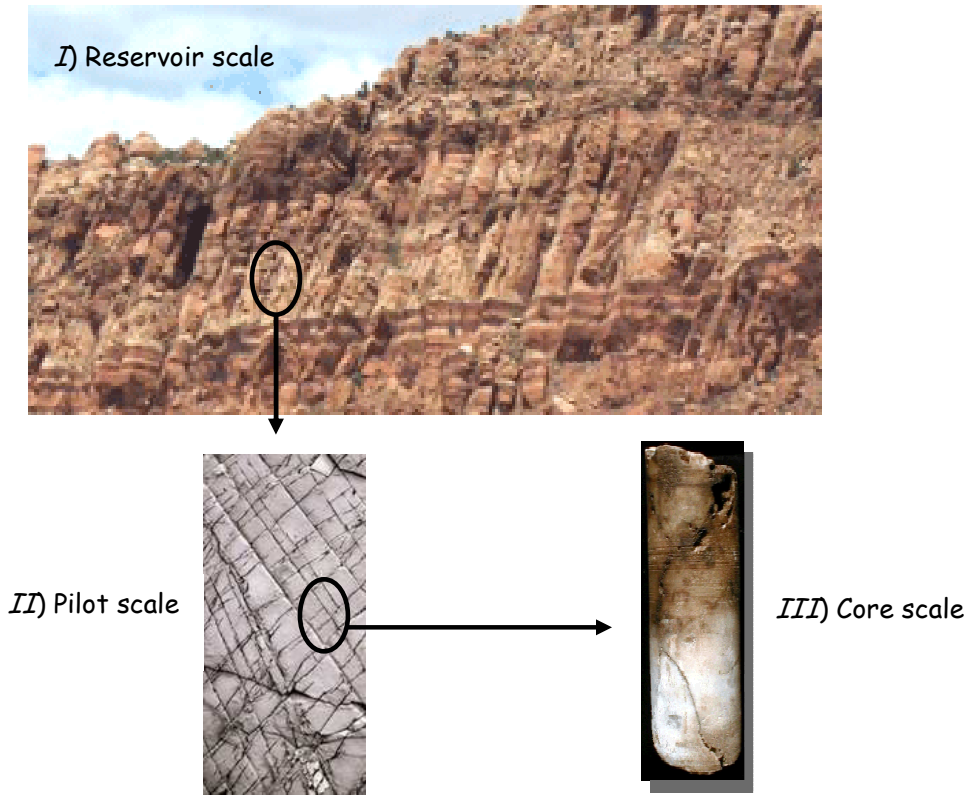


Figure 2.11. Heterogeneous structure of the fractured reservoir at different scales.

Based on this observation at different scales, we may construct a simplified geometrical model (Kfoury 2004) to describe the hetrogeniety at different scales (figure 2.12) . It is important to mention that, in reality, there may be some intermediate scales between the

scales presented in this model. The general characteristics of different scales could be described as follow:

Pore scale: The dimension of pore scale is about the diameter of the grain or the pore, and the fluid flow can be described by Navier-Stokes equation.

Core scale: The dimension of the core scale is few centimeters and the Navier-Stokes fluid flow equation can not be applied directly to this scale and some homogenization is necessary to obtain a so-called continuum medium description. Generally it is assumed that the Darcy law is applicable at this scale.

Large scale: The dimension of this scale is several meters at which the governing equations are derived from upscaling of the Darcy scale equations, taking into account heterogeneity in transport properties.

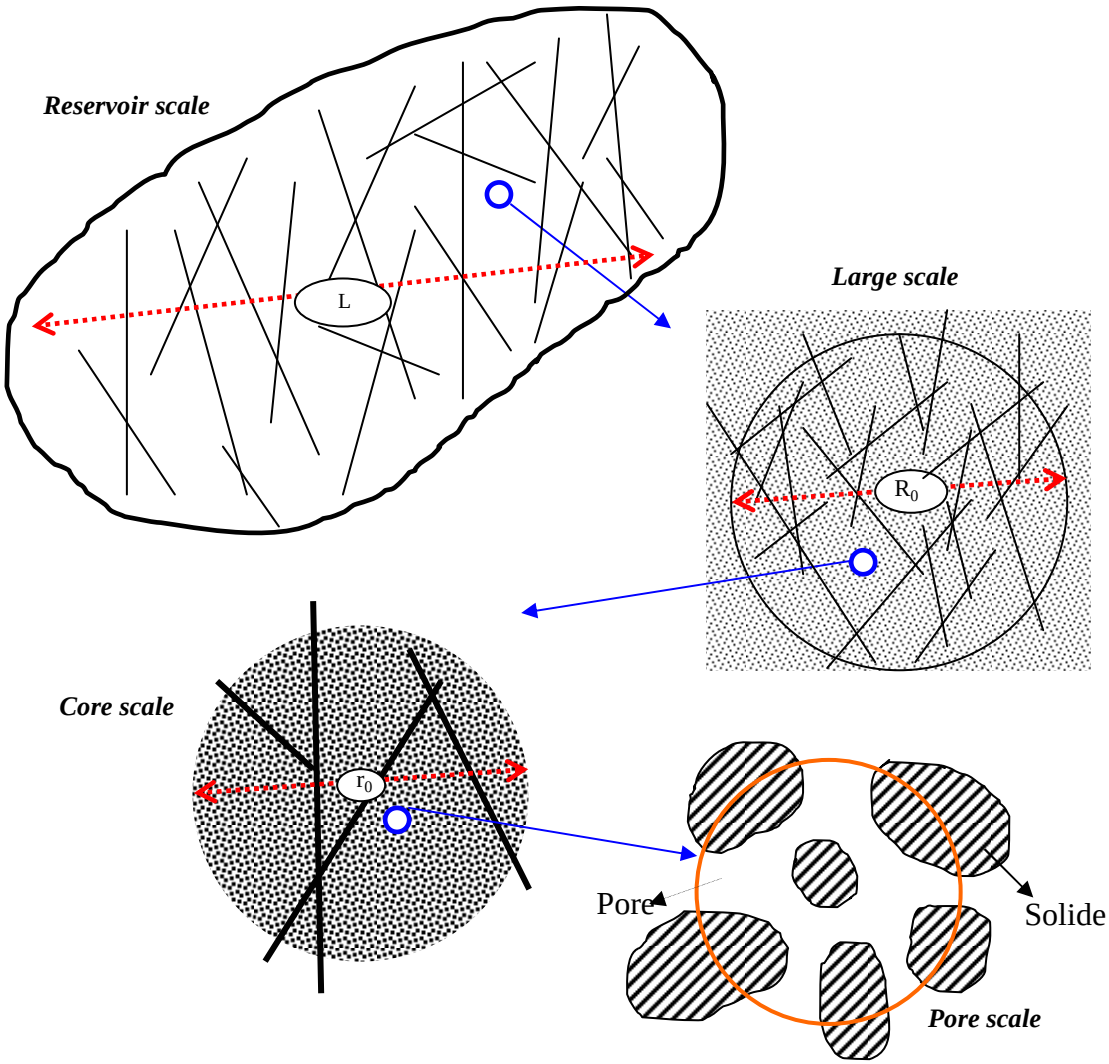


Figure 2.12. Simplified representation of the heterogeneity in fractured reservoir at different scales.

The fractures which cut the reservoir rock in various directions delineate a bulk unit referred to as the matrix block unit or simply matrix block (Van Golf-Racht 1982). The scale of a matrix can vary from a few centimeters to a few meters. The aperture of the fracture also

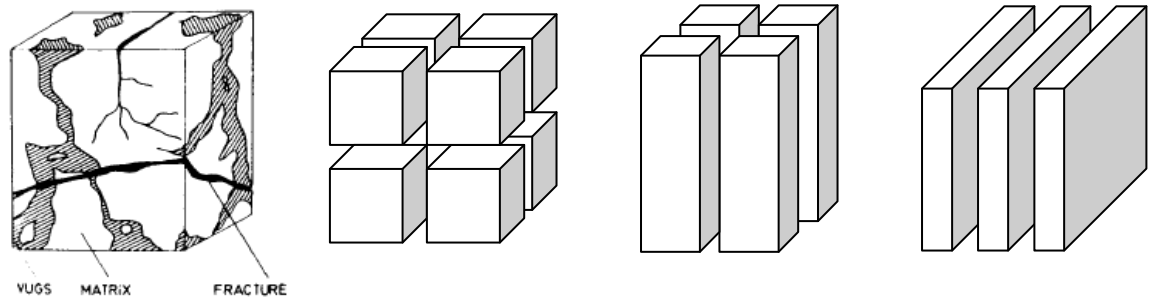
varies between less than one millimeter to a few centimeters. The volume of the fracture in a unit volume of the reservoir rock is considerably smaller (<1%) than the volume of the matrix such that we can consider the following relation (Van Golf-Racht 1982): $\phi_f \prec\prec \phi_m$

At field scale we may observe large conductive channels called faults (Henn et al. 2004). In this study we are not dealing with such objects. Our focus is on local and pilot (intermediate) scales where we assume no fault is present. The same relation can be considered for the permeability as the fracture is considerably more permeable than the matrix: $K_m \prec\prec K_f$

The large scale is not a unique scale as it depends on the objective of the problem. As mentioned before, in our case, this scale represents a block(s) of a few meters which seems to be suitable for the simulation of the inter-well scale processes.

2.4.2 Idealized representation of the fractured reservoir

Depending on the direction of the tectonic events and the predominance of one compared to the others, different unit blocks may be seen in a geological system. This complex fracture-matrix structure could be reduced, at least in some cases, to matrix block of simple geometry (parallelepiped, cubes, sphere, etc.) separated by uniform spaced intervals which represent the fractures (figure 2.13b). The size and shape of these blocks depend on *fracture density* and type of fractures. If the horizontal fracture density is equal to its vertical density the matrix block approaches cube shape (Van Golf-Racht 1982).



a) Real matrix block *b*) Sugar box *c*) Matches *d*) Slides

Figure 2.13. Basic idealized models of a fractured matrix.

Warren and Root (1963) developed the first idealized model to represent the fractured reservoir based on the model presented by Barenblatt et al. (1960), by considering the discrete matrix block between the connected network of fractures also known as “sugar–box” model (figure2.13b). It is important to note that, in reality, the surface of the fracture may not be smooth and its aperture and length may not be constant even at the core scale.

It must be emphasized that these reduction of a real, complex, fractured system to an array of simple geometries is really a rough representation that will result in a lack of many of the characteristics of the real system. This can be more illustrated by looking at the results obtained by Kfoury et al. (2004).

Two main reservoir types can be distinguished based on the origin of the porosity (primary or secondary) in a fractured reservoir (Estebenet et al. 2001):

- Single porosity
- Double porosity

The difference between these two is that in the first one, practically there is no porosity in the matrix while for the second type, the matrix is also porous. From the fluid flow point of view this idealization of fractured porous media can be done in different ways:

- If matrix permeability is negligible then all the flow occurs in the fracture network and matrix will play the role of a source term (*single permeability dual porosity*).
- When matrix permeability is also considerable, then convective flow also can occur in matrix (*dual permeability and porosity*)

It is important to mention that matrix blocks can be either disconnected or connected. In the petroleum domain most of the simplified reservoir models use the sugar-box geometry while in the study of heterogeneous porous media, in general other geometries, like sphere in cube or cylinder in cube, have been applied by researchers.

2.4.3 Simplified geometry

A simplified geometry for matrix and fracture is shown in Fig (2.14) which is the same as the Warren and Root (1963) model. As shown in this figure, fractures have two main directions perpendicular to each other. In this way each matrix block is surrounded by fractures. The figure illustrates that the matrix blocks are not connected. We also assume that, in our study, both matrix and fracture are permeable media, however, the permeability in the fracture is significantly larger than in the matrix.

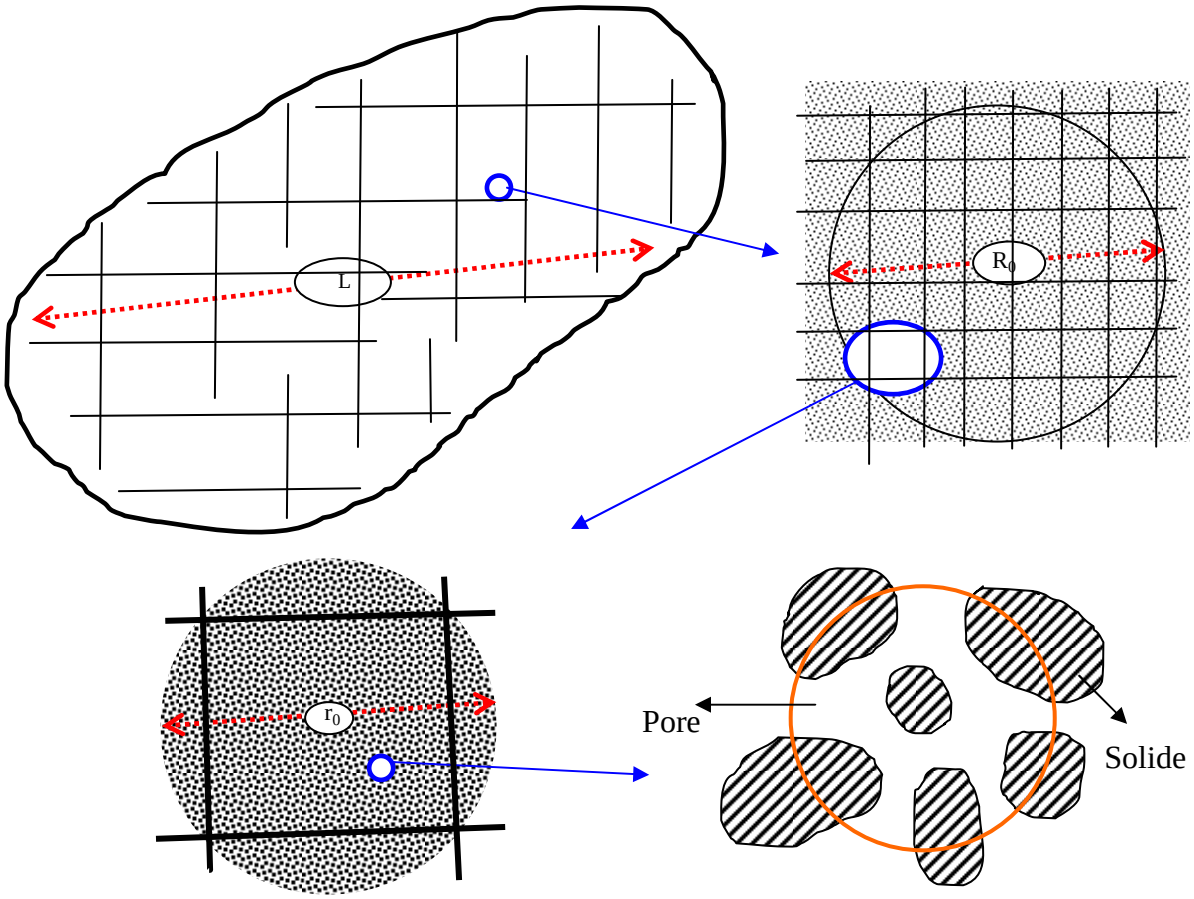


Figure 2.14. Simplified representation of the fracture and matrix in our study.

2.4.4 Fluid flow modeling in fractured reservoirs

Due to a very complex structure of the fractures, performing a detailed simulation even for single phase flow within a fractured medium is very difficult. To simulate the transport

phenomena, some averaged description of the flow field is necessary. Different methods are developed for performing this averaged description such as: Volume averaging (VA), Homogenization, Random walk, Fractal approach etc. Here we present the application of the VA method as an upscaling tool. Details about the mathematical background of this method may be found in a book written by Whitaker (1999) and the application of the method for different cases may be found in the extensive publications of Quintard and Whitaker (1995, 1996 and 1998) and Ahmadi et al. (1998). Using this method, one can start with the pore scale equations and, by doing some mathematical manipulations, a macroscopic model can be derived for Darcy scale. Further averaging could also be performed to derive a larger scale representation based on Darcy-scale equations. In this way there are two main approaches:

One-equation model

Starting from pore scale transport equations, one can consider matrix and fracture as a single homogenized medium at the local scale (or even field scale) and derive transport equations using effective parameters. However, this model is simpler and less costly in computation time, but it can not model some processes as they are observed in the field (Ahmadi et al., 2007). Using such a simplified model one should be always aware of its limitations.

Two-equation model

In some transport phenomena (i.e., solute transport) in heterogeneous porous media, non-ideal behavior was observed at the field scale, which could not be explained by a classical one-equation advection-dispersion model (Ahmadi et al. 2007 and Golfier et al. 2007). For these cases, two-equation model could provide better results. In this approach, matrix and fracture are considered as two homogenized medium at local (or field scale). Transport equations can be written for each medium separately and coupled with each other with an exchange term(s).

One or two-equation model, why?

When the undergoing process in a porous medium involves both heat and mass transfers, to verify if a one or two equation model is applicable for a specific scale, one should think of the conditions whether the thermal, mechanical and mass equilibrium assumptions are satisfied for that scale or not. Here we present some literature concerning the validity condition for these assumptions.

Local thermal equilibrium

In the study of transient heat conduction in a porous medium using the VA method, Whitaker (1999) developed the mathematical constraints for local thermal equilibrium to be valid. When local thermal equilibrium is not valid, one should write the heat transport equation for each phase. Whitaker (1999) explained the condition when the temperature deviation compared to the averaged temperature is negligible for both phases.

$$\begin{aligned} \langle T_\beta \rangle^\beta &= \langle T \rangle + \hat{T}_\beta \,,\ \langle T \rangle >> \hat{T}_\beta \\ \langle T_\sigma \rangle^\sigma &= \langle T \rangle + \hat{T}_\sigma \,,\ \langle T \rangle >> \hat{T}_\sigma \end{aligned} \qquad \textbf{(2-6)}$$

In the above mentioned equation the intrinsic averaged temperature is represented in terms of the spatial averaged temperature and the Darcy-scale deviation. After some mathematical manipulation, he concluded that, for local thermal equilibrium to be valid, one of the following conditions should be satisfied:

- Volume fraction of one of the phases tends to zero
- Physical properties of the phases are very close

- $\left(\frac{l_{\beta\sigma}}{L}\right)^2$ tends to zero

where $l_{\beta\sigma}$ is the small length scale defined by following equation and L is the length scale on which the average temperature is changing.

$$l_{\beta\sigma}^2 = \frac{\varepsilon_\beta \varepsilon_\sigma k_{\beta\sigma}}{a_v h} \quad \textbf{(2-7)}$$

Quintard and Whitaker (1995) studied several porous systems to identify the condition of local thermal equilibrium. They presented the following equation for the difference of the temperature in two domains for the local thermal equilibrium to be valid:

$$\frac{\langle T_\beta \rangle^\beta - \langle T_\beta \rangle^\sigma}{\Delta \langle T \rangle} = O\left(\frac{l_{\beta\sigma}}{L}\right)^2 [O(1-10)] \quad \textbf{(2-8)}$$

The parameter $l_{\beta\sigma}$ is the same as presented before and it is the ratio of conduction in the unit cell to the exchange between two phases, when the conduction is more important than the exchange; the value of this parameter will be large. On the other hand, one can expect when conduction is more important, the characteristic time for conduction will be small thus resulting in a $\left(\frac{l_{\beta\sigma}}{L}\right)^2$ that becomes larger than one. Under such a condition, the difference between temperatures of the two phases is significant and the two-equation model must be used. This approach in which the difference of the desired averaged parameter (i.e., temperature) in two phases is minimized to verify the equilibrium condition is the basis for study of mechanical and mass equilibrium.

Mechanical equilibrium

Quintard and Whitaker (1998) studied the condition of mechanical equilibrium at large scale for a slightly compressible single phase. Assuming an isotropic medium at Darcy scale, they found that, for a steady state process and a one dimensional case, all constrains are satisfied for large scale mechanical equilibrium. They also emphasized that for multi-dimensional or transient flows, one needs to verify carefully the estimations of the spatial derivatives which then will lead to such a constraint.

According to these constraints, for an isotropic system at Darcy scale, one large scale pressure field could be applicable if the following conditions are satisfied:

- Permeabilities of two regions are close to each other
- The compressibility of two regions considered are the same
- Volume fraction of one region becomes negligible

Mass equilibrium

In the study of active solute transport in heterogeneous porous media, Quintard and Whitaker (1998) also proposed some constraints associated with the large scale mass equilibrium. Based on these constraints they concluded that the conditions for mass equilibrium are as follow:

- Nearly equal capacitance factor
- Nearly equal regional velocity
- Regional dispersion tensors are nearly equal

The capacitance factor here plays the same role as the heat capacity does in heat transfer study.

Ahmadi et al. (1998) developed a general two-equation model using the VA method for the solute transfer in heterogeneous porous media. they found that, in the case of active solute dispersion, a one-equation model is not able to correctly predict the behaviour of such a system while the result of a two-equation model was satisfactory. Ahmadi et al. (1998) also compared their results with the work of Marle et al. (1967) (see Ahmadi et al. 1998). In the case of passive dispersion in a stratified system, it is found that, for the asymptotic condition, the response of a two-equation model is the same as a one-equation non-equilibrium model developed by Marle et al. (1967) (see Ahmadi et al. 1998). But for a transient condition the two-equation model provides better predictions.

Empirical categorization

Based on an experimental work, Zinn et al. (2004) (see Golfier et al. 2007) proposed an empirical categorization of possible transport regimes for the passive solute transport in a binary heterogeneous system. Figure (2.15) shows the schematic of the experimental setup used by Zinn et al. According to this empirical plot, Golfier et al. (2007) presented a slightly modified version of such a regime (figure 2.16).
In this classification, two Péclet numbers were defined as follows to measure the relative importance of the convection and diffusion.

$$Pe_{\omega\omega} = \frac{\langle V_\omega \rangle^\omega a}{D_\omega^*} \quad \textbf{(2-9)}$$

$$Pe_{\eta\omega} = \frac{\langle V_\eta \rangle^\eta a}{D_\omega^*}\left(\frac{a}{L}\right) \quad \textbf{(2-10)}$$

Here a is the characteristic length (radius) of the inclusions, L is the characteristic length of the more conductive phase, $\langle V_\omega \rangle^\omega$ is the velocity in inclusions and $\langle V_\eta \rangle^\eta$ is the velocity in more permeable zone and D_ω^* is the effective diffusion in the inclusions.
The first Péclet number represents the characteristic time for diffusion in the inclusion to characteristic time of convection across the inclusion. The second is the so-called mixed region Péclet number, representing the ratio of convective flux in the more permeable zone to the diffusive flux in the inclusion (characteristic time for diffusion in the inclusions to characteristic time of convection crosses the more permeable zone).
Fractured petroleum reservoirs are known to be heterogeneous porous media which contain low permeability matrix and highly conductive fractures. In such a system, one can expect diffusion dominated process in the matrix and convection dominated transport in the fracture. Such behavior is extensively discussed by many researchers (Warren and Root 1963, Bourbiaux and Granet 1999 and Lim and Aziz 1995) in the petroleum literature. Most of the secondary recovery processes consist of the injection of a fluid into an oil reservoir to recover the remaining oil in the matrix by any proper matrix-fracture interaction processes.

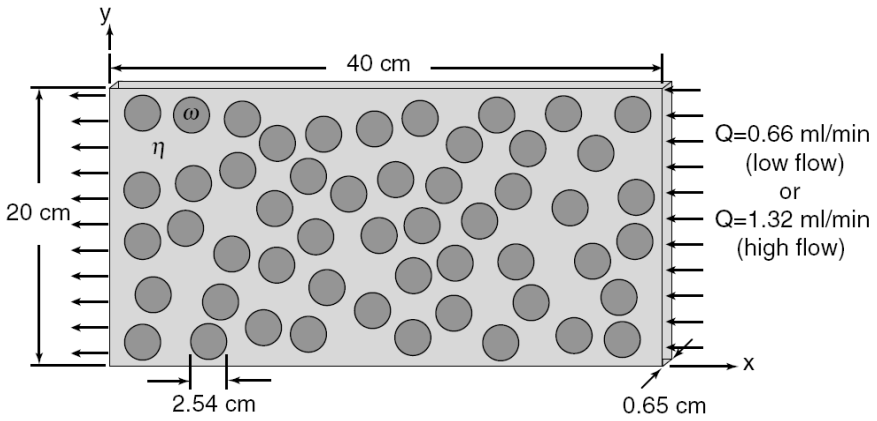


Figure 2.15. Experimental system used by Zinn et al. (2004, see Golfier et al. 2007).

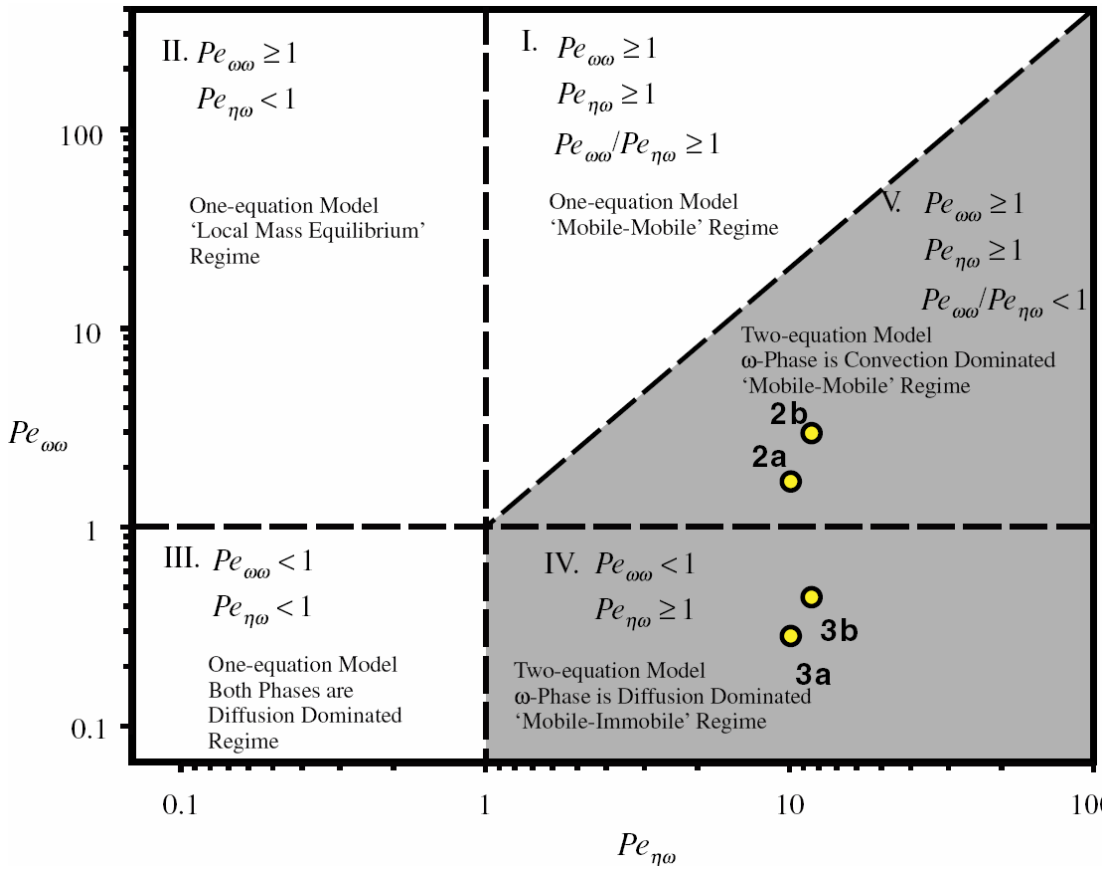


Figure 2.16. Empirical categorization of one or two-equation model based on Péclet number.

This injected fluid will pass through the high conductivity fractures while interacting with the adjacent matrix block. In such a condition, one can expect that $Pe_{\eta\omega}$ (equation 2-10) is always larger than one. Matrix block by itself is a low permeability porous medium in which the convective term is not generally pronounced and with enough confidence one can consider the convection in the fracture to be considerably higher than in the matrix. Assuming that the presented plot in figure (2.16) is valid as a representation of the mass transfer processes in fracture reservoir, two-equation models may be good candidates.

Process heterogeneity

Based on the current knowledge of the combustion process presented in the literature, we introduce the description shown in figure (2.17) which shows the presence of different phases at pore scale. According to the published literature both in petroleum and filtration combustion domains, it is known that high temperature combustion takes place in a relatively thin zone compared to the size of the porous medium (Bousaid and Ramey 1968, Schulte and de Vries 1985, Bagci 1998). Some examples were already presented in Table (2.1). This table shows that the thickness of this front is less than 10 cm for most of the cases. The combustion zone is a place in which major changes occur in temperature and the oxygen, oil, coke and water concentrations. Due to the limitation in the size of measuring devices (i.e., thermocouples) the magnitude of the changes may be even larger than what is reported in the literature. It would be also interesting if one could trace the pressure changes in this zone. This significant change across a small distance suggests that any upscaling method should respect such a sharp change. Otherwise the time and length scale assumptions in an averaging procedure could be violated. For example, if we consider the averaging volume larger than the combustion zone then it will be difficult to respect the upscaling constraints. Under this condition the characteristic length scale of deviation terms will be on the same order of magnitude as averaged terms.

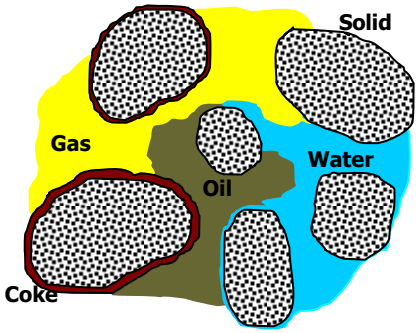


Figure 2.17. Pore scale description of the combustion process.

2.4.5 Two-equation models

According to the previous sections, in the study of highly contrasted property media which is the case of fractured reservoir, when dealing with the active process (absorption or reaction), one-equation models may not be adequate to model the process at large scale. Having this in mind and also considering the large hydraulic conductivity difference between two domains and the presence of a relatively thin reaction zone (few centimeters), it seems that two-equation models may be more suitable.

General two-equation models

Two-equation models, also called two-domain description of the heterogeneous porous medium, were first introduced by Barenblatt et al. (1960). In this two-equation model, averaged equations were considered for fracture and matrix separately and these two equations were coupled with an exchange term. The continuum approach which was used successfully for the fluid flow in a conventional porous media may be used for heterogeneous media as well.

Considering low permeability high fluid storage matrix, and high permeability low storage fracture, Warren and Root (1963) used the same approach as Barenblatt et al. (1960) to model the fractured petroleum reservoir. For a quasi steady state condition in the matrix, Warren

and Root (1963) proposed an analytical solution for these sets of equations using *Laplace transformation*. In their model matrix is impermeable and it communicates with the fracture from its boundaries with a well known exchange term. The large scale pressure equation for matrix and fracture reads:
In the matrix continuum:

$$\varepsilon_m c_m \frac{\partial P_m}{\partial t} = -\frac{K_m}{\mu}\alpha(P_m - P_f) \qquad \textbf{(2-11)}$$

In the fracture continuum:

$$\varepsilon_f c_f \frac{\partial P_m}{\partial t} - \frac{K_f}{\mu}\nabla^2(P_f) = \frac{K_m}{\mu}\alpha(P_m - P_f) \qquad \textbf{(2-12)}$$

K_m and K_f are the large scale permeabilities for matrix and fracture respectively and α is a shape factor that depends on the geometry of the block. So if the geometry of the block is chosen, this factor can be calculated.
As the assumption of constant shape factor was adopted in these equations, this model cannot capture the transient behavior of the process. Many researchers have been dealing with further development of this exchange term to predict the production from the fractured reservoir more accurately. Here we will present a short review. However, a more complete review can be found in Hassanzadeh and Pooladi-Darvish (2006), Chen (1989), Rangel-German and Kovscek (2005) and Bourbiaux and Granet (1999) and Landereau at al. (2000).
Quintard and Whitaker (1996) used the volume averaging method to calculate the shape factor of the single phase flow of slightly compressible flow. Bourbiaux and Granet (1999) derived the shape factor for two-dimensional matrix-fractured transfer based on single phase fine grid simulation.
In the context of solute transport, Quintard et al. (1998) and Ahmadi et al. (2007) investigated the mass exchange coefficient for a porous medium with non spherical geometry for the inclusions using the volume averaging method; they also provided constraints for the range of the validity of this model. Study of the solute transfer is more complex than the single phase flow which has been used to study the matrix-fracture transfer in the petroleum literature, as the advection-diffusion of the solute is also important.
Following, is the first-order mass transfer model for passive solute transport proposed by Golfier et al. (2007).

$$\frac{\partial\langle C_\eta\rangle^\eta}{\partial t} = \nabla.\left[D^*_{\eta\eta}.\nabla\langle C_\eta\rangle^\eta\right] - \langle v_\eta\rangle^\eta.\nabla\langle C_\eta\rangle^\eta - \varepsilon_\eta^{-1}\phi_\eta^{-1}\alpha^*\left(\langle C_\eta\rangle^\eta - \langle C_\omega\rangle^\omega\right) \qquad \textbf{(2-13)}$$

$$\frac{\partial\langle C_\omega\rangle^\omega}{\partial t} = \nabla.\left[D^*_{\omega\omega}.\nabla\langle C_\omega\rangle^\omega\right] - \langle v_\omega\rangle^\omega.\nabla\langle C_\omega\rangle^\omega + \varepsilon_\omega^{-1}\phi_\omega^{-1}\alpha^*\left(\langle C_\eta\rangle^\eta - \langle C_\omega\rangle^\omega\right) \qquad \textbf{(2-14)}$$

in which the $D^*_{\eta\eta}$ and $D^*_{\omega\omega}$ are the total dispersion coefficients in the η and ω medium respectively. The last term in both equations is the exchange term in which α is the effective mass transfer coefficient, which in first order models is constant. This two-equation model is based on the solution of steady state closure problems. As stated by Golfier et al. (2007) this assumption is more accurate when the characteristic time of two regions are in the same order of magnitude. However when the characteristic time for one region is considerably larger than the other, the steady-state closure problem becomes less accurate. Under this condition, the assumption of constant exchange coefficient is not valid.

Estebenet et al. (2001) used the continuous random walk method to derive the shape factor. Good agreements were obtained compared to numerical results. Penuela et al. (2002) developed a time dependent shape factor and then implemented it in the dual porosity model for simulation. Discrete simulation of the fracture was used by Sarda et al. (2002) to evaluate the shape factor, which was spatially dependent on the local matrix and fracture properties.
The important point is that most of the work has been done on single phase flow considering a quasi steady state transfer between matrix and fracture. Hassanzadeh and Pooladi-Darvish (2006) considered also fracture pressure variation which was not considered in previous works and concluded that the shape factor depends on the pressure in the fracture and its changes with time.
Most of the works in the context of the petroleum engineering and environmental studies did not take into account the temperature changes when dealing with the fluid flow in fractured porous media; while the study of the combustion in porous media is associated with an important temperature effect.

Mixed model

When the transport inside the matrix block also becomes important, the assumption of lumped matrix which communicates with the fracture with an exchange term may introduce some error in the solution (Golfier et al. 2007). Dual media simulators using large scale equations incorporate the Darcy-scale fields characteristics through some effective properties like exchange terms. For some processes (i.e., heat transfer and gravity segregation), it is difficult to find pertinent effective parameters. Hence the use of mixed model, for which a Darcy-scale equation for the matrix is coupled with the averaged (large scale) equation in the fracture, seems to be suitable (Estebenet et al., 2001).
In a recent study of solute transport in highly heterogeneous porous media, Golfier et al. (2007) compared the result of the two-equation constant exchange coefficient with the mixed model. In the mixed model, the equations for the more permeable region (η) are upscaled while for the less permeable region (ω), they were kept at Darcy scale in an approximate way, especially by using "representative" matrix block instead of the real complex matrix geometry. For the less permeable zone, only the mass diffusion was considered. Following are the mass conservation equations and boundary conditions for two regions:

High permeability region:

$$\frac{\partial \langle C_\eta \rangle^\eta}{\partial t} = \nabla.\left[D^*_{\eta\eta,mixed}.\nabla \langle C_\eta \rangle^\eta \right] - \langle v_\eta \rangle^\eta \nabla \langle C_\eta \rangle^\eta + \underbrace{\frac{\varepsilon_\eta^{-1}\varphi_\eta^{-1}}{V_\eta} \int_{A\eta\omega} n_{\eta\omega}.(\varepsilon_\eta D^*_\eta.\nabla C_\eta)dA}_{Interface\quad exchange} \qquad \textbf{(2-15)}$$

low permeability region:

$$\varepsilon_\omega \frac{\partial C_\omega}{\partial t} = \nabla.\left[\varepsilon_\omega D^*_\omega.\nabla C_\omega\right] \qquad \textbf{(2-16)}$$

and the boundary conditions are:

$$C_\omega = \langle C_\eta \rangle^\eta \text{ on } A_{\eta\omega} \qquad \textbf{(2-17)}$$

$$n_{\eta\omega}.(\varepsilon_\omega D^*{}_\omega.\nabla C_\omega) = n_{\eta\omega}.(\varepsilon_\eta D^*{}_\eta.\nabla C_\eta) \text{ on } A_{\eta\omega} \qquad \textbf{(2-18)}$$

The dispersion tensor ($D^{*}_{\eta\eta,mixed}$) could be derived using the same manipulation as for two-equation models. For the boundary condition the deviation of the concentration in the fracture at the interface is neglected. The difficulty that remains with this model is that the interface between two regions should be explicitly known (in this case at Darcy scale) however by assuming that the matrix blocks are independent of each other and their geometry is constant, then a representative geometry could be considered. In this way one or several representative unit cells may be defined to describe the porous media (Golfier et al. 2007). The concept of representative block, which may be questionable but is necessary, otherwise the mixed model would not offer a significant improvement compared to a direct Darcy-scale simulation.
Golfier et al. (2007) also indicated that constant mass exchange coefficient provides a reasonable prediction of the observed breakthrough curve; however it did not allow a good representation of the tailing that was observed in the data. It is concluded that the mass exchange predicted via quasi-steady state assumption could potentially be improved with the mixed model. As mentioned earlier and proved in Debenest and Quintard (2008), the two-equation model does a better job than the mixed model when some advection occurs also in the matrix (so-called mobile-mobile system).
Another example of the application of mixed model can be found in Hager et al. (2000) for steam drying of a bed of porous spheres. In the area between the spheres there is a flow of super heated steam which removes the initial water in the spheres by evaporation. The spheres are modeled using the first step upscaled equations (Darcy scale) while the area between them is modeled with the large scale averaged equations. Further simplification of the problem was possible if the condition of symmetric temperature and evaporation is assumed in the sphere.
Some other methods have been applied to address the shortcomings of dual media simulators, such as pseudo-curves and the subgridding method (Golfier et al. 2007). Another important modification is the use of multi-rate models in which instead of one single exchange coefficient a series of coefficients may be adopted to capture the transient behavior of the system. Each of these coefficients could be considered as an additional region that communicates with the fracture. Such a model is very complex as the concentration in each additional region is defined with the transport equation that is coupled with each of the other regions (Golfier et al. 2007).

Exchange term for multiphase flow in heterogeneous porous media

When dealing with the multiphase flow in a porous medium, immediately the capillary and relative permeabilities effects appear and in the case of fractured systems the exchange term also plays an important role. Although the exchange term for single phase flow has been studied extensively in the past, this is not the case for multiphase systems.
In the study of immiscible two-phase flow in heterogeneous porous media Quintard and Whitaker (1998) used the VA method to model transport at large scale. By applying certain length scale constraints and assuming that at the interface of the two fluid at pore scale the pressure and capillary effects are dominant and also considering a non-moving contact line for the closure problem, they introduced the Darcy scale model equations. Based on this model and local mechanical equilibrium assumption, the one-equation model for large scale was derived. To derive the large scale equation a quasi-steady closure problem was assumed. They relaxed this restriction of the quasi-steady closure in their next work (Quintard and Whitaker 1995).
In the study of matrix-fracture transfer for multiphase system, Rangel-German and Kovscek (2005) found that the shape factor depends on the driving mechanism as well as the partial or complete filling of the fracture. From experimental work on the imbibition process and further mathematical development, an expression for the location of water front in the matrix block is

proposed which is then used to calculate the exchange term. This experiment also leads to a new time dependent shape factor:

$$\sigma_s(t) = \frac{A(t)}{Vl(t)} \tag{2-19}$$

where *A(t)* is the area of the matrix block contacted by water and *V* is the volume of the block. *l* is the distance between the saturation at the fracture and matrix averaged saturation, which is defined by :

$$l = \frac{\int_0^L S_w(x,t)dx}{\bar{S}_{wm}(t)} \tag{2-20}$$

in which S_w is the water saturation and $\bar{S}_{wm}(t)$ is the averaged water saturation in the block.
By neglecting the gravity and mass diffusion effects, the following exchange function is proposed for water imbibition and pressure driven process:

$$\tau = \sigma_p VK \frac{k_{rw}}{\mu_w}(\bar{P}_{wm} - P_{wf}) - \sigma_s V \alpha_h (S_{w\max} - \bar{S}_{wm}) \tag{2-21}$$

where the σ_p is the shape factor for pressure driven process and σ_s is the shape factor for the capillary imbibition driven process and α_h is the hydraulic diffusivity.
Sarma and Aziz (2004) introduced a new shape factor both for single and multiphase systems. In the multiphase case, they studied water injection in fractured reservoir. By assuming that only pressure diffusion and capillary imbibition are the dominant production mechanisms they derived an exchange term which is a combination of these two driving forces. Thus two shape factors are introduced for each process. Comparing the production simulation of a single block surrounded by fractures for both the conventional and new shape factors with the fine grid reference solution, they observed that the new shape factor produces more accurate results.

2.4.6 Summary

The following is a summary of the second part.

- The upscaling of complex problems such as combustion with a strong coupling of heat and mass transfer seems to be very complicated. Large scale upscaling of transport processes has been mostly limited to relatively simple cases (i.e., single phase, slightly compressible, solute transport). In other words, applying some upscaling methods such as volume averaging for a complex problem like combustion seems to be very challenging.
- From the structure of the combustion front, it is evident that on a relatively small distance, large changes happen. This seems to be one of the major obstacles for the macroscopic representation of the problem using upscaling tools. For example, some traditional assumptions of volume averaging method may be violated.
- Determination of the exchange term even for a simple process in case of highly heterogeneous system is still under investigation. Especially for the early time of the process where the transient effects are important. For multiphase systems, this exchange term may be even more complex and the effect of the underlying physics should be taken into account.
- Whatever is the model for large scale it is always necessary to verify its accuracy by comparing its result with the result of the lower scale model. Thus one needs to

perform some simulation at Darcy scale using an appropriate numerical tool, to know firstly if the model can handle the process with sufficient accuracy by comparing with some reference data (i.e., experimental); Secondly to decide about the upscaling approach.

- Due to all difficulties mentioned before for modeling and upscaling of the multiphase flow with combustion process in a fractured system, there is not a numerical tool based on the volume averaging method that can treat this problem. The only available numerical tools are the commercial codes developed by petroleum companies. In our study we will use one of these codes but we have to verify the assumptions and simplification associated with them.

Notations (chapter 3)

$A_{i\pi}$	Pre-exponential factor for species *i*
A_0	Pre-exponential factor
c_g	Gas heat capacity, (J/kg.°C)
c_s	Solid heat capacity, (J/kg.°C)
c_r	Product heat capacity, (J/kg.°C)
c^*	Total heat capacity, (J/kg.°C)
C_p	Total heat capacity, (J/m^3.°C)
C_s	Solid heat capacity, (J/m^3.°C)
C_g	Gas heat capacity, (J/m^3.°C)
C_{O2}	Oxygen mole fraction
C_0	Initial/ boundary value of oxygen mole fraction
$D_{\pi i}$	Pore scale diffusion, (m^2/sec)
D^*	Darcy scale effective diffusion (m^2/sec)
$\underline{\underline{\mathbf{D}}}_{\pi i}$	Effective diffusion tensor at Darcy scale for species *i*, (m^2/sec)
E_i	Activation energy for species *i* reaction, (J/mole)
E	Activation energy, (J/mole)
$\vec{\mathbf{g}}$	Gravity acceleration vector, (m/s^2)
h_π	Phase enthalpy, Darcy scale, (J/kg)
$\underline{\underline{\mathbf{I}}}$	Unit tensor
i	Species indicator, otherwise, constant
$\underline{\underline{\mathbf{k}}}$	Effective conductivity tensor at Darcy scale, (W/m.°C)
$\underline{\underline{\mathbf{K}}}$	Absolute permeability tensor, (m^2)
k^*	Darcy scale effective conductivity, (m^2/sec)
k_g	Gas phase thermal conductivity, Darcy scale, (W/m.°C)
k_f	Fluid phases thermal conductivity, Darcy scale, (W/m.°C)
k_s	Solid phase thermal conductivity Darcy scale, (W/m.°C)
$k_{r\pi}$	Relative permeability
K_i	Equilibrium K-value
L	Characteristic length, (m)
m	Constants in the reaction rate otherwise signifies the matrix
m'	Constants in the reaction rate
n	Constant
P_π	Darcy scale pressure, (Pa)
P_c	Capillary pressure, (Pa)
P_{nw}	Non-wetting phase pressure, (Pa)
P_w	Wetting phase pressure, (Pa)
P	Total pressure, Darcy scale, (Pa)
P_g	Gas phase pressure, Darcy scale, (Pa)
P_{O2}	Oxygen partial pressure, (Pa)
$q_{\pi i}$	Reaction heat for species *i* (J/kg)
q	Reaction heat, (J/kg)
q_{out} q_{in}	Heat injection or production, (J/m3)
$r_{\pi i}$	Rate of the reaction for species *i* in phase π.
R	Universal gas constant, (J/mole.°C)
S	Source or sink mass flux, (kg/m^3.s)
T	Darcy scale temperature, (°C)
T_{ref}	Reference temperature, (°C)
t	Time, (s)
U_π	Internal energy of the phase, Darcy scale, (J/m^3)
u_c	Combustion front velocity, (m/s)
$\vec{U}$	Darcy scale velocity, (m/s)
v_g	Darcy scale gas phase velocity, (m/sec)
v_o	Darcy scale oil phase velocity, (m/sec)
$\mathbf{v}_\pi$	Darcy phase velocity, (m/s)
V_π	Phase volume, Darcy scale, (m^3)
W	Reaction rate
X	Dimensionless distance
x	*x* direction
y	*y* direction
Z_π	Phase compressibility

Greek symbols

α^*	Darcy scale effective thermal diffusivity, (m^2/sec)
α_T	Transversal dispersion coefficient, (m)
Ω_i	The stoichiometry coefficient

θ	Phase indicator, otherwise, dimensionless temperature
ε	Porosity
ε_π	Volume fraction of the phase
μ_π	Dynamic viscosity, (Pa.s)
η	Solid fuel conversion
π	Phase indicator, otherwise, Pi number
τ	Tortuosity at Darcy scale, otherwise dimensionless time
ρ_π	Darcy scale density (kg/m^3)
ρ^*	Total mass density, (kg/m^3)
ρ_f	Fuel mass density, (kg/m^3)
ρ_{f0}	Initial fuel mass density, (kg/m^3)
ρ_s	Solid mass density, (kg/m^3)
ρ_s	Solid mass density, (kg/m^3)
ρ_g	Gas mass density, (kg/m^3)
$\omega_{\pi i}$	Mass fraction of species *i*
ω_{oxygen}	Oxygen mass fraction

Dimension less numbers

Pe_g	Péclet number based on gas velocity
Pe_o	Péclet number based on front velocity Péclet number based on oil velocity
Le	Lewis number
Da	Damköler number

Chapter 3. Numerical study of the propagation of a combustion front in a fractured system

In this chapter the numerical study of ISC in fractured systems is presented. We begin with the validation of the numerical tool and then the simulation result at core, single block and multi-block cases are presented.

3.1 Validation of the simulator

Experimental results showed that the oil combustion process in fractured core is governed by oxygen diffusion. Fractured carbonate reservoirs are known to have usually very low matrix permeability which provides a more favorable condition for diffusion dominant processes (Van Golf Rasht 1982, Schulte and De Vries 1985 and Greaves et al. 1991). Our aim in this part is to verify the validity of simulation results of the available numerical tool (the CMG[1] thermal reservoir simulator; STARS) in case of a diffusion dominated combustion process in a petroleum reservoir. To do this, first we will present the mathematical model that is implemented in this numerical tool. Then we will perform some step by step validation procedure starting from simple cases and then increasing the problem complexity. Firstly, the oxygen diffusion in a fractured system without any reaction will be compared with the available analytical solution. This is just to make sure that, when appropriate time and space discretization is used, the numerical tool is able to reproduce the exact mathematical solution with acceptable accuracy. However, it may not be possible to use the same discretization when one tries to simulate a complex problem like ISC. Secondly, the simulation of solid-gas combustion process will be compared with analytical results from Aldushin and Matkowsky (2000). This process is less complex compared to the oil combustion because there is only one mobile phase (gas). Finally, we will compare the simulation results of crude oil combustion in a non-fractured core with the available experimental data. This case involves a complete ISC problem where water, oil and gas phases are present as well as a reactive solid phase (coke).

3.1.1 Mathematical model of the combustion process in porous media

To perform the modeling of ISC process in fractured reservoir at scale larger than Darcy-scale (i.e., pilot scale), one will follow an upscaling process to derive the corresponding transport equations at that scale. The Darcy-scale equations are the starting point of this procedure. However, the Darcy-scale equations are themselves an upscaled version of the pore scale equations. Transport equations (Navier-Stokes equations) are written at the pore-scale where the continuum assumption is valid. For this reason, one needs to derive the transport equation at Darcy-scale from those at pore-scale. Considering all the complexity both from geometrical and process point of view, Darcy-scale equations may contain some simplifications and constraints, which is the case for most of the simulation tools in chemical and petroleum engineering domains.

Governing equation for heavy oil combustion at Darcy-scale

Based on current knowledge of the combustion process of heavy oils in porous media, we can consider the following governing equations for this process. Here we consider that there are mainly four phases in our problem: oil, gas, water and solid. The oil and gas phases are multi-

[1] : Computer Modelling Group.

component (i.e. hydrocarbon components in oil and gas phases, water also in gas phase), solid phase containing inert solid and coke. However water is considered to have only one component. In general, all these phases may be in contact with each other. Reactions are taking place in the oil, gas and on the surface of the solid phase (when coke is present). A fraction of oil phase is immediately solidified and becomes a reactive solid component called Coke. Reactions in oil and gas phases are homogeneous but the coke reaction is heterogeneous, but, because of the upscaling procedure, here both appear as sources or sink terms in the averaged equation.

Mass conservation

The equation for the mass conservation for component *i*:

$$\frac{\partial(\varepsilon_o\omega_{oi}\rho_o+\varepsilon_g\omega_{gi}\rho_g+\varepsilon_w\omega_{wi}\rho_w+(1-\varepsilon)\omega_{si}\rho_s)}{\partial t}+\nabla.\left[\varepsilon_o\omega_{oi}\rho_o\mathbf{v}_o+\varepsilon_g\omega_{gi}\rho_g\mathbf{v}_g+\varepsilon_w\omega_{wi}\rho_w\mathbf{v}_w\right]$$
$$=\nabla.\left(\varepsilon_o\rho_o\underline{\underline{\mathbf{D}}}_{oi}.\nabla\omega_{oi}+\varepsilon_g\rho_g\underline{\underline{\mathbf{D}}}_{gi}.\nabla\omega_{gi}+\varepsilon_w\rho_w\underline{\underline{\mathbf{D}}}_{wi}.\nabla\omega_{wi}\right)+\sum_{i=1}^{n}r_{i\pi}+\sum(S_{out}-S_{in}) \quad \textbf{(3.1)}$$

The $r_{i\pi}$ is the rate of the reactions and are of Arrhenius type:

$$r_{i\pi}=\varepsilon_\pi A_{i\pi}e^{\left(\frac{-E_i}{RT}\right)}(\omega_{i\pi}\rho_\pi)^{m'}(\omega_{oxygen}P_g)^m \quad \textbf{(3.2)}$$

S_{out} and S_{in} are the sink and source terms i.e., production and injection wells. The total dispersion coefficient is defined as:

$$\underline{\underline{\mathbf{D}}}_{\pi i}=\frac{D_{\pi i}}{\tau}\underline{\underline{\mathbf{I}}}+\alpha_T\|\mathbf{v}_\pi\|\underline{\underline{\mathbf{I}}} \quad \textbf{(3.3)}$$

Momentum conservation

Reservoir simulation tools are normally using Darcy's law in its general form which is also an averaged form of the Navier-Stokes equation. The permeability of each phase is represented as the product of the absolute permeability of the porous medium and the relative permeability of that phase. There are several ways to introduce the relative permeability. It is often written as a function of phase saturation(s) and may be introduced either as an empirical correlation or as a table in the input data file. The simulator is able to take into account the effect of the temperature on relative permeability and viscosity (STARS User Manual, 2008). Darcy's law is assumed applicable for all fluid phases.

$$\mathbf{v}_\pi=-\frac{\underline{\underline{\mathbf{K}}}k_{r\pi}}{\mu_\pi}.(\nabla P_\pi-\rho_\pi\vec{\mathbf{g}}) \quad \textbf{(3.4)}$$

Energy conservation

Conservation of the energy may be represented as the following equation:

$$\frac{\partial(\varepsilon_o\rho_oU_o+\varepsilon_g\rho_gU_g+\varepsilon_w\rho_wU_w+(1-\varepsilon)\rho_sU_s)}{\partial t}+\nabla.\left[\varepsilon_oh_o\rho_o\mathbf{v}_o+\varepsilon_gh_g\rho_g\mathbf{v}_g+\varepsilon_wh_w\rho_w\mathbf{v}_w\right]$$
$$=\nabla.\left(\underline{\underline{\mathbf{k}}}.\nabla T\right)+\sum_{i=1}^{n}q_{i\pi}+\sum(q_{out}-q_{in}) \quad \textbf{(3.5)}$$

in which the $q_{i\pi}$ is the reaction heat(s) and q_{out} and q_{in} are the heat withdrawal or injection by the wells. In order to have closed form of the above mentioned differential equation we may need some auxiliary relations which are:

$$\varepsilon_o + \varepsilon_g + \varepsilon_w = \varepsilon \text{ and } \varepsilon = f(P) \tag{3.6}$$

$$\sum_{i=1}^{n} \omega_{\pi i} = 1 \tag{3.7}$$

$$P_c = P_{n-wet.} - P_{wet.} \tag{3.8}$$

$$K_i = \frac{\omega_{gi}}{\omega_{li}} \tag{3.9}$$

$$h_\pi = U_\pi + P_\pi V_\pi \tag{3.10}$$

$$P_\pi V_\pi = Z_\pi RT \tag{3.11}$$

3.1.2 Validation case: One and two dimensional diffusion tests

We will compare simulation results of one and two dimensional oxygen diffusion with the analytical solution available in literature. There is only gas phase in the porous medium and there is no temperature and pressure change during the diffusion process. The porosity is 40% in both cases. A large oxygen bank was considered to be attached to the porous system to assure constant oxygen concentration at the inlet. This will mimic the Dirichlet boundary condition (i.e., constant oxygen concentration). Initially the oxygen concentration is equal to zero in the porous medium. The length of the porous medium is considered to be large enough so that the oxygen concentration remains zero at the other end during the simulation time. The characteristics of the simulation model are presented in Table (3.1).

Table 3.1. Characteristics of the one and two dimensional diffusion simulation model.

Case	Grid	Block size (m)	Effective Diffusion coefficient (m^2/sec)
1D	142×1× 1	0.003×0.048 ×0.03	6.667E-6
2D	100×100×1	0.003×0.003×0.048	6.667E-6

The analytical solution of this initial-boundary value problem was found in Carslaw and Jaeger (1959):

Initial and Boundary conditions

$$\begin{cases} 1)\ \ t = 0, x \Rightarrow C_{O2} = 0 \\ 2)\ \ t > 0, x = 0 \Rightarrow C_{O2} = C_0 \\ 3)\ \ t > 0, x \to \infty \Rightarrow C_{O2} = 0 \end{cases} \tag{3.12}$$

the solution:

$$C_{O2}(x,t) = C_0\left[1 - erf\left(\frac{x}{2\sqrt{D^* t}}\right)\right] = C_0 erfc\left[\frac{x}{2\sqrt{D^* t}}\right] \tag{3.13}$$

For the two-dimensional diffusion problem, a square porous block is considered which is surrounded by a large oxygen bank. Like the one dimensional case, this oxygen bank is also non porous and only the gas phase is filling the porous medium. During the process, oxygen

concentration at each side of the square was kept constant (Dirichlet condition). Like in the previous case there was not any source or sink term in the system and the pressure and the temperature are constant. The concentration in a semi infinite rectangle of *2l* width that initially has unit concentration and of which the faces are kept at zero concentration in a dimensionless form is:

$$C_{O2}(x,t)=\frac{4}{\pi}\sum_{n=0}^{\infty}\left(\frac{(-1)^n}{(2n+1)}\right)\exp\left(\frac{-D^*(2n+1)^2\pi^2 t}{4l^2}\right)\cos\left(\frac{(2n+1)\pi x}{2l}\right) \quad \textbf{(3.14)}$$

Initial and Boundary conditions:

$$\begin{cases} 1)\ \ t=0, x \Rightarrow C_{o2}=1 \\ 2)\ \ t>0, x=\begin{cases} l \\ -l \end{cases} \Rightarrow C_{O2}=0 \\ 3)\ \ t>0, x=0 \Rightarrow \dfrac{\partial C_{O2}}{\partial x}=0 \end{cases} \quad \textbf{(3.15)}$$

based on this, the solution of a finite square with the dimensions of *2l* will be:

$$C_{O2}(x,y,t)=C_{O2}(x,t)\times C_{O2}(y,t) \quad \textbf{(3.16)}$$

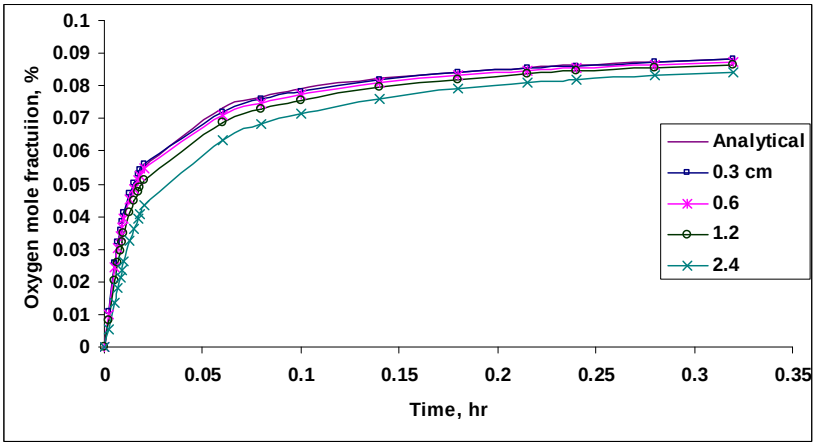


Figure 3.1. Oxygen mole fraction vs. time at 0.03m from the inlet, grid size effect.

Our problem is the same as the above mentioned case but the boundary and initial conditions are different, where initially the dimensionless concentration in porous system is zero and then it is kept equal to one at all boundaries. By changing the variable, the above mentioned solution was used for our problem.

Comparison between simulation results and the analytical solution for 1D diffusion (figure, 3.1) shows that, grid size smaller than 1.2 cm, gives results very close to the analytical solution. In 2D cases, one can expect to get results close to the analytical solution, if the grid size is smaller than 2.4 cm (figure, 3.2). The results (one and two dimensional) are in good agreement with the analytical solution, showing that the numerical tool is able to handle one and two dimensional diffusion process, using small enough grid size, with reliable results. However it should be noted that in a complex combustion process using this grid size may not be affordable.

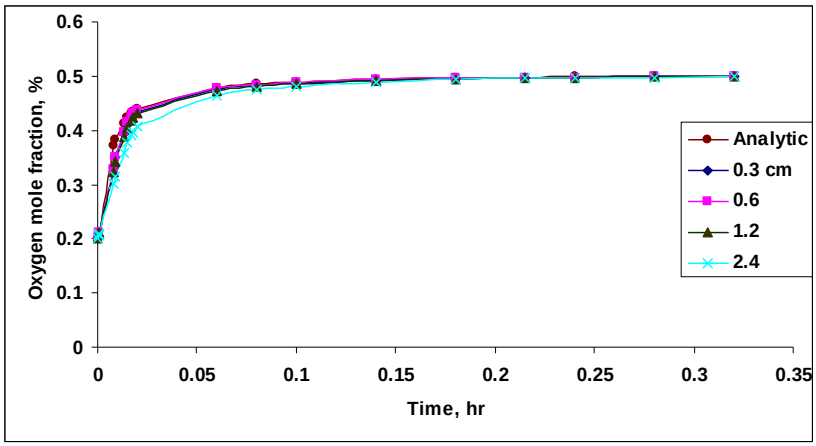


Figure 3.2. Oxygen mole fraction vs. time at 0.03m from the sides, grid size effect.

3.1.3 Validation case: one dimensional solid-gas combustion test

A two-phase (solid-gas) combustion problem in a porous medium initially containing a solid fuel is simulated using the thermal reservoir simulator. Figure (3.3) shows the geometry of the system for this problem. Simulation input data are given in Table (3.2).

Table 3.2. Characteristics of the one dimensional combustion model.

Case	Grid	Porous slab dimensions (m)	Diffusion coefficient (m^2/sec)
1-D combustion	188×1×13	1.5E-3×4.8E-2×1.5E-2	6.6667E-6

The porosity is 40% and initially contains the solid fuel (100 kg/m^3) and the inert gas. Similar to the one-dimensional combustion problem, a constant oxygen concentration was imposed at the inlet of the porous medium using a large block which acts as an oxygen bank connected to the one dimensional porous slab. It is considered that the temperature has no effect on the oxygen diffusion coefficient. There is no injection or production well and the reaction stoichiometry is defined so that an equal numbers of moles are consumed and produced in the gas phase to prevent any convective flow. Under this condition, the combustion process is supposed to be governed by oxygen diffusion.

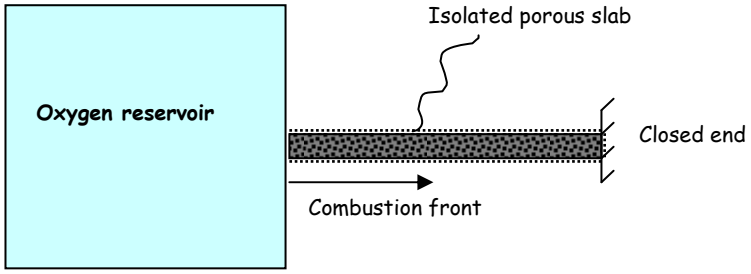


Figure 3.3. Schematic of one dimensional solid-gas combustion model.

Aldushin and Matkowsky (2000) solved this problem analytically considering an infinite reaction rate which results in a sharp reaction front (sheet like). The model describing combustion in porous media involves continuum description for fluid flow, heat and mass transfer at Darcy scale. It is assumed that the diffusion driven combustion that we are dealing with leads to a slowly propagating wave so that local thermal equilibrium may be assumed between the gas phase and solid matrix. The following equations are described in this model:

- *The overall reaction scheme is:*

$$(Fuel)+\Omega(Oxidizer)\rightarrow\Omega_{gr}(Gaseous\quad product)+\Omega_{r}(Solid\quad product) \tag{3.17}$$

in which Ω(s) are the stoichiometry coefficients and the net gas production in the reaction is defined by Ω_g according to:

$$\Omega_g=\Omega_{gr}-\Omega \tag{3.18}$$

- *Governing equations based on the moving coordinate system attached to the front:*

Energy conservation
$$C_P\left(\frac{\partial T}{\partial t}-u_c\frac{\partial T}{\partial x}\right)=\nabla.(k^*\nabla T)-c_g\rho_g v_g.\nabla T+Q\rho_{fo}W \tag{3.19}$$

Oxygen mass conservation
$$\frac{\partial(\rho_g C_{O2})}{\partial t}-u_c\frac{\partial(\rho_g C_{O2})}{\partial x}=-\nabla.(\rho_g v_g C_{O2}-D^*(\rho_g\nabla C_{O2}))-\Omega\rho_{fo}W \tag{3.20}$$

Gas phase mass conservation
$$\frac{\partial\rho_g}{\partial t}-u_c\frac{\partial\rho_g}{\partial x}=-\nabla.(\rho_g v_g)+\Omega_g\rho_{fo}W \tag{3.21}$$

Fuel mass conservation
$$\frac{\partial\eta}{\partial t}-u_c\frac{\partial\eta}{\partial x}=W \tag{3.22}$$

Assuming Darcy's law is valid for the gas movement, so:

$$\vec{U}=-f\nabla P \tag{3.23}$$

In which *f* is the filtration coefficient and *U* is the Darcy velocity of the gas phase. Total heat capacity was defined as:

$$C_P=c_f\rho_f+c_s\rho_s+c_r\rho_r+c_g\rho_g \tag{3.24}$$

Considered effective densities, also using the following auxiliary equations

a) ρ_i =constant (3.25)

b) $\rho_r=\rho_{fo}\Omega_r\eta$ (3.26)

c) $\rho_f=\rho_{fo}(1-\eta)$ (3.27)

d) $W=A_0\exp(\frac{-E}{RT})(1-\eta)(P_{O2})$ (3.28)

(3.29)

Reaction rate was considered to be of the Arrhenius type. The assumption of a sheet like reaction front divides the problem in two regions; one from the inlet to the reaction point and the second from the reaction point to the point where the initial temperature is still not disturbed by combustion. The solution of this problem for front velocity, considering the adiabatic condition around the porous medium and the following initial and boundary condition (equation 3.30) is obtained.

$$\begin{cases} 1)\quad t=0,x\Rightarrow C=0,T=T_0 \\ 2)\quad t>0,x=-x_f\Rightarrow C=C_0,T=T_0 \\ 3)\quad t>0,x\rightarrow\infty\Rightarrow C=0,T=T_0 \\ 4)\quad t>0,x=0\Rightarrow C\big|_{0+}=C\big|_{0-}=0,T\big|_{0+}=T\big|_{0-}=T_{front} \end{cases} \tag{3.30}$$

assuming quasi-steady approximation of equation (3.21) the front velocity was calculated as:

$$u_c = \frac{D^* \rho_g}{x_f \rho_{f0}} \times \frac{\ln(1+\overline{\Omega}_g C_0)}{\Omega_g} \quad \textbf{(3.31)}$$

Where $\overline{\Omega}_g$ is

$$\overline{\Omega}_g = \frac{\Omega_g}{\Omega} \quad \textbf{(3.32)}$$

The front position x_f is the point where the oxygen concentration is equal to zero (according to infinite large reaction rate). The front velocity calculated using this analytical solution and the one calculated using the simulation results (based on the zero oxygen concentration in the block) is given in Figure (3.4).

Comparing the simulation and analytical results, we found that there is a good agreement between them if we use reasonable numerical parameters (i.e. grid size equal to 10^{-3} m). Small fluctuations in the simulation results may be related to the way that we calculated the velocity. It was based on the difference of the front position at two locations divided by the time spent for the front to travel between these two points. In this way it is assumed that the velocity is constant between these two points, which is a simplifying assumption. This is more important at the initial times where the velocity change is important.

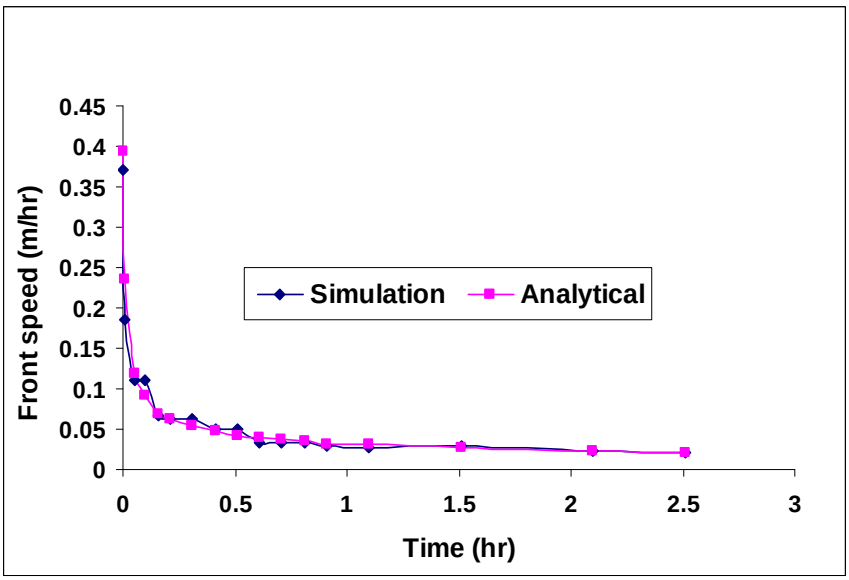


Figure 3.4. 1-D solid-gas combustion front velocity, simulation and analytical solutions.

3.1.4 Crude oil combustion in a non-fractured core

Crude oil in situ combustion simulation at the core-scale was done using the available thermal reservoir simulator. Conventional dry combustion simulation was performed based on data published by Kumar (1991). Result will be compared with the experimental data and numerical simulation results published by Kumar.

Simulator input data

The input data used by Kumar in his simulator and the corresponding data that we used in our simulator are presented in the table (3.3).

Reaction scheme and kinetic data

In his paper, five reactions presented are based on the work of Lin et al. (see Kumar 1987) in which two reactions were considered for the cracking (light oil and heavy oil cracking). In our work we have used the same model but one reaction is considered for the cracking and that is the cracking of heavy oil (table 3.4). This model is proposed by CMG and we found better temperature prediction with this model.

Table 3.3. Simulation input data.

Parameter	Initial data used in our simulator
Combustion type	Forward, dry, top-to-down ISC
Core dimension (m)	x = 0.049; y=0.049; z=0.67
Number of grid cell	(x=1 ; y=1 ; Z=12)
Porosity	0.414
Absolute permeability	12700 md
Three phase relative permeability	Stone's 2
Pressure	136.05 bar
Temperature	310.7 °K
Oil saturation	65.4%
Gas saturation	17.8%
Water saturation	16.8%
Rock thermal conductivity	2.76 (W/M.°K)
Rock compressibility	1.45038×10^{-2} (kPa^{-1})
Rock heat capacity	2.31 ($J/m^3.K$)
Water-oil relative permeability	Kumar and Garon (1991)
Gas-oil relative permeability	Kumar and Garon (1991)
Oil properties	
API gravity	26
Molecular weight	290 (kg/ kg mole)
Heavy oil pseudo component Mw	675 (kg/ kg mole)
Light oil pseudo component Mw	156.7 (kg/ kg mole)
Coke Mw	13.1 (kg/ kg mole)
Heavy oil specific gravity	0.99
Light oil specific gravity	0.8
Heavy oil compressibility	73.5×10^{-6} (kPa^{-1})
light oil compressibility	73.5×10^{-6} (kPa^{-1})
K-values .	Kumar (1987)

Table 3.4. Reaction kinetic model and parameters.

1) Heavy oil cracking	HO ---------- $2.154\ LO + 25.96\ Coke$
2) Heavy oil combustion	$HO + 60.55\ O_2$ ---------- $51.53\ IG^* + 28.34 H_2O$
3) Light oil combustion	$LO + 14.06\ O_2$ ---------- $11.96\ IG^* + 6.58 H_2O$
4) Coke combustion	$Coke + 1.18 O_2$ ---------- $IG^* + 0.55\ H_2O$
	*: *Inert gas(CO_x and N_2)*

Reaction	A, pre-exponential factor		E, activation		Heat of reaction	
	Field	SI	(BTU/mole)	(J/ mole)	(BTU/mole)	(J/ mole)
1	$4.165\times10^{5+}$	4.165×10^{5}	27000	3.14×10^{7}	40000	4.65×10^{7}
2	$3.02\times10^{10++}$	4.395×10^{9}	59540	1.3849×10^{5}	18.555¤	4.315893×10^{7}
3	$3.02\times10^{10++}$	4.395×10^{9}	59540	1.3849×10^{5}	18.555	4.315893×10^{7}
4	$4.17\times10^{4++}$	6.069×10^{3}	25200	5.8615×10^{4}	18.555	4.315893×10^{7}

$^+$: (h^{-1}), $^{++}$: ($h^{-1}psi^{-1}$ or $h^{-1}Kpa^{-1}$), ¤: Assumed to be the same as value obtained for crude (Kumar 1987).

3.1.5 Comparison of simulation results with Kumar's experiment

We have chosen three parameters for validation based on available experimental data in Kumar's paper (1987): the cumulative oil and water production and the peak temperature.

Oil and water production

Cumulative oil and water production from simulation results and the corresponding values reported by Kumar are presented in Figure (3.5). Cumulative oil production predicted by the simulator shows a good match with experimental results. The history match of water production is good until 14hr of production but, for the rest of the production time, the simulator shows over prediction while total production is the same as in the experimental data. This could be due to the representation of the relative permeability data. Kumar also mentioned that the relative permeability data were modified to obtain a good match. Modification of relative permeability curves may result in a better match for water production; nevertheless, these results are still close enough to experimental data.

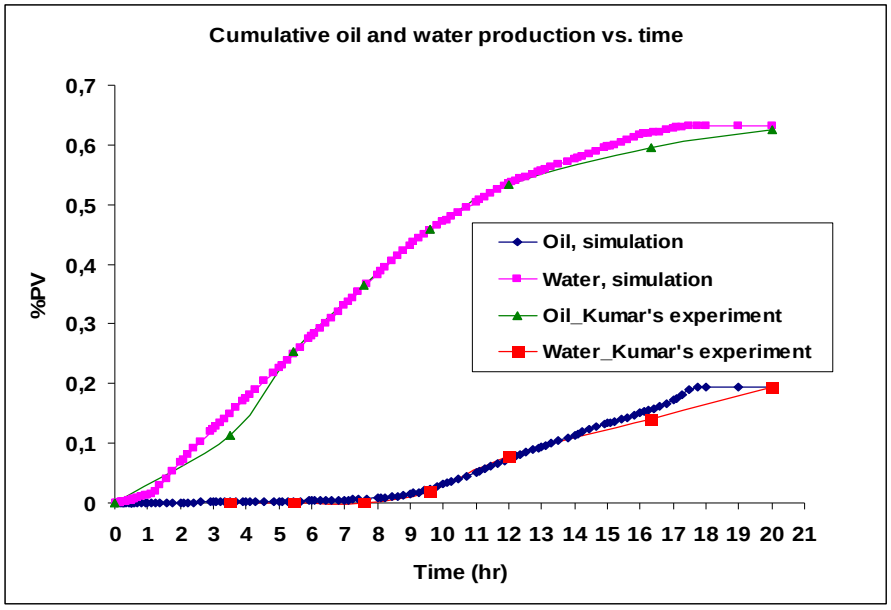


Figure 3.5. Cumulative oil and water production, comparison of simulation and experiment.

Peak temperature

Peak temperature as a function of distance along the core is presented in Figure (3.6). Generally, there is fairly good agreement between experimental data and simulation result. For the first block, simulated peak temperature is lower than the experimental one. This could be due to difference in initial heating time during the ignition period. The initial heating time (ignition time) is not mentioned in Kumar's paper and consequently the ignition temperature also is not precise. The peak temperature predicted by the simulator is close to the experimental value and the difference is less than 50°C, which seems to be reasonable.

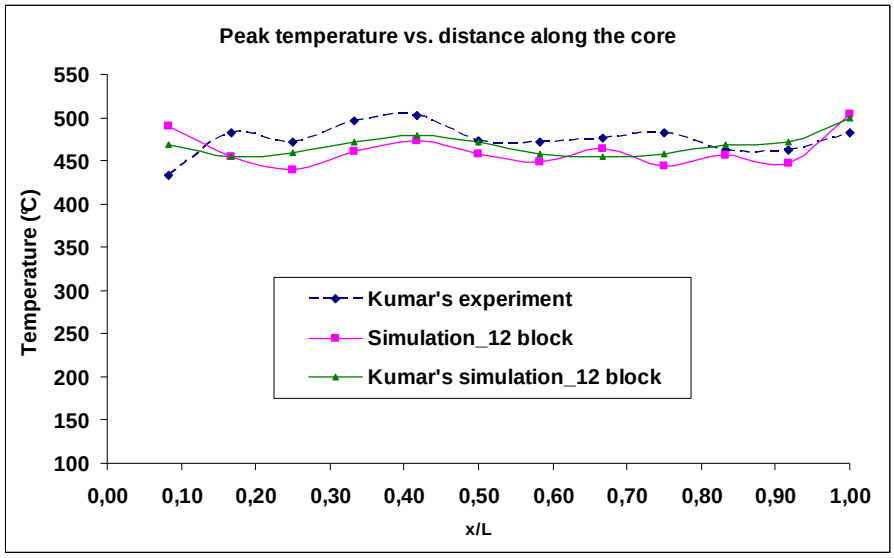


Figure 3.6. Peak temperature along the core length, simulation and experimental results.

There are some fluctuations of peak temperature along the core both in experimental data and simulation results. These fluctuations of simulated peak temperature could be related to the corresponding coke concentration. Figure (3.7) shows the change of coke concentration along the core, and the respective peak temperature. It is evident that the increase in coke concentration leads to the increase in peak temperature considering the adiabatic condition in this problem.

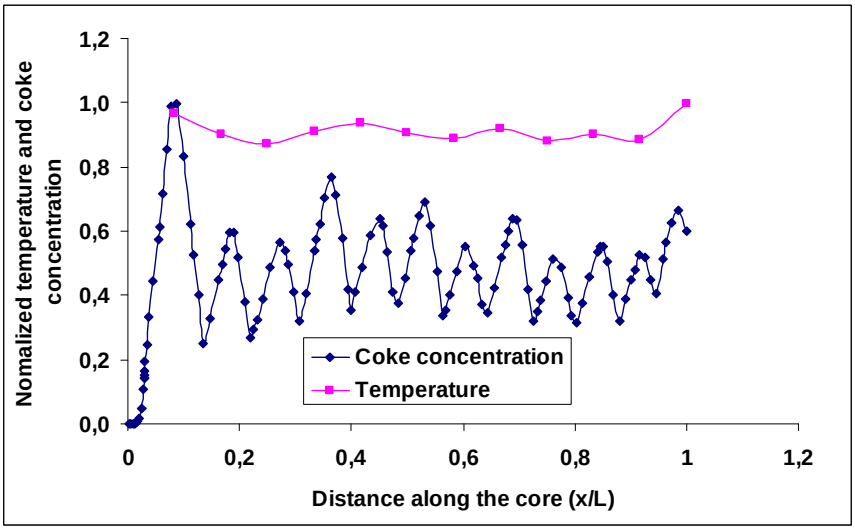


Figure 3.7. Peak temperature and coke concentration along the core (12 block).

In each block down stream of the combustion front, the quantity of the coke is increasing as the temperature increases, until the combustion front reaches that block, then the produced coke begins to be consumed by the oxidation reaction.

Effect of grid size

Simulation results showed that, in general, peak temperature decreases with decreasing grid size. These results are in agreement with Kumar's numerical simulation using 24-blocks, although the predicted temperature in our case is somehow lower than both Kumar's experimental and numerical results (figure 3.8). This difference in the first two or three blocks could be due to different ignition procedure and for the other blocks it could be due to

different relative permeability curves and end-points. However, the general trend in both cases (our simulation and Kumar's simulation) is quite similar. In the simulation results, the peak temperature decreases along the core after a small initial increase. This initial increase could be related to the high amount of coke produced during the ignition period and the further decrease may be explained by the fact that the light oil fraction increases along the core as the combustion front advances. This will lead to lower coke concentration as the heavy oil cracking down stream is reduced.

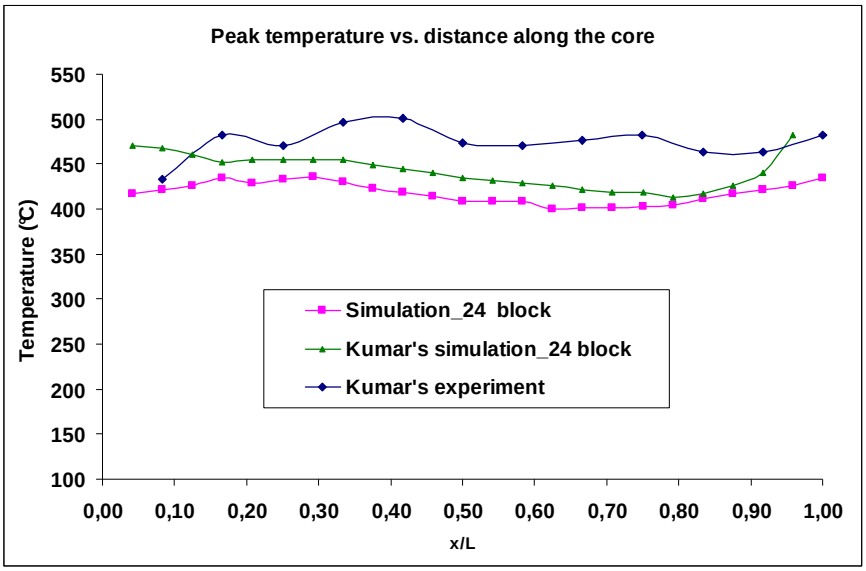


Figure 3.8. Simulation result for 24 block, comparison with Kumar's results.

Kumar explained that the lower peak temperature for the 24-block case compared to the 12-block case is related to the lower fuel (coke) availability associated with the former case. As he mentioned, this can also explain the faster combustion front movement in the 24-block case compared to 12-block case. The lesser amount of fuel in 24-block case is consumed in less time and the combustion front progresses faster. Oil production history in our simulation showed that in the 24-block case the oil was drained somehow faster compared to the 12-block case, which confirms the same hypothesis made by Kumar.

Figure (3.9) shows the coke concentration for 12-block and 24-block tests along the core. In both cases more coke generates at early time of the process. The lower temperature in the 24-block case could be due to lower coke content. The oscillations observed in Figure (3.9) are related to the number of blocks and the fact that the quantity of the injected air is not enough to consume all the produced coke ahead of the combustion front when it reaches that position. On the other hand, one may expects smoother curves using more refined grid.

Further refining with 48 blocks showed that coke concentration in this case is less than the 24-block case for later time of the burning process. It shows that the coke content is dependens on the grid size. However it is important to mention that the coke content is not only dependent on this parameter but also depends on the oil saturation history. The ignition temperature in all cases were the same, thus at early time of the process, (4 or 5 hours) the produced coke in all cases is not very different. At later time, the average oil saturation of the fine model in the block close to the combustion front (where cracking takes place) is somehow lower than that of the coarse model (8% in 12-block, 4% in 24 block and 2% in 48-block). This causes that less amount of coke is produced in the fine grid model. It is very challenging to explain the fluctuations of the coke content in this figure, as it is function of temperature and fluid saturation(s) history.

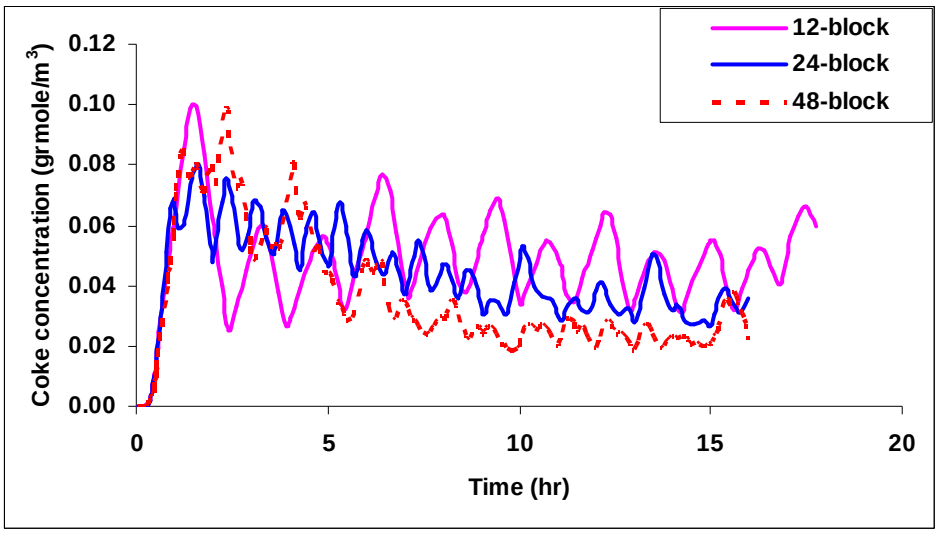


Figure 3.9. Comparison of the coke content for 12, 24 and 48-block cases.

3.1.6 Summary

Simulation results showed that for relatively simple cases (oxygen diffusion and gas-solid combustion) our numerical tool is able to produce reasonably accurate results. In case of crude oil combustion in a conventional tube, we were able to reproduce the oil and water production observed in the laboratory, as well as the peak temperatures, with acceptable accuracy. Temperature variations along the core in simulation results could be correlated to the amount of coke produced during the reaction. The amount of generated coke decreases when grid size decreases. It is important to notice that matrix permeability in Kumar's experiment is 12700 md which is very high compared to the matrix permeability in most of fractured reservoirs. One should take this into account for practical purposes. Another important point is that the validation was obtained for non-fractured porous media so performing some fractured-core experiments and comparing the results with simulation, seems to be necessary in order to use the numerical tool with more confidence.

3.2 Simulation of oil combustion in a fractured core

In this part, our aim is to, (1) identify the extinction/propagation condition of the combustion front in a fractured system and, (2) in case of a sustained combustion process understand the governing oil production mechanism(s). To this end we will perform some core-scale simulations with the data (Kumar 1987) that we used to validate our numerical tool.

3.2.1 Simulation model

The reason for using core-scale simulations is that we can perform some fine grid simulations. At the same time we may have the possibility to verify the results with present experimental data or with possibly available experimental results in the future. The geometry of the simulation model is presented in Figure (3.10) and the characteristics of this model are given in Table (3.5).

The core dimensions and the grid size of matrix and fracture are shown in Table (3.6). The petrophysical properties of the core and the oil properties are similar to the ones we used in the previous chapter (Kumar 1987). We simulated a medium oil with 26°API gravity. However, we are interested in studying heavy oil. The reason for studying a medium oil is the lack of a complete data set for heavy oil at the time of performing the simulation work. For oil-water and gas-oil relative permeability, Kumar's (1987) data was used and for the fracture

we used a cross type relative permeability (Tabasinejad et al. 2006 and STARS User Manual 2008).

Table 3.5. Simulation input data.

Parameter	Unit	Value
Reservoir T , P	(°K, kPa)	311, 13.8×10^{3}
Oil gravity	°API	26
Porosity	(%)	40
Permeability (matrix, fracture)	(md)	12700, 127×10^{4}
Oil saturation	(%)	65.4
Water saturation	(%)	17.8
Gas saturation	(%)	16.8
Oxygen diffusion coefficient	(m^2/s)	0.667×10^{-5}
Matrix tortuosity	-	1.5
Air injection rate	(m^3/hr)	0.0142
Air injection flux	(m^3/m^2.hr)	4.52
Core cross sectional area	(m^2)	3.143×10^{-3}

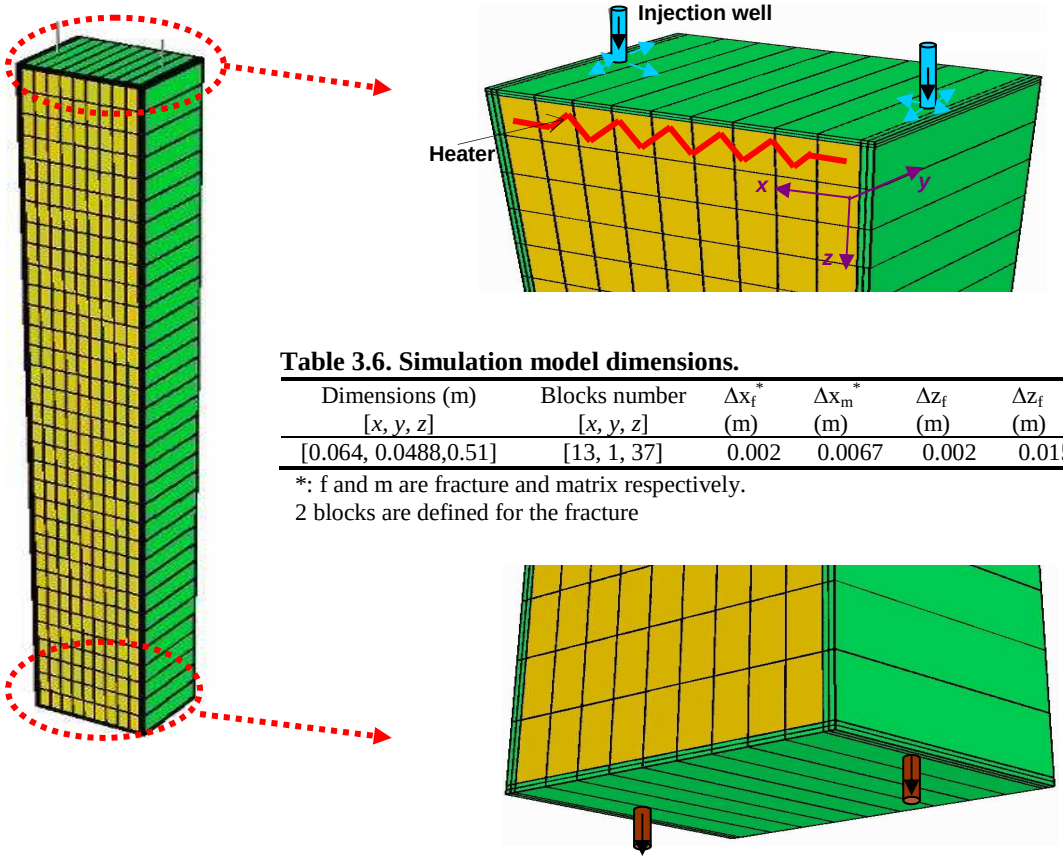


Table 3.6. Simulation model dimensions.

Dimensions (m) [*x*, *y*, *z*]	Blocks number [*x*, *y*, *z*]	Δx_f^* (m)	Δx_m^* (m)	Δz_f (m)	Δz_f (m)
[0.064, 0.0488,0.51]	[13, 1, 37]	0.002	0.0067	0.002	0.015

*: f and m are fracture and matrix respectively.
2 blocks are defined for the fracture

Figure 3.10. Schematic of the fractured core model.

For oil phase relative permeability, Stone-II model was used. The same reaction, for oil cracking and combustion, was used as in the case of homogeneous porous medium. It is assumed that the capillary pressure is negligible both in matrix and fracture. In the fracture, this assumption may be reasonable as the aperture is large (0.002 m). In the matrix, the high temperature process may minimize capillary pressure effects as the surface tension reduces with the temperature increase; i.e. for water-air the surface tension is 72.7 and 10.5 (mN/m) at 20 and 310°C respectively (Lide 2004).

Initially, the core is at reservoir temperature, pressure and fluid saturation conditions. It is positioned vertically to mimic a so-called top-down process where air is injected from the top and oil is produced from the bottom. Air was injected into the top fractures (third block from each side) using two vertical wells and oil is produced by two vertical wells at the same corresponding position at the bottom. When air injection begins, at constant rate, a constant bottom-hole pressure constraint applied to the production well. Constant heat flux is also injected into the first row of blocks at the core top. The heat injection was maintained for 24 minutes until the ignition starts in the core; this time is considered to be of the same order as that used for non-fractured core.
The air injection was stopped when the temperature in the producing wells reached 300 °C. This also corresponds to the time where nearly all matrix oil has been produced and only coke remained in the end blocks.

3.2.2 Typical combustion of crude oil in fractured core (base-case)

A typical combustion simulation using the data presented in Table (3.5) was done and this run is considered as a base case. Cumulative oil and water production are presented in Figure (3.11).

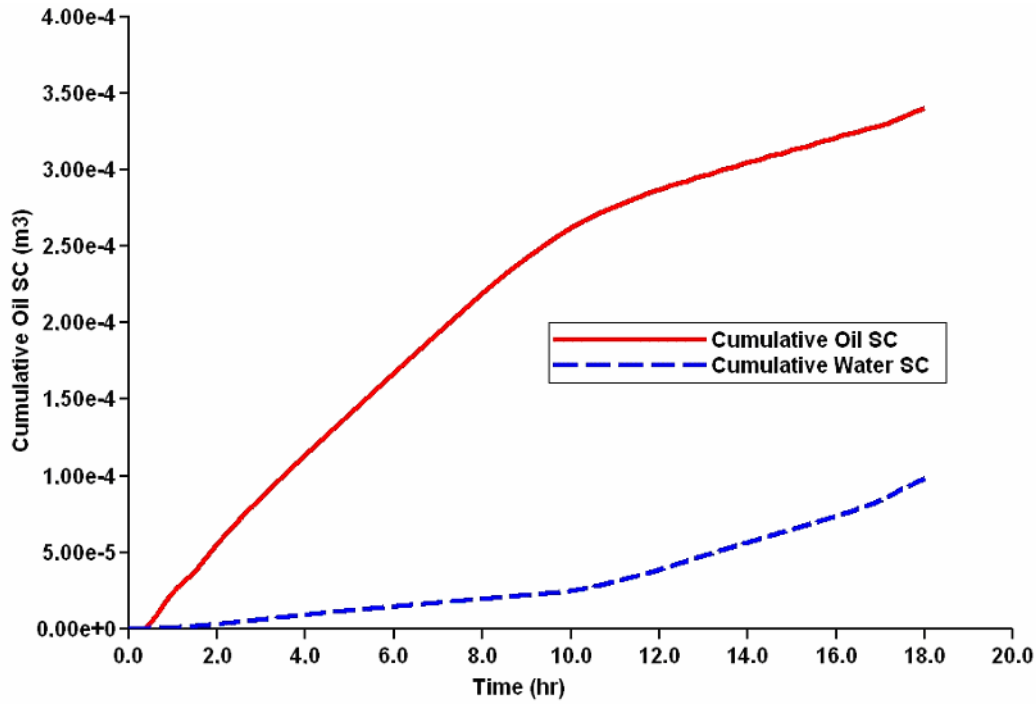


Figure 3.11. Cumulative oil and water production under ISC (base case).

After an initial delay, the oil production rate is relatively constant until approximately 10 hr, which corresponds to about 80% of total oil production, and then it declines gradually. The same behavior exists for water production, but after 10 hr the water production rate starts to decline. The initial delay is the time for combustion to develop and the following constant production rate suggests a constant front velocity. Declining of oil production rate in the second period is based on the fact that most of the oil has been produced already and the average oil saturation (thus the relative permeability) is reduced. The situation is reverse for water as it is produced during the reactions; hence its saturation and relative permeability increase. Temperature variation along the core centre is shown in Figure (3.12).

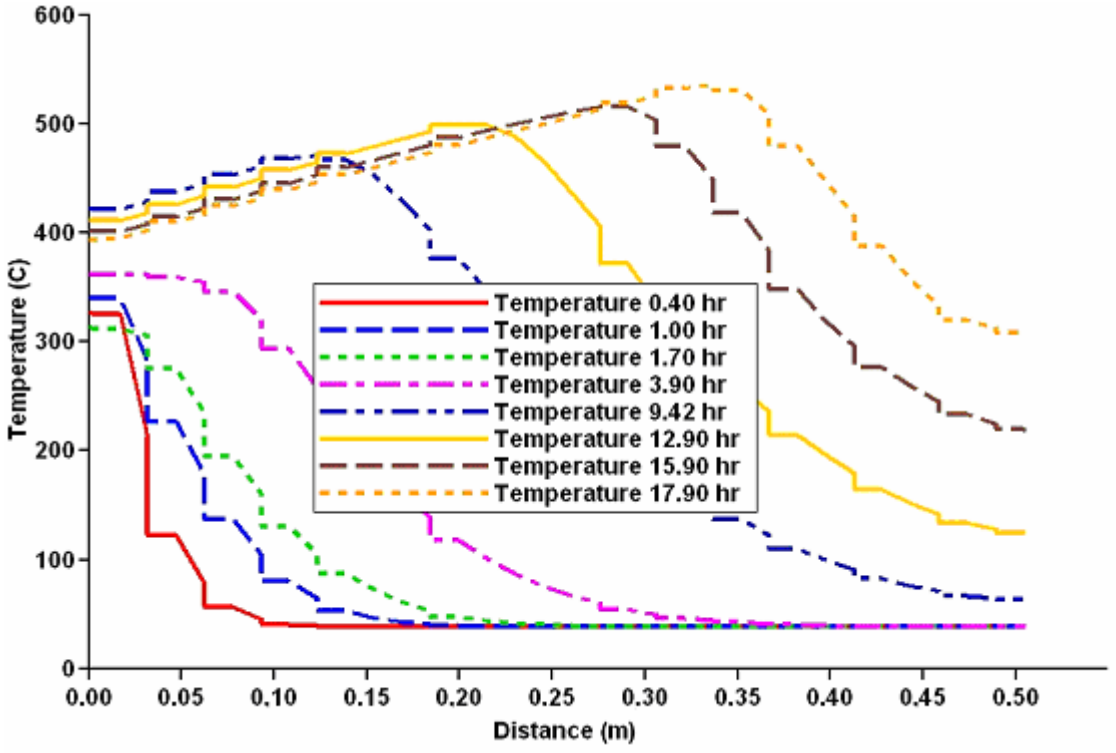


Figure 3.12. Temperature profiles at the core center during ISC (base-case).

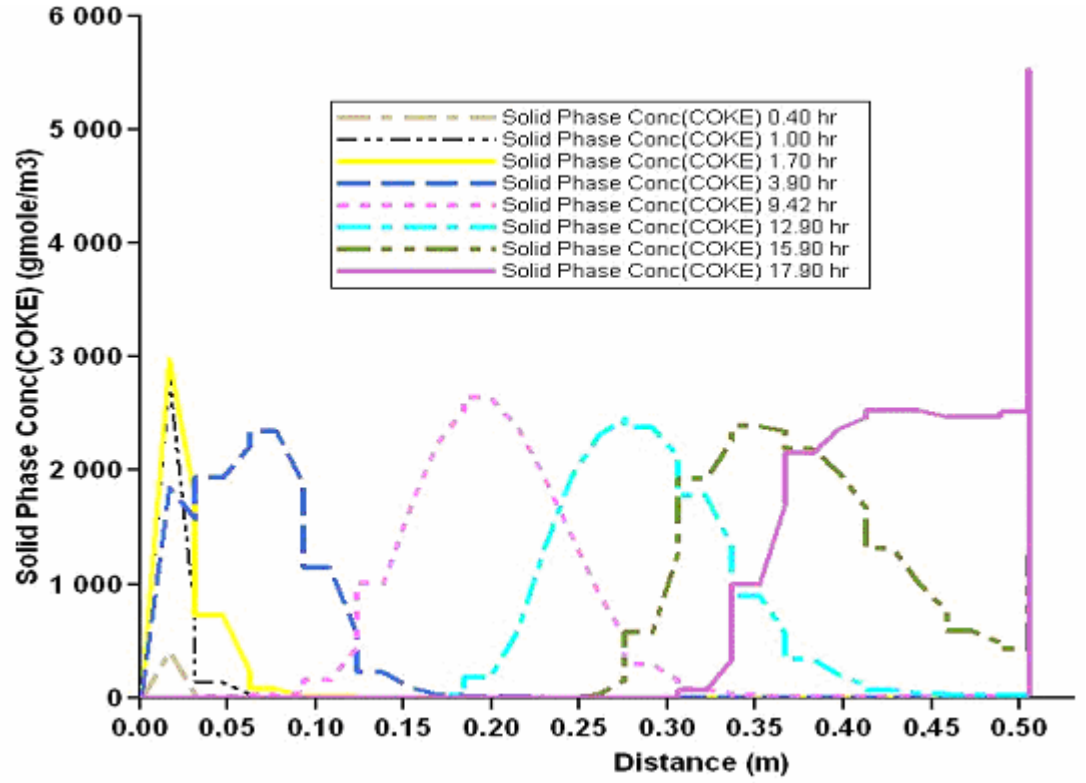


Figure 3.13. Coke concentration profiles at the core center during ISC (base-case).

The ignition temperature is 325 °C and, after that, the peak temperature is increasing until the end of the simulation while in a non fractured core the temperature is constant or slowly decreasing with time.

This could be due to the increase in coke concentration as shown in Figure (3.13). The amount of oil which has been burnt during the combustion is calculated to be 13% of the total initial mass of the oil while for non fractured core it is 6.4%, thus the temperature increase is due to more oil burning in the fractured system. The increase in peak temperature was also associated with the burning zone expansion which is shown in appendix (A.1.2). The thickness of the combustion zone plays a very important role when one is willing to perform upscaling work. Here we observe that, instead of having a constant value, the thickness is variable. The oxygen influx into the matrix is less than the rate of coke generation and this will result in combustion zone expansion and peak temperature increase. Another reason is that not all the injected air passes through the matrix due to its lower permeability compared to the fracture, so the cooling efficiency of injected air is somehow lower than in the non fractured combustion case. One can expect smoother curves for both temperature and coke concentration, by increasing the vertical resolution of the simulation grid.

3.2.3 Extinction/propagation condition

Many parameters may have an influence on the behavior of a combustion process in heterogeneous media, i.e., air injection rate, oxygen diffusion, oil and porous matrix reaction characteristics, fracture spacing, matrix permeability, etc. (Van Golf Rasht 1982, Schulte and De Vries 1985, Greaves et al. 1991, Awoleke 2007 and Tabasinejad et al. 2006).
Among these parameters, in a first step, we will study the effect of oxygen diffusion and of the matrix permeability. The former is believed to govern the crude oil combustion in the fractured core (Schulte and De Vries 1985 and Greaves et al. 1991) and the latter is related to the inherent characteristics of carbonate reservoirs, which have naturally low permeability (yet in a typical combustion tube experiment, permeability is usually very high compared to that in a real reservoir).
Several computations were performed using different values of oxygen diffusion and matrix permeability. The cumulative oil production as a function of oxygen diffusion and matrix permeability is shown in Figure (3.14) which in turn reflects the *extinction or propagation* of the combustion front. The *x* and *y* axis are the ratios of the oxygen diffusion coefficient and permeability to their respective reference value where the reference is the base case. The *z* axis is the cumulative oil production. The base case corresponds to maximum oxygen diffusion and relative permeability (Kumar's experiment). In this figure, zero production means that the combustion is not sustained, however, in such case there is a small amount of production due to natural gravity drainage. In this case, after the initial heating period (0.4 hr), when the electrical heaters are switched off, the temperature starts to decrease immediately or after a short time.

Main conclusions

From this Figure (3.14) it is evident that the sustained combustion in the matrix is strongly dependent upon the oxygen diffusion coefficient. When it is 50 times smaller than in the base case, the combustion front does not propagate through the core. However, if we reduce the permeability even 1000 times, the combustion is still sustained. On the other hand, the diffusion coefficient has not a significant influence on oil production while oil production decreases sharply if we reduce the permeability 10 times.

Some preliminary tests showed that, for some cases where we do not have combustion, changing the initial condition may lead to propagation of combustion, i.e., higher injection rate, longer initial heating time and more oil saturation in the first block.
The projection of Figure (3.14) on a *x-y* plane shows the extinction/propagation condition more clearly. This is shown in Table (3.7) in which the propagation and extinction are indicated with red and blue circles, respectively. One can notice an interesting behavior in this

figure: in some cases, for a constant diffusion coefficient, we will enter the propagation zone by reducing matrix permeability.

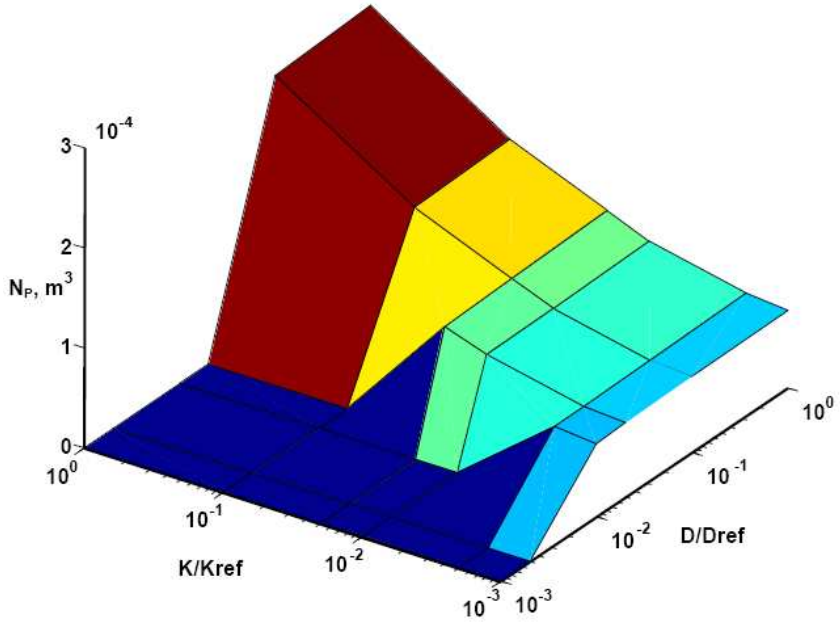


Figure 3.14. Oil production vs. oxygen diffusion and matrix permeability.

This situation corresponds to the points indicated in dotted rectangle; between [K0.1, D0.02] and [K0.02, D0.02]. In both cases, the oxygen diffusion coefficient is the same but the latter has a permeability 5 times lower than the former. We can detect the same behavior between [K0.02, D0.02] and [K0.02, D0.02].

Table 3.7. Extinction/ propagation diagram on x-y plane.

K/K_{ref} \ D/D_{ref}	1	0.1	0.02	0.01	0.002	0.001
1	●	●	○	○	○	○
0.1	●	●	○	○	○	○
0.02	●	●	●	○	○	○
0.01	●	●	●	○	○	○
0.002	●	●	●	●	○	○
0.001	●	●	●	●	○	○

To explain the behavior of our system, we may recall the fact that, for any sustained combustion reaction, we need three essential elements: fuel, heat and oxygen. By reducing the diffusion coefficient, one can expect the extinction of the combustion reaction due to lack of oxygen delivery to the reaction zone; however, for a constant oxygen diffusion we need to find the reason for non sustainable combustion when increasing the permeability. Tracing the oil saturation and coke concentration as a source of fuel, and the temperature as a source of heat, may be helpful. To this end, we have shown these fields in Appendix (A). From a heating point of view, the condition is the same for all cases until the electrical heater is turned off. Therefore, we map these fields for the times close to the moment at which heater is turned off.

Effect of oxygen diffusion

Figure A.1.2 shows the temperature profile for case denoted [K0.1, D0.1] and the case [K0.1, D0.02]. The temperature in the former is starting to be higher compared to the later case just after the heater shuts down. However, oil saturations seem to be similar and coke content is approximately the same until 1hr. Thus, the increase of temperature could be related to higher oxygen diffusion in the [K0.1, D0.1] case compared to the [K0.1, D0.02] case. If we look more precisely to the first row at the top of the matrix, where the heater is located, and trace the temperature profile at the time of heater shutdown, we find the profiles indicated in Figure (3.15).

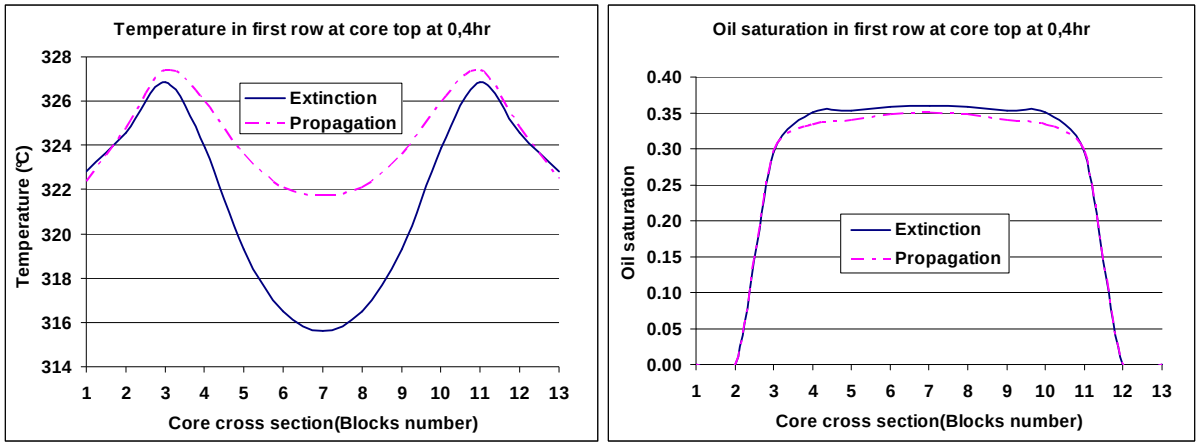


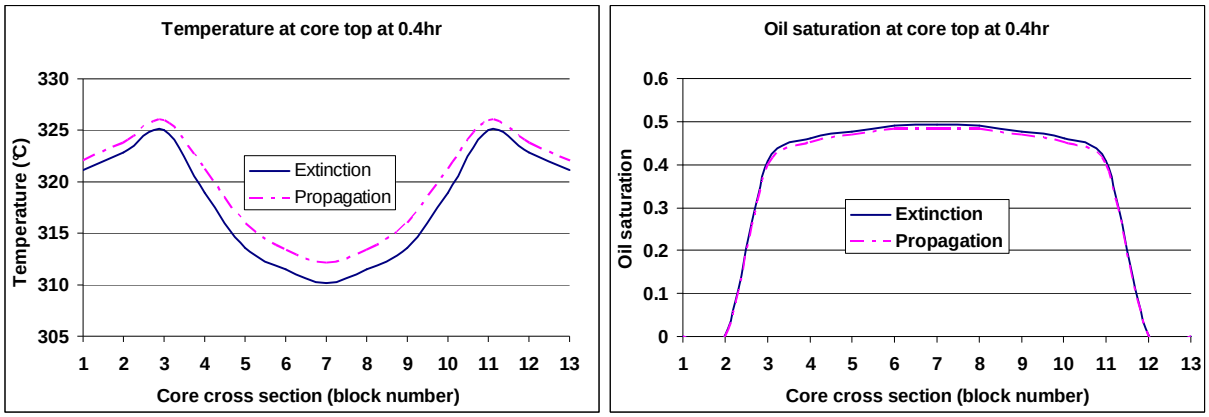
Figure 3.15. Temperature and oil saturation in first row [K0.1, D0.1] and [K0.1, D0.02].

This Figure (3.15) shows that, even with the same heating history until 0.4hr, the temperature in [K0.1, D0.1] case is slightly higher due to higher oxygen diffusion.

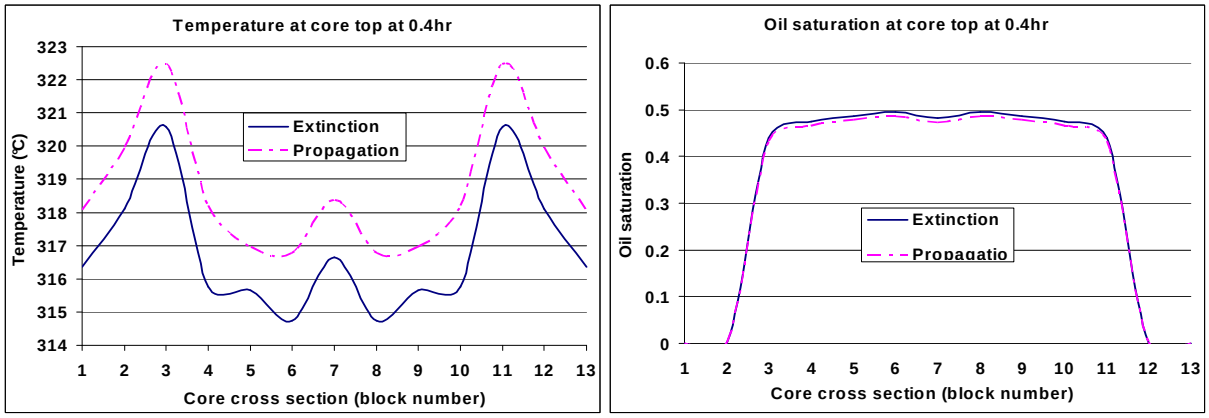
To be more general about the effect of diffusion, the above analysis should be completed for other points in Table (3.7). The temperature and oil saturation profiles for those points that have equal permeability but different diffusion coefficient are shown in figure (3.16). All curves are corresponding to the first row on the matrix top at time 0.4hr.

It seems that all cases show a similar behavior, that is, the oil saturation is the same for all cases. However the temperature is different, except for the [K0.001, D0.001] case. For this case, the difference in temperature and saturation profiles is not so evident. In all cases, the temperature in the matrix is decreasing toward the centre except in [K0.01, D0.02] and [K0.01, D0.01] cases for which there is a small peak at the centre. Average temperature in the fracture is lower than in the matrix for high permeability cases and, as the matrix permeability decreases, the temperature in the fracture is higher than in the matrix.

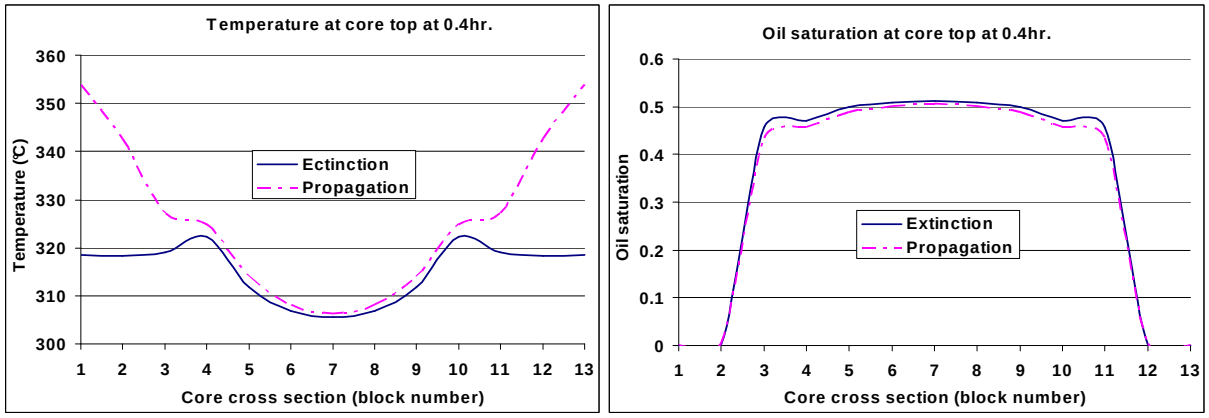
From these figures, it could be possible to conclude that, due to lower temperatures, the combustion front was not self-sustained in the extinction cases. This lower temperature is in turn due to lower oxygen diffusion coefficient because both the oil saturation (fuel) and the initial heating history (heat) are the same. Thus one may find out that the extinction is due to lack of oxygen. However, one can make this conclusion when the permeability is high (> 20md) thus for low permeabilities this conclusion could be violated.



[K0.02,D0.02] and [K0.02_D0.01]▲



[K0.01, D0.02] and [K0.01, D0.01]▲



[K0.002, D0.01] and [K0.002, D0.002]▲

[K0.001_D0.01] and [K0.001_D0.01] ▼

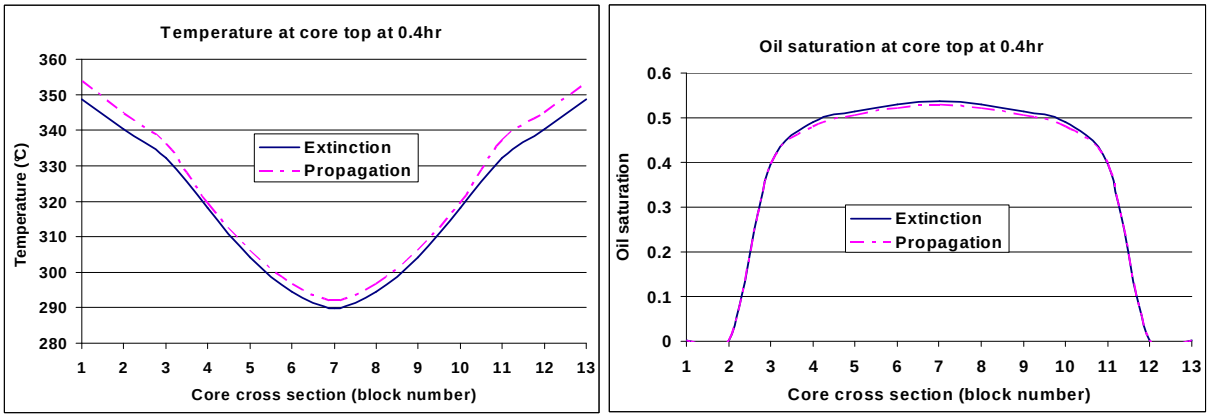


Figure 3.16. Temperature and saturation profiles for different points in the Table (3.7).

Effect of matrix permeability

There are two cases in Table (3.7) (shown in dotted rectangles) in which decreasing the matrix permeability has led to combustion sustainability. Following the same procedure as we did for diffusion effect, the temperature, oil saturation and coke content fields for [K0.1, D0.02] and [K0.02, D0.02] cases are shown in Figure A.2.1-A.2.3 in Appendix A. Permeability in the first case is 5 times higher than in the second one. Comparing the temperature profiles, we observe that the difference is small until 0.62hr and then, for the less permeable case, increases slowly. Oil saturation profile shows that when the heater is turned off, the saturation is higher for less permeable matrix meaning that the more permeable one drains faster, as expected. The coke concentration is rather the same until 1 hr for both cases. Looking more precisely at the first row on top of the matrix, the temperature profile at 0.4hr is even a bit lower for the less permeable case while the oil saturation is higher (see figure 3.17). Thus, one can conclude that in the less permeable case more fuel is available for combustion during the initial time.

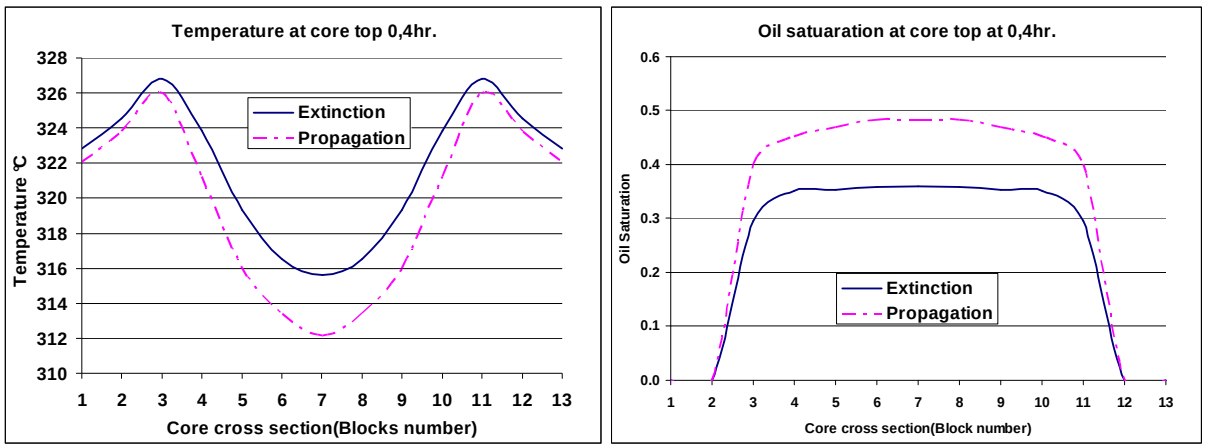


Figure 3.17. Temperature and saturation profiles for [K0.1, D0.02] and [K0.02, D0.02].

Now we may pay attention to the other two points on Table (3.7), which have the same diffusion coefficient but different permeability and for which there is propagation for one and extinction for the other. The temperature and oil saturation profiles for those points that have equal diffusion coefficients but different permeabilities are shown in Figure (3.18).

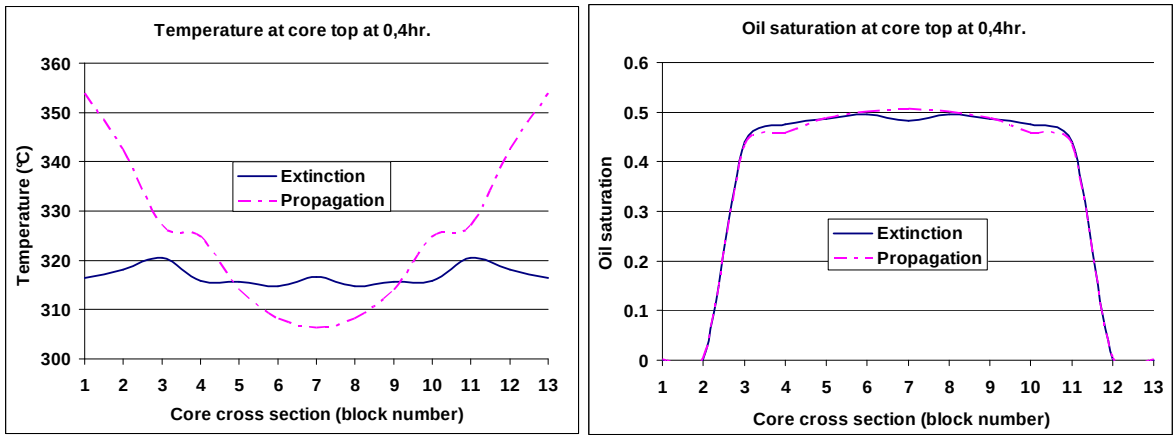


Figure 3.18. Temperature and saturation profiles for [K0.01, D0.01] and [K0.002, D0.01].

Unlike the previous case, where the difference in oil saturation was remarkable between the two cases, here they are almost superimposed. However, the temperature profiles are different; they do not show the same behavior as in the previous case. It seems that, applying the same hypothesis as for the previous case which says "the oil drains faster in high permeable matrix so there will not be sufficient fuel to support the combustion after heater turn off", may not be reasonable in this case as the system behaves differently.

3.2.4 Analysis based on dimensionless numbers

From the analysis of diffusion and permeability effect it was not possible to find a completely comprehensive explanation of the combustion behavior. This led us to think of some dimensionless numbers based on which it may be possible to predict more precisely the extinction/propagation of the combustion front. However, it must be emphasized that we are dealing with a complex, highly coupled, non-linear system. Therefore, we know at least theoretically that a finite set of dimensionless numbers may not be enough to describe all possible features. Anyway, we believe that this can be helpful to the analysis, with proper caution.

The dimensionless numbers are calculated at the combustion front location. The front thickness is equal to few blocks in the *z*-direction in which the value of the different parameters are not constant. The average of the desired parameters was considered to calculate the dimensionless numbers. At initial time of the process, the combustion front is not fully developed (it consists of 4 blocks in z direction), so we calculated an average of parameters in these blocks.

Péclet number

The Péclet number is the ratio of the convective to the diffusive transport. It is calculated for the matrix as initially there is no oil present in the fracture and simulation results showed that no oil will be produced from the fracture for the base-case during the process. In other cases with lower permeability a very small amount of oil will be produced through the fractures. We have:

$$Pe_g = \frac{v_g l}{D^*} \tag{3.33}$$

in which, $l = L/2$ and L is the width of the matrix block (0.06m), v_g is the gas phase Darcy scale velocity and D^* is the effective diffusion coefficient defined as: $\frac{D_{molecular}}{\tau}$ in which τ is the matrix tortuosity.

For the base case the gas phase average velocity (Darcy velocity) in the matrix was about 0.1 (m/hr), so the matrix Péclet number will be:

$$Pe_g = \frac{0.1 \times (0.06/2)}{0.024} = 0.125$$

We are also interested to calculate a Péclet number (Pe_o) which is based on the velocity of the oil phase (v_o), we may have:

$$Pe_o = \frac{v_o l}{D^*} \tag{3.34}$$

This Péclet number is comparing the rate of the oxygen delivery with the rate of fuel (oil) leaving the reaction zone. Considering the oil phase velocity equal to 3×10^{-3} (m/hr):

$$Pe_o = \frac{3\times10^{-3} \times (0.06/2)}{0.024} = 4.16\times10^{-3}$$

These calculations showed that the oil phase velocity at the front location is about two order of magnitude lower than the gas phase velocity, which seems to be meaningful due to very low oil saturation at this location. It reveals also that the process is diffusion dominated. The Pe_g and Pe_o for other points on Table (3.7) are presented in Table (3.8). Data in this table shows that the process is under low Péclet number or, on the other hand, diffusion controlled. The gas phase Péclet number has the same order of magnitude in all cases, however this is not true for the oil phase Péclet.

Table 3.8. Values for Pe_g and Pe_o for different points on Table (3.7).

Case	Vg (m/hr)	Pe_g	Vo (m/hr)	Pe_o	Propagation
[K1,D1] (Base-case)	0.1	**0.12**	0.003	**0.0042**	**Yes**
[K0.1, D0.1]	0.02	**0.25**	0.003	**0.042**	**Yes**
[K0.1, D0.02]	0.01	**0.62**	0.006	**0.42**	**No**
[K0.02, D0.02]	0.01	**0.62**	0.003	**0.16**	**Yes**
[K0.01, D0.02]	0.01	**0.62**	0.001	**0.089**	**Yes**
[K0.01, D0.01]	0.007	**0.95**	0.0013	**0.16**	**No**
[K0.002, D0.01]	0.01	**1.25**	0.0006	**0.082**	**Yes**

The low Pe_o for base case could be due to very low oil saturation as the oil is already drained because of the high permeability. It could be seen that, for the extinction cases ([K0.01, D0.01] and [K0.1, D0.02]), the Pe_o is higher compared to the propagation cases ([K0.02, D0.02], [K0.002, D0.01]) which have the same oxygen diffusion. The reason for extinction in these cases could be the *lack of fuel existence in the combustion zone* as it is already drained due to relatively higher permeability.

Damköhler number

The Damköhler number is the ratio of reaction rate to the transport rate. In our problem, we have four reactions, so we need to define which one should be considered in the calculation. Removing all reactions except heavy oil combustion led to extinction while removing coke production and combustion, we had still propagation. Removing only the coke combustion, we still had the propagation but the simulation stopped because of a fatal error, apparently because of high coke concentration. Removing all reactions except the light oil combustion led to extinction of the combustion. It seems that the combustion of light and heavy oil plays an important role in our system. Thus we consider light oil (or heavy oil) combustion in the calculation. The reaction temperature is assumed to be 350°C and the maximum gas phase velocity in the matrix is 0.1 m/hr.

$$Da = \frac{Rate \times l}{v_g} = \frac{Ae^{(\frac{-E}{RT})} \times [P_{O2}] \times L/2}{v_g} \qquad \textbf{(3.35)}$$

$$= \frac{4.395\times10^{9} \times \exp(\frac{-3.3091\times10^{4}}{1.987\times623}) \times [1.3837\times10^{4} \times 0.21] \times 0.06/2}{0.1} = 9.4$$

Here, it is assumed that the pressure is equal to the bottom-hole pressure (1.3837×10^4kPa) and that oxygen volume fraction in the reaction zone is the same as in the injected air. Calculating the Damköhler number based on diffusive transport and considering oxygen diffusion in matrix equal to 0.024 m^2/hr, we have:

$$Da = \frac{Rate \times l^2}{D^*} = \frac{Ae^{(\frac{-E}{RT})} \times (L/2)^2}{D^*} = \frac{4.395\times10^9 \times \exp(\frac{-3.3091\times10^4}{1.987\times623}) \times [1.3837\times10^4 \times 0.21] \times (0.06/2)^2}{0.024} = 1.2 \quad \textbf{(3.36)}$$

Damköhler number values show that the reaction is faster than the transport. It is calculated for the condition that the gas velocity or oxygen diffusion are maximum (base-case) thus for other cases the Damköhler number is higher than the one for the base case. The Damköhler number is not constant because both temperature and oxygen concentrations are varying during the process. Figure (3.19) shows the rate of the oxygen moles reacted as a function of time.

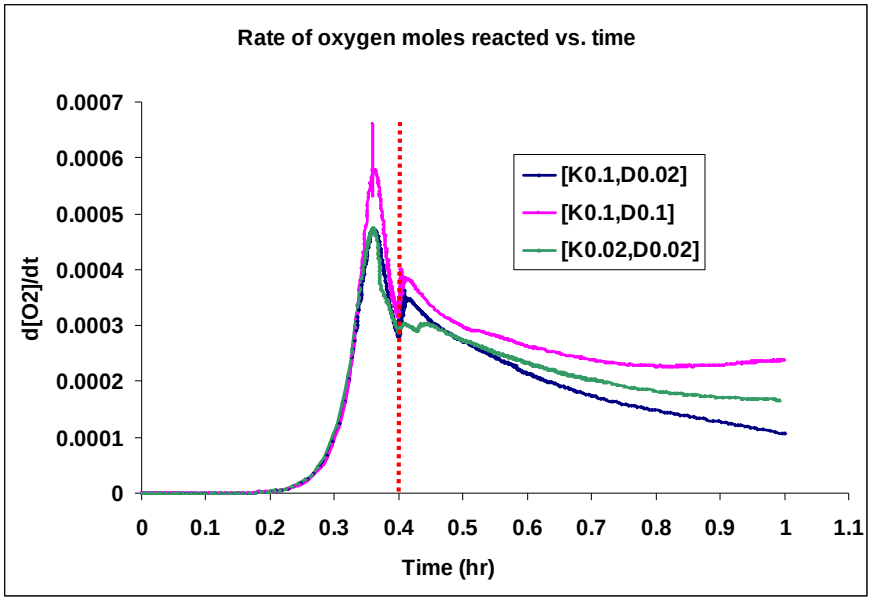


Figure 3.19. Rate of reacted oxygen vs. time.

The rate of oxygen consumption is the same until the time of heater shut off (0.4hr, indicated by dotted line), for the two cases that have the same diffusion coefficient, while it is higher for the case with higher diffusion coefficient even before heater shut off.
During a short period after heater switch off the rate of oxygen consumption is lower for [K0.02, D0.02] compared to [K0.1, D0.02] but, as time is passing, the situation becomes reverse and finally the combustion front propagates in the first case and stops in the second case. This might be another evidence for our hypothesis that *the lack of enough fuel availability* in the high permeability case is the cause of extinction.

Lewis number

The Lewis number is defined as:

$$Le = \frac{\alpha^*}{D^*} \quad \textbf{(3.37)}$$

in which α^* is the equivalent thermal diffusivity and the D^* is the effective mass diffusivity in the matrix.

$$\alpha^* = \frac{k^*}{\rho^* c^*} \tag{3.38}$$

There are several ways to calculate the equivalent thermal diffusivity of the porous medium; here we use the geometrical approach for the thermal conductivity and the saturation-weighted for the heat capacity and the density (STARS User Manual 2008 and Kaviany 1995).

$\frac{k^*}{k_f} = \left(\frac{k_s}{k_f}\right)^{\varepsilon}$ in which ε is the matrix porosity

The calculation is done for the initial reservoir condition in which the saturation in oil, gas and water are 0.65, 0.17 and 0.18 respectively.

$c^* = 125.5\ (\frac{J}{kg.K})$, $k^* = 1.01\ (\frac{J}{m.s.K})$, $\rho^* = 1488\ (\frac{kg}{m^3})$

$$\alpha^* = 0.54\times10^{-6}\ (\frac{m^2}{s})$$

$$D^* = 0.67\times10^{-5}\ (\frac{m^2}{s})$$

The Lewis number will be: $Le = 0.09$

This means that mass diffusion is faster than the thermal diffusion.

Thermal Péclet number based on combustion front speed

Combustion front speed based on the maximum temperature was calculated for the base case. It is not constant during the process; however it stabilizes after a certain time. The calculated value is $0.01<V_f<0.03$ (m/hr). Taking the average value of 0.02 (m/hr), the thermal Péclet number will be:

$$Pe_c = \frac{u_c l}{\alpha^*} = \frac{0.02\times(0.06/2)}{8.78\times10^{-4}} = 0.68 \tag{3.39}$$

which means that thermal conduction is faster than the combustion front movement. It is also in favour of the local thermal equilibrium assumption.

Péclet number based on combustion front speed and oxygen diffusion

$$Pe_c = \frac{u_c l}{D^*} = \frac{0.02\times(0.06/2)}{0.024} = 0.025 \tag{3.40}$$

This shows that the front is moving very slowly compared to the diffusion of oxygen.

Based on these dimensionless numbers, we conclude that the matrix is governed by a diffusion controlled process. Local thermal equilibrium assumption is valid as the rate of heat transfer by conduction is faster than the heat generated in combustion reaction (based on front velocity). Although there are uncertainties about the Damköhler number time scale, we can conclude that the reaction characteristic time is in general smaller than the transport characteristic time of the oxygen.

3.2.5 Horizontal configuration

To distinguish the gravity effect on extinction and propagation, the same operating condition is applied to the fractured core which was positioned horizontally. Changing the K and D in

horizontal configuration will lead to a considerable shift in the extinction/propagation diagram (see Table 3.9) compared to vertical configuration (table 3.7). These results show that, for horizontal configuration, even with very low oxygen diffusion, we still have combustion. The oil saturation profiles in the horizontal situation show that the fracture always contains considerable amount of oil.

K/K_{ref} \ D/D_{ref}	1	0.1	0.02	0.01	0.002	0.001
1.0						
0.1						
0.02						
0.01						
0.002						
0.001						

Table 3.9. Extinction/ Propagation diagram for horizontal configuration (red: propagation, blue: extinction.

That is why the combustion front will propagate, even with low diffusion values. In fact we can always have oil combustion which is present in the fracture. Having large oil saturation in fracture also increases the pressure drop and more oxygen can pass through the matrix compared to a vertical situation. However, the horizontal situation is an ideal case and in reality the gravity effects exist in any in situ combustion recovery process.

3.2.6 Oil production mechanisms

During the in situ combustion process, many production mechanisms that participate in oil production are playing at the same time. To distinguish the effect of each driving force we tried to study the effect of each mechanism separately whenever it was possible.

Comparison with non-fractured core

Comparing oil production in fractured (base case) and non fractured core shows that the oil recovery factor in the latter was higher than in the former. The results are presented in Figure (3.20).

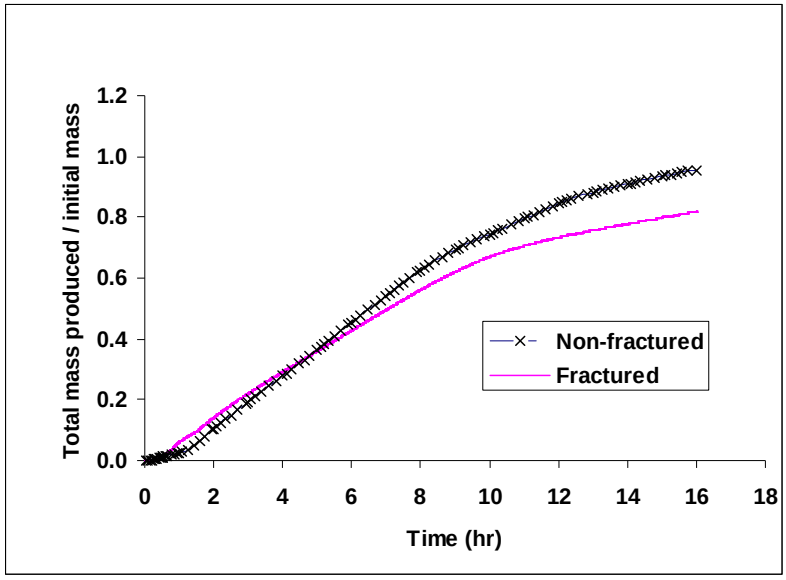


Figure 3.20. Mass of oil produced in fractured and non-fractured cores.

Both cases show very low oil production at initial time that corresponds to the time at which combustion develops. The fractured system is producing faster than the non-fractured until about 5hr; however the differences are small. After that, production in the fractured core is lower than in the non-fractured case. One can observe that the difference between the oil productions in two systems is not noticeable. This could be due to a very permeable matrix hiding the fracture effects.

Natural gravity drainage

The driving force for oil production from fractured reservoir is initially coming from reservoir natural pressure. However, here we do not apply any pressure gradient except the head of the oil column in the matrix block. Thus, we would like to study the role of natural gravity drainage on the oil production. To this end we may keep the same geometry as the base case, removing all reactions and let the system drain by gravity. Oil production under only gravity drainage was very slow and less than 8% of oil was produced during 20 hours, which is a typical burning time in the ISC process. So, the natural gravity drainage is unlikely to be of economical interest.

Oil production in vertical and horizontal configurations

Another test was carried out to determine the combustion effect on cumulative oil production in presence or absence of gravity. Oil production in vertical fractured core was compared with the one of the horizontal configuration. The results are presented in Figure (3.21). As indicated in this figure, oil production in the vertical position is considerably faster than in the horizontal case, which confirms that gravity plays an important role in the oil production.

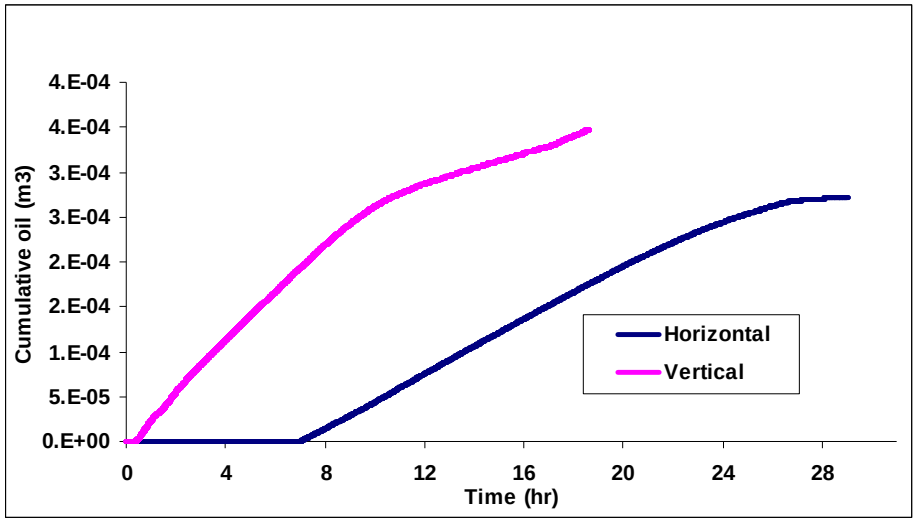


Figure 3.21. Cumulative oil production in horizontal and vertical configurations.

This is shown also in Figures (3.22) where oil saturation in vertical and horizontal positions could be compared. The direction of oil phase velocity vectors that are associated with Figure (3.22) shows that, in the vertical situation, almost all oil is produced via the matrix while considerable amount of oil is produced by fractures when the system is positioned horizontally.

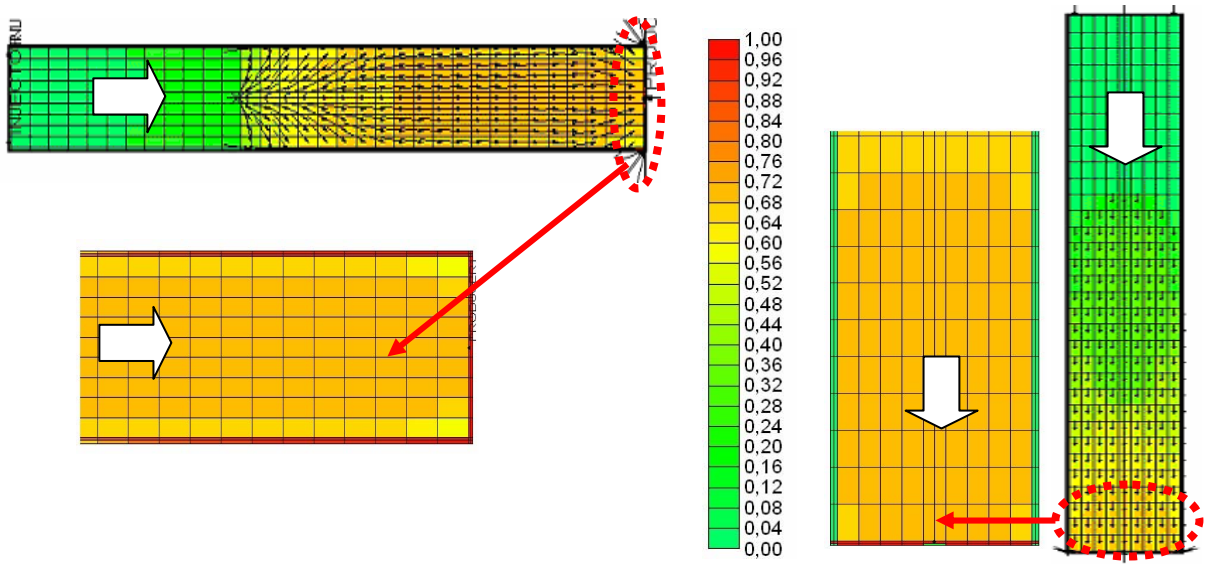


Figure 3.22. Oil saturation and oil phase velocity vectors in vertical and horizontal configurations.

Oil production via ISC and programmed heating

In this case, the same temperature as observed in ISC process is applied by external heaters to the core. When using heaters, all reactions were removed from the model. The heat front moves with the same temperature and speed as the combustion front was programmed to pass through the core.

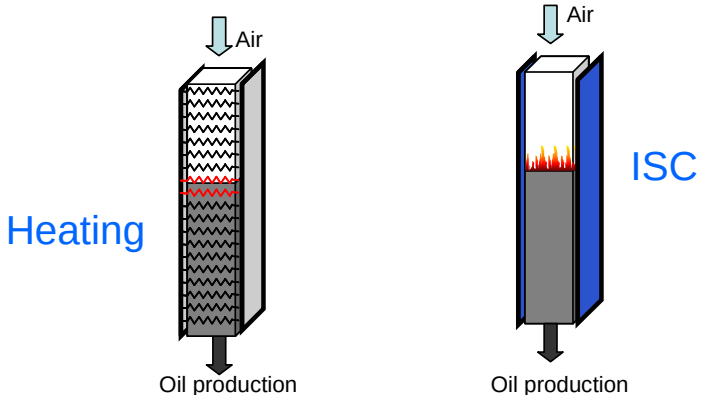


Figure 3.23. Schematic of the system under ISC and electrical heating.

Figure (3.23) shows a schematic drawing of these two cases and Figure (3.24) presents the oil production via ISC and programmed heating. The cumulative oil production by programmed heating after 15 hours is the same as ISC and even a bit more (2%). It indicates that temperature effects are predominant factors for oil production and non thermal effects, such as differential pressure generated during the oxidation reaction, do not play a major role. This could be also explained by the fact that, the pressure gradient generated during the ISC will be damped by the high permeability of the matrix, initial gas saturation (18%) as well as the fractures.

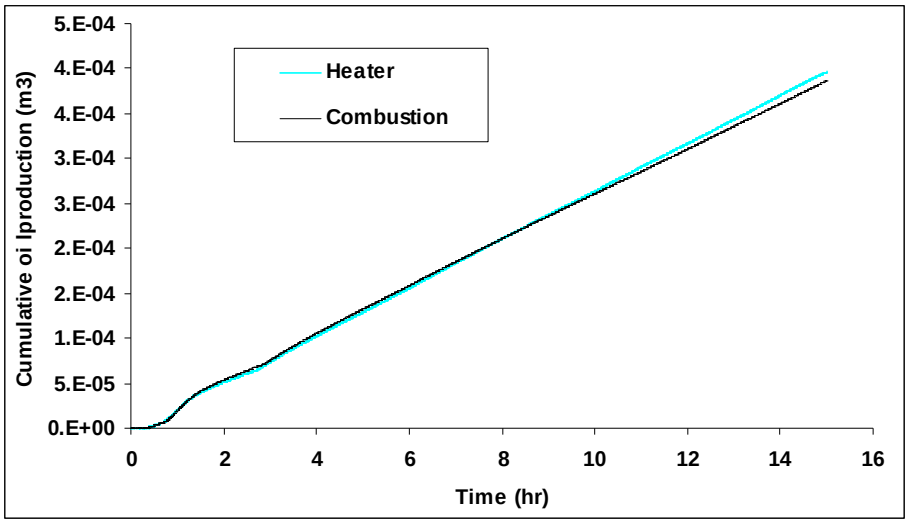


Figure 3.24. Oil production via in situ combustion and electrical heaters.

3.2.7 Shape of the coke zone

Figure (3.25 a) shows the effect of the oxygen diffusion coefficient on the shape of the coke zone after 10 hr of production. Coke is immobile and, when produced by the cracking reaction, it remains in place until it reacts with the oxygen. Low oxygen diffusion coefficient will result in coke zone expansion. On the other hand, when the matrix permeability is reduced (see Figure (3.25 b) it has no such effect, while the coke zone is slightly elongated. This indicates that the shape of coke zone changes with the oxygen diffusion**.**

Another observation in this Figure (b) is that the coke zone concentration is higher near the fractures. The reason for that could be the higher temperature in matrix edges compared to the temperature in the centre, which causes more heavy oil to be cracked and subsequent higher coke concentration.

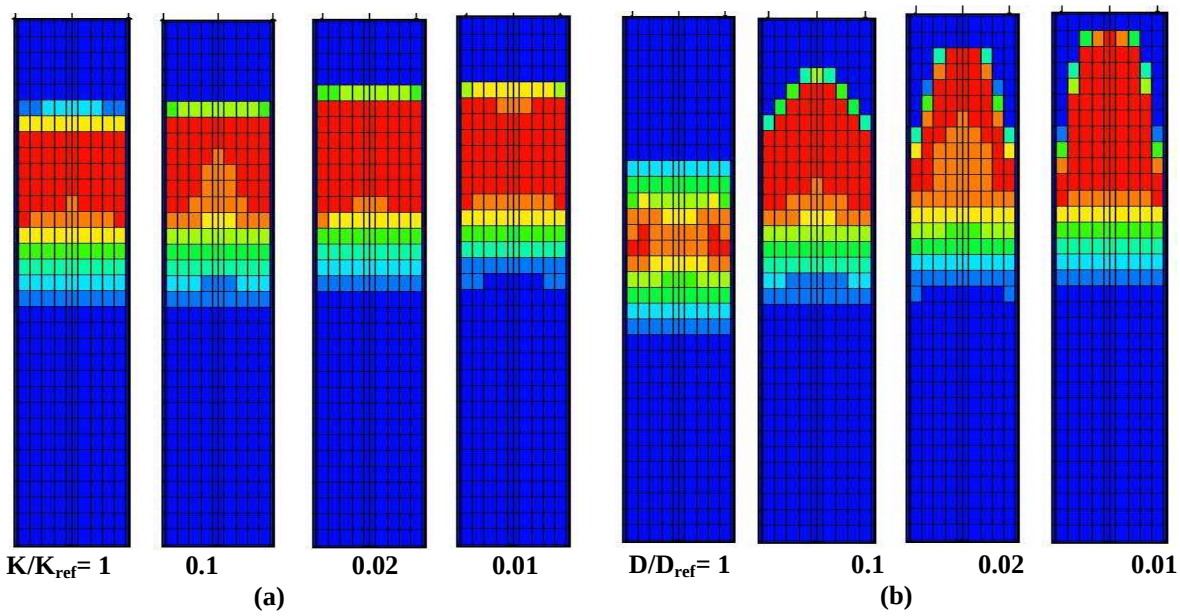


Figure 3.25. Shape of the coke phase when permeability or oxygen diffusion is varying.

3.2.8 Summary

Simulation results show that in situ combustion is feasible for medium oil at the fractured core-scale. The peak temperature and the extent of the coke zone were increasing during the process while these two parameters are rather constant in conventional combustion. The possible explanation is the higher rate of coke generation compared to coke oxidation in fractured system in which the oxidation reaction rates depend on oxygen delivery. For a given time, the shape and length of the coke zone was observed to be dependent on oxygen diffusion coefficient while matrix permeability seems to have minor effect on that. Oxygen diffusion coefficient was found to have a major influence on extinction/ propagation of combustion and matrix permeability to play an important role on oil production. Keeping constant matrix permeability and reducing the oxygen diffusion coefficient will lead to extinction which could be due to lack of oxygen in the combustion zone. Temperature profile in the combustion zone showed that this argument could be justified in most of the cases. In some non-propagating situations, when the oxygen diffusion was kept constant, reducing the matrix permeability resulted in combustion front propagation. This suggests a lack of fuel to support the combustion in higher permeability case. This also could be somehow explained by the reaction rate and the oil phase Péclet number.

Prediction of extinction/propagation conditions based on either oil saturation, coke concentration and temperature profiles or dimensionless numbers seems to be very challenging. Defining some pertinent dimensionless numbers for this aim may help but was not completely discriminating, which is not surprising given the coupled, non-linear nature of the problem. Considering the characteristics of the porous matrix for the base-case, the simulation results showed that more fuel was consumed during the ISC in a fractured system compared to non-fractured case. This result is in agreement with the coke zone expansion and peak temperature increase that was observed in fractured core. Gravity drainage and thermal effects were found to be important in oil production. Any possible pressure gradient generation during the ISC process seems to have a minor effect on oil production. However, one should keep in mind that very high permeability of the matrix may hide some possible driving forces like gas drive and pressure generation.

3.3 Simulation of ISC process in a single matrix block

Two-dimensional simulation of a single matrix block surrounded by fractures was studied. The geometry of the system is shown in Figure (3.26). Because of the symmetry that exists in this problem, we have simulated half the block (in the *x*-direction).

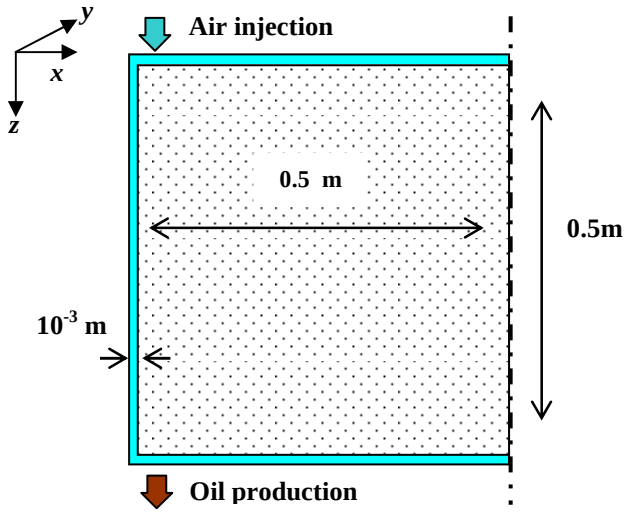


Figure 3.26. Schematic of a model used for single block simulation.

We also simplified the 3-D block geometry to a 2-D slab, neglecting the influence of the fractures in front of, and behind, the block. The fracture at the bottom of the block was wider (0.025 m) than that on its side allowing for better production control. Block dimensions in *x*, *y* and *z* directions were 1, 0.05 and 0.5 (m) respectively. The matrix block was discretized by 16×16 grid blocks in *x* and *z* directions and two grid blocks were considered for fractures which resulted in a 20×20 simulation grid. The same reservoir properties, initial condition and reaction scheme were used as in the previous part except that here oil was made more viscous at initial reservoir condition (4000 cp). Air was injected onto the fracture from the top-left and oil was produced also from the fracture at the bottom-left of the simulation domain. Heat losses to the block surroundings were considered to be zero.
Here, we present some observations of the combustion process in a single block.

3.3.1 Temperature

The temperature profile along the matrix block diagonal from the top left to the bottom right is shown in Figure (3.27). Peak temperature and size of the high temperature zone inside the block increase during the production. After ignition (1 hour), the peak temperature increases to about 410 °C (at 10 hours) and then remains relatively constant until 50 hours, after which it starts to increase again.

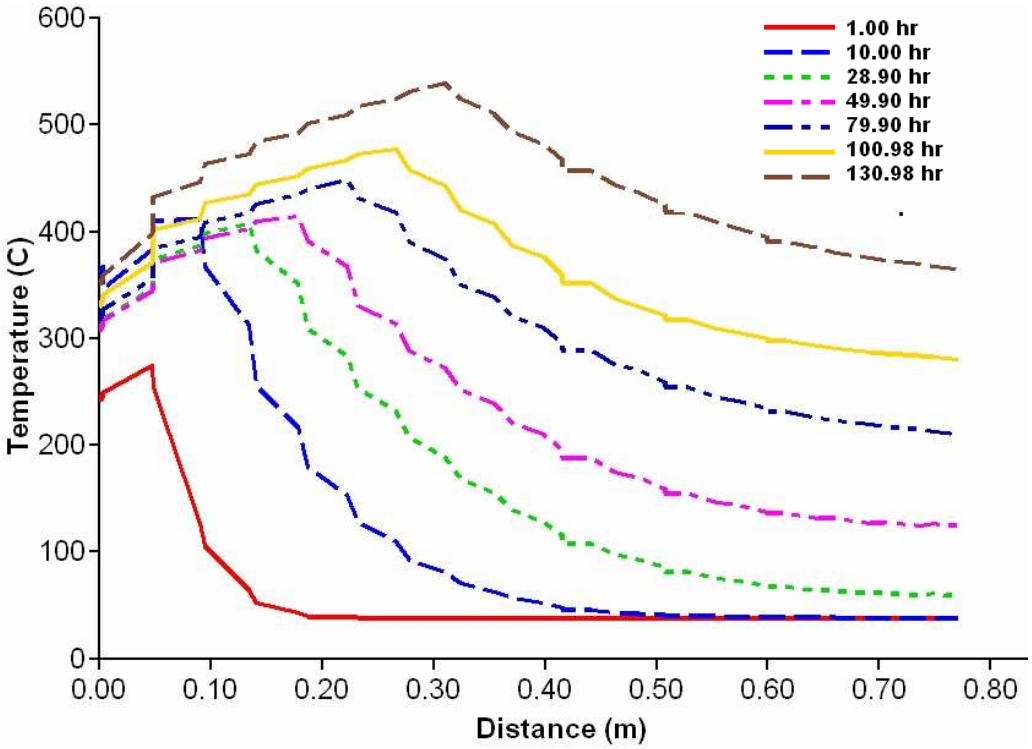


Figure 3.27. Temperature along the block diagonal at different times for K=1270 md.

To explain the behavior of the system we may try to compare the magnitude of different processes that are involved in heat transfer during combustion. In this regard, instead of treating the whole system, which is very complex, we will analyze some simpler cases for which dimensionless numbers may be derived. The simplified version of this process is a filtration combustion (FC) in which a combustion front passes through a porous matrix, initially containing a solid fuel. This process has been studied by many researchers (Debenest et al. 2005; Aldushin and Matkowski 2000). To determine the behavior of a FC process, Debenest et al. (2005) used the parameter Δ:

$$\Delta = \frac{\varepsilon C_g (v_g - u_c)}{[\varepsilon C_g + (1-\varepsilon)C_s]u_c} \approx \frac{\varepsilon C_g v_g}{(1-\varepsilon)C_s u_c} \tag{3.41}$$

When Δ>1, heat is transferred from upstream (behind the front) to downstream (ahead of the front) by convective gas flow. Δ=1 corresponds to a situation where heat remains in the vicinity of the reaction front and when Δ<1 there is no convective heat transfer from upstream to downstream. This analysis is based on the hypothesis that the dominant heat flow regime is gas convection. In our case, however, we expect that heat conduction is also significant.
To start the analysis we may write the energy balance equation in the form used by Aldushin and Matkowski (2000) for a 1-D system of solid-gas combustion in a coordinate system that is moving with the combustion front:

$$C_P\left(\frac{\partial T}{\partial t} - u_c \frac{\partial T}{\partial t}\right) + \varepsilon C_g v_g \frac{\partial T}{\partial x} = k^* \frac{\partial^2 T}{\partial x^2} \tag{3.42}$$

$$C_P = (1-\varepsilon)C_s + \varepsilon C_g \tag{3.43}$$

This energy balance is written in 1-D for a region near the combustion front. Upstream of the front, the fluid is in a gas phase and downstream at the vicinity of the combustion front the oil saturation is equal or less than its residual saturation and no water is present due to high temperature. Under this condition it is reasonable to consider only solid and gas phase in the energy equation.
Choose the following dimensionless variables:

$$X = \frac{x}{L},\ \tau = \frac{t}{t^*},\ t^* = \frac{L}{u_c},\ \theta = \frac{T}{T_{ref}} \tag{3.44}$$

Here L is the length of the matrix and t^* is the time for combustion to travel the matrix length. Usually the gas phase heat capacity is negligible compared to solid phase heat capacity in Eq.3.43. Thus the equivalent heat capacity is:

$$C_P \approx (1-\varepsilon)C_s \tag{3.45}$$

Eq. 3.42 can be written as:

$$\frac{u_c C_P}{L}\frac{\partial \theta}{\partial \tau} + \left(\frac{\varepsilon C_g v_g}{L} - \frac{C_P u_c}{L}\right)\frac{\partial \theta}{\partial X} = \frac{k_{eq}}{L^2}\frac{\partial^2 \theta}{\partial X^2} \tag{3.46}$$

Dividing both sides by $\frac{k^*}{L^2}$, we have:

$$\frac{(1-\varepsilon)C_s u_c L}{k^*}\frac{\partial \theta}{\partial \tau} + \left[\frac{\varepsilon C_g v_g L}{k^*} - \frac{(1-\phi)C_s u_c L}{k^*}\right]\frac{\partial \theta}{\partial X} = \frac{\partial^2 \theta}{\partial X^2} \tag{3.47}$$

We can write this equation as:

$$Pe_c \frac{\partial \theta}{\partial \tau} + \left[Pe_g - Pe_c\right]\frac{\partial \theta}{\partial X} = \frac{\partial^2 \theta}{\partial X^2} \tag{3.48}$$

in which the Pe_c and Pe_g are the thermal Péclet numbers based on combustion front and gas phase velocities respectively.

To determine the order of magnitude of each parameter we used the simulation result to calculate the gas phase velocity and the combustion front velocity. Calculation based on the simulation results for a typical case (K=1270 md) showed that the average gas phase velocity is in the order of 10^{-6} m/s close to the front position. The front velocity is not constant. At the initial times it is of the order of 5×10^{-6} m/s and then it reduces to 5×10^{-7} m/s and even smaller at later times. Typical values for gas and solid phase volumetric heat capacity are 7.5×10^{4} and 3.2×10^{6} J/m^3°C, respectively. Thermal conductivity was calculated to be 1.0 W/m.°C and the porosity of the medium is 40%. The Péclet numbers are:

$$Pe_g = \frac{\varepsilon C_g v_g L}{k^*} = \frac{0.4\times7.5\times10^{4}\times10^{-6}\times0.5}{1.01} = 0.02 \quad \textbf{(3.49)}$$

$$Pe_c = \frac{(1-\varepsilon)C_s u_c L}{k^*} = \frac{0.6\times3.2\times10^{6}\times5\times10^{-7}\times0.5}{1.01} = 0.45 \quad \textbf{(3.50)}$$

Comparison of these two parameters shows that heat transfer due to front movement is more important than gas phase convective heat transfer and both of them are less important than heat transfer by conduction. The combustion front velocity decreases with time and thus at later time, heat transfer due to front movement also decreases.

Based on this calculation we may explain the temperature behavior as follows: The initial increase in peak temperature is due to the development of the combustion process where the combustion front velocity is high and the rate of heat generation by combustion is higher than the rate of heat transfer.

Subsequently the relatively constant temperature suggests that the heat produced by the combustion process is transported mainly by conduction to the colder parts of the block. Finally when the heat front reaches the symmetric no-flow boundary on the right side of the computation domain (middle of the matrix block), peak temperature starts to increase as conduction heat transfer is limited by this boundary.

Gas phase velocity vectors in Figure (3.28) indicate that the gas phase does not bring the heat from upstream to the front (unlike the FC process), but rather remove heat from it. In this figure the red color region shows the maximum temperature or the combustion front location. This is another indication that conduction heat transfer is dominant.

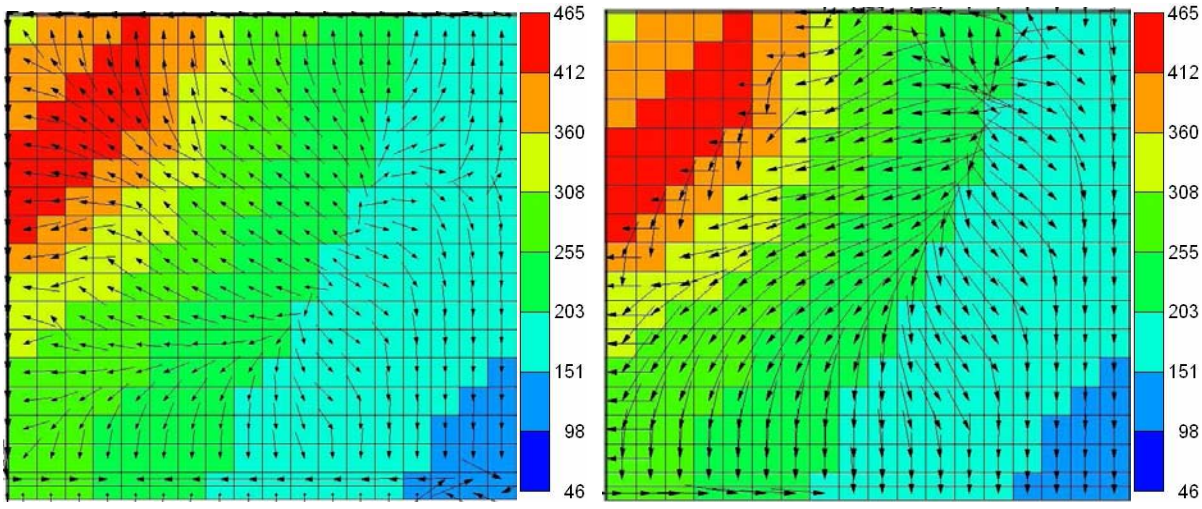


Figure 3.28. Temperature profile and gas phase velocity vectors (left), temperature profile and oil phase velocity vectors (right).

Oil phase velocity is shown in Figure (3.28) using flow vectors. The oil phase just ahead of the front drains relatively vertically but far from the front the drainage is inclined. This is because the oil at the upper right part of the simulation domain has lower viscosity than the oil underneath it. Velocity of the oil phase adjacent to the front is 10^{-9} m/s and far from the front it is about 3×10^{-8} m/s. The oil phase thermal Péclet number near the front is:

$$Pe_o = \frac{v_o L}{\alpha^*} = \frac{10^{-9}\times 0.5}{0.54\times10^{-6}} = 0.9\times10^{-3} \quad \textbf{(3.51)}$$

This value shows that heat transfer by the oil phase just ahead of the front is negligible compared to conductive heat transfer.
The oil phase thermal Péclet number far from the front is:

$$Pe_o = \frac{v_o L}{\alpha^*} = \frac{3\times10^{-8}\times 0.5}{0.54\times10^{-6}} = 0.027 \quad \textbf{(3.52)}$$

This value indicates that although heat transfer by the oil phase far from the front is more important than heat transfer near the front, still the conductive heat transfer is more important than convective heat transfer.
Considering an oxygen diffusion coefficient equal to 0.67×10^{-5} m^2/s and a characteristic length of 0.5 m for the matrix, the Péclet number for the gas phase is:

$$Pe_g = \frac{v_g L}{D^*} = \frac{10^{-6}\times 0.5}{0.67\times10^{-5}} = 0.08 \quad \textbf{(3.53)}$$

This value shows that the process of oxygen delivery to the combustion front is also diffusion dominated.

Péclet number in the fracture

Gas phase velocity inside the fracture is in the order of 10^{-3} m/s. The Péclet number in the fracture is:

$$Pe_g = \frac{v_g L}{D^*} = \frac{10^{-3}\times 0.5}{10^{-5}} = 50 \quad \textbf{(3.54)}$$

which shows that the oxygen transport in the fracture is convection dominated.
To calculate the thermal Péclet number inside the fracture we consider the air heat capacity and thermal conductivity as 7.5×10^4 $J/m^3°C$ and 4×10^{-2} W/m.°C. The thermal Péclet number is then:

$$Pe_g = \frac{C_g v_g L}{k_g} = \frac{7.5\times10^4\times 0.5}{4\times10^{-2}} \approx 10^5 \quad \textbf{(3.55)}$$

These calculations show that the main transport mechanism for both heat and mass in the fracture is convection.

3.3.2 Coke zone

Figure (3.29) shows the coke concentration across the diagonal of the block between left upper corner and the right lower corner of the symmetry section of the matrix block in Figure (3.26). The size of the coke zone increases during the production while the maximum coke concentration remains relatively constant. This shows that the heat transport ahead of the combustion front is faster than the advance of the combustion front. On the other hand, the

coke consumption by the combustion process is slower than its generation by the cracking reaction.

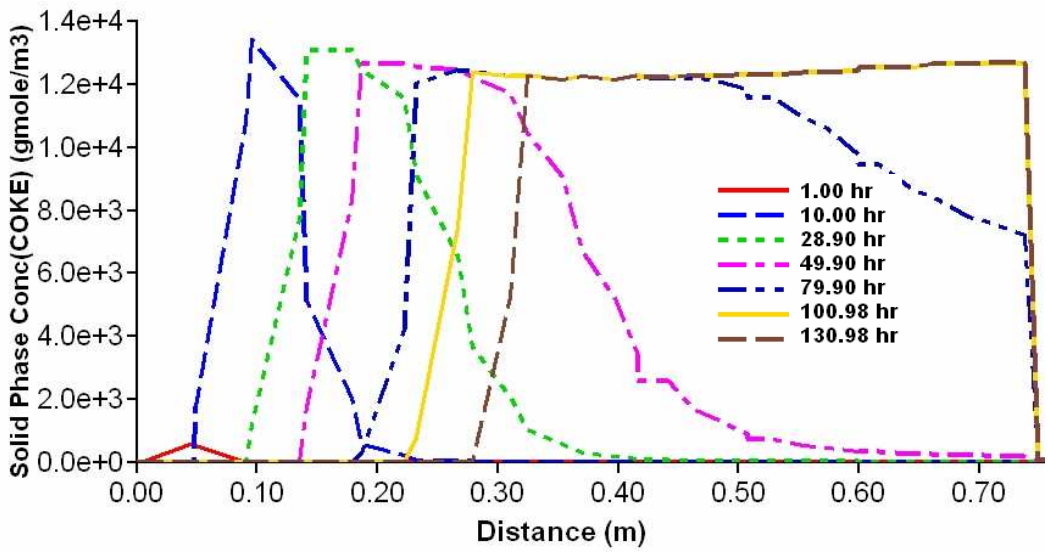


Figure 3.29. Coke concentration along the diagonal of the simulation domain for different times for K=1270 md.

It is important to mention that values for coke concentration may not be necessarily generalized, but our aim here is mainly to show how the extent of the coke zone evolves during the ISC process. Another important point is that the coke concentration also depends on the reaction scheme and it may vary for different oils.

3.3.3 Oil saturation

The oil that is mobilized due to heating will form a so-called oil bank ahead of the high temperature combustion front. Initially this narrow thickness, high oil saturation zone will form close to the combustion front (figure 3.30.). This happens because a large portion of the block is still at low temperature at which oil is not mobile. Under this situation most of the oil production occurs through the vertical fracture. As the combustion front progresses, the size of the oil bank increases and finally it touches the matrix bottom and causes the oil to be produced by the matrix as well. This increase of oil bank size may be explained by the fact that heat transfer is faster than combustion front movement. At later times (>50 hours) one can distinguish two main fronts for oil saturation: The one which is close to the combustion zone with a jump from zero to about 25% saturation and the oil bank which is far from it with oil saturation jumping to a value larger than the initial oil saturation. At later times no oil will be produced by the vertical fracture as the oil-bank is far away from it.

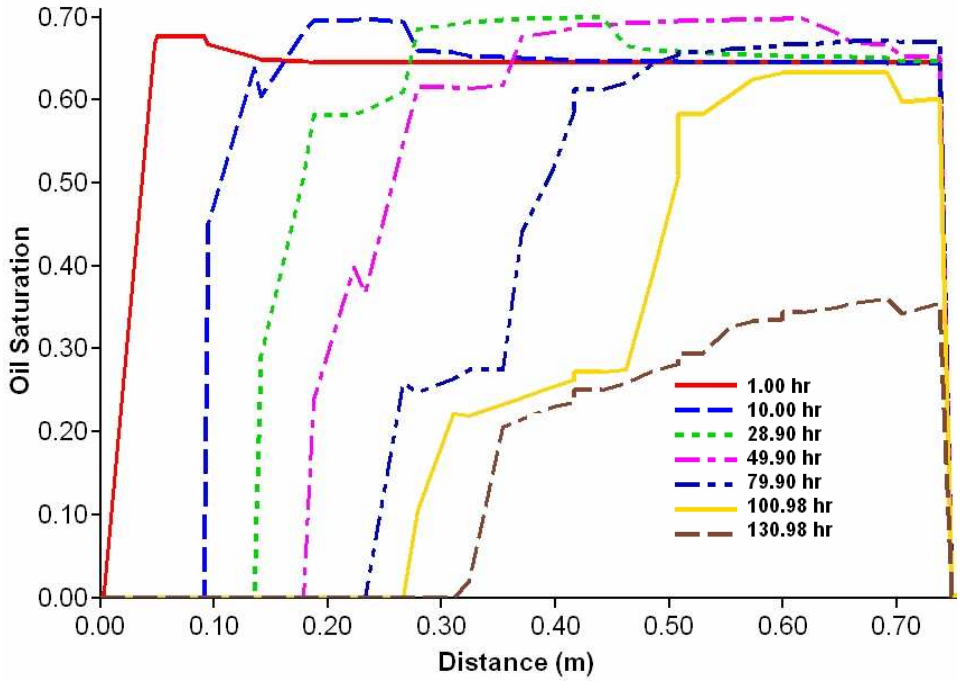


Figure 3.30. Oil saturation along the block diagonal at different times for K=1270 md.

3.3.4 Combustion front velocity

Figure (3.31) shows the front velocity calculated based on the oil saturation profile shown in Figure (3.29). This figure shows that front velocity decreases with distance. Comparing these results with the analytical solution of the diffusion dominated combustion process studied by Aldushin and Matkowski (2000) reveals that the combustion process in our case is also governed by diffusion.

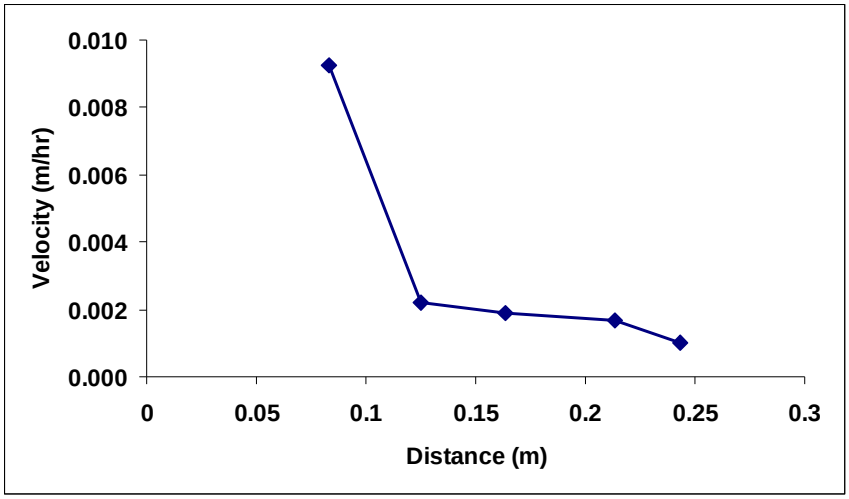


Figure 3.31. Combustion front velocity based on the oil saturation profile.

We can make a similar comment about the front velocity as that we made for coke concentration. The velocity values could be different for another oil or reaction scheme but we emphasize the fact that the velocity decreases with time and it shows that the process is diffusion dominated.

3.3.5 Water saturation and steam plateau

In a typical in situ combustion process, water is produced in the gas phase, as a product of combustion reactions. Also, due to high temperature associated with the combustion front, part of the water that initially exists in the reservoir vaporizes. Water in the gas phase, when reaching a cooler region of the reservoir (downstream the combustion), condenses and produces a so-called water bank. The steam generated during ISC and the water bank are known to influence oil production (Butler 1991, Castanier and Brigham 2003, Sarathi 1999); the former can have a stripping effect and the latter may act as a hot water drive. Based on the condensation temperature of water and vaporized hydrocarbon, different zones may develop in a conventional ISC process. Typically, the steam plateau and water bank are ahead of the oil bank (Castanier and Brigham 2003).
Figure (3.32) shows the position of the water bank during ISC in the single block with surrounding fractures.

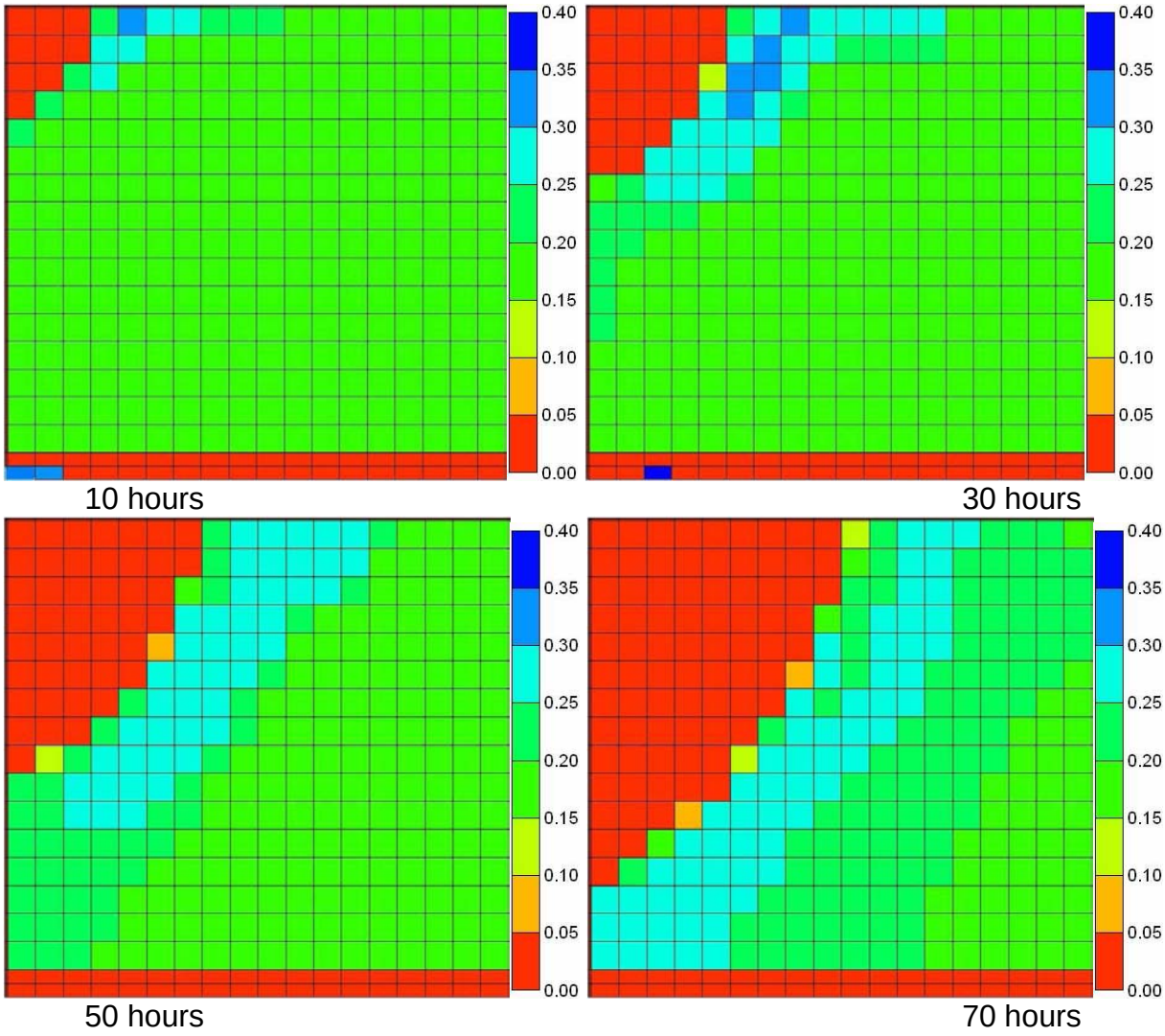


Figure 3.32. Water saturation evolution with time (K=1270 md).

The relative position of the water saturation compared to the oil bank and combustion front in the fractured system is somehow different compared to what is typically observed (Castanier and Brigham 2003) in a conventional ISC. The vaporized water and the water vapor which is produced by combustion reactions tend to move toward the upper part of the block. This is

due to its density which is becoming lower than that of the liquid phases. The water vapor, when reaching the cooler regions, condenses and starts to drain. As shown in this figure, initially the water bank position is not completely downstream of the combustion front. Later, when the water saturation increases, it starts to move downward. This figure also shows that the size of the water bank increases with time. This behavior is somehow different from the conventional expectation about the steam plateau and water bank.

3.3.6 Oil upgrading

Oil upgrading is characterized by the amount of heavy oil that is transformed to light oil due to the cracking reaction. Another product of this reaction is coke, of which the amount inside the matrix increases during the production time.

Cracking reactions occur in two different temperature ranges. Heavy oil cracking that takes place below 350°C, called visbreaking, which reduces the oil viscosity. The high temperature cracking produces coke and light hydrocarbon (Monin and Audibert 1985, Castanier and Brigham 2003). However low temperature oxidation reactions that occur at temperature below 350°C, produce some complex components with high viscosity. Thus the oil upgrading is a result of the combination of all these different reactions.

Experimental study of ISC in a fractured core (Greaves et al. 1985) showed significant upgrading of Wolf Lake oil with enriched air (32% oxygen in air). With normal air, the API gravity of the oil was increased by 3 degrees. Application of ISC at field scale showed an oil upgrading of as much as 6° API (Ramey et al. 1992). In an attempt for in situ upgrading Atabasca bitumen, Xu et al. (2001) found that low temperature oxidation followed by temperature increase (i.e. steam injection) can significantly reduce viscosity. An experimental study done by Xia and Greaves (2001) on bitumen applying a SARA-based analysis, showed signification increase, 8° in oil API gravity. Castanier and Brigham (2003) proposed sulfur removal by using some water soluble additives. A review of possible upgrading process can also be found in their work. In another work on comparison between ISC and steam distillation of two Canadian crudes, Freitag and Exelby (2006) reported that, opposite to common belief, before steam breakthrough, the properties of the produced oil are much more influenced by steam distillation than by cracking reactions. They also found that increases in the recovery due to a combustion front effect were much more pronounced for the heavier oil than those due to steam (79% higher compared to steam flooding recovery for Wolf Lake).

Figure (3.33) shows the cumulative production of heavy oil, which corresponds to 2.5% of the initial volume of heavy oil in place. This reveals that more than 97% of the heavy oil has been cracked. This is a huge upgrading that may not occur in reality. Literature results show that oil upgrading occurs during ISC and it could be significant. Our simulation results also show significant upgrading. However, in our simulation model we did not incorporate LTO reactions nor the visbreaking processes. In an experimental study on Athabasca bitumen, Moore et al. (1992) reported that the negative temperature gradient region plays an important role in the oil kinetics and it should be incorporated in numerical simulation in order to obtain reliable results. In another paper (Moore et al. 1996) it is also mentioned that oil recovery is dependent to the nature of the low temperature oxidation reactions. Another important point is that, in our simulation, only two components are considered for the oil phase thermodynamics representation, which is also a strong simplification. The fact that we have increased the viscosity of the oil without changing the reaction scheme could be another reason for this extensive upgrading. Having this in mind, a stricter judgment on the extent of upgrading in a fractured system should be assessed by experimental results.

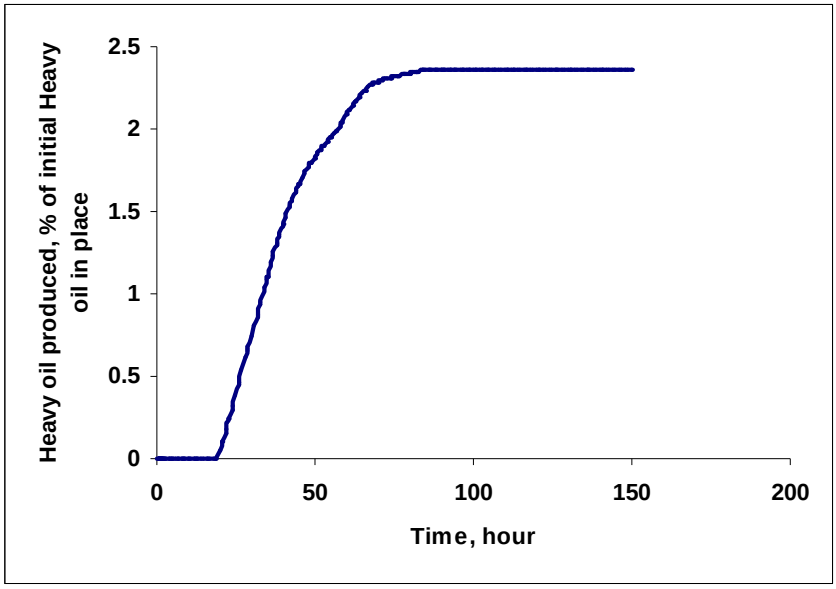


Figure 3.33. Cumulative volume of heavy oil produced as a fraction of initial volume, both measured at standard condition.

3.3.7 Oil production

Cumulative oil production at standard condition as a function of time is presented in Figure (3.34) for three cases with different matrix permeability.

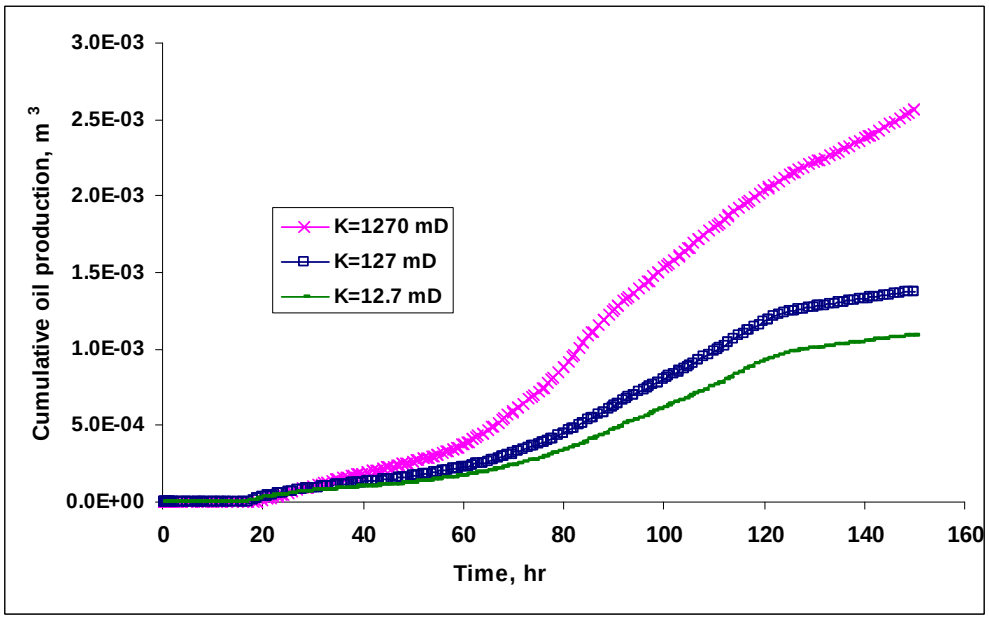


Figure 3.34. Cumulative oil production at standard condition for different matrix permeability.

The air injection rate is 0.3 m^3/hr for all cases. Oil production during the initial phase (<60 hours) is small due to high viscosity (4000 cp) of the oil at reservoir condition and later production increases as heat penetrates into the matrix block. The cumulative oil produced increases as matrix permeability increases. The increase of the oil production after 60 hours in high permeable (1270 md) matrix is more pronounced than that in the other two cases. A transition time of 60 hours corresponds (for the high permeable case) to the time at which the

oil bank reaches the matrix vertical symmetry no-flow boundary. Figure (3.35) shows the progress of the oil bank during production. The oil bank size is maximal when it reaches this boundary.

In the study of ISC for a fractured system at laboratory scale, Greaves et al. (1991) reported that more than 75% of the oil was produced during the first half of the burn period. This is not the case in a block where most of the oil production occurs at the second half of the production period. We believe that the shape of the combustion front in a tube is totally different from that in the matrix block. In the tube, after an initial time period necessary for development of combustion, the front will pass through the tube from top to bottom without horizontal displacement. However in a block, both vertical and horizontal advancement of the combustion front occurs and consequently the resulting heat transfer will affect the amount of mobilized oil and eventually the production.

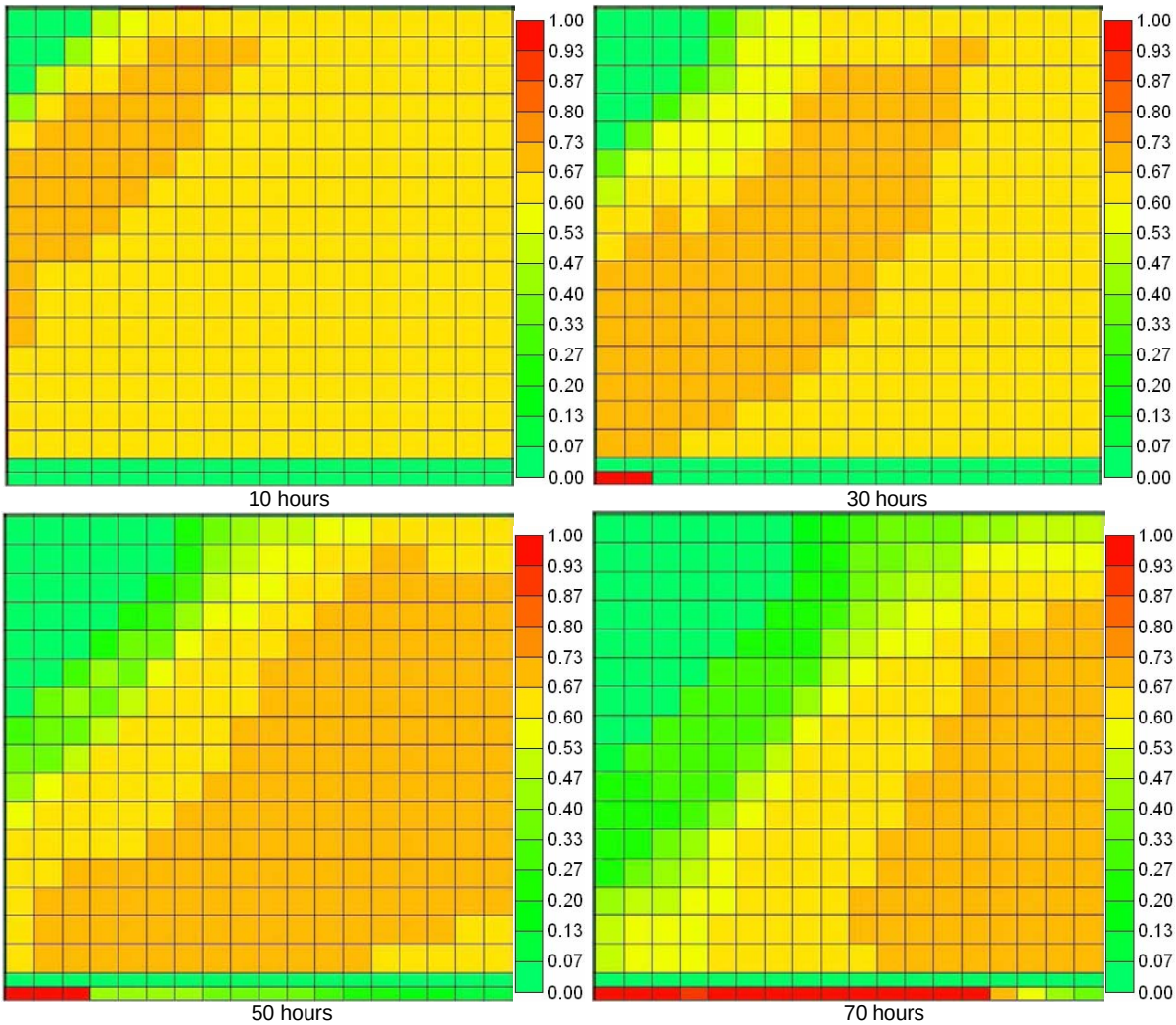


Figure 3.35. Oil saturation during ISC in a single matrix block (K =1270 md).

3.3.8 Summary

Simulation of ISC at the matrix block scale showed that the underlying process is diffusion dominated both for heat and mass (i.e. oxygen) transfer. Heat transfer due to the movement of the combustion front velocity is less important than heat transfer by conduction; this is the reason for the observed increase of combustion front temperature during the process. In this multi front process, different zones can be distinguished for oil saturation and temperature

with sizes that vary over time. The relative size of the heat and saturation zones and the change of their size during the burning process suggest that any upscaling method should take into account these phenomena. On the other hand, for a multi-block situation, homogenizing the matrix block as a single node in the simulation model may introduce large errors as the nature of the process inside the matrix is highly heterogeneous. More detailed mathematical manipulation is needed to address this issue based on the characteristic length scale of the processes on-going in the matrix and the averaged values of different parameters.

3.4 Multi-block simulation

The aim of multi-block simulation is to identify the behavior of the combustion process in a case where more than one block is present in the system. This is basically to identify the possible interferences of the blocks on each other and the eventual effect on the length scale of the combustion process parameters.

In this model the same reservoir and fluid parameters as the single block case were used. The model characteristics are presented in Table (3.10) and Figure (3.36) shows a schematic of the model. In this figure bold lines are fractures and for each block a number is designated. This number will be used to present the results corresponding to that specific block.

Ignition is started in the first block at the top-left of the model and air is injected in this position also (both in the matrix and the fracture). The fluids are produced at the bottom-right of the model. There is no heat loss from the reservoir to the surroundings and the capillary pressure is considered to be negligible both for the oil-water and oil-gas systems.

Table 3.10. Parameters of multi-block simulation model.

Parameter	***Value***
Porosity %	40
Permeability (matrix), md	1270
Permeability (Fracture), md	127000
Injection rate, m^3/hr	0.4
Initial saturation	
Oil	0.66
Water	0.18
Gas	0.16
Temperature, °C	37
Pressure, kPa	137
Reservoir dimension, m	1.2×0.2×1.8
Grid (*x*, *y*, *z*) number	50×1×74
Block dimension, m	0.3×0.2×0.3
Fracture aperture, m	1.5e-3

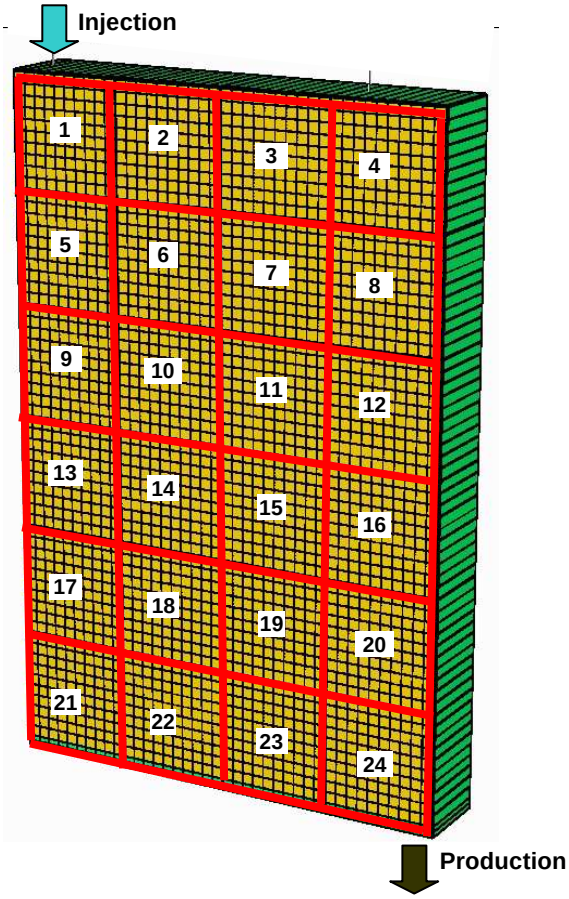


Figure 3.36. Schematic of the multi-block model.

3.4.1 Temperature profile

Figure (3.37) shows the temperature for three different times. Generally, the temperature increases with time, which may be partly due to the adiabatic reservoir assumption. At 10 hr the combustion front (high temperature) is still in the first block (ignition block) and it has slightly touched the second block. At this time, the combustion front is somehow inclined and in the first block, it is in advance compared to the other blocks at the top of the reservoir. At 20 hr the front is mainly in the first and second block and the general form of the front is less inclined. At later time (60 hr) the high temperature front is present in different blocks (2, 3, 5 and 6). Although the size of the high temperature zone is less than the size of a block and it is inclined, the low temperature front seems to be horizontal downstream. The position of the production well causes the combustion gases to flow toward the right side of the reservoir thus the temperature front moves also mainly towards the right side.

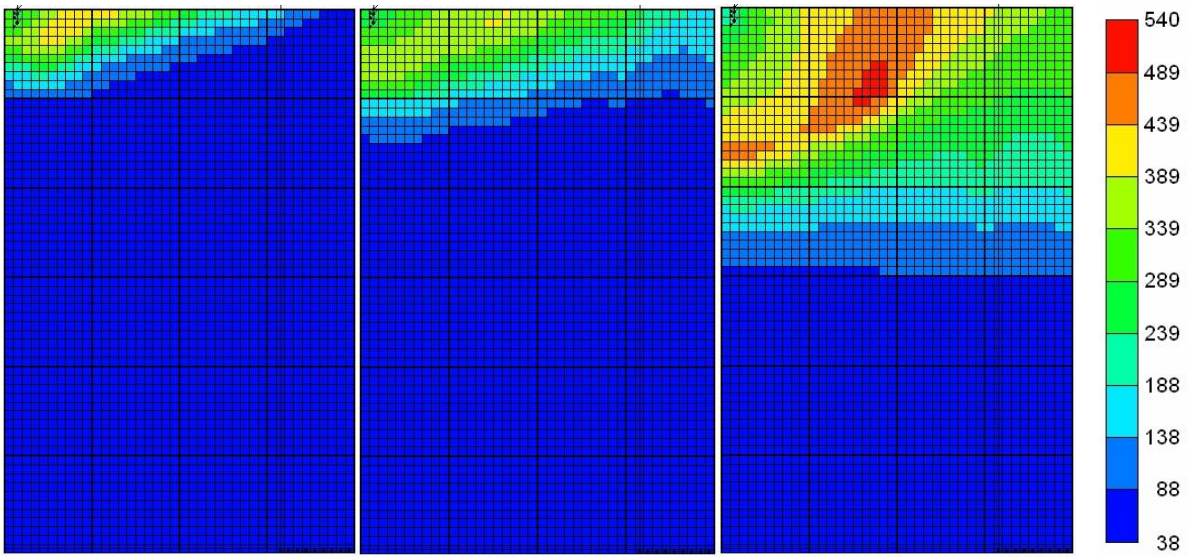


Figure 3.37. Temperature (°C) profile for different simulation time.

3.4.2 Fluid saturations

The oil saturation profiles are presented in Figure (3.38) for the same time intervals as the temperature profiles. Generally, the oil saturation front is somehow inclined at the beginning of the burning process and it becomes relatively horizontal later. The area with residual oil saturation (<0.2) also increases with time, which shows that the combustion front moves slower than the oil saturation front.

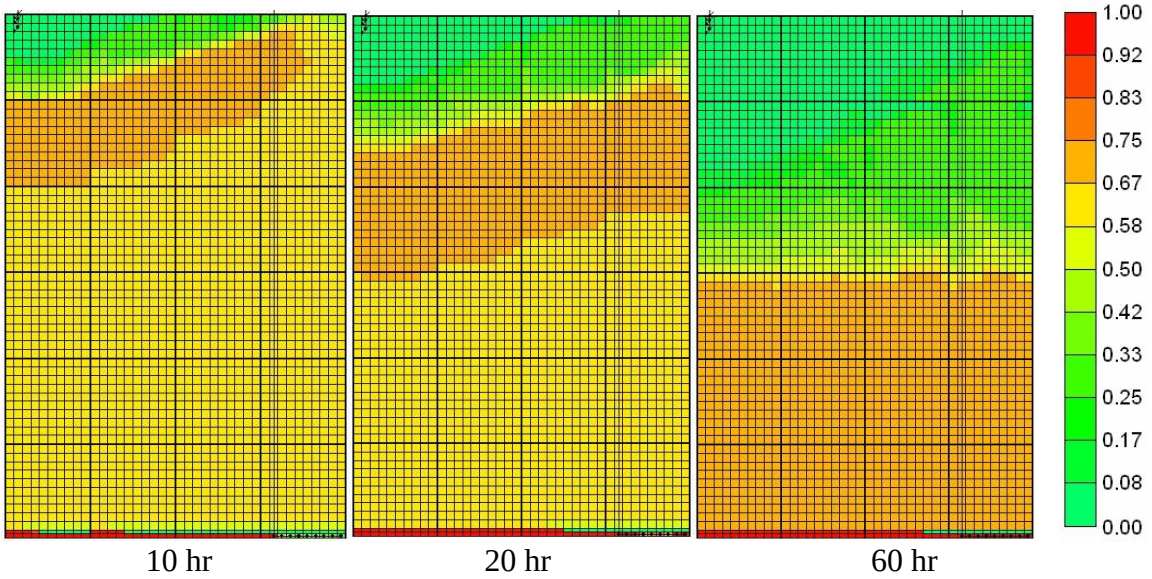


Figure 3.38. Oil saturation profile for different simulation time.

The water saturation profile exhibits an interesting behavior which is somehow different than what one expects normally from a typical combustion process where the water bank is downstream of the combustion front. As shown in figure (3.39), water saturation increases in the blocks at the top of the reservoir, which is not exactly downstream of the combustion front. We may explain this behavior with the presence of the fractures and the fact that the

production gases tend to stay at the top of the system. We remind also that these gases flow mainly toward the right side of the reservoir according to the position of the production well. The water bank which is formed at the top of the reservoir flows downward and sweeps more oil in the blocks underneath (figure 3.38).

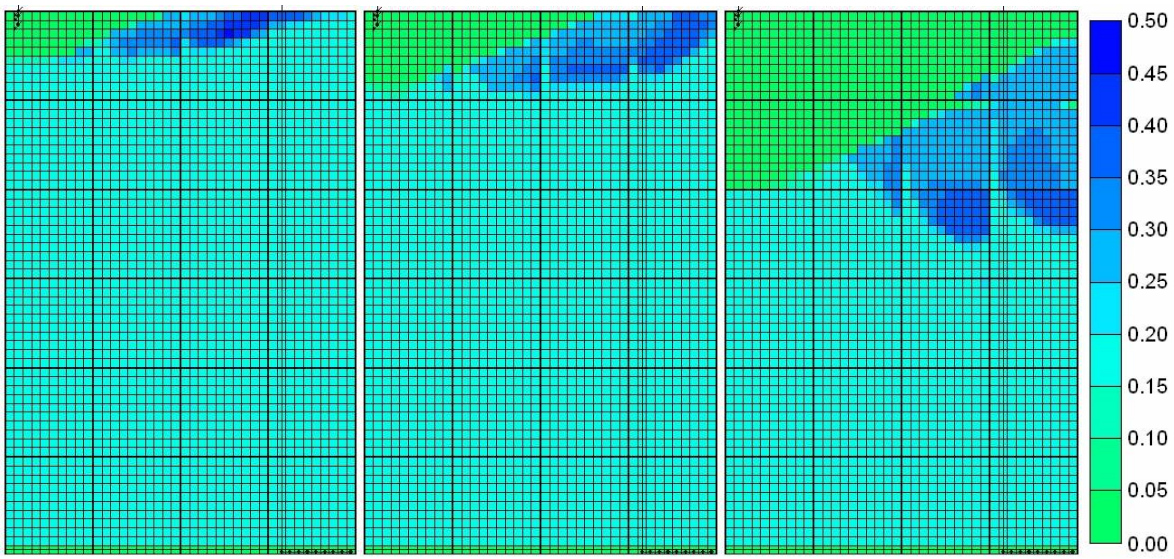


Figure 3.39. Water saturation profile for different simulation times.

3.4.3 Coke zone

Figure (3.40) presents the coke zone evolution during the ISC process. The extent of this zone increases with time which is another indication that the combustion front progresses slower than the heat transfer front. The maximum coke content can be found close to the area where the temperature is high or where the oil saturation is considerable. The first area is at the left side (block 5 and 6) and the second one is mostly at the right side (blocks 4 and 8).

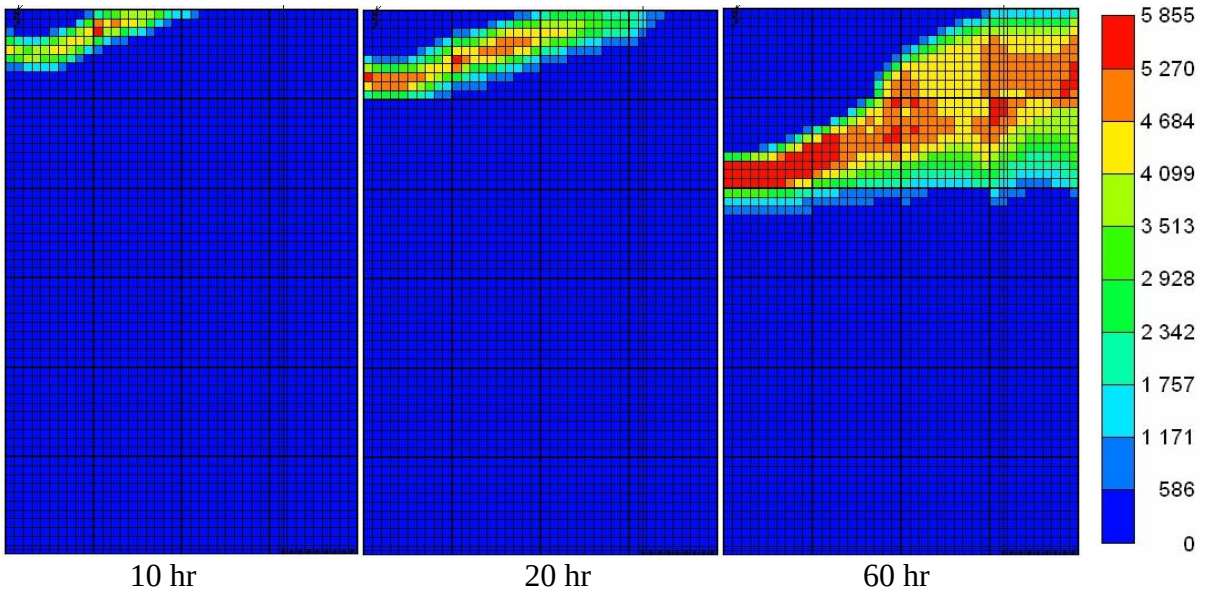


Figure 3.40. Coke concentration (gmol/m^3) profile for different simulation times.

3.4.4 Oil production

Oil production rate and the cumulative oil produced are illustrated in Figure (3.41). Until 10 hr from the beginning of the air injection, oil production is negligible. This is the time necessary for the oil that has expelled from the matrix block at the top of the reservoir to reach the production well at the bottom. Then, there is a sharp increase in the oil production rate which may be due to the arrival of an oil bank from fractures. If we look at the oil saturation profile (figure 3.38), at the time of this sharp increase in the oil production rate, the oil bank is still far away from the production well, however the oil saturation in the fractures at the bottom of the system is very high. Then the oil production decreases slightly, which could correspond to the tail of the oil bank in the fracture. A second increase of the oil production rate occurs at about 60 hr, this is the time when the main oil bank reaches the bottom of the reservoir. A relatively constant production plateau remains until 140 hr and after this time the production decreases. This somehow constant production rate may suggest a heat assisted gravity drainage production mechanism. Cumulative oil production shows that about 84% of the initial oil in place is produced.

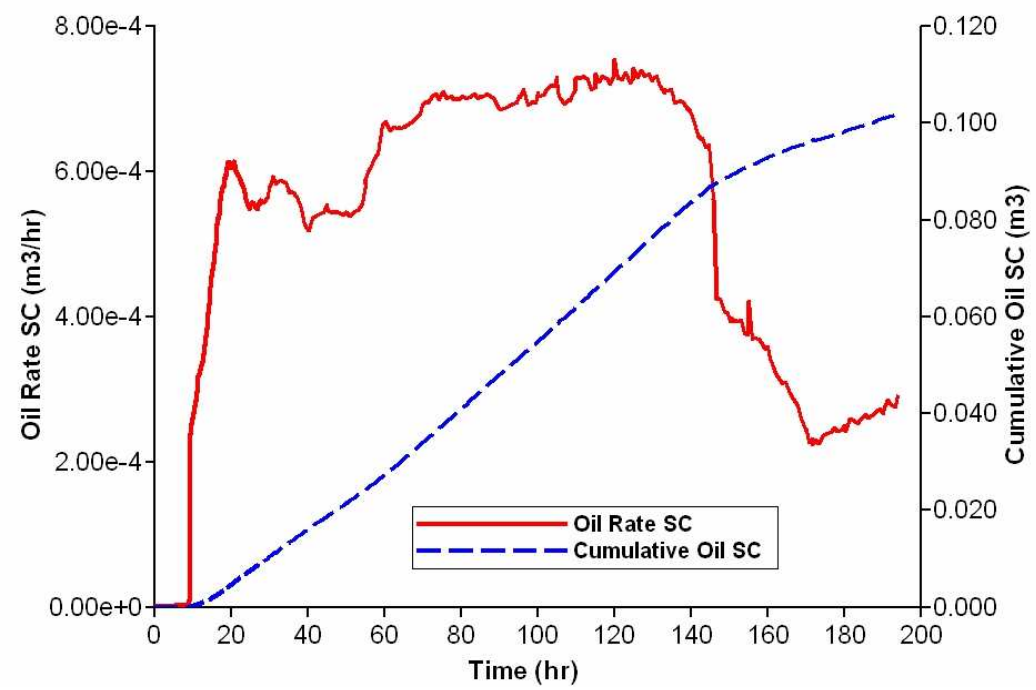


Figure 3.41. Oil production rate and the cumulative oil produced at standard condition.

3.4.5 Average temperature and mole fraction

As indicated in the second chapter in the study of two medium problems, the difference of the averaged parameter in two domains is an indicating factor to verify whether one or two equation models are suitable for upscaling or not. In the multi-block case, the averaged temperature and oil phase mole fraction in the fracture and matrix are calculated during the burning process. Figure (3.42) shows the average temperature for some blocks and the surrounding fractures. Here, the fracture average temperature, related to each block, corresponds to the average of the temperature in the fractures (horizontal and vertical) around that block.

It shows that, at early time, the average temperature in the matrix and in the fracture are the same in all the blocks mentioned in this figure which is in favor of a one equation, local equilibrium heat transfer model. When the combustion starts in the first block, this

temperature becomes higher in the matrix than in the fracture because of the liberated heat due to combustion in the matrix. At later time, these two temperatures become almost equal. This corresponds to the time that combustion front has already swept the first block. In the blocks number 3 and number 6, which are downstream of the process, at early time, the temperature in the fracture is slightly higher than the matrix for some time and then gradually the situation becomes vice versa. This is when the combustion front enters in the block and causes the average temperature in the matrix to become higher than in the fracture. At still later time, the average temperature in the matrix and in the fracture are equal in both cases which show that the burning has finished in these blocks.
In the blocks number 12 and 24, which are far from the ignition point, the matrix and fracture average temperatures are nearly equal. However for block number 12 the average temperature in the fracture is slightly higher than in the matrix. This is basically because of the fact that this block is closer to the ignition point and thus the fluids going in the fractures around this block are hot. Except in the first block, generally the average temperature in the matrix and the fracture are close to each other. It shows that the characteristic time for heat transfer in the matrix and in the fracture are of the same order of magnitude. This suggests that for upscaling this process in a fractured system, a one equation model may be enough accurate to simulate the temperature evolution.

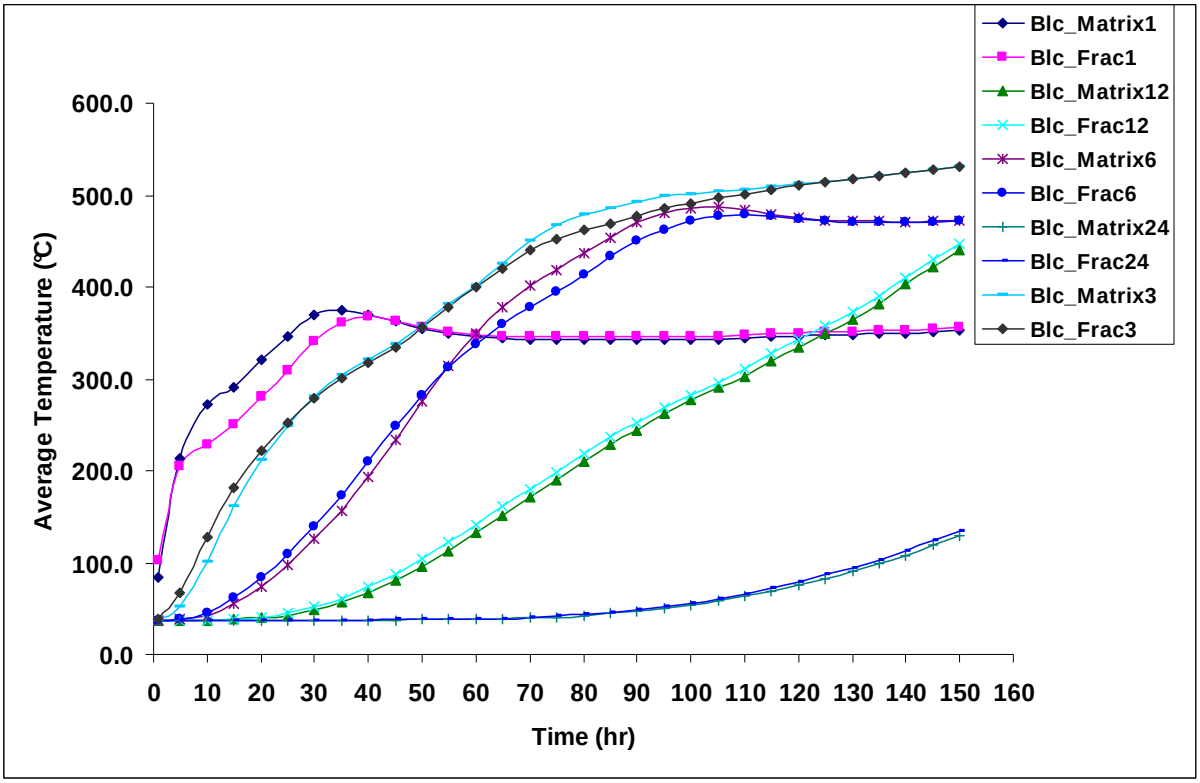


Figure 3.42. Average temperature in matrix blocks and corresponding fractures.

The same calculation as we did for temperature is done also for mole fraction. The average light oil mole fraction is presented in Figure (3.43). In the first and second blocks, the average mole fraction in the matrix and fracture (after 10 hr) decreases with time. The average mole fraction in the fracture is less than in the matrix. One can observe relatively the same behavior for the third and fourth blocks. In the fourth block the mole fraction increases slightly in the matrix which is as a result of the heavy oil cracking.

Figure (3.44) shows the light oil mole fraction in the blocks 9 and 10, which are far from the ignition point. As it is shown in these figures, the average mole fraction for matrix and fracture at initial time are equal, which shows that this part of the reservoir has not yet been affected by the combustion process. Later, the mole fraction increases both in the matrix and the fracture except for the fracture around block number 9. The reason is that part of the oil which drained from the above matrix into the fracture can be reimbibed in the matrix underneath this fracture. It should be also mentioned that in this simulation there is no capillary pressure thus the condition is more favorable for reimbibition.

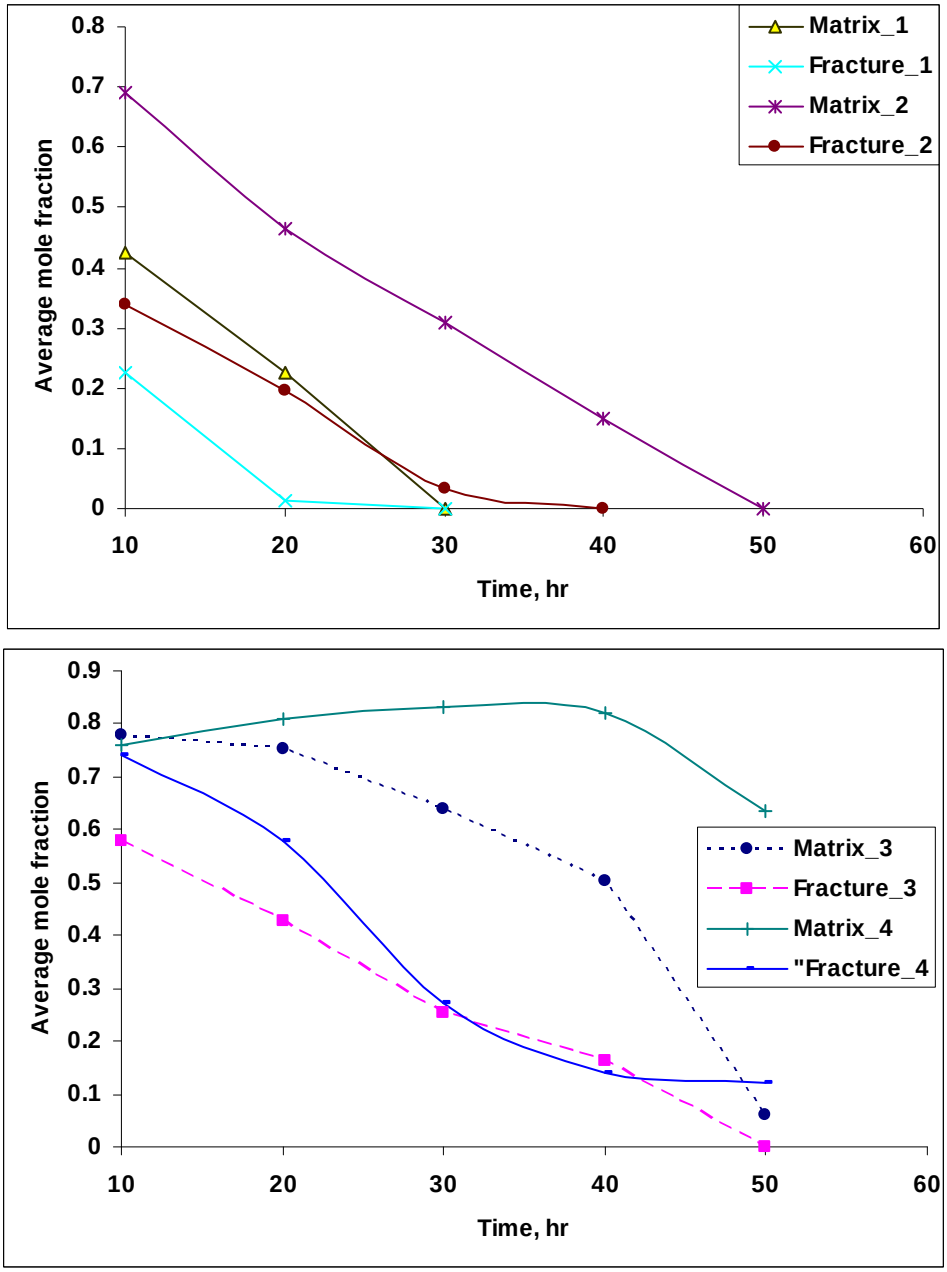


Figure 3.43. Average light oil mole fraction in matrix blocks and corresponding fractures.

In Figure (3.44), at initial time the difference between the average mole fraction in the matrix and in the fracture is not considerable, later, this difference increases. The important point about these two Figures (3.43 and 3.44) is that for all matrix and fracture pairs, the average mole fraction in the matrix and fractures are different during some periods of the burning

process. This behavior indicates that in order to represent the oil saturation in upscaled model one needs to consider the matrix and fracture separately and define an equation for each one. From this observation representing the oil saturation of both the matrix and the fractures in a single equation may introduce considerable error in the results.

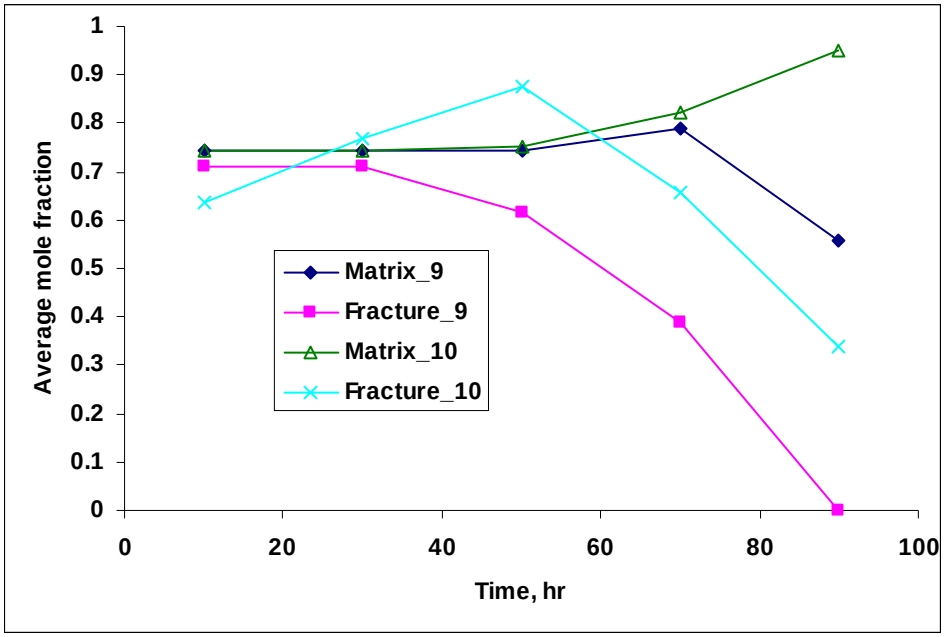


Figure 3.44. Average light oil mole fraction in matrix blocks and corresponding fractures (cont.).

Here we note that, in the present simulation model, pressure in the matrix and the fracture burning process was relatively the same for a constant depth, which is not surprising considering the high permeability of the matrix block (1270 md). Thus, these results are obtained for a condition where the oil production is governed mainly by the gravity and thermal effects.

3.4.6 Horizontal and vertical extension of the temperature

It is illustrated in the second chapter that according to the combustion literature, the combustion front is a position in which rapid changes happen (i.e., temperature, concentration). Our simulation at core and single block scales also confirmed this heterogeneity associated with these parameters. In the upscaling process the knowledge about the heterogeneity of the process under study plays a crucial role. Temperature and oil saturation profiles in the horizontal and vertical direction of the model can give us an idea about the extent of this heterogeneity. Figure (3.45) shows the temperature profile in the horizontal direction and Figure (3.46) shows this profile in the vertical direction. One can observe the presence of the peak temperature in both cases; however the temperature change in the horizontal direction is less significant than that in the vertical direction. Sharp temperature change in the vertical direction (more than 100°C in less than 0.15 meter) implies that any upscaling procedure should respect this change in which the characteristic length of the temperature change is less than the block scale.

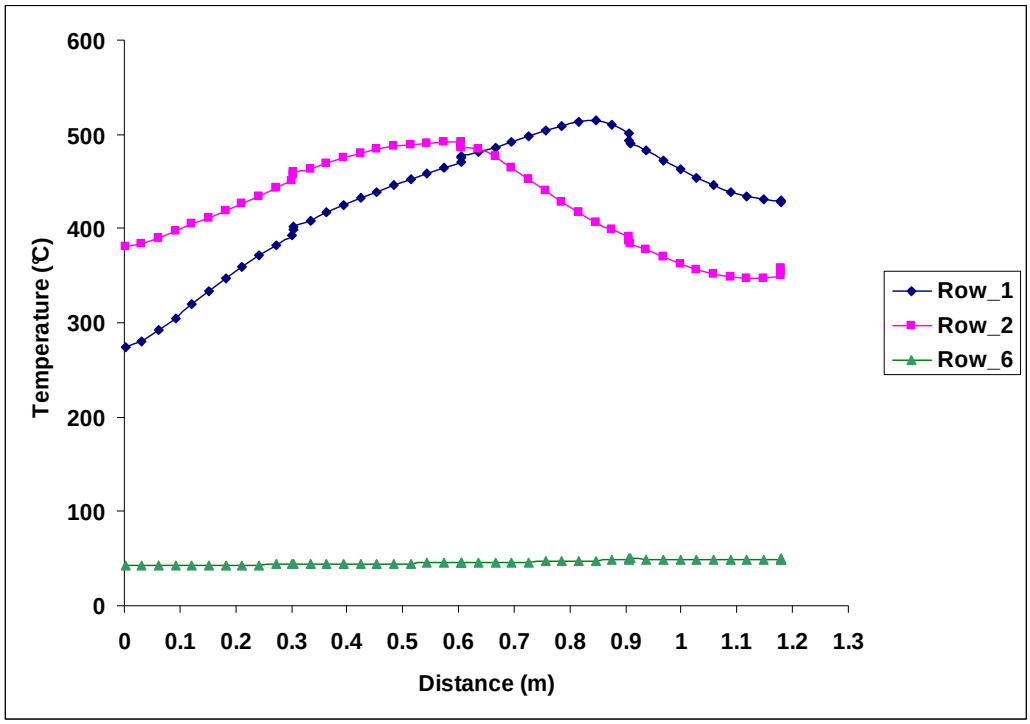


Figure 3.45. Temperature profiles in the horizontal direction.

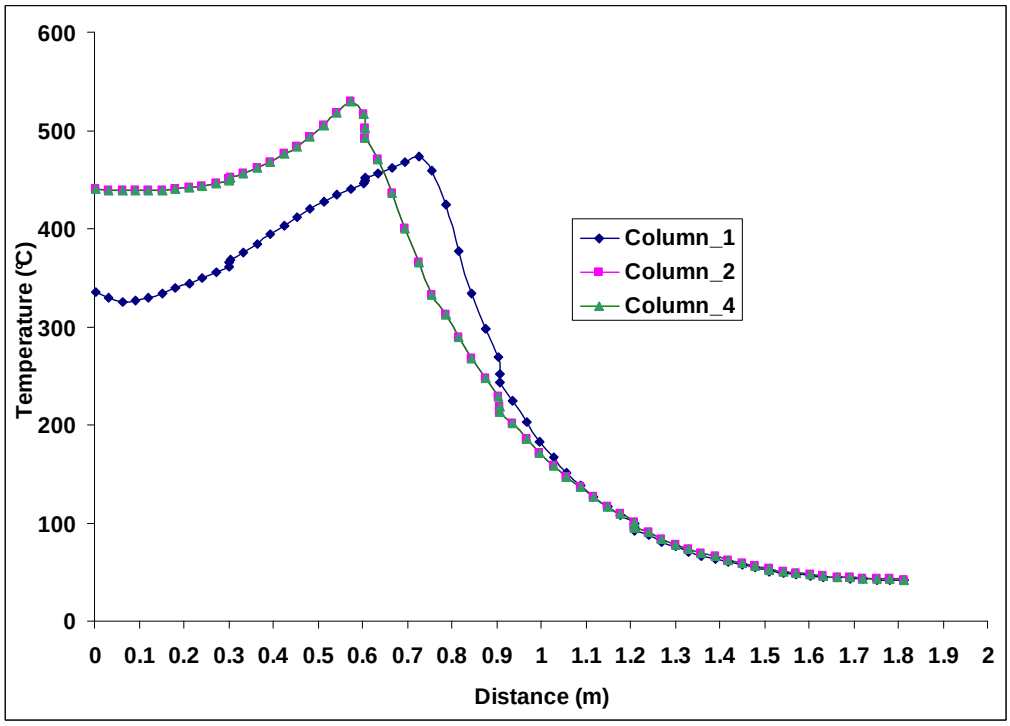


Figure 3.46. Temperature profiles in the vertical direction.

3.4.7 Summary

The simulation results show that the combustion front moves slower than the heat and mass transfer fronts. At the beginning of the process where the combustion front is developing, the oil saturation and temperature profiles are inclined but, after that, they become horizontal. However, the high temperature side of the temperature profile is still inclined. Production gases tend to move toward the upper part of the reservoir. This behavior causes the development of a water bank not necessarily at the downstream of the combustion process but rather detached from it. About 84% of the initial oil in place is produced.

Average temperature in the matrix block and the corresponding fractures are relatively close to each other (except for the ignition block), which may suggest the application of one-equation model for upscaling. However in order to perform upscaling for this system one should be aware of relatively rapid change of temperature in a distance smaller than the block length. Average mole fraction in the matrix and the fracture indicate that, one may need a two-equation model to represent the mass transfer in the upscaled model.

Chapter 4. Experimental analysis of ISC in fractured carbonates

This chapter presents the results of the experimental part of this thesis. The main reason for performing these experiments was to verify core simulation results and to obtain better understanding of the ISC process in the real world.

As mentioned in chapter two, we found only two experimental works in the literature concerning the ISC in fractured systems, which contain relatively detailed information about the experimental procedure. These studies have been done by Schulte and De Vries (1985) and Greaves et al. (1991). In both of these works, it is found that the combustion front can propagate in the fractured system. Greaves et al. (1991) applied the operating pressure ranging from 483 to 1724 kPa but the operating pressure is not mentioned explicitly in the work of Schulte and De Vries. However, the maximum working pressure of their experimental setup was 4000 kPa. We found also two other works with less details (Miller et al. 1983 and Awoleke 2007) where the authors indicate that the presence of severe heterogeneities prevented the combustion front to propagate through the fractured core. The operating pressure in the first work (Miller et al.) was 140 kPa and the corresponding value in the second one (Awoleke) was 700 kPa. The importance of mentioning the operating pressure is that most of these works are done at relatively low pressure condition. These somehow controversial results indicate that our knowledge about the ISC in fractured systems is not enough mature; even the propagation condition at laboratory scale is a matter of debate.

We have done two types of experiments: combustion tube tests and kinetic cell analysis. The main part of the work is the combustion tube runs. Several experiments were done to investigate the propagation of the combustion front in a fractured core, while the kinetic cell study was mainly to identify the qualitative influence of the presence of fractured carbonate porous medium on the kinetic of the combustion. We also used the kinetic cell results to adjust the kinetic parameters in our simulation study. The aim of this simulation work is to verify whether we can reproduce, at least qualitatively, the experimental observations of the combustion tube. These results are presented at the end of this chapter.

4.1 Material and methods

4.1.1 Experimental set up

The main elements of the experimental set-up are the combustion tube and the kinetic cell shown in Figure (4.1). The combustion tube and the kinetics cell are connected to a gas analyzer, traveling thermocouple, and data logging system. Two high pressure cylinders provide the injection gases (air or nitrogen). Injection gas goes through a series of filters (0.2 to 10 micrometer) before its flow rate is metered and controlled by a mass flow controller (Brooks 5058E). Then it is injected either into the combustion tube or into the kinetic cell. At the outlet of the combustion tube, liquid is separated from the gaseous products. This separator is equipped with two valves which allow collecting the produced oil during the burning process. The gas stream leaving the separator is cooled by a water condenser and dehumidified using a drierite column. A back pressure regulator is placed to control the pressure both in the combustion tube and the kinetic cell experiments. The effluent gases pass through a second gas flow meter. This flow meter is used to ensure proper sealing of the system. A part of the effluent stream flows through two acid scrubbers containing potassium permanganate and the other part is vented. The scrubbed effluent is then directed to a Xentra gas analyzer (model 4200). The gas analyzer measures oxygen, carbon dioxide, carbon

monoxide, and methane concentration once per minute. The effluent gases from the kinetic cell pass also through the water condenser and the rest of the passage line is the same as for the combustion tube.

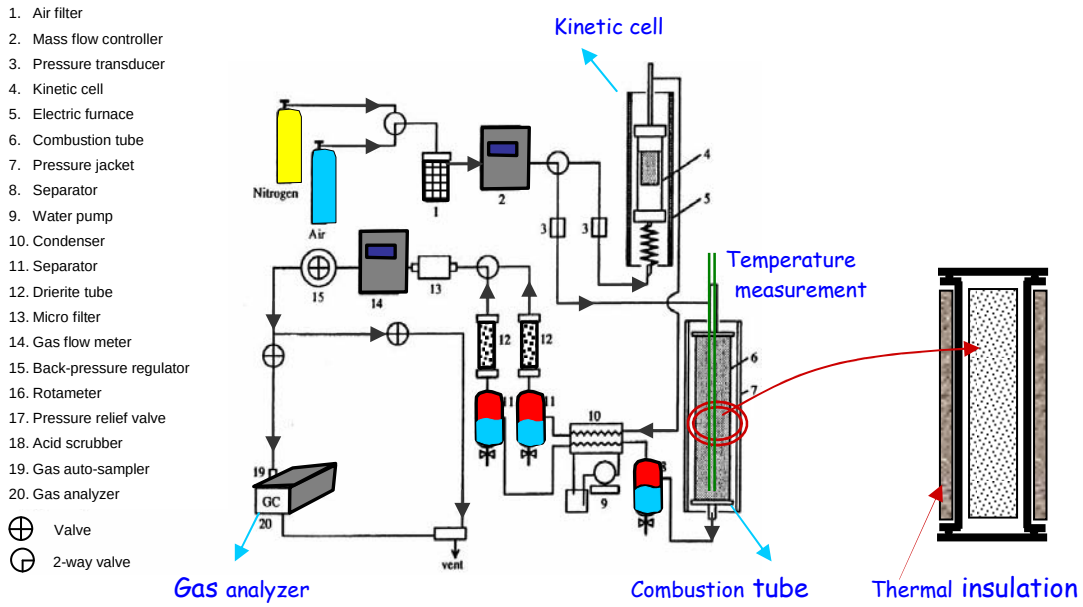


Figure 4.1. Schematic of the experimental setup (taken from Castanier and Brigham 2003).

Temperatures are recorded every centimeter along the length of the tube using a "thermal well". The thermal-well is a 1/8 inch (0.32 cm) stainless steel tube, few centimeters longer than the tube of which one end is closed and the other end is open in order for the thermocouple to be able to travel within the tube. The closed end of the thermal-well is placed in the tube and the other end goes through the upper flange and three-way injection line at the top of the tube. A special connection closes the space between the injection line and the thermal-well to keep the sealing of the system. In this way the inside of the thermal-well tube becomes completely isolated from the combustion tube inside. However, heat can pass through and be measured by the thermocouple placed inside the thermal-well.

In this experiment, the thermocouple was of J-type. In the case where the tube was filled with a homogeneous sand pack, temperature was measured in the tube centre and in the case of a fractured system it was measured in the fracture. During the kinetics cell runs, temperatures were measured in the centre of the cell.

The combustion tube is made of stainless steel (316) with a wall thickness of 1.3 mm. It is 1.0 m long with an inner diameter of 7.5 cm. An image of the combustion tube is shown in Figure (4.2). The maximum pressure limit of the combustion tube is 1360 kPa (~200 psi). During the experiment, this thin walled tube is placed inside an insulated explosive-proof jacket. For homogeneous experiments, the tube was packed with a multiphase mixture of sand, clay, oil and water. The composition is given in Table (3.5). Hereafter, we call this mixture the "oil-sand" mixture. Mixture composition was the same for both the kinetic cell and the combustion tube. For heterogeneous runs, the porous core was initially saturated with water and oil using a special designed core holder and then mounted into the combustion tube. The preparation of the oil-sand mixture and the saturated core is presented later.

We used the Wilmington heavy oil with 15 ° API. The viscosity of this oil at 49°C is 117~223 cp. The same procedure was done to saturate small cores for kinetic cell experiments. All

cores used in this study were made from Berea sandstone with average porosity and permeability of 20% and 100~200 md respectively.

During the combustion process, a traveling thermocouple measured the temperature as a function of time and distance from the tube top. A measurement interval of 1-5 cm was generally used depending on the temperature profile and front velocity. The kinetics cell is a thick-walled stainless steel (316) cylinder that is 13.3 cm long and 4.8 cm (O.D) in diameter (figure 4.3) situated inside a cylindrical furnace. The furnace temperature is controlled according to the desired heating procedure. Air is injected from the bottom of the cell. Prior to injection, air flows through coiled 3.2 mm tubing and is preheated. The maximum working pressure of the kinetics cell is 68 atm (~ 1000 psi).



Figure 4.2. Combustion tube image, left: in horizontal position with electrical heater attached to the far end, right: in the vertical position.



Figure 4.3. Kinetic cell image with the heating coil at the bottom.

4.1.2 Oil-sand mixture preparation

To prepare the oil-sand mixture, a desirable amount of dry clean sand (mesh 60) was weighted according to the composition presented in Table (3.5) and then carefully mixed with the clay (powder) in a pot. The mixing was done manually. Then, water was added and the mixing was continued. In the last step, an electrical mixer was used while oil was added to the system. The mixing was continued for about an hour to obtain a reasonably uniform mixture.

Table 4.1. Composition of the porous medium in the kinetic cell.

Run	Weight (%)			
	Sand	Oil	Water	Clay
Homogeneous mixture	84	7	7	2
Carbonate	84	7	7	2
Consolidated core	93	5	2	-

The mass based compositions presented in this table correspond to 35 and 33% of the oil and water saturations in the oil-sand mixture respectively and 75 and 25% of the oil and water saturation in the consolidated core respectively.

4.1.3 Consolidated core saturation

To obtain the initial saturations in consolidated cores, the dry core was first covered by a stretch plastic film except from two ends, and then placed in a core holder. Figure (4.4) shows an image and a schematic of the core holder. The role of this plastic cover was to prevent the early breakthrough from the core surroundings during the water and oil injection and ensure a stable displacement. The design of the core holder also allowed us to use an overburden liquid (water) to prevent any oil and water passage from the core surroundings (between the core surface and the plastic cover).

At the beginning of the saturation procedure, the core holder was connected to a vacuum pump and the core was vacuumed for about 12 hours. Then, the connection valve with the vacuum pump was closed and the system was connected to a vessel containing distilled water in order to suck the water into the core by vacuum. The water connection valve was closed when no water was able to be further sucked by the vacuum. The core holder was positioned vertically and the water connection valve was connected to a water injection pump for further water injection. Water was injected from the bottom in order to have a favorable condition for a stable displacement considering the mobility ratio of air to water. The injection was done at low rate (1 cc/min) and approximately two pore volumes of water were injected. The pore volume of the core was calculated to be equal to the total injected water volume minus the produced water volume. In the next step the connection to water injection pump was replaced by an oil injection pump. Oil injection was done from the top of the core holder as mentioned previously, considering the fact that the oil density was lower than the water density. Oil injection was continued until the breakthrough point. We should mention that with this kind of heavy oil very stable displacement was observed during the oil injection. The produced water and injected oil volumes are recorded and used to calculate the initial saturations.

Before presenting the results, we want to emphasize that ISC tube runs in our study were relatively exploratory as our experimental protocol was different from what we found in the literature (Schulte and De Vries 1985, Greaves et al. 1991 and Miller et al. 1983). The main difference is the way in which we did the thermal insulation of the tube. Thermal insulation is necessary to minimize the heat losses from the tube wall in order to perform the experiment as close as possible to an adiabatic condition. In the literature, hot-guard devices were used, i.e., electrical heaters were placed all along the tube in combination with a controller to heat the tube surface (during the ISC experiment) in order to compensate for heat loss to the

surrounding. Instead, we used an efficient insulation material to minimize heat losses. The disadvantage of the hot-guard devices is that some undue heating may occur because of the fact that the width of the heating element is usually larger than the combustion front thickness. For example, Greaves et al. (1991) used 11 heating elements for a tube of 76 cm long which gives a length of about 8 cm per each heating element.

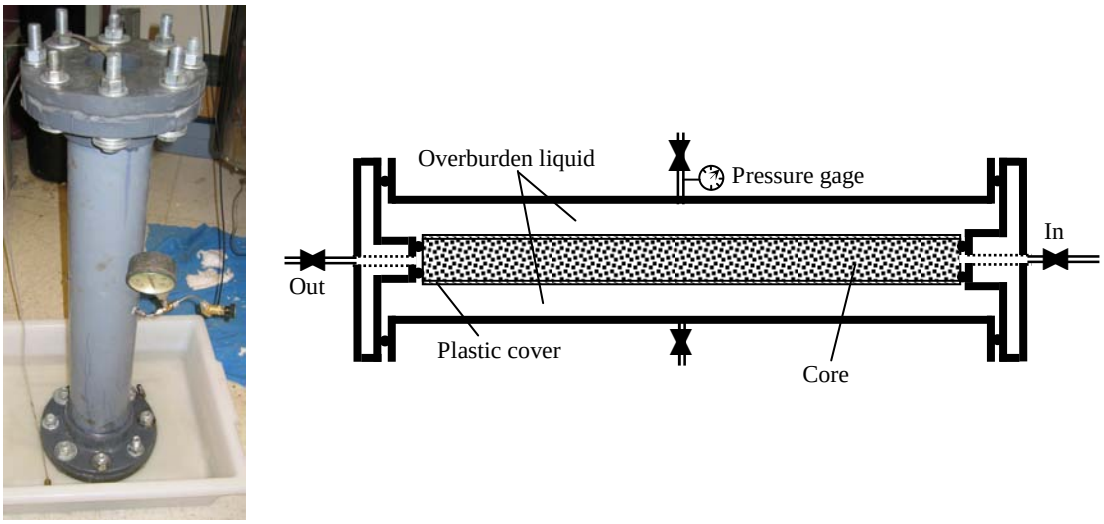


Figure 4.4. Core holder image (left) and a schematic of the coreholder (right).

The thickness of a typical combustion front is less than 5 cm (based on our observation in a homogeneous experiment). When the thickness of the heating element is larger than the front thickness, extra heat may be added to the system by electrical heaters. On the other hand, using thin (~1 cm width) heaters where each heater needs two thermocouples (one inside and another outside the combustion tube) make the experimental procedure very complicated and sometimes not feasible. In our study design, we did not add any heat (except the initial heating needed for ignition) during the combustion process to verify if the combustion is self-sustained or not.
Another important feature of this setup is the temperature measurement method. Unlike the previous studies on fractured ISC in which some fixed thermocouples were placed inside the tube, here we used a traveling thermocouple. This feature permits us to measure the temperature wherever along the tube center axis or along the fracture, which leads to more flexible and repeatable measurement as well as better localization of the combustion front position. This method also requires less thermocouples.

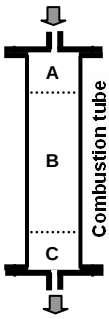
4.2 Combustion tube experiments

A summary of all tube runs is presented in Table (3.6). We have done one ISC tube test using oil-sand mixture inside the tube. This run is considered as combustion in a homogenous system and also as a base case to identify the general behavior of this oil under an ISC process. All other tests were conducted using an heterogeneous medium inside the combustion tube. To reach the ignition temperature in all runs an electrical heater was used and during its operation (about 3 hrs) nitrogen was injected into the tube. When the ignition temperature was reached (about 450 °C in the tube/ core centre) nitrogen was replaced by air.

Table 4.2. Experimental condition for tube runs.

Run	Inj. Rate (l/min)	Oxygen (%)	S_{oi}	S_{wi}	Length A*(cm)	Length B*(cm)	Length C*(cm)	Frac. width (mm)
1	2	21	35	33	-	-	-	-
2	2	21	>50	-	18	47	15	5
3	1	21	68	32	10	50	20	1
4	1	21	70	30	0	50	30	5
5	1	60	67	33	0	50	30	5
6	1	21	35	33	0	50	30	-

*: A, B and C position are shown on the combustion tube image.



4.2.1 Combustion in a non-consolidated porous medium

Homogeneous porous medium

A conventional ISC tube test was done using a non-consolidated porous medium (run 1). The combustion tube which is shown in Figure (4.2) consists of four flanges and a thin wall stainless steel tube. Two of these flanges are welded to each end of the tube and the other two removable flanges are attached to each of the fixed flanges with 12 bolts. A high pressure metal connection is provided with each of the removable flanges to connect the injection gas line to the tube at the top of the tube and the bottom of the tube to the separator. There is a metal gasket between each flange pairs to provide the sealing during the operation. Before filling the tube, a metal screen is glowed to the interior side of the flange to prevent any sand carry over into the production line and the separator. Then the removable flange is attached to the fixed flange at the end of the tube and the tube is positioned vertically. Figure (4.5) illustrates the tube composition for this run.

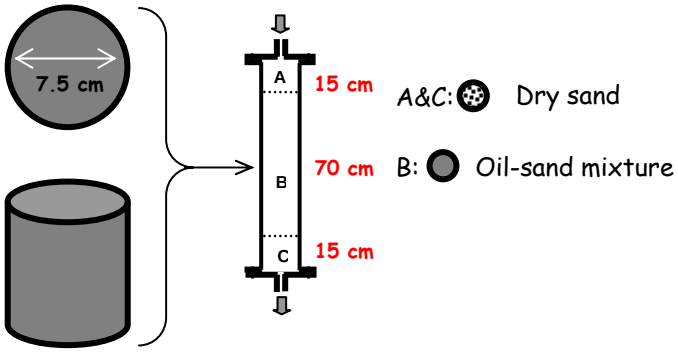


Figure 4.5. Combustion tube composition, run 1.

The tube was filled with the oil-sand mixture in the following way. The first 15 cm of the tube bottom was filled with the dry coarse sand (average 20 mesh) to prevent the possible blockage of the production line with the fine sands in the oil-sand mixture. Then, the thermal-well was placed in the tube centre and the oil sand mixture was charged into the tube. Another 15 cm at the top of the tube was also filled with the dry coarse sand to uniformly distribute the injected gases (especially air) on the tube cross section. When the filling was finished the top flange (removable) was placed and attached to the fixed flange by bolts. Then the tube was pressure tested for any leakage using nitrogen.

The electrical heater was placed on the tube wall (outer side) at the same level as the interface of the oil-sand mixture and the coarse sand at the top of the tube. The heater thickness was approximately 5 cm. Then the tube was carefully covered with the insulation sheets. Finally the combustion tube was placed inside the explosion-proof jacket and on the top it was connected to the injection line and from the bottom to the separator.

Injection starts with the nitrogen and at the same time the electrical heater is turned on. The injection rate is the same as the desired air injection flow rate. Once the ignition temperature reached, the nitrogen is replaced by oxygen. The temperature which corresponds to the temperature at the time of the ignition is measured along the tube. This procedure is repeated in all experiments to achieve the ignition condition. Next temperature measurements are done at about 30 minutes time intervals. The exit gas composition is recorded continuously by the gas analyzer. Air injection is replaced by nitrogen injection when the combustion front reached a position near (about 20 cm) the tube bottom.

Figure (4.6) shows the profile of the gases at the tube outlet. Air injection starts at 90 minutes and about 10 minutes later CO_2 concentration increases up to 14% which indicates that high temperature combustion was established inside the tube. The high initial value for CO_2 production rate could be due to higher fuel content produced during the operation of the electrical heater. Small fluctuations in the CO_2 profile may be due to small heterogeneities in the sand pack. The CO profile also illustrates a stable condition during the air injection. Methane production which is also an indication that the cracking reactions starts before air injection and reaches its maximum (5%) right after the air injection starts. Then after that, methane concentration decreases and remains less than 1% during the burning process. The initial increase in methane concentration may be due to the high temperature condition reached at the beginning of the air injection which, in turn, caused more cracking reactions to take place. Another thing that may have a contribution to lower methane concentration during air injection compared to nitrogen injection is that part of the liberated methane reacts with the oxygen in the gas phase. Oxygen concentration in the effluent gases is almost zero, except for the points where there is a fluctuation. This confirms that approximately all injected oxygen was consumed by the combustion process.

The temperature profile along the tube centre shown in Figure (4.7) also proves that the high temperature combustion front has traveled all along the core. The profiles shown in this figure are for the time after which the air injection starts. The initial high temperature (at 20 and 55 min) may be explained by the same reason as mentioned for high initial CO_2 concentration. After this initial high temperature period, temperature profiles show a relatively stable condition where the average peak temperature is around 450 °C and the average front velocity is calculated (based on the peak temperatures) to be about 20 cm/ hr.

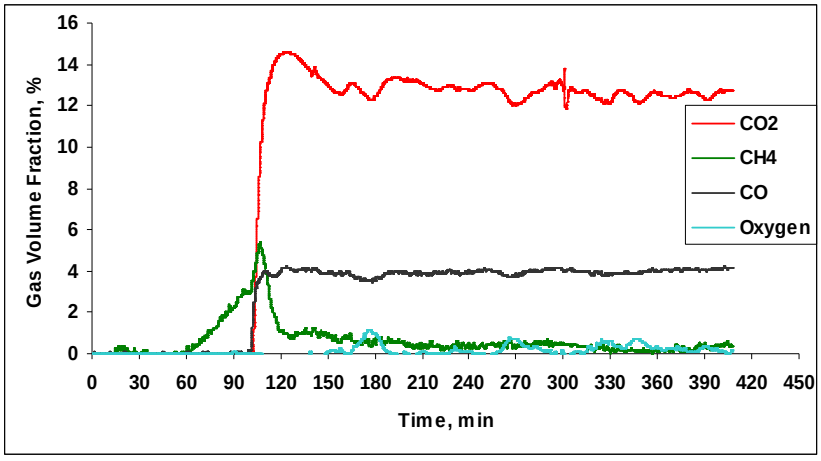


Figure 4.6. Gases profile at the exit of the combustion tube, run 1.

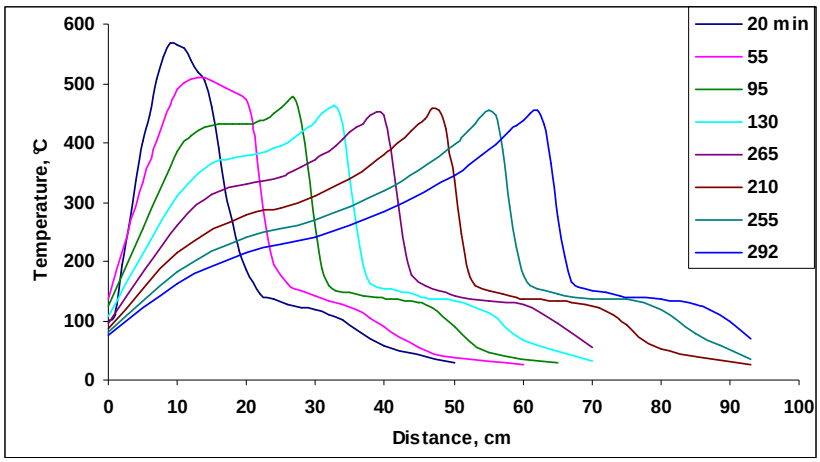


Figure 4.7. Temperature profile along the core centre, run 1.

Sharp temperature decrease across a small distance (about 5cm) ahead of the combustion front indicates a situation which is closer to the reaction leading condition (see chapter 2). Presence of a steam plateau which corresponds to the horizontal part of the temperature profile just ahead of the peak temperature (right side) is also another important observation. According to the steam table the temperature of the saturated steam at 100 psi (680 kPa) is about 169°C. The beginning of the steam plateau in Figure (4.7) corresponds to a temperature of about 160°C which also confirms the presence of the steam plateau.

Heterogeneous porous medium

To study the effect of heterogeneities in a non-consolidated system on the ISC process, an experiment was designed in which part of the combustion tube was filled with two porous media of different permeabilities. In this experiment the combustion tube was filled in the same manner as the previous experiment except that 40 cm of the homogeneous oil-sand mixture at the top of the tube was replaced by a heterogeneous mixture (run 6). In this heterogeneous mixture, as shown in Figure (4.8), a cylinder of about 6.3 cm of diameter at the centre of the tube was filled with the oil-sand mixture.

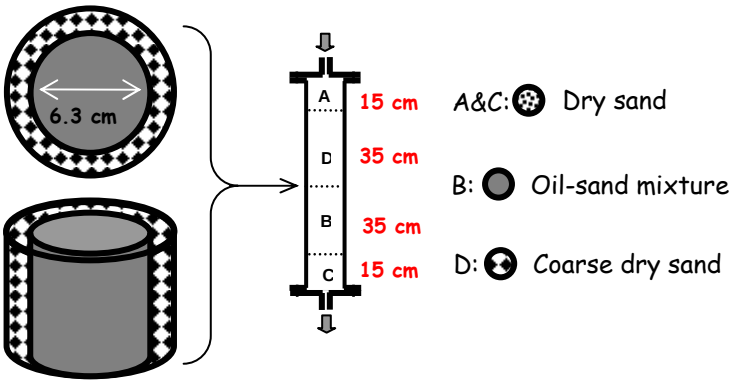


Figure 4.8. Composition of the combustion tube, non-consolidated heterogeneous experiment (run 6).

The annulus between this cylinder and the tube wall (0.6 cm opening) was filled with the coarse dry sand of about 10 mesh. In this way the permeability ratio between the two media is calculated to be on the order of 100 ($\frac{K_{coarse}}{K_{fine}} \approx 100$).

The effluent gases composition for this experiment is shown in figure (3.5). From this figure, we see that the ignition was done successfully as the initial CO_2 concentration increases up to 12% while oxygen production is very small. The value of 12% for CO_2 concentration is the same as what we observed in the homogenous experiment which shows a reasonable propagating condition. CO and methane concentrations also confirm a reasonable ignition condition. The CO_2 concentration then starts to decrease and after approximately 3 hours becomes stable around 7%. During this period the oxygen concentration increases and finally stabilizes at about 6%. CO and methane concentrations show also a small decrease.

After being stabilized for about 1.5 hours, the CO_2 concentration gradually increases and oxygen concentration decreases. This behavior shows that the combustion process was self sustained in this heterogeneous system.

The temperature profiles which are presented in figure (4.10) also confirms a good ignition condition where the temperature at the tube centre reached about 500 °C after 10 minutes of the air injection beginning. But the initial high temperature decreases with time until it becomes relatively constant around 350 °C. This value is considerably lower than the peak temperature observed in the homogeneous experiment (450°C). We may consider two reasons for that: (1) part of the injected oxygen does not react with the oil thus the generated heat is less than in the previous case, (2) part of the system does not contain any oil as the annulus was filled with dry sand, thus less fuel is available. The slopes of the temperature curves ahead of the front in the heterogeneous case are noticeably less than in the homogeneous case. It may be because of the effect of heat transfer though the annulus where the gas velocity is higher than in the oil-sand mixture. It is possible that part of the liquid was also passed through the annulus and caused some heat transfer. The presence of the coke like material in the annulus after the experiments confirms this hypothesis.

This experiment demonstrates that the combustion front can propagate in such a heterogeneous system. However one should keep in mind that the permeability of the oil-sand mixture is considerably high (few thousand Darcy) which may permit the oxygen to penetrate into the mixture and react with the oil.

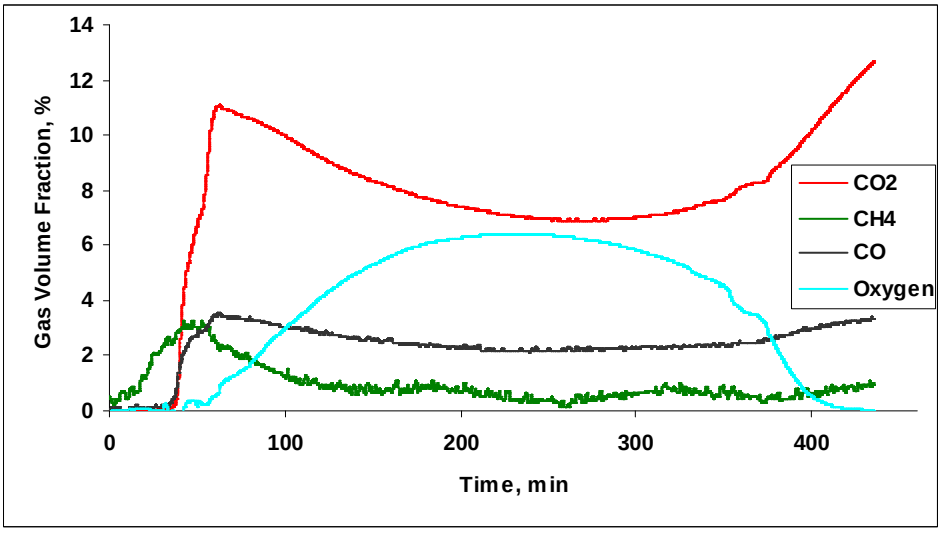


Figure 4.9. Gases profile at the exit of the combustion tube, run 6.

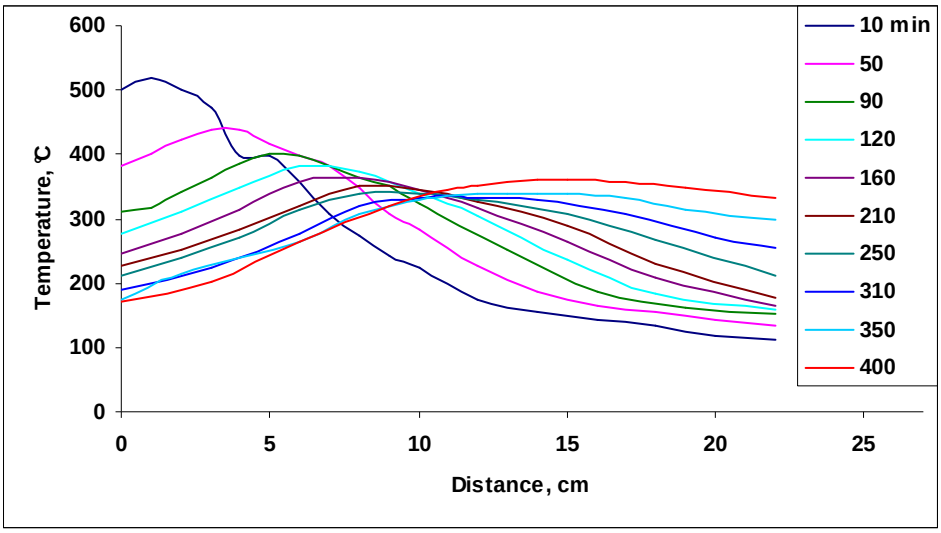


Figure 4.10. Temperature profile along the core centre, run 1.

4.2.2 Combustion in a consolidated porous medium

Small and large scale heterogeneity

We intended to start the consolidated experiments with the one in which, we thought, the condition was more favorable for the combustion front to propagate. That is why in this experiment the upper part of the tube, close to the ignition point, was filled with saturated core pieces and the lower part with a consolidated core. The tube is prepared in the following way: A saturated core of 50 cm long and 6.3 cm of diameter, was cut in two parts, then one part was further broken in to different pieces (5 cm average). In the other part, a 2 cm diameter hole was drilled all along the core in the core centre. Then the combustion tube was filled as it is shown in Figure (3.7), where 15 cm of the tube bottom was filled with a homogeneous oil-sand mixture, then the 25 cm core (with the hole inside) was placed on top of it while the hole inside the core and the annulus between the core and the tube wall was filled also with the oil-sand mixture. In the next step the core pieces were placed (corresponding to a total length of about 22 cm) and the spaces between them were filled with the oil-sand mixture. Another 18 cm on top of the tube was filled with the oil-sand mixture. This corresponds to run 2 in Table (3.6).

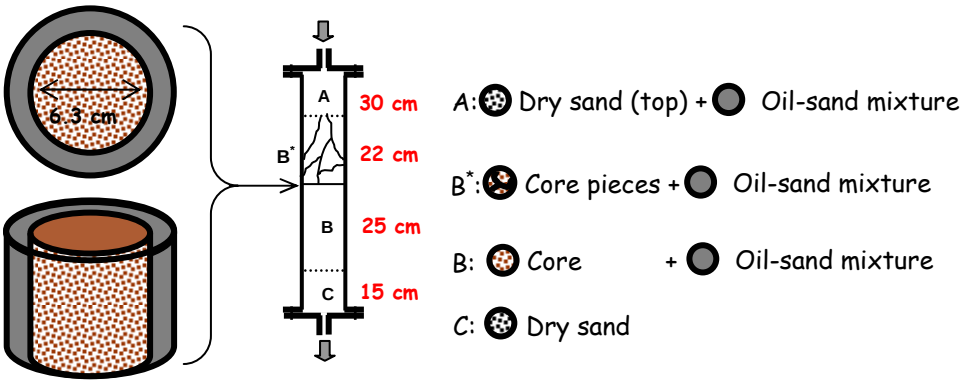


Figure 4.11. Composition of the combustion tube, consolidated experiment (run 2).

Combustion started in the oil-sand mixture on top of the core and the behavior of the combustion front was monitored when it traveled downward into the heterogeneous part of the tube. The composition of the effluent gases and the temperature in the tube centre are presented in Figure (4.12). From gases and temperature profiles, one can observe that the ignition was relatively successful (CO_2 concentration about 11%) however the oxygen concentration gradually increases after the ignition. This oxygen production could be related to the initial temperature which seems not to be high enough in order to have all injected oxygen consumed by the reactions. There is an increase in the CO_2 level (and also in the peak temperature), at the time equal to about 100 min which corresponds to the time that the combustion front is getting close to the heterogeneous part of the tube (core pieces). This temperature increase may be related to the presence of heterogeneity in the oil-sand mixture close to the core pieces or to the higher oil saturation in the core pieces (>50%) compared to the oil-sand mixture (35%). The methane profile also shows an interesting behavior in this section (core pieces) and that is: the average methane concentration (approximately 3%) is higher than that of the homogeneous experiment (<1%). We mentioned previously that methane production is the result of the cracking process, thus this observation could be an indication of the fact that oil cracking is more significant in the consolidated system than in the non-consolidated one. High temperature front had ceased when it had approached the large scale heterogeneity. The extinction situation is indicated by high values of oxygen concentration in the exit gas (>16%) or the low peak temperature (< 350°C).
This situation is associated with a considerable decrease in CO_2 level as well as methane and CO concentrations.
A post run image of this experiment is shown in Figure (4.13), which illustrates that the combustion front passed through the small scale heterogeneities but not through the large scale one. Another interesting observation is the form of the black area (coke) on the magnified image at the middle, which shows that the burning process was possibly governed by the flow of the oxygen from the high permeability areas around this piece into the core body (shown by horizontal arrows in the right side of the figure). The cone shaped (dotted red line) form of the black area may confirm this hypothesis. The temperature in this experiment is measured at the tube centre. The temperature profiles for this experiment show also the presence of the steam plateau but it is less significant than in the base case (run 1).
The combustion velocity is not constant during the burning process. If we calculate this velocity based on the peak temperatures, we find that the combustion front advances slowly at the beginning of the process (until 50 min). Then the front moves with relatively constant velocity (about 10 cm/hr) until 150 min. Then the front velocity decreases here after, where it is calculated to be approximately 5 cm/hr until 260 min.

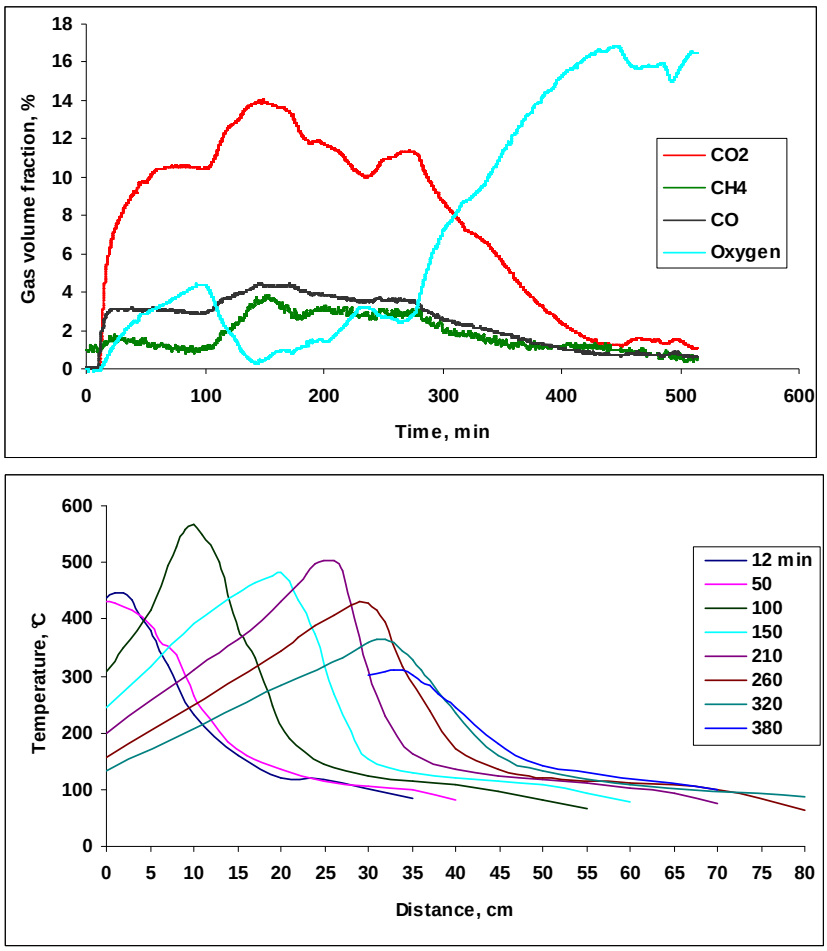


Figure 4.12. Gas analyzer results (top) and temperature profile along the core centre (bottom) for run 2.

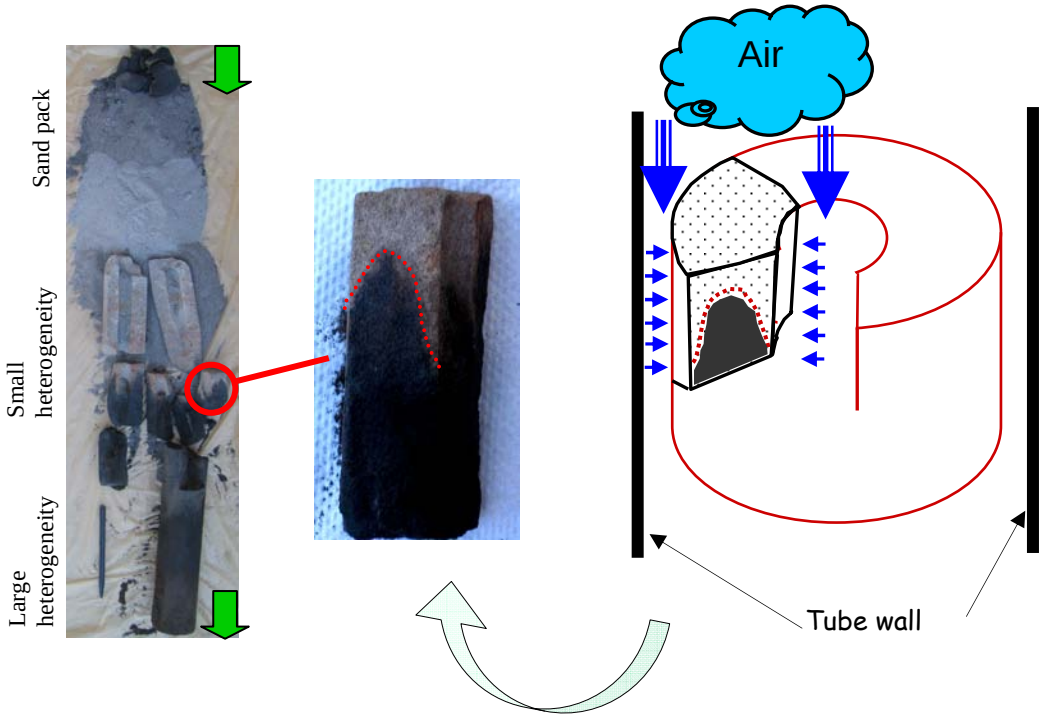


Figure 4.13. Post run image of run 2.

Effect of fracture permeability

Two different permeabilities for the fracture were applied in this experiment. We used also two different core diameters. This was mainly because of the available material during this experimental campaign. However, the same combustion tube was used in all experiments. In the first experiment, fracture width was 1 mm and it was completely empty (run 3). In the second experiment, the fracture width was 5 mm and it was filled with dry sand (run 4). In the first one, the electrical heater was placed so that the ignition started in the sand pack but, in the second one, it was directly started from the core. In both experiments, the high temperature front was not sustained (figures 4.14,4.15) and the high temperature after ignition (>500 °C) decreased below 350 °C after replacing the nitrogen by air. These results also show that, with an empty fracture, the extinction was faster than with a filled one. This is indicated by the time during which the oxygen concentration reaches high values (16 % >). This can be clearly seen in Figure (4.14) and (4.15) on gas profiles, i.e., the CO_2 concentration in the run 3 decreases faster than in the run 4.

Temperature profiles in the Figure (4.14) and (4.15) do not show a distinct steam plateau. We remind that the temperature in both of these cases was measured in the fracture. It may explain that the steam plateau was inside the consolidated core thus it had less significant effect on the temperature changes in the fracture.

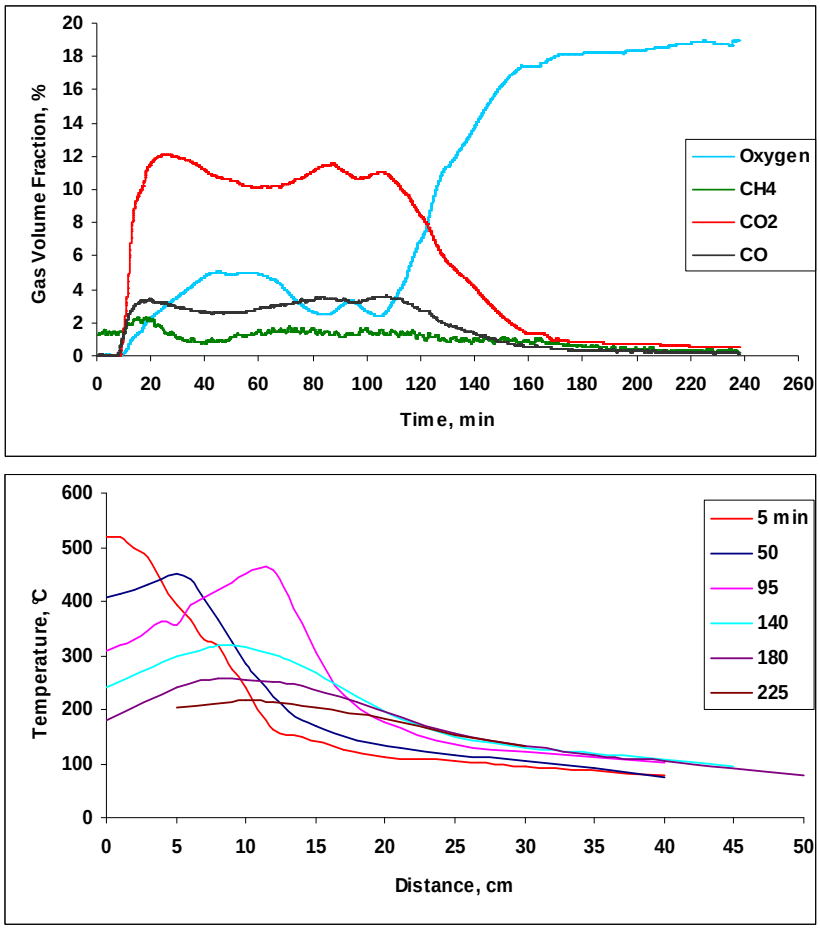


Figure 4.14. Gas analyzer results (top) and temperature profile along the core (bottom) for run 3.

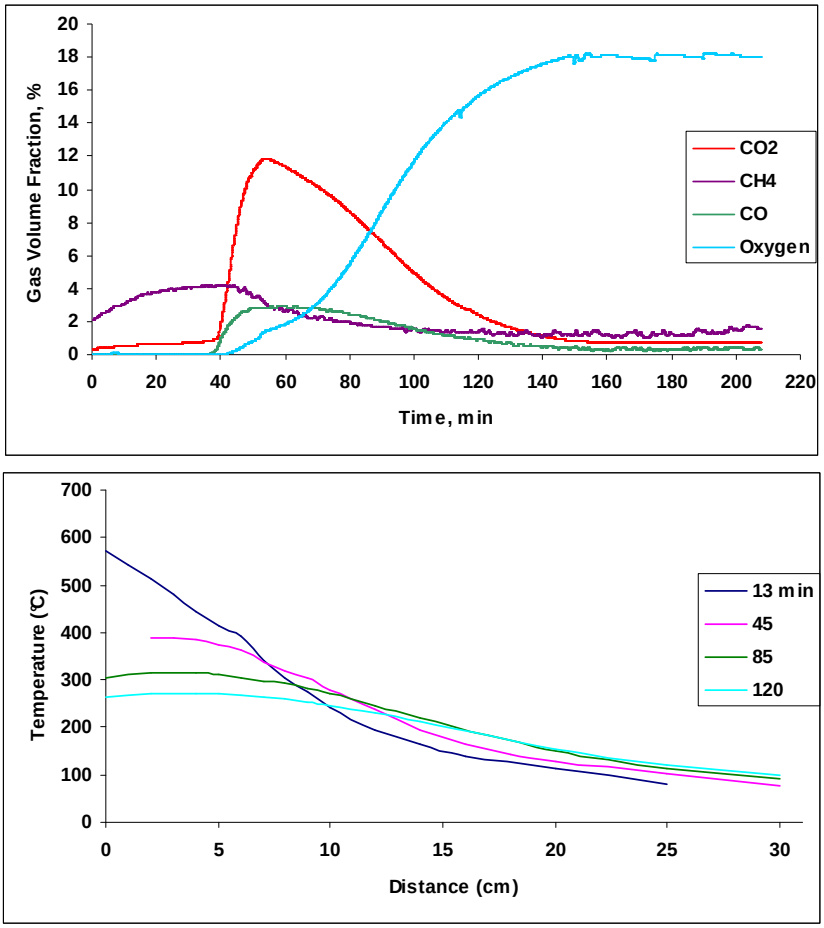


Figure 4.15. Gas analyzer results (top) and temperature profile along the core (bottom) for run 4.

Post-run observations showed that in the second case (run 4) while the combustion process was not sustained the combustion front had advanced a few centimeters (4 cm). The images are not presented here. This was not the case in the first test (run 3) where almost no high temperature front entered into the matrix. Presence of a sand layer (1~2 cm thickness) with high coke content on the top of the core was another indication that the combustion front could not travel from the sand pack to the core. That is why we decided to perform all next runs with the same core geometry as in the run 4. The presence of coke in the fracture in the second case revealed that some oil had been expelled into the fracture during the heating period and subsequent combustion.

Several other runs were done using normal air (21 % oxygen) and applying different parameters such as higher (2 l/min) and lower (0.5 l/min) air injection rates, oil-sand filled fracture and higher pressure (14 bar) inside the tube; none of them led to the propagation of a high temperature front. However, in some cases, for example higher pressure, the extinction was slower than the lower pressure experiment. In all cases, we improved the insulation layer around the tube to further decrease heat losses to the surroundings but it was found that this parameter was not play an important role in preventing the propagation. Post-run results demonstrated that considerable amount of coke was found remaining close to the high temperature front inside the core.

These results, considering both the high ignition temperature (>450 °C) initially provided by the heater and the use of an efficient thermal insulation, indicate that the reason for extinction could have been the lack of oxygen delivery into the matrix. The amount of oxygen which

enters into the matrix was limited due to low permeability of the matrix. That is why we decided to increase the oxygen concentration in the injected air.

Effect of oxygen diffusion

A run was done applying higher oxygen concentration (60 %) in the injected air (run 5). To do so, the normal air bottle in the experimental setup was replaced by an enriched air bottle which contained 60% of oxygen and 40% of nitrogen. The idea was to increase mass rate of oxygen diffusion into the matrix. Injection rate was 1.0 l/min and tube pressure was 1414 kPa. The results are presented in Figure (4.16). Here, one can observe that, after initial ignition in which the CO_2 concentration increases and reaches about 30 %, it decreases and after 150 min it becomes stable. After having been stable for about 100 min, it increases again. This second increase shows that the combustion in this case was self sustained because in all previous cases (with consolidated core), after the first decline it had never increased. The figure also shows a second decline in the CO_2 profile and further increase, which could be explained by the possible presence of the heterogeneities in the system (both in the matrix and the fracture). One can also observe that, even with the high temperature combustion (propagation condition), oxygen concentration at the exit is high (18 %).

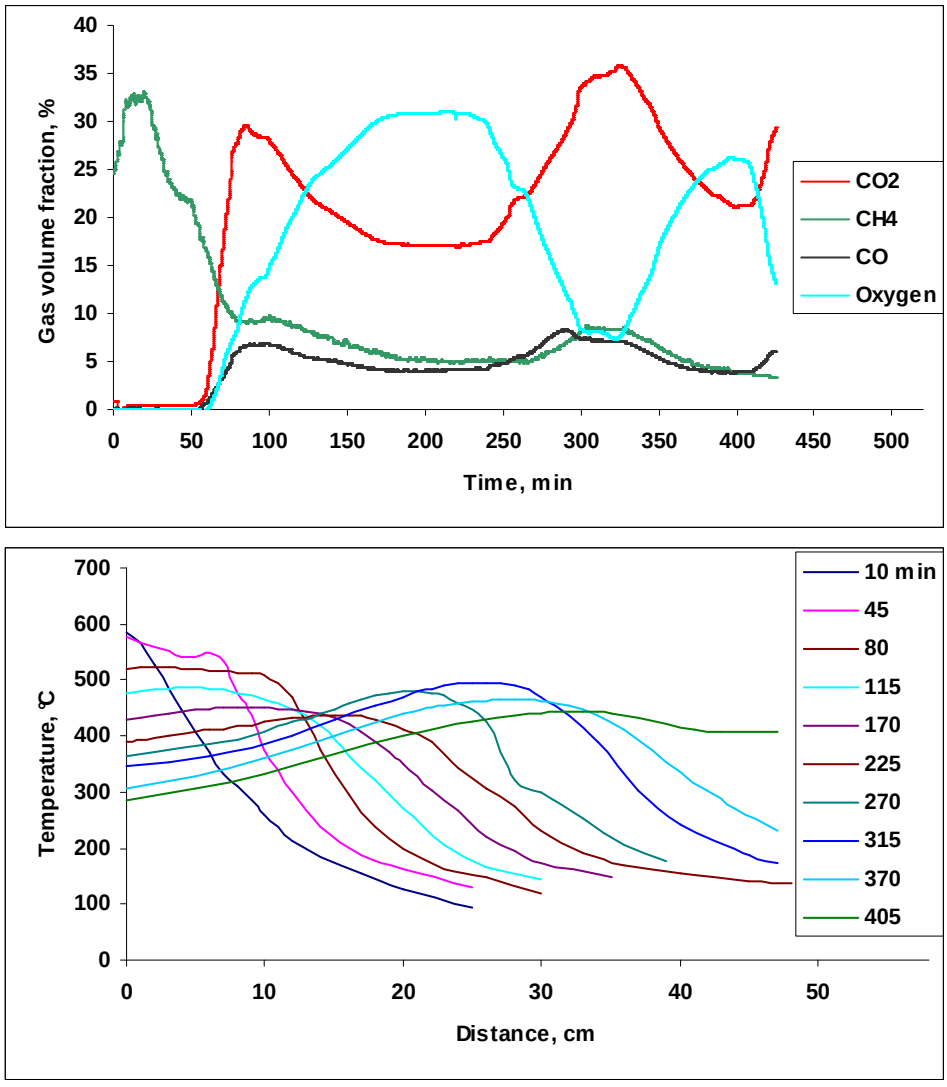


Figure 4.16. Gas analyzer results (top) and temperature profile along the core (bottom) for run 5.

The optimum condition under which the oxygen concentration in the exit stream becomes as low as possible should be determined using different values of oxygen concentration in the injected gas. This is crucial for the ISC process design in fractured reservoirs. The optimum condition could be found either by performing some experiments or doing simulation with a validated simulator.

The temperature profile inside the fracture (figure 4.16) demonstrates that a high temperature front was achieved and that it sustained during the burning process. Comparing this result with the temperature profile of the homogeneous case (run 1) indicates that the temperature profile in the homogeneous case is steeper than in this case, both ahead and behind the combustion front. This is because of the fact that heat losses from the porous matrix in a fractured system are less important than in the non fractured system. The fracture by itself acts as a barrier of heat loss for the matrix. Previous works also mentioned the same behavior (Greaves et al. 1991). The appearance of the steam plateau is less significant in this experiment compare to the ISC in a homogeneous system (run 1).

These results reveal that enriched air is necessary to obtain a self-sustained ISC process in the fractured system at low pressure. Here we emphasize that our experiments were done at relatively low pressure (max. 1414 kPa). However, performing the same experiments with high pressure one may obtain the propagation condition with normal air. The oxygen concentration in the fracture under a high pressure condition may be enough to provide a sustainable combustion. However, doing such experiments requires special equipment and the use of a sophisticated experimental procedure with possibly higher costs and longer time.

4.3 Kinetic cell experiments

As mentioned earlier, the target of the kinetic cell study was to qualitatively compare the effect of some parameters on the kinetics of the combustion process. The effect of calcium carbonate, which is inherently present in the fractured reservoirs, and the effect of consolidated matrix are studied. The effect of the consolidated matrix here is, in fact, replacing the oil-sand mixture by a consolidated core. Both of these cases are compared with a reference case where the porous medium inside the kinetic cell was an oil-sand mixture (non-consolidated). The composition of the porous medium in the kinetic cell is presented in Table (4.3).

Table 4.3. Composition of the porous media in the kinetic cell.

Run	Solid type	Weight (%)			
		Solid	Oil	Water	Clay
Homogeneous mixture	Clean sand	84	7	7	2
Carbonate	Pure $CaCO_3$	84	7	7	2
Consolidated core	Berea sandstone	93	5	2	-

4.3.1 Kinetics in a non-consolidated medium

Homogeneous mixture (base case)

In our first experiment, the kinetics of oil combustion in a non-consolidated system without carbonate was studied. The cell was filled in the following manner: first the cell cavity was properly cleaned with compressed air. Then, about 3 cm of the cell bottom was filled with dry coarse sand. The role of this sand pack is to uniformly distribute the air flow. Then the oil-sand mixture was charged into the cell. Then a thermocouple was placed at the cell centre and, finally, the cell was closed by putting the upper flange. At the end, the entire cell with the coiled tube on the bottom (see figure 4.3) was placed inside the furnace. Then, the furnace was turned on the cell temperature and the effluent gas composition were recorded. Figure

(4.17) shows the profile of effluent gases volume fraction from the kinetic cell. The oxygen profile shows the volume fraction of oxygen in the injection gas minus the oxygen volume fraction measured by the gas analyzer at the exit. Under the hypothesis of approximately equal mass in- and out flow rates, the resulted value is proportional to the oxygen consumption rate. The CO_2 and CO profiles are the mole fractions of these gases at the analyzer exit. These profiles show a conventional behavior of ISC kinetics in a porous medium (Fassihi et al. 1984, Audibert and Vossoughi 1991) which consists of two peaks in two different temperature ranges. The first peak corresponds to low temperature oxidation (LTO) and the second peak to high temperature oxidation (HTO).

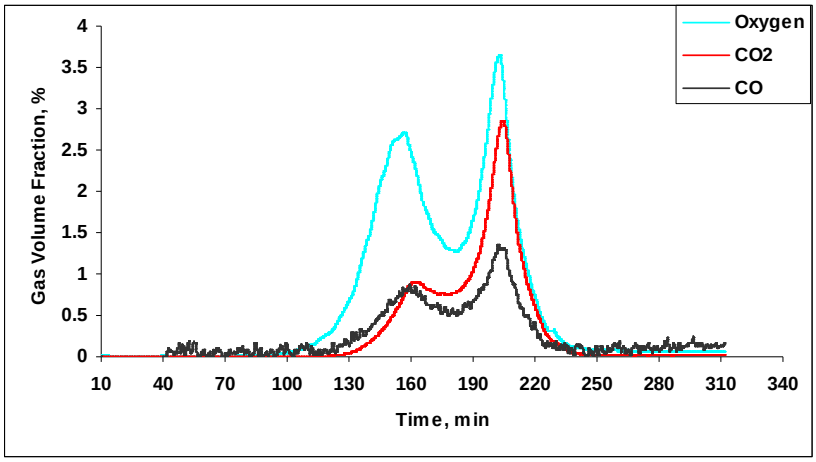


Figure 4.17. Kinetic cell results for homogeneous mixture (base case).

The temperature of the cell for this experiment is indicated in the Figure (4.18). In this figure, the second vertical axis shows the oxygen volume fraction (as indicated in figure 4.17). The temperature controller was programmed to linearly increase the cell temperature; however this profile is not completely linear. This could be due to some initial transient heat transfer effects and the fact that the stainless steel is not highly conductive to homogenize the cell temperature. Another important observation of this profile is the presence of two small peaks at about 158 and 204 minutes, which correspond to the energy release during the LTO and HTO reactions respectively.

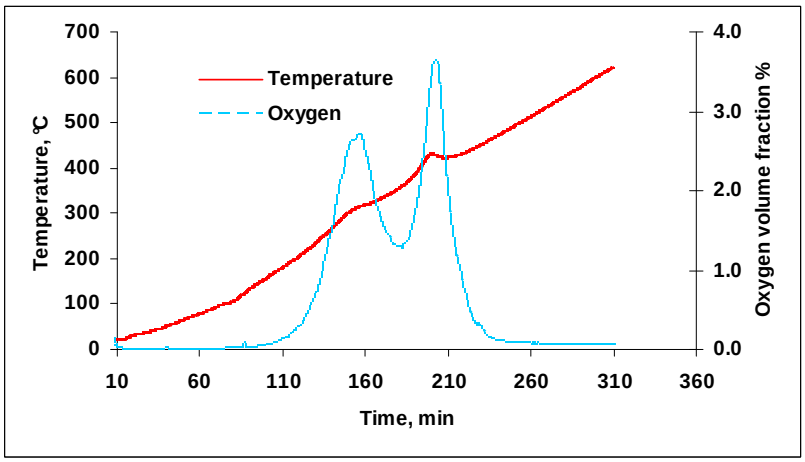


Figure 4.18. Temperature of the kinetic cell.

Effect of carbonate

In this experiment the oil-carbonate (with pure $CaCO_3$) mixture was prepared using the same protocol as for the oil-sand mixture. Figure (4.19) shows the volume fractions of gases produced from the kinetic cell for oil-carbonate mixture. A comparison of this figure with Figure (4.17) indicates that the kinetics is considerably modified. The HTO peak for oxygen consumption in the absence of carbonate is more significant than the LTO peak, but, in presence of carbonate, a reverse situation was observed. However, this is not the case for CO_2 production. For the LTO peak, it is less important than for the HTO peak in both cases. It seems that the presence of carbonate matrix favors low temperature reactions and, mainly those consume oxygen without significant CO_2 generation. In this figure the fluctuations associated with the CO profile makes it difficult to judge about the evolution of this profile, but the general trend shows that the CO content is slightly higher in the LTO peak than in the HTO peak. This trend is different from what we observe in the base case (Figure 4.17).

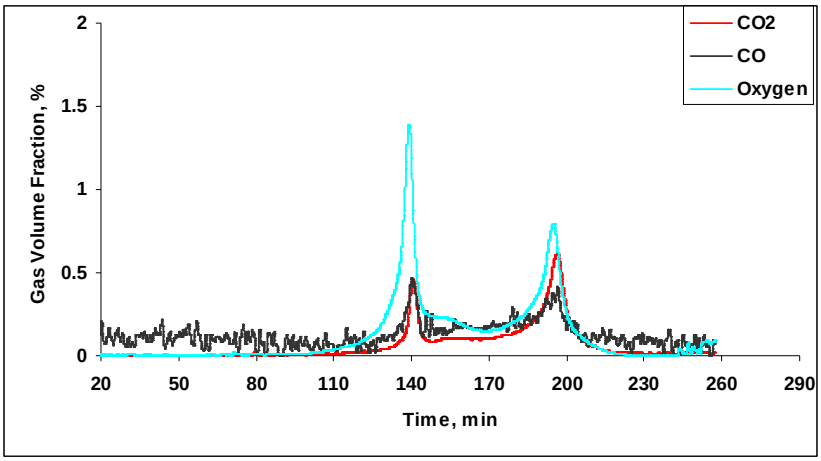


Figure 4.19. Kinetic cell results for the oil-carbonate mixture.

4.3.2 Kinetics in a consolidated medium

Consolidated matrix

In this experiment, we replaced the oil-sand mixture with a consolidated core. We applied the same procedure to provide the initial saturations as we did for the consolidated core in the combustion tube experiment except that, here, a small core holder was used. The core diameter was slightly smaller than the inner diameter of the cell, which provides an annulus around the core when it is placed inside the kinetic cell (figure 4.20). This small distance (about 1 mm) between the cell wall and the core outside diameter could be considered as a fracture which is shown in Figure (4.20). The bottom part of the cell was filled with dry sand. The kinetic behavior of the core is shown in Figure (4.21). Comparing this figure to the base case (figure 4.17), we can see that the low temperature peak has completely disappeared and the high temperature peak becomes more significant.

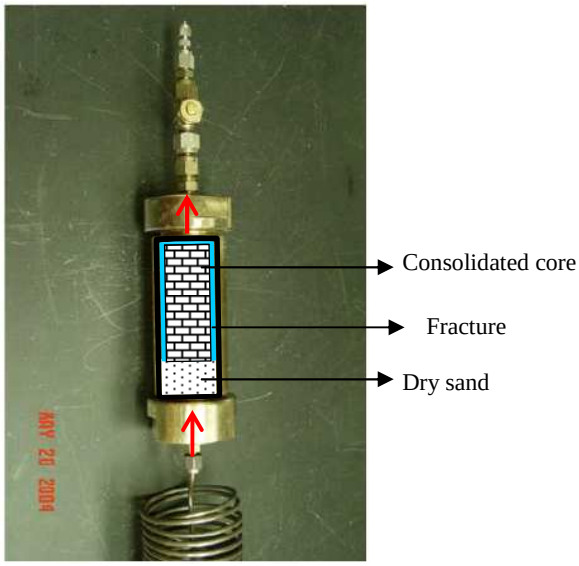


Figure 4.20. Kinetic cell composition in the consolidated core experiment.

These observations may indicate that the nature of oxygen delivery to the reaction zone is different for non-consolidated and consolidated systems. A possible explanation is that, in the former case, due to the high permeability of the porous medium which is also homogeneously distributed, enough oxygen is present for the reactions so the reaction kinetics is rate limiting. In the latter, the amount of oxygen which enters into the consolidated matrix is limited due to low permeability of the matrix. This makes the kinetics in the non-consolidated case to be constrained by limited supply of oxygen.
The low permeability matrix in turn does not allow the oil to be produced from it as easy as the oil-sand mixture. Thus, we expect that more oil, in the form of fuel, remains in the matrix, which, eventually burns at high temperature and makes the HTO peak more significant.

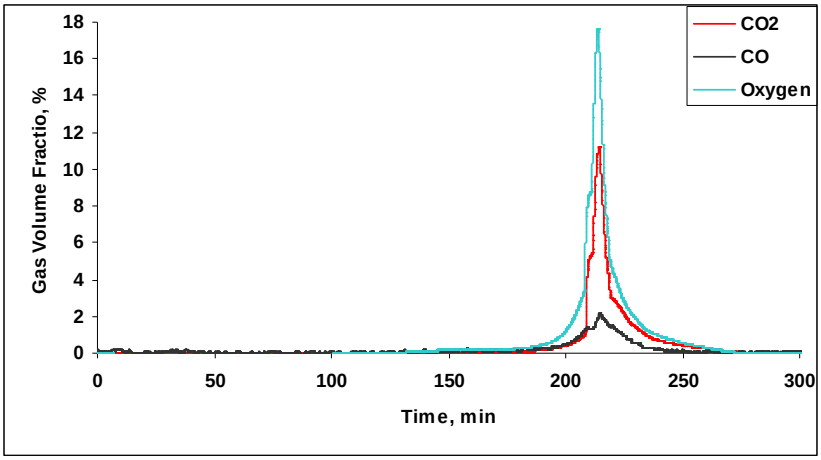


Figure 4.21. Kinetic cell results for consolidated core.

Core pieces

In another experiment in which the consolidated core was replaced by some core pieces (with average characteristic length of 1.0 cm), we observed the same behavior but less significant as we did with the entire core. In this experiment, a consolidated core was initially filled with water and oil according to the same procedure as we did in the consolidated experiment. Then, the core was broken into small pieces. These small pieces were charged to the kinetic

cell. The composition of the cell is shown in Figure (4.22) and the gas composition from the kinetic cell is illustrated in Figure (4.23). The LTO peak in this experiment is present unlike what we observed with the entire consolidated core but it is less significant than for the homogeneous experiment (figure 4.17). Comparing these three experiments, one can observe a trend where the LTO peak vanishes when the size of the consolidated matrix increases.
These results show that the combustion kinetics in a consolidated system can be different from that in non-consolidated system. This has to be taken into account for simulation of ISC in a fractured reservoir. We notice that these experiments should be considered as an observation step and we do not aim to derive a complete set of kinetic parameters based on these two experiments. However, we believe that these results are some evidences for an important modification in the combustion kinetics in fractured systems. More elaborated experiments are needed to fulfill the requirement of appropriate kinetic parameters in such a porous medium, which is beyond the scope of this study.

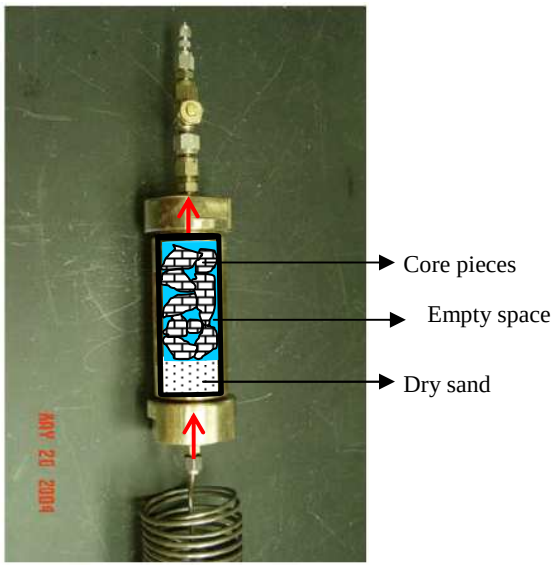


Figure 4.22. Kinetic cell composition in the core pieces experiment.

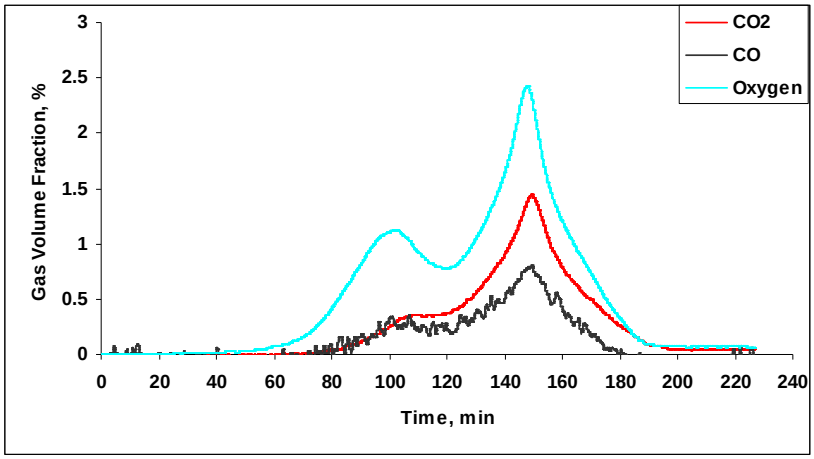


Figure 4.23. Kinetic cell results for core pieces.

4.4 Numerical simulation

In this part, we present the numerical simulation results obtained for the kinetic cell and the combustion tube using a commercial thermal reservoir simulator (STARS). These simulations could be seen as some preliminary results in order to verify the same tendency as we observed in the experiments rather than a complete history match work. This is because of the fact that the experimental work by itself was somehow exploratory, especially for the tube runs, considering the new experimental setup. Another important notice is that a thorough history match study calls for a complete set of input data for oil, sand, relative permeabilities as well as the reaction parameters. These complete sets of input data were not available in our study.

4.4.1 Kinetic cell simulation

The kinetic cell simulation was only done for the homogeneous case with the oil-sand mixture. For carbonate mixture and the consolidated case, the system is much more complex due to the complicated reaction scheme for carbonate and highly coupled transport and reaction for the consolidated case. In the case of consolidated core we may need a complete data set for the relative permeability and the capillary pressure curves in presence of the temperature change in order to be able to simulate the process with acceptable accuracy. Study of these two cases in more details calls for a separate study.

Starting with the dataset published by Kumar (1987) and modifying some input parameters, it was possible to reproduce the results obtained in the experiment. Modified parameters are the activation energy, pre-exponential factor, reaction heat, stoichiometry coefficients and the gas-oil K-value. The reaction scheme used in this simulation is presented in Table (4.4).

It is important to note that this reaction scheme is highly simplified compared to what actually happens in reality. The reason for this simplification is the limitation of the simulation time. Another important point is that, based on the initial model presented by Kumar (1987), LTO reaction in our model consists of the oxidation reaction of light oil which produces CO_2, water and energy. Thus any LTO reaction in which the oxygen participates in the hydrocarbon molecule and produces more viscous product was not considered.

Table 4.4. Reaction scheme used in kinetic cell simulation

5) Heavy oil cracking	***HO ---------- 2.5 LO +21.78 Coke***
6) Heavy oil combustion	***HO + 60.55 O_2 ---------- 51.53 IG^* + 28.34 H_2O***
7) Light oil combustion	***LO + 60.06 O_2 ---------- 39.92 IG^* + 25.1 H_2O***
8) Coke combustion	***Coke + 1.18O_2 ---------- IG^* + 0.55 H_2O***
	****: Inert gas((CO_x and N_2)***

Reaction	A, pre-exponential factor		E, activation		Heat of reaction	
	Field	SI	(BTU/mole)	(J/mole)	(BTU/mole)	(J/mole)
1	$4.167\times10^{8+}$	4.167×10^{8}	3.01×10^{4}	7.00×10^{4}	0.0	0.0
2	$5.160\times10^{8++}$	7.508×10^{7}	5.00×10^{4}	1.16×10^{5}	5.25×10^{6}	1.22×10^{7}
3	$2.167\times10^{5++}$	3.153×10^{4}	3.40×10^{4}	7.90×10^{4}	1.00×10^{6}	2.32×10^{6}
4	$4.167\times10^{7++}$	6.063×10^{6}	5.10×10^{4}	1.19×10^{5}	1.50×10^{4}	3.49×10^{4}

$^{++}$: (h^{-1}), $^{+}$: ($h^{-1}psi^{-1}$ or $h^{-1}Kpa^{-1}$)

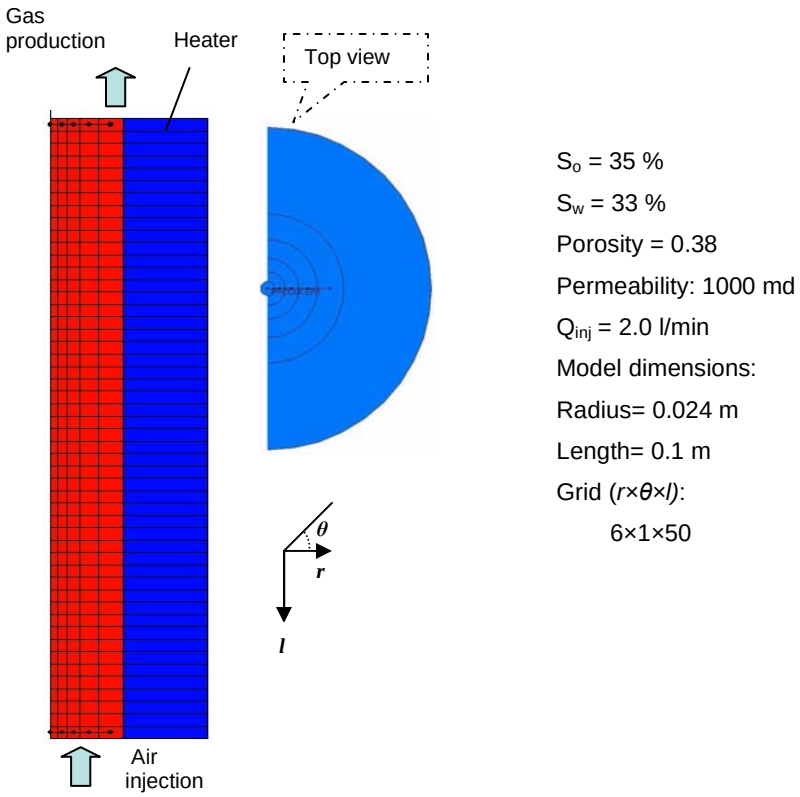


Figure 4.24. Kinetic cell simulation model and some important model parameters.

The simulation model and some important parameters of this model are presented in Figure (4.24). In this model, the radial geometry is used in which, due to vertical symmetry of the problem, only half of the kinetic cell is modeled. An injection well is positioned at the bottom and a production well at the top of the model. Air is injected from the bottom and combustion gases produced from the top. The temperature of the porous medium increases by a heater which is situated around it and provides the same temperature ramp as observed in the experiment.

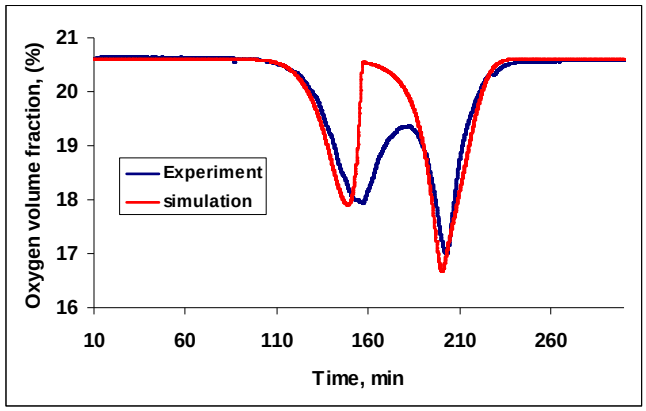


Figure 4.25. Oxygen volume fraction in the homogeneous kinetic cell.

Figure (4.25) shows the profile of the oxygen concentration at the exit of the kinetic cell. In our reaction model, the combustion process is considered to be complete, meaning that there is no carbon monoxide (CO) production in the combustion reaction. That is why, here, we only compare the oxygen profile and not the CO_2 and CO profiles. The oxygen profiles confirm an acceptable agreement between the simulation and the experiment results.
The difference between two profiles, which is more significant in the first peak, may come from the fact that, in the simulation model, we highly simplified the reactions and specially the LTO part. These simplifications are the reduced number of reactants and reactions and, as we explained earlier, no oxygen addition reaction was considered in our model. Another point is that the matching procedure was done manually and the presented case is the best one achieved. An automated matching procedure may produce better results.

4.4.2 Combustion tube simulation

Using the validated model of the kinetic cell in the previous part, some combustion tube simulations were done for the fractured systems. As we observed from the consolidated kinetic cell experiments, the reaction kinetic for these systems may not be the same as for non-consolidated one for the same oil. Our attempt to obtain a reasonable match for a the consolidated kinetic cell was not successful, which could be due to lack of some reliable input data. That is why we assumed that the reaction parameters of the non-consolidated case may be applicable for the consolidated one at least for qualitative comparison. The aim of these simulations was to investigate the propagation and extinction condition of the combustion front. Like the kinetic cell simulation, here we used the radial geometry as shown in Figure (4.26) and due to the radial symmetry only half of the tube is simulated. The top view of the model is shown in the left side of this figure. The parameters of the model are also demonstrated in this figure.
Initial saturations are the same as for the experiment. For oil-water and gas-oil relative permeability the data published by Kumar (1987) was used and for the fracture we used a cross type relative permeabilities (Tabasinejad et al. 2007, Delaplace et al. 2004). For oil phase relative permeability, the Stone II model was introduced. It is assumed that the capillary pressure is negligible both in matrix and fracture. In the fracture, this assumption may be reasonable as the aperture is large (0.002m). In the matrix, it is assumed that the high temperature process may minimize capillary pressure effects.
Initially, the core is at reservoir temperature and pressure. It is positioned vertically and air is injected from the top and oil is produced from the bottom. When air injection starts, with constant rate and constant bottom-hole pressure, a constant heat is also applied though blocks in which the electrical heaters are situated. The position of the electrical heater is shown in the Figure (4.26). The heat injection is maintained for 2.5 hrs, which corresponds to the temperature of 450 °C at the core centre, which is also the ignition temperature. The blocks above and below the electrical heaters (in the same vertical layer) have the same thermal properties as the thermal insulation that we used in the experiment. The heat loss from this layer to the surrounding is modeled by some large blocks that contain air and are attached to this layer.
Figure (4.27) shows the temperature profile versus distance in the fracture along the core. With normal air, after the initial ignition (around 450 °C), the temperature decreases below 330 °C after 3.9 hr which leads to extinction condition. This is not the case for enriched air where the high temperature (relatively equal to the ignition temperature) maintains after the same period of time.

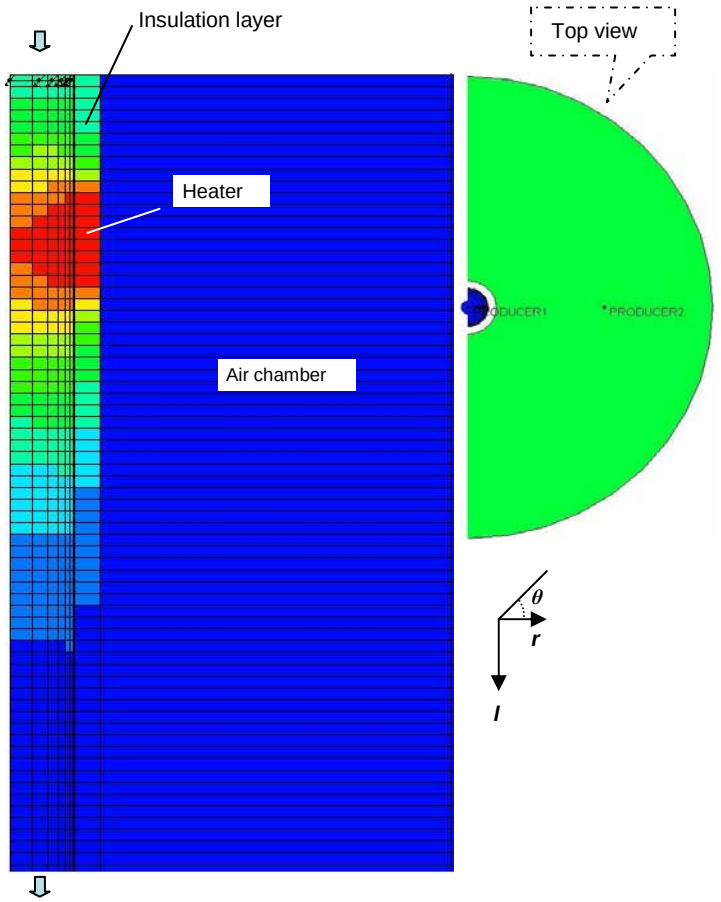


Figure 4.26. Combustion tube simulation model and some important model parameters.

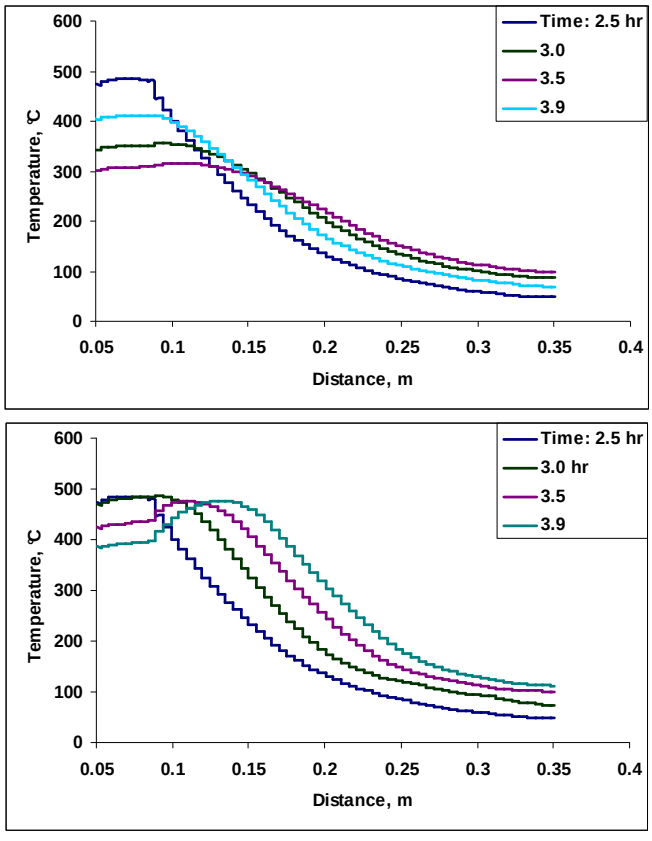


Figure 4.27. Temperature versus distance; Top: normal air, Bottom: enriched air (60% O_2).

This behavior may be explained by the form of the coke profile in Figure (4.28). In this figure, for normal air (left), a small amount of coke has been consumed during 3.5 hours while, for enriched air, considerable amount of coke has reacted. The higher consumption of coke with the enriched air is due to the higher oxygen availability in this case.
The oxygen profile (figure 4.29) also confirms this observation. With normal air, the oxygen concentration in the porous matrix is considerably lower than in the case with enriched air.

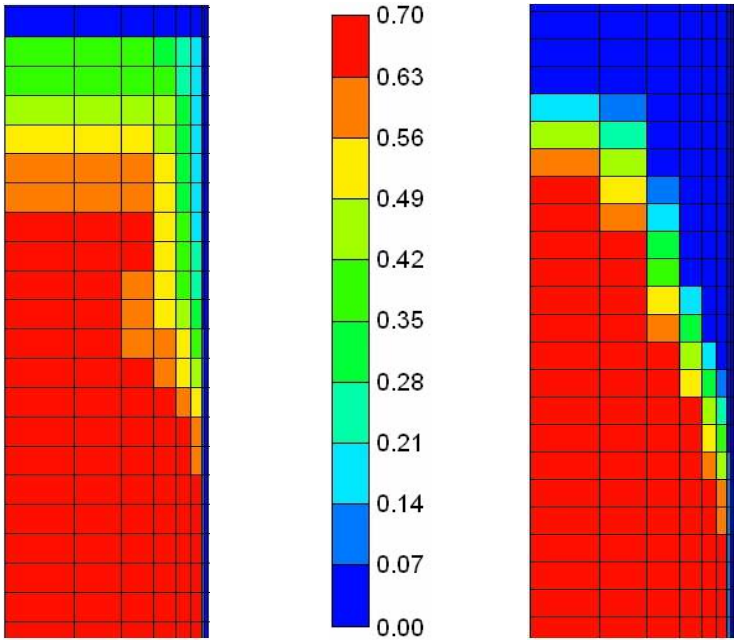


Figure 4.28. Coke profile at time = 3.5 hr; left: normal air, right: enriched air.

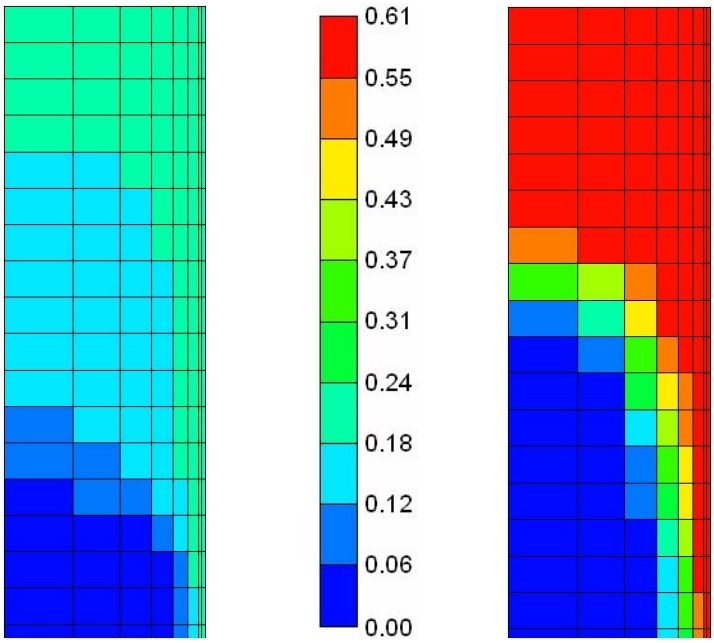


Figure 4.29. Oxygen mole fraction at time = 3.5 hr; left: normal air, right: enriched air.

When the oxygen concentration is low, the combustion reaction is less significant and can not generate enough heat to compensate the heat losses, thus the high temperature front ceases.
In this simulation study, it is found that, when normal air is injected in which the oxygen concentration is 21%, the high temperature combustion front could not propagate and the temperature close to the ignition point (electrical heater) decreases after the ignition is achieved. However, when the oxygen concentration increases in the injected air (60%) the combustion is self sustained and we are in the propagation mode.
This result confirms qualitatively the experimental observation, which emphasizes the fact that the mass flux of oxygen into the porous matrix is an important factor to have a sustainable combustion front in fractured systems. This is somehow similar to what we found in our previous simulation study on the combustion in fractured cores (see chapter 3). In the previous study the oil properties (medium oil of 26° API) and the reaction scheme were taken from a paper published by Kumar (1987) and the geometry of the model was Cartesian. The results of that study showed that, while the matrix permeability plays a major role in the oil production, the determining factor for the combustion front propagation is the oxygen diffusion coefficient.
Our experimental results also showed that the oxygen diffusion was the controlling factor for the propagation of ISC front. However, we did not practice different matrix permeabilities to address the effect of permeability ratio between the matrix and the fracture, but, from some preliminary runs with filled or empty fractures, we found that this parameter does not change the propagation condition. However, one should keep in mind that in real geological systems, the matrix permeability and the diffusion coefficient are correlated.

4.4.3 Summary

In the study of a non-consolidated heterogeneous system with about 100 times permeability ratio of the matrix and the fracture, after the ignition, combustion front propagation through the tube was sustained. A combustion tube study of consolidated media showed that, in case of air injection (21% oxygen). A high temperature combustion front can propagate through small scale heterogeneities but it can not propagate through large scale heterogeneities. It seems that with normal air (21% oxygen), the propagation condition does not change when changing the fracture permeability (filled or empty) in a consolidated case. The fact that an increase in oxygen concentration allowed to propagate the combustion front suggests that oxygen diffusion into the matrix is the determining parameter for combustion propagation.
Presence of carbonate can modify the kinetics of ISC in the porous medium. This should be considered in the application of ISC in fractured reservoirs. Study of the consolidated system kinetics showed that it is significantly different from non-consolidated system kinetics. Both of the above mentioned issues need a detailed study in order to better understand their effect(s) on the combustion process behavior.
Simulation results showed the same qualitative behavior observed in both in the kinetic cell and combustion tube experiments.

Chapter 5. Conclusions and perspectives

This chapter presents a global overview of the manuscript and gives a perspective for future studies in this area.

5.1 Conclusions

Once again, we draw the reader's attention to the main target of this thesis, which is, to study the ISC process at inter-well scale in a fractured reservoir using the available numerical tools. In this regard we reviewed the literature concerning the in situ combustion process in fractured reservoirs. Based on the current knowledge about the ISC process and fractured reservoirs, two main challenges were distinguished, at small and large scales, which of course, are related to each other. A good understanding of the small scale behavior of the system is a crucial step for large scale studies.
The complexity associated with this process has been leading the petroleum industry to have less appeal to the application of the ISC process. As the consequence, the literature resources about this process, especially in fractured reservoirs, are limited. Based on the available literature, the following aspects are distinguished as some open questions concerning the ISC in porous media and fractured reservoirs:

- *In situ combustion*

The condition under which the combustion process in a fractured system is sustained is not fully understood. The oil recovery mechanism in fractured systems under ISC process is also another important issue and the contribution of different recovery mechanisms should be addressed (i.e., evaporation and expansion, steam drive, gas drive, gravity drainage, etc.). There is a question on whether one can use the reaction schemes which are developed and used in homogenous system, for a highly heterogeneous medium like a fractured reservoir. In carbonate reservoirs, the interaction of carbonate matrix with the combustion reaction calls for more detailed study (Fadaei et al. 2009). Regarding the modeling and simulation of the process at the reservoir scale, to our knowledge, very little references can be found in the literature.

- *Fractured reservoirs*

Large scale upscaling of transport processes has been mostly limited to relatively simple processes. Thus, the upscaling of complex problems such as combustion with a strong coupling of heat and mass transfer seems to be very complicated. In an ISC process, large changes happen over a relatively small distance. This seems to be one of the major obstacles for the macroscopic representation of the problem using upscaling tools. Determination of a pertinent exchange term (in two-equation models) even for a simple process in case of highly heterogeneous system is still under investigation, especially for the early time of the process. This is more challenging in the case of multiphase systems.
To our knowledge, large scale simulation of fractured reservoirs is currently feasible only by using two-medium (two-equation) models. Due to all difficulties mentioned before for modeling and upscaling of the multiphase flow with combustion process in a fractured system, there is not a numerical tool based on the volume averaging method that can treat this

problem. The only available numerical tools are the commercial codes developed by petroleum companies.

We started with the small scale challenges which mainly concern the feasibility of the ISC in fractured system, the influence of some reservoir/operational parameters as well as the oil production mechanisms. To do so, in the first step, a commercial thermal reservoir simulator (STARS) was used. To perform the simulation study, one of the main issues is the availability and the reliability of the input data (i.e., oil, reservoir properties and more importantly the chemical reactions parameters). We used the data published by Kumar (1987).

Simulator validation

The simulator validation was done for different processes by comparing the simulation results with analytical solutions (for simple processes) and experimental results (for oil combustion). It is confirmed that the simulator is able to handle the ISC process with acceptable accuracy. We recall that we studied a single porosity model not a dual porosity in our simulation work.

Core scale simulation

Fractured core scale simulation showed that, in situ combustion is feasible for medium oil. The peak temperature and the extent of the coke zone were increasing during the process while these two parameters are rather constant in conventional combustion. For a given time, the shape and length of the coke zone was observed to be dependent on oxygen diffusion coefficient while matrix permeability seems to have minor effects on that. Oxygen diffusion coefficient was found to have a major influence on extinction/ propagation of combustion and matrix permeability to play an important role on oil production.
Prediction of extinction/propagation conditions based on either oil saturation, coke concentration and temperature profiles or dimensionless numbers seems to be very challenging. Defining some pertinent dimensionless numbers for this aim may help but was not completely discriminating, which is not surprising given the coupled, non-linear nature of the problem. Considering the fuel consumption, the simulation results showed that more fuel was consumed during the ISC in a fractured system than in a non-fractured case. Gravity drainage and thermal effects were found to be important in oil production. The pressure gradient generation during the ISC process was not significant and seems to have a minor effect on oil production.

Core scale experiment

Further study of the ISC process at small scale was done by performing some combustion tube experiments and kinetic cell tests. Doing the combustion experiments was important considering the controversial results in the literature regarding the propagation condition of the ISC in fractured systems. Also these experiments provided us with a verification of our numerical tool. We also studied some aspects of the ISC process which have not been studied before (i.e., effect of filled or empty fracture and ISC in the heterogeneous non-consolidated system)
In the study of a non-consolidated heterogeneous system where the permeability ratio of the matrix to the fracture was about 100, after the ignition, combustion front propagation through the tube was sustained. Combustion tube study of consolidated media showed that, in case of air injection (21% oxygen), a high temperature combustion front can propagate through small scale heterogeneities but it can not propagate through large scale heterogeneities. It seems that with normal air (21% oxygen), the propagation condition does not change when changing the fracture permeability (filled or empty) in a consolidated case. The fact that an increase in oxygen concentration allowed to propagate the combustion front suggests that oxygen

diffusion into the matrix is the determining parameter for combustion propagation. Simulation of the tube experiments also showed the same behavior qualitatively.
Some kinetic cell tests were also conducted in which we found that the presence of carbonate can modify the kinetics of ISC in the porous medium. This should be considered in the application of ISC in fractured reservoirs. Study of the consolidated system kinetics showed that it is significantly different from non-consolidated system kinetics.

Single-block scale simulation

The importance of the single block simulation is to investigate the two dimensional behavior of the ISC in fractured system. Simulation results showed that the underlying process is diffusion dominated both for heat and mass (i.e. oxygen) transfer. Heat transfer due to the movement of the combustion front velocity is less important than to heat transfer by conduction. In this multi front process, different zones can be distinguished for oil saturation and temperature with sizes that vary over time. The relative size of the heat and saturation zones and the change of their size during the burning process suggest that any upscaling method should take into account these phenomena.

Multi-block scale simulation

The simulation results show that the combustion front moves slower than the heat and mass transfer fronts (same as what we observed in the single block case). Production gases tend to move toward the upper part of the reservoir. The position of the water bank is not necessarily downstream of the combustion process but rather detached from it.
Average temperature in the matrix block and the corresponding fractures are relatively close to each other (except for the ignition block), which may suggest the application of a one-equation model for upscaling. However, in order to perform upscaling for this system one should be aware of relatively rapid changes of temperature in a distance smaller than the block length.
To upscale the mass transfer, one needs to use at least two-equation models to represent the transport in the matrix and the fracture.

5.2 Perspectives

Simulation, Darcy scale

Our simulation study was based on the input data which corresponds to a medium oil. In order to study the heavy oil combustion, one needs the corresponding input data for oil properties, relative permeabilities as well as the reaction parameters.
Further simulator validation with the corresponding experimental data of the fractured systems, where the diffusion dominated exchanges between matrix and the fracture are important, can increase the reliability of the numerical tool.

Experiment

More combustion tube experiments of “propagating situation” are necessary to address the effect of some operational and reservoir properties on the behavior of the combustion process. Post-run images of propagating condition may help to verify the extension of different zones. Tube test under CT scanner may help to distinguish the relative position of oil, gas and water fronts. Performing some tube experiments at reservoir condition (higher pressure) with normal air to verify the possible propagation situation may also be desirable.
In core scale experiments, the radius of the core is normally less than 0.1m. In this situation, the characteristic time for diffusion and conduction is small, which is in favor of propagation situation. Especially, two dimensional effects are not visible in the tube experiment. Thus, performing some experiments at a larger scale (2 or 3-D model of 0.5 m length) may be

helpful to better address the two dimensional effects, especially heat losses ahead of the combustion front.
In the kinetic cell experiment, the effect of carbonate matrix and the consolidated porous media were studied qualitatively. Further experiments are needed to study these effects quantitatively. This may lead to a new set kinetic parameters which could be derived for a oxygen limited situation.

Upscaling

The upscaling issue remains the most challenging aspect of the ISC in fractured systems considering the heterogeneous nature of the fractured reservoirs and highly non-linear characteristics of the ISC process.
Here, we present the upscaling of a simplified version of the ISC process using the method of volume averaging. The idea is to verify whether or not the large scale (upscaled) model, derived with this method, is able to produce the same results as we obtained with Darcy scale (DNS) model. Only the conductive transport in the matrix and the fracture is considered and oil combustion is simplified to the coke combustion. The combustion reaction is considered to be of Arrhenius type and the reaction takes place only in the matrix. The system is under adiabatic condition except from the left side, where, a constant temperature is applied. The schematic of this model is presented in Figure (5.1). This is a two dimensional model that consists of an array of matrix blocks which are surrounded by fractures. Some main characteristics of the model are presented in Table (5.1).

Table 5.1. Model parameters.

Parameter	***Value***
Unit cell dimension, m (*x, y*)	0.19, 0.19
Matrix dimension, m (*x, y*)	0.18, 0.18
Fracture dimension, m (*x, y*)	0.19, 0.0055
Model dimension, m (*x, y*)	1.6, 0.2
Thermal conductivity ratio (k_m/ k_f)	10
Heat capacity ratio $(\rho Cp)_m$/ $(\rho Cp)_f$	1.6×10^3

We started with the Darcy scale equations for each medium as presented in the following equations
For the matrix:

$$(\rho C_p)_m \frac{\partial T_m}{\partial t} = \nabla.\left(k_m^*.\nabla T_m\right) + q_{rxn} \qquad \textbf{(5.1)}$$

For the fracture:

$$(\rho C_p)_f \frac{\partial T_f}{\partial t} = \nabla.\left(k_f^*.\nabla T_f\right) \qquad \textbf{(5.2)}$$

The boundary and initial conditions:

$$T_m = T_f \quad \text{at} \quad A_{mf} \qquad \textbf{(5.3)}$$

$$n_{mf}.(k_m^*.\nabla T_m) = n_{mf}.(k_f^*.\nabla T_f) \quad \text{at} \quad A_{mf} \qquad \textbf{(5.4)}$$

$$T_m = T_f = T_i \quad \text{at} \quad t = 0 \qquad \textbf{(5.5)}$$

$$T_f = T_c \quad \text{at} \quad x = 0 \qquad \textbf{(5.6)}$$

These equations are averaged over the representative cell which is shown in Figure (5.1). More details about the mathematical manipulation are presented in appendix (B).
Starting with Darcy scale equations and performing the averaging over the representative volume (unit cell, figure 5.1), also assuming the steady state closure problem (see appendix B), governing equations for large scale are derived. The closure problem resulted to a set of differential equations based on closure variables, by solving which the effective parameters for the large scale are derived. The equations are solved using COMSOL Multiphysics software.

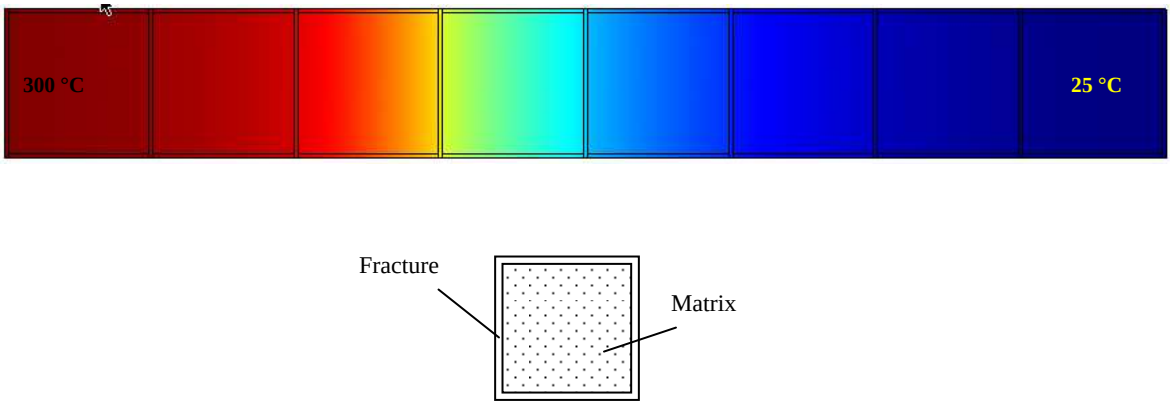


Figure 5.1. Schematic of the Darcy scale model (top) and the unit cell (bottom).

We examined two cases with two (small and large) Damköhler numbers. Figure (5.2) shows the dimensionless temperature versus dimensionless distance for two different times for a case of small Damköhler number. For the Darcy scale model, this temperature corresponds to the volume averaged temperature calculated over the representative block. This figure shows that the upscaled model is able to reproduce the small scale temperature with reasonable accuracy. Thus when the reaction characteristic time is larger than the transport characteristic time, one can use the upscaled model.
On the other hand, when the Damköhler number is large, the upscaled model results are different from the small scale results. This is illustrated in Figure (5.3). At initial times of the process, where the temperature is not high, the upscaled model is able to predict relatively the same result as the small scale one. When the temperature increases, however, the reaction term becomes more important, and the model is not able to reproduce the small scale temperature.

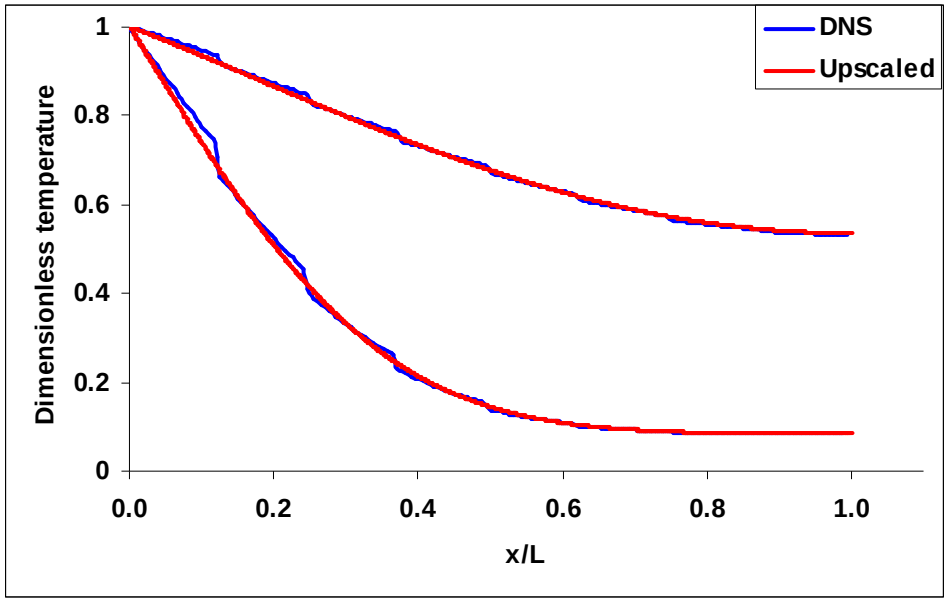


Figure 5.2. Dimensionless temperature vs. distance (Damköhler =0.3).

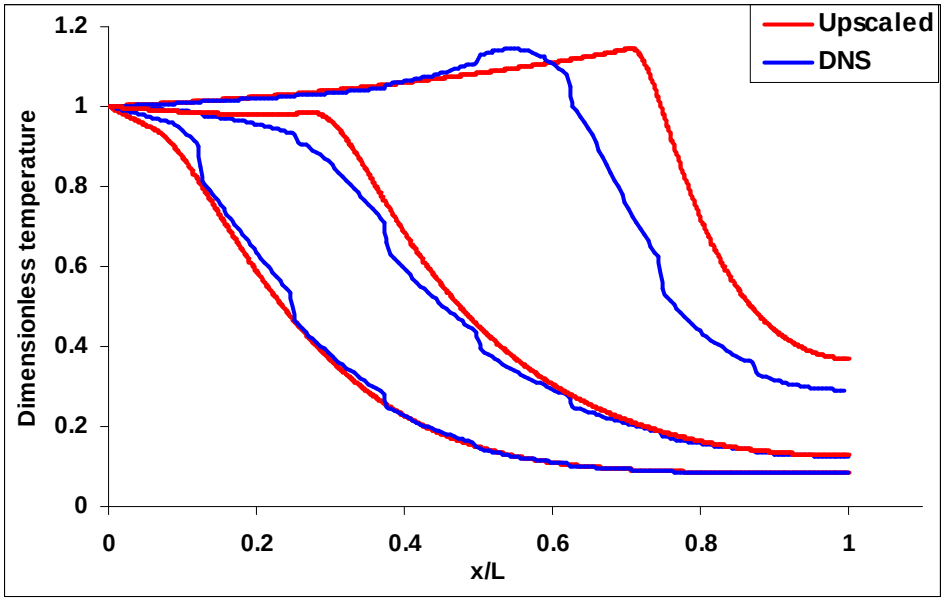


Figure 5.3. Dimensionless temperature vs. distance (Damköhler =30).

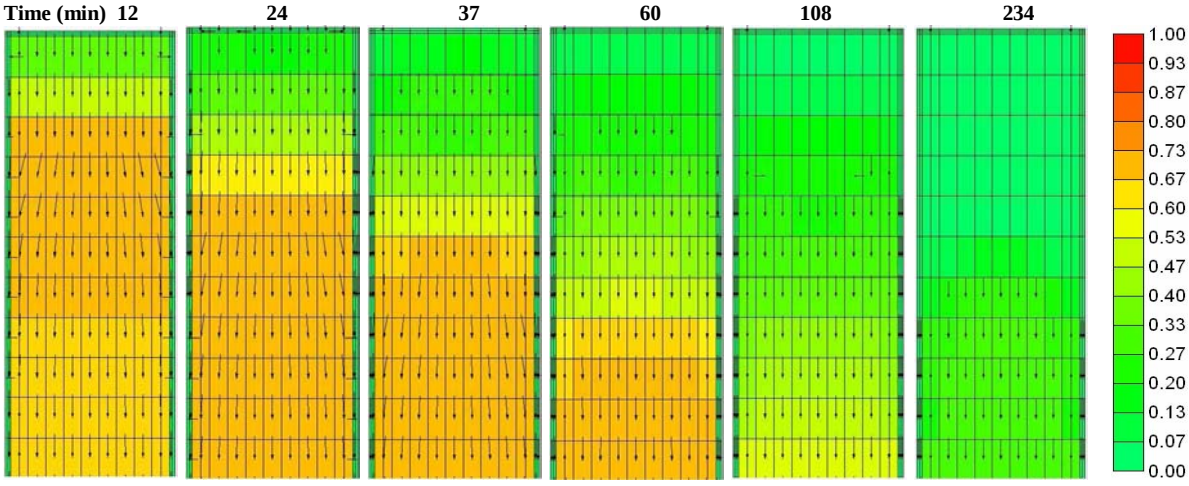
To our knowledge, this kind of problem, where the reaction term is of Arrhenius type is not treated in the literature using the volume averaging method. From this point of view these results also indicate that the method can be used to handle this kind of problems. However the results for high Damköhler number do not show a reasonable match with the small scale results. Upscaling the high Damköhler case may call for handling a closure problem in a non steady state which makes the problem very complicated. This is a challenging step for the future work on this subject. It should be emphasized also that, the present case is highly simplified compared to the oil combustion in porous media.

APPENDIXES

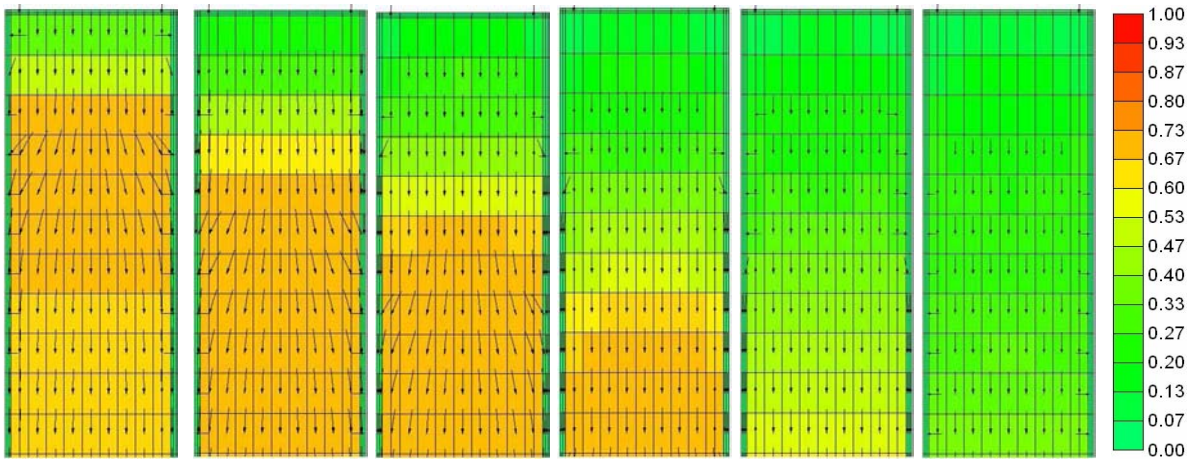
A. Combustion in fractured core

A.1 Effect of oxygen diffusion coefficient on ISC

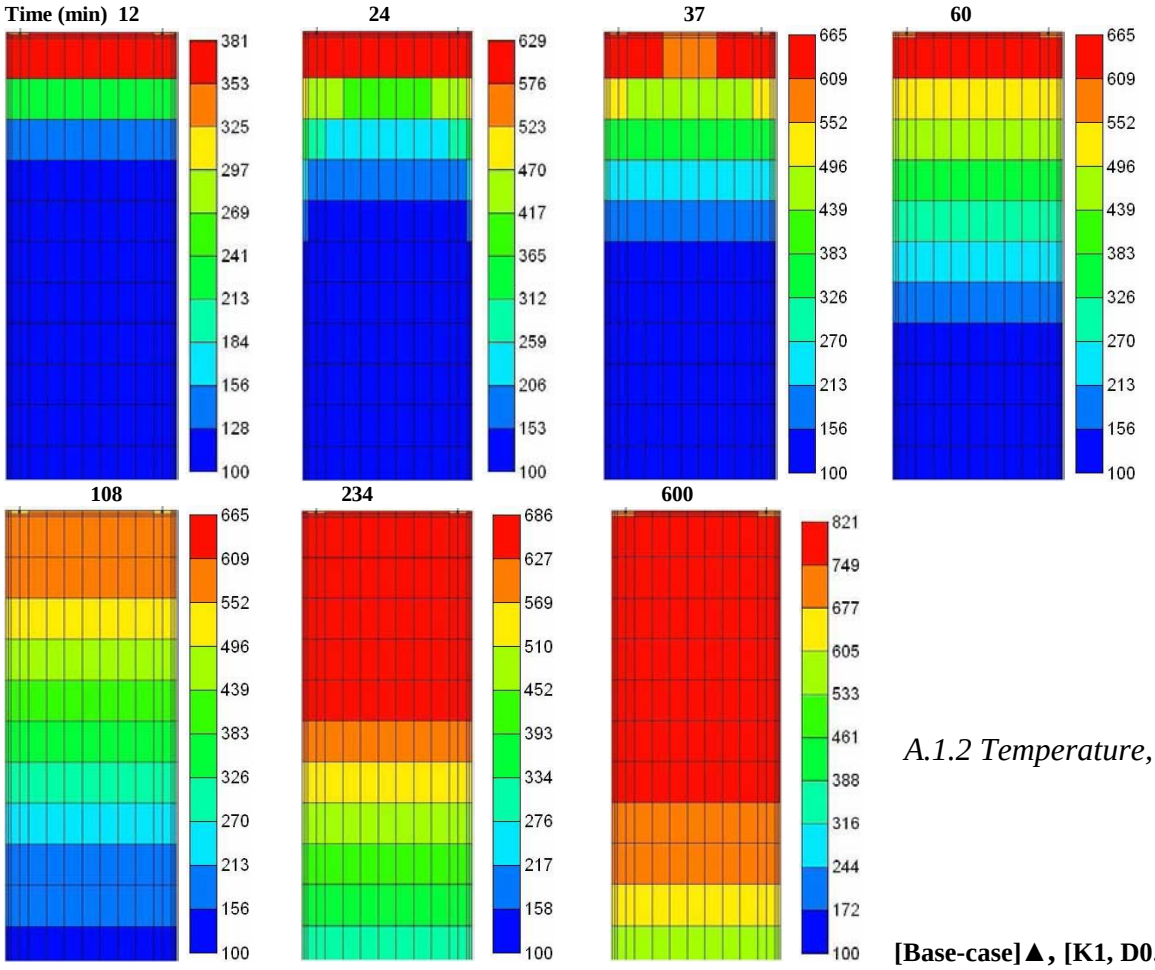
A.1.1 Oil Saturation



[Base-case]▲

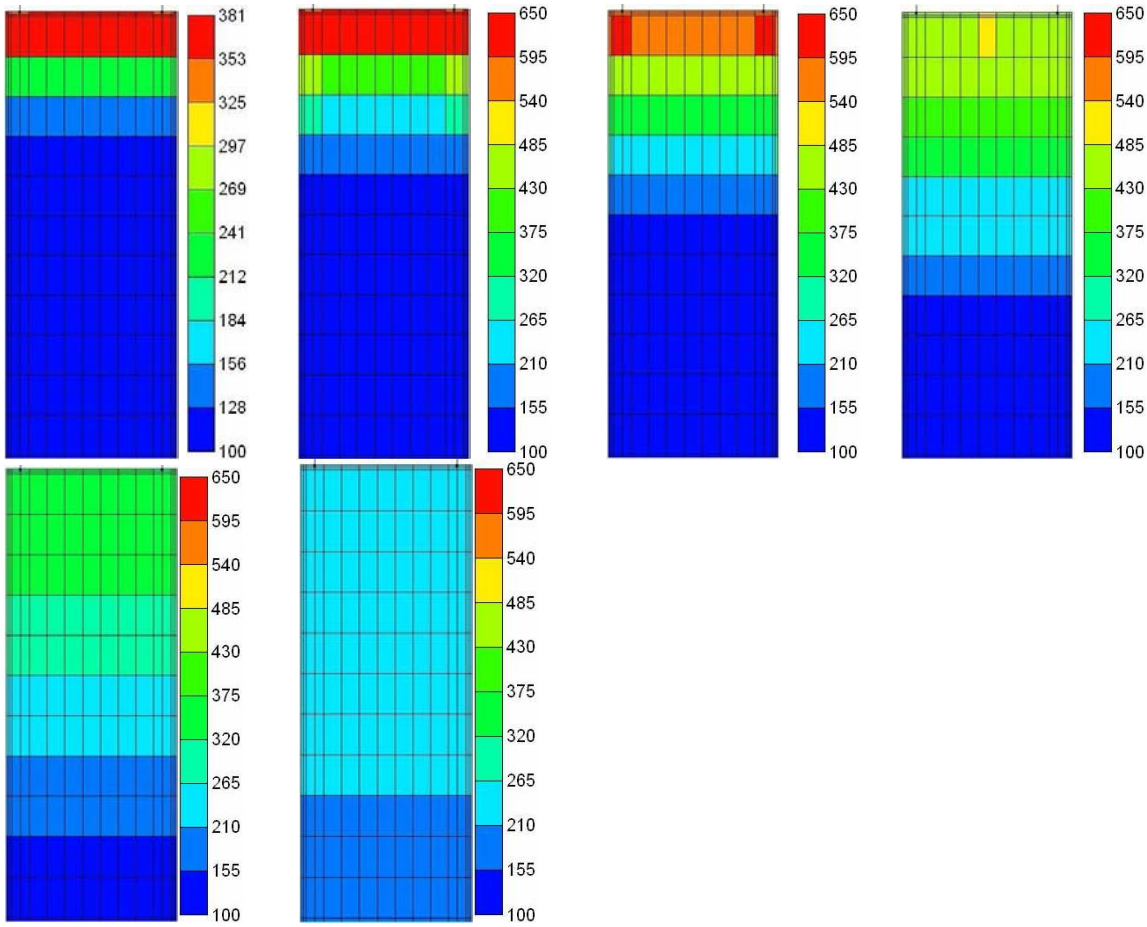


[K1, D0.02]▲

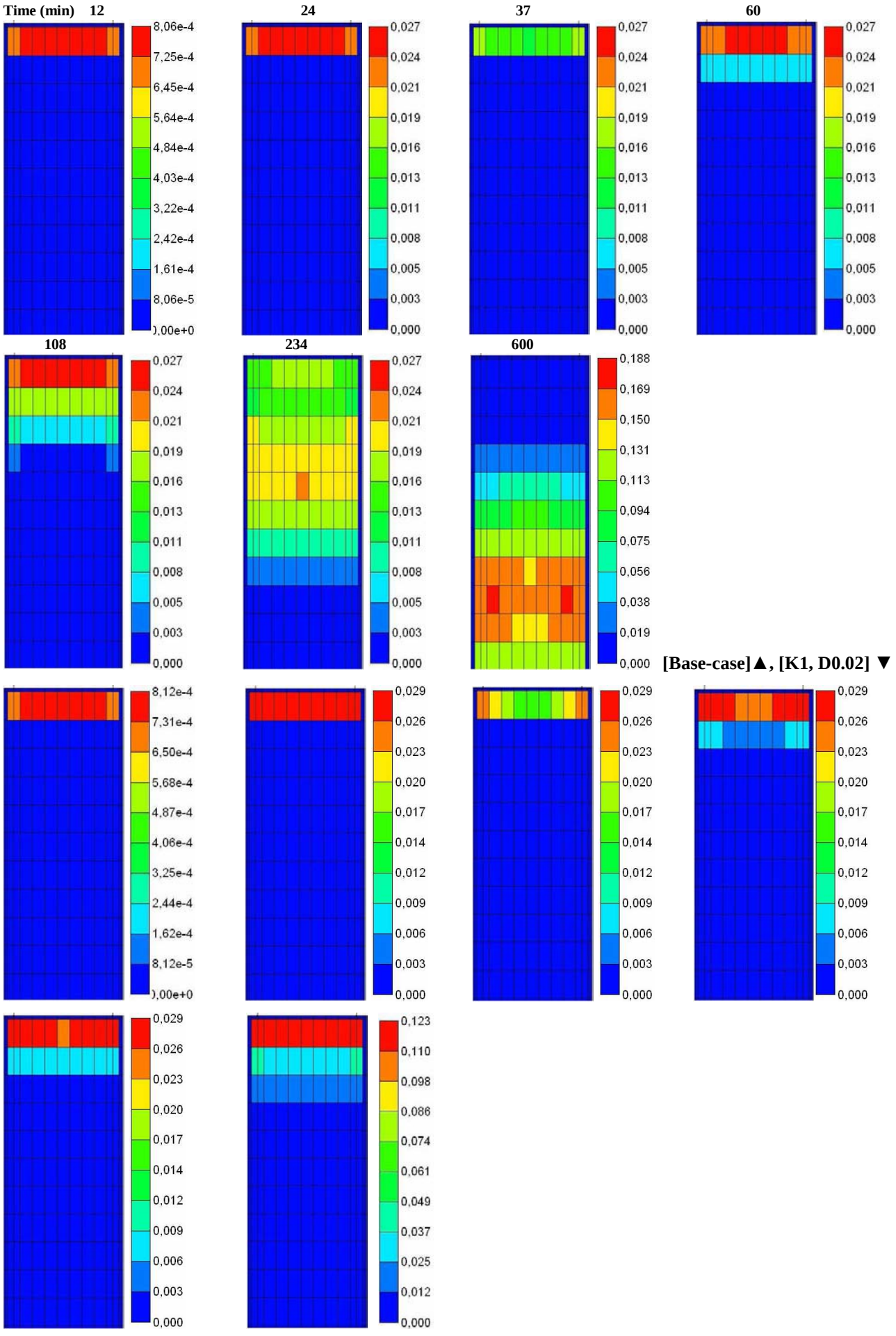


A.1.2 Temperature, (°C)

[Base-case]▲, [K1, D0.02] ▼

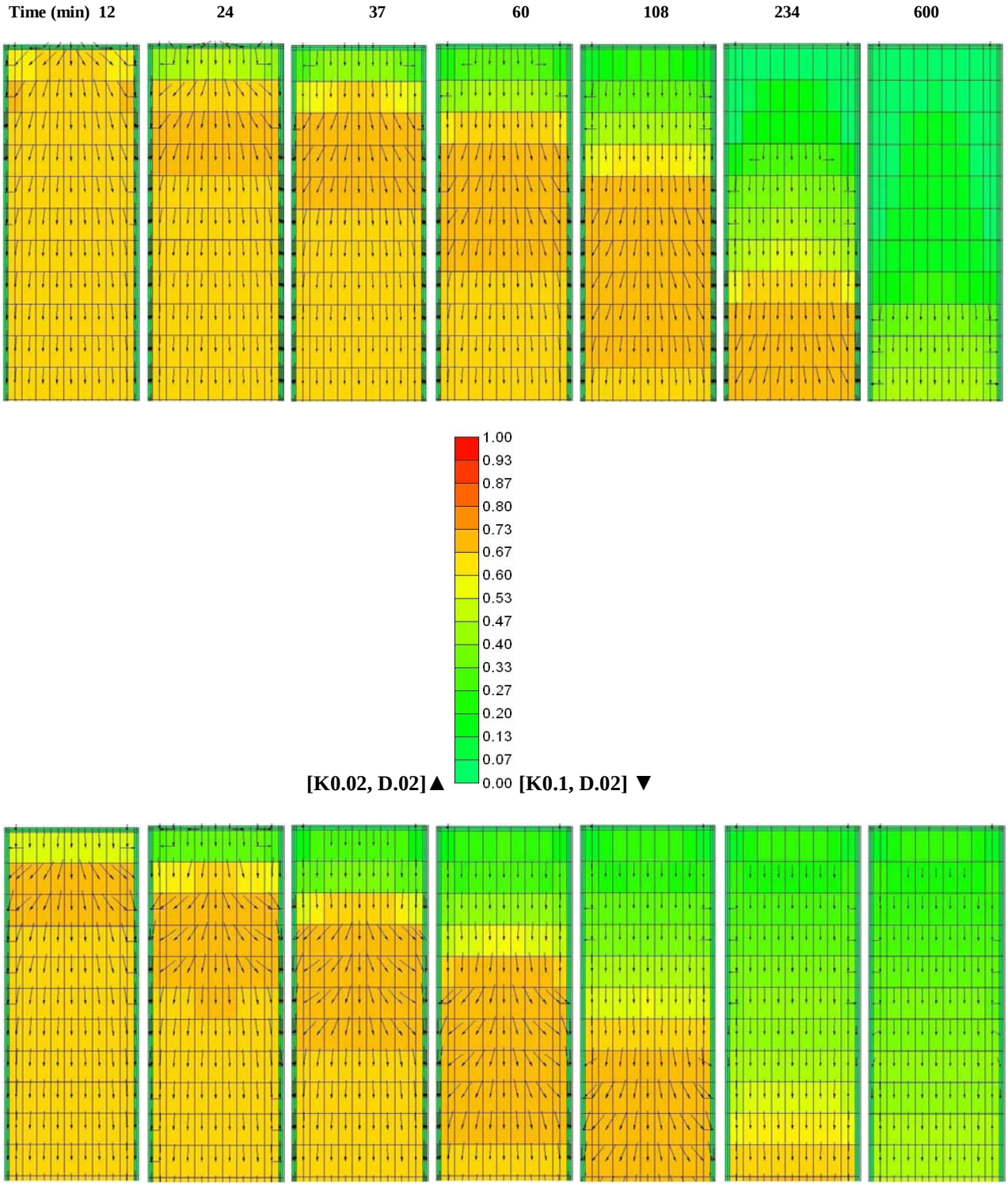


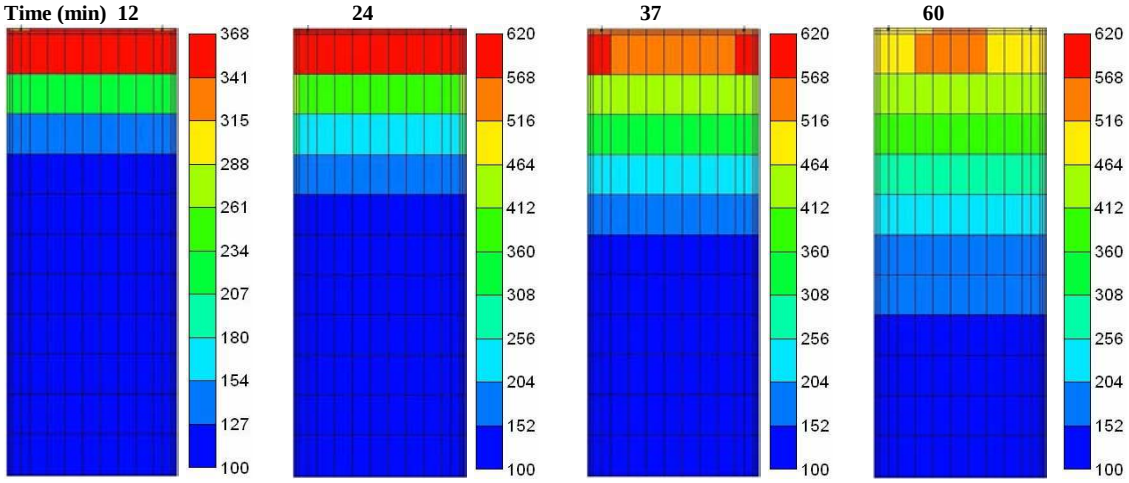
A.1.3 Coke concentration (lbmole/ ft^3)

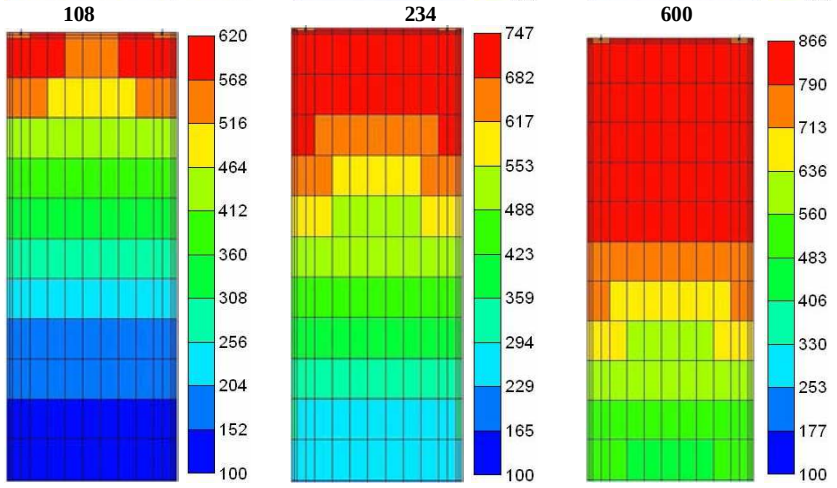


A.2 Effect of matrix permeability on ISC

A.2.1 Oil saturation

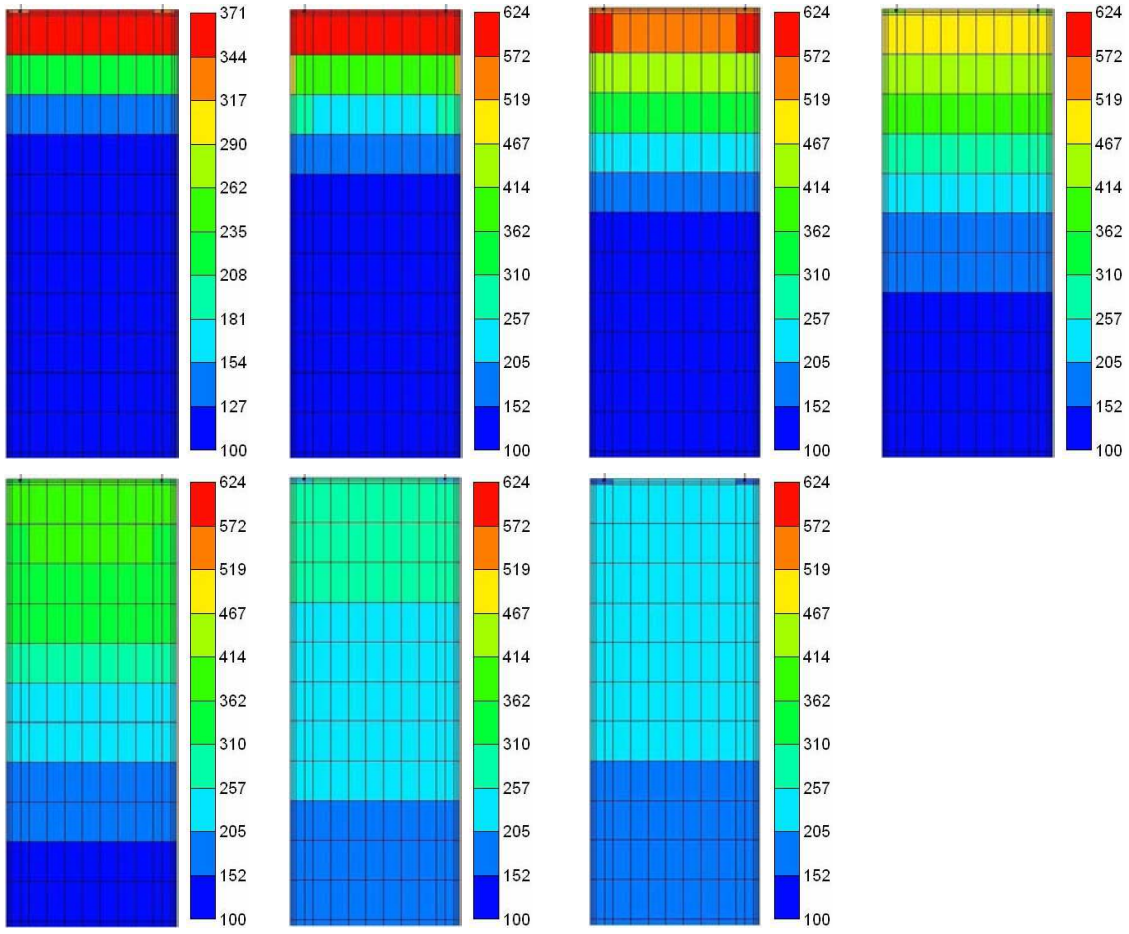






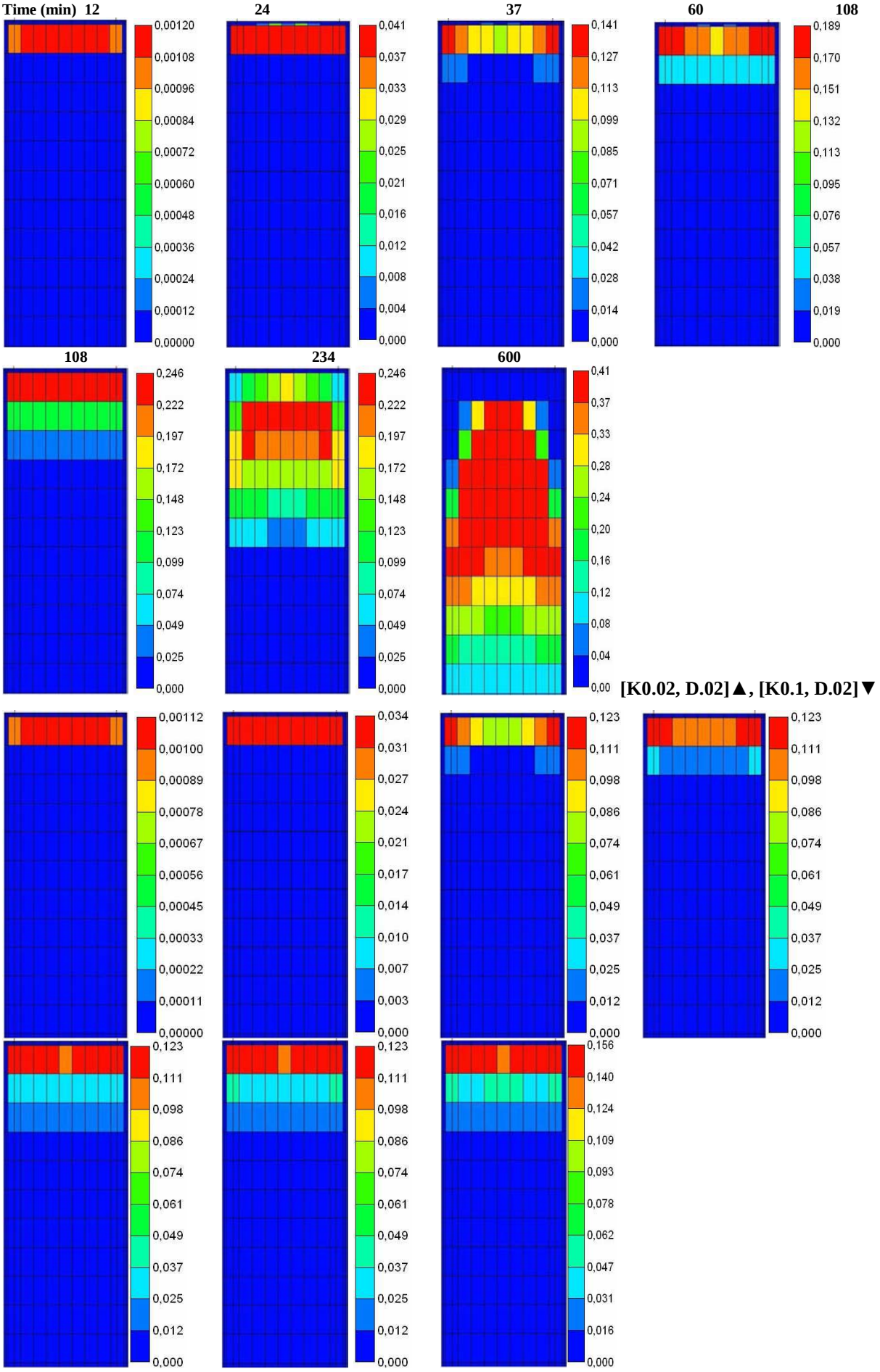
A.2.2 Temperature, (°C)

[K0.02, D.02] ▲, [K0.1, D.02] ▼



Appendix A

A.1.3 Coke concentration (lbmole/ ft^3)



Notations (Appendix B)

A_{mf}	Interface between two phases, (m^2)
A_0	Pre-exponential factor, (1/s)
a_V	specific surface area, (m^2/m^3)
$\mathbf{b}_{mm}$	
$\mathbf{b}_{mf}$	
$\mathbf{b}_{ff}$	Closure variables, vector, (m)
$\mathbf{b}_{fm}$	
C_p	Specific heat capacity, (J/kg.K)
E	Activation energy, (J/mole)
H_{rxn}	Reaction heat, (J/m3)
k_π^*	Darcy scale thermal conductivity, (W/m.K)
$\mathbf{K}_{\pi\pi}$	Large scale thermal conductivity
$\mathbf{K}_{\pi\theta}$	tensor, (W/m.K)
L	Large scale length scale
l	Small scale length scale
m, f	Matrix and fracture indicators
$n_{\pi\theta}$	The normal vector at the interface
R	Universal gas constant, (J/mole.K)
q_{rxn}	Reaction term
s_m	Closure variable, scalar
s_f	
t	Time, (s)
T_π	Darcy scale temperature
$\mathbf{u}_{mm}$	
$\mathbf{u}_{mf}$	Transport coefficient in the large
$\mathbf{u}_{ff}$	scale model
$\mathbf{u}_{fm}$	
V_π	Volume of the phase, (m^3).
V	Volume of the averaging volume, (m^3)
$\mathbf{x}, \mathbf{y}$	Vector
$\langle\ \rangle$	Average property
$\sim$	Deviation term.
ρ	Density, (kg/m^3)
π, θ	Phase indicators

B. Upscaling of the solid-gas combustion using the volume averaging method

In this appendix, we present a short overview of the volume averaging method and the mathematical development for upscaling of the solid-gas combustion. The mathematical manipulations are based on a paper published by Quintard and Whitaker (1993) and a book written by Whitaker (1999) on the subject of volume averaging.

B.1 Introduction

In order to perform the averaging of the transport equation in the volume averaging method, a volume of V is considered as the averaging volume based on which those equation are averaged. Figure (B.1) shows this volume, in which, the volume of each individual phases are represented as (here we replaced β by *f* and σ by *m*)

$$V = V_m(x) + V_f(x) \tag{B-1}$$

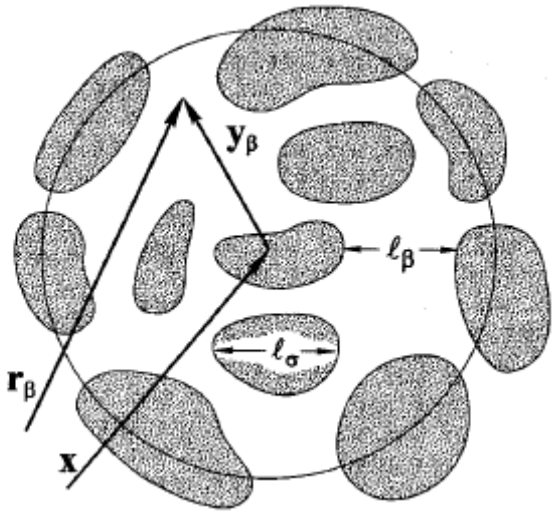


Figure B.1. Averaging volume and the position vectors (taken from Quintard and Whitaker 1993).

In this figure, the centroid of the averaging volume is located by a position vector *x*, and other positions in this volume by vector *y*. The superficial average is defined by

$$\langle \psi_m \rangle \big|_x = \frac{1}{V} \int_{V_{m(x)}} \psi_m(x + y_m) dV_y \tag{B-2}$$

The intrinsic average is defined as

$$\langle \psi_m \rangle^m \big|_x = \frac{1}{V_m(x)} \int_{V_{m(x)}} \psi_m(x + y_m) dV_y \tag{B-3}$$

Normally in the volume averaging literature these two averages are represented in a simplified form as

$$\langle \psi_m \rangle = \frac{1}{V} \int_{V_m} \psi_m dV \tag{B-4}$$

$$\langle \psi_m \rangle^m = \frac{1}{V_m} \int_{V_m} \psi_m dV \quad \textbf{(B-5)}$$

these two averages are related to each other by

$$\langle \psi_m \rangle = \varepsilon_m \langle \psi_m \rangle^m \quad \textbf{(B-6)}$$

in which, ε_m is the porosity of the phase *m* or $\frac{V_m}{V}$.

In a transport equation, in order to do the averaging of the gradient or divergence term, one can use the following relation (Whitaker 1999).

$$\langle \nabla \psi_m \rangle = \nabla \langle \psi_m \rangle + \frac{1}{V} \int_{A_{mf}} \mathbf{n}_{mf} \psi_m dA \quad \textbf{(B-7)}$$

In the process of averaging to obtain the governing equation based on the averaged parameters, the following decomposition is used.

$$\psi_m = \langle \psi_m \rangle + \tilde{\psi}_m \quad \textbf{(B-8)}$$

in which, $\tilde{\psi}_m$ is the deviation term.

B.2 Solid-gas combustion in fractured porous medium

The governing equation for heat transfer in the matrix and the fracture are presented in the chapter (5). This particular solid-gas combustion problem in which only conduction heat transfer is considered, is very similar to the problem of two-phase thermal conduction studied by Quintard and Whitaker (1993) using the volume averaging method. However, in our problem there is an extra reaction term. Here, we will follow the same development as done by Quintard and Whitaker (1993) for upscaling. We present the assumptions concerning the reaction term, simplifying the problem in a way that allows us to treat the same closure problem as presented by Quintard and Whitaker (1993).

We recall the equations presented in the chapter (5).

For the matrix

$$(\rho C_p)_m \frac{\partial T_m}{\partial t} = \nabla . \left(k_m^* . \nabla T_m \right) + q_{rxn} \quad \textbf{(B-9)}$$

For the fracture

$$(\rho C_p)_f \frac{\partial T_f}{\partial t} = \nabla . \left(k_f^* . \nabla T_f \right) \quad \textbf{(B-10)}$$

The boundary and initial conditions:

$$T_m = T_f \qquad \text{at} \quad A_{mf} \quad \textbf{(B-11)}$$

$$n_{mf} . (k_m^* . \nabla T_m) = n_{mf} . (k_f^* . \nabla T_f) \qquad \text{at} \quad A_{mf} \quad \textbf{(B-12)}$$

$$T_m = F_m(r_m), \quad T_f = F_f(r_f) \qquad \text{at} \quad t = 0 \quad \textbf{(B-13)}$$

$$T_m = I_m(r_m, t), \qquad \text{at} \quad A_{me} \quad \textbf{(B-14)}$$

$$T_f = I_f(r_f, t), \qquad \text{at} \quad A_{mf} \quad \textbf{(B-15)}$$

Here the A_{mf} represents the interface of *m* and *f* phases within the averaging volume in Figure (B.1), where A_{me} and A_{mf} represent the entrance and exit of the *m* and *f* phases respectively.

Generally the condition at A_{me} and A_{mf} are known only in terms of the average quantities (see Quintard and Whitaker 1993).

By averaging the equation (B-9) we have:

$$\left\langle (\rho C_p)_m \frac{\partial T_m}{\partial t} \right\rangle = \left\langle \nabla.\left(k_m^*.\nabla T_m\right)\right\rangle + \left\langle q_{rxn} \right\rangle \qquad \textbf{(B-16)}$$

The reaction rate is assumed to be of zero the order, so the liberated heat by the reaction is

$$q_{rxn} = A_0 \exp\left(-E/RT\right) \times H_{rxn} \qquad \textbf{(B-17)}$$

With this definition, the reaction term is only the function of temperature. Using the Taylor series and neglecting the higher terms, for an arbitrary function F, we have

$$F(T) = F\left(\langle T\rangle\right) + \left(T - \langle T\rangle\right)\frac{\partial F}{\partial T}\Big|_{T=\langle T\rangle} + \left(T - \langle T\rangle\right)^2 \frac{\partial^2 F}{\partial T^2}\Big|_{T=\langle T\rangle} + \ldots \qquad \textbf{(B-18)}$$

Using the decomposition presented in equation (B.8) we have

$$F(T) = F\left(\langle T\rangle\right) + \left(\tilde{T}\right)\frac{\partial F}{\partial T}\Big|_{T=\langle T\rangle} + \left(\tilde{T}\right)^2 \frac{\partial^2 F}{\partial T^2}\Big|_{T=\langle T\rangle} + \ldots \qquad \textbf{(B-19)}$$

Replacing F by the reaction heat equation gives

$$q_{rxn} = A_0 \exp\left(-E/R\langle T_m\rangle^m\right)H_{rxn} + \tilde{T}_m\left[A_0 H_{rxn}\frac{E}{R\langle T_m\rangle^{m^2}}\exp\left(-E/R\langle T_m\rangle^m\right)\right] + \ldots \qquad \textbf{(B-20)}$$

Performing the average of the equation (B.9) and doing further manipulation as presented by Quintard and Whitaker (1993) gives

$$\begin{aligned} \varepsilon_m (\rho C_p)_m \frac{\partial \langle T_m\rangle^m}{\partial t} &= \nabla.\left(\varepsilon_m k_m^* \nabla \langle T_m\rangle^m\right) + \nabla.\left(\frac{k_m^*}{V}\int_{A_{mf}} \mathbf{n}_{mf}\tilde{T}_m dA_{mf}\right) \\ &+ \frac{1}{V}\int_{A_{mf}} \mathbf{n}_{mf}.k_m^* \nabla T_m dA_{mf} + \langle q_{rxn}\rangle \end{aligned} \qquad \textbf{(B-21)}$$

Further manipulation of the last term on the right side gives

$$\begin{aligned} \langle q_{rxn}\rangle &= \frac{1}{V}\int_{V_m}\left(A_0 \exp\left(-E/R\langle T_m\rangle^m\right)H_{rxn} + \tilde{T}_m\left[A_0 H_{rxn}\frac{E}{R\langle T_m\rangle^{m^2}}\exp\left(-E/R\langle T_m\rangle^m\right)\right]\right)dv \\ &= \varepsilon_m A_0 H_{rxn}\exp\left(-E/R\langle T_m\rangle^m\right) + \frac{A_0 H_{rxn} E}{R\langle T\rangle^2}\exp\left(-E/R\langle T_m\rangle^m\right)\langle \tilde{T}_m\rangle \end{aligned} \qquad \textbf{(B-22)}$$

Now applying the decomposition presented in the equation (B.8), to the equation (B.9), we have

$$(\rho C_p)_m \frac{\partial \langle T_m\rangle^m}{\partial t} + (\rho C_p)_m \frac{\partial \tilde{T}_m}{\partial t} + = \nabla.\left(k_m^*.\nabla\langle T_m\rangle^m\right) + \nabla.\left(k_m^*.\nabla\tilde{T}_m\right) + q_{rxn} \qquad \textbf{(B-23)}$$

Replacing the reaction term in the above equation by equation (B.22), and then subtracting it from equation (B.21) we have the following equation. Here, we followed the same development presented by Whitaker (1999), except for the reaction term.

$$(\rho C_p)_m \frac{\partial \tilde{T}_m}{\partial t} = \nabla.\left(k_m^*.\nabla \tilde{T}_m\right) - \frac{\varepsilon^{-1}}{V}\int_{A_{mf}} \mathbf{n}_{mf}.k_m^*\nabla \tilde{T}_m dA_{mf} + \frac{A_0 H_{rxn} E}{\varepsilon_m R\langle T_m\rangle^{m^2}} \exp\left(-E/R\langle T_m\rangle^m\right)\left(\langle \tilde{T}_m\rangle - \tilde{T}_m\right) \quad \textbf{(B-24)}$$

The average of the deviation term is usually considered to be equal to zero (see Whitaker 1999), thus the above equation reduces to

$$(\rho C_p)_m \frac{\partial \tilde{T}_m}{\partial t} = \nabla.\left(k_m^*.\nabla \tilde{T}_m\right) - \frac{\varepsilon^{-1}}{V}\int_{A_{mf}} \mathbf{n}_{mf}.k_m^*\nabla \tilde{T}_m dA_{mf} - \frac{A_0 H_{rxn} E}{\varepsilon_m R\langle T_m\rangle^{m^2}} \exp\left(-E/R\langle T_m\rangle^m\right)\left(\tilde{T}\right) \quad \textbf{(B-25)}$$

Assuming that the closure problem is quasi-steady

$$0 = \nabla.\left(k_m^*.\nabla \tilde{T}_m\right) - \frac{\varepsilon^{-1}}{V}\int_{A_{mf}} \mathbf{n}_{mf}.k_m^*\nabla \tilde{T}_m dA_{mf} - \frac{A_0 H_{rxn} E}{\varepsilon_m R\langle T_m\rangle^{m^2}} \exp\left(-E/R\langle T_m\rangle^m\right)\left(\tilde{T}_m\right) \quad \textbf{(B-26)}$$

The estimation of the conduction term will be (see Whitaker 1999)

$$\nabla.\left(k_m^*.\nabla \tilde{T}_m\right) = O\left(\frac{k_m^* \tilde{T}_m}{l_m^2}\right) \quad \textbf{(B-27)}$$

and the estimation of the interfacial flux term is (see Whitaker 1999)

$$\frac{\varepsilon^{-1}}{V}\int_{A_{mf}} \mathbf{n}_{mf}.k_m^*\nabla \tilde{T}_m dA_{mf} = O\left(\frac{\varepsilon^{-1} k_m^* \tilde{T}_m}{l_m L}\right) \quad \textbf{(B-28)}$$

in order to compare the significance of the reaction term with two other terms in equation (B.26), we need to evaluate the multiplier term of $\tilde{T}_m$ in the last term of this equation. To this end, we consider $\langle T_m\rangle^m$ equal to the combustion front temperature. However this is not a constant value and varies with time. Values for other parameters are presented in Table (B.1). We note that, here, the pre-exponential factor is considered to be equal to 10, which corresponds to the low Damköhler number in chapter (5). Generally in fractured reservoirs, the volume fraction of the fractures is very small, thus one can consider the ε_m very close to 1.

Table B.1. Parameters for estimation of the reaction term.

Parameter	A_0 *(1/s)*	E *(J/mol)*	H_{rxn} *(J/m^3)*	k^*_m *(W/(m.°C)*	$\langle T_m\rangle^m$ *(°C)*	R *(J/mol.K)*
Value	10	6.8×10^{-4}	2.25×10^{7}	1.5	200	8.314

Based on these values

$$\frac{A_0 H_{rxn} E}{\varepsilon_m R\langle T_m\rangle^{m^2}} \exp\left(-E/R\langle T_m\rangle^m\right) = \frac{10\times 2.25e7\times 6.8e4}{8.314\times(200)^2}\exp\left(\frac{-6.8e4}{8.314\times 473}\right) \cong 1.0 \quad \textbf{(B-29)}$$

estimations of the two other terms in equation (B.26) are

$$\frac{k_m^*}{l_m^2} = \frac{1.5}{(0.18)^2} = 46 \qquad \textbf{(B-30)}$$

$$\frac{k_m^*}{l_m L} = \frac{1.5}{0.18 \times 1.6} = 5 \qquad \textbf{(B-31)}$$

One should note that the value of $\langle T_m \rangle^m$ plays an important role in this comparison. Figure (B.2) shows how the multiplier term of $\tilde{T}_m$ in the equation (B.26) changes with temperature.

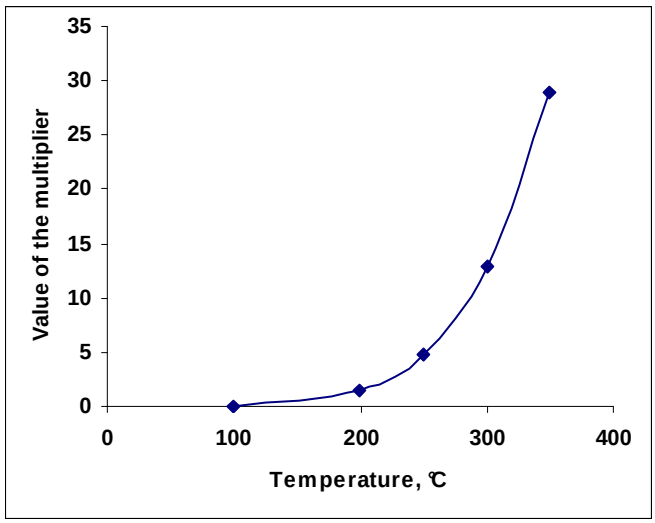


Figure B.2. How the multiplier term changes with temperature.

It is illustrated that, for small temperature values, the reaction term becomes negligible, but when temperature increases, this term becomes important compared to the conduction and interfacial exchange terms. Based on this figure, we assume that the last term in the equation (B.26), is negligible compared to the other terms. However we remind that this is valid only for relatively low temperatures.

Under this condition, the closure problem becomes identical to the one presented by Quintard and Whitaker (1993), to which we refer the reader for further mathematical manipulations.

According to the developments presented in the above mentioned reference, the following closure problem is obtained.

In the matrix

$$k_m^* . \nabla^2 \tilde{T}_m = \frac{\varepsilon_m^{-1}}{V} \int_{A_{mf}} \mathbf{n}_{mf} . k_m^* \nabla \tilde{T}_m \, dA_{mf} \qquad \textbf{(B-32)}$$

in the fracture

$$k_f^* . \nabla^2 \tilde{T}_f = \frac{\varepsilon_f^{-1}}{V} \int_{A_{mf}} \mathbf{n}_{mf} . k_f^* \nabla \tilde{T}_f \, dA_{mf} \qquad \textbf{(B-33)}$$

The boundary conditions

$$\tilde{T}_m = \tilde{T}_f + \langle T_f \rangle^f - \langle T_m \rangle^m \qquad \text{at} \quad A_{mf} \qquad \textbf{(B-34)}$$

$$\mathbf{n}_{mf} . k_m^* \nabla \tilde{T}_m = \mathbf{n}_{mf} . k_f^* \nabla \tilde{T}_f + \mathbf{n}_{mf} . k_f^* \nabla \langle T_f \rangle^f - \mathbf{n}_{mf} . k_m^* \nabla T_m{}^m \qquad \text{at} \quad A_{mf} \qquad \textbf{(B-35)}$$

According to Quintard and Whitaker (1993), this form of the closure problem suggest the following representations for $\tilde{T}_m$ and $\tilde{T}_f$.

$$\tilde{T}_m = \mathbf{b}_{mm}.\nabla\langle T_m\rangle^m + \mathbf{b}_{mf}.\nabla\langle T_f\rangle^f - s_m\left(\langle T_f\rangle^f - \langle T_m\rangle^m\right) + \zeta_m \qquad \text{at } A_{mf} \qquad \textbf{(B-36)}$$

$$\tilde{T}_f = \mathbf{b}_{fm}.\nabla\langle T_m\rangle^m + \mathbf{b}_{ff}.\nabla\langle T_f\rangle^f + s_f\left(\langle T_f\rangle^f - \langle T_m\rangle^m\right) + \zeta_f \qquad \text{at } A_{mf} \qquad \textbf{(B-37)}$$

In which ζ_m and ζ_f are arbitrary functions and $\mathbf{b}_{mm}$ and $\mathbf{b}_{mf}$,…, s_m and s_f are known as closure variables.

Quintard and Whitaker performed further mathematical manipulation in which these closure variables are presented in terms of a plausible set of boundary value problems. By solving these set of problems they presented the upscaled equations. Here we followed the same manipulations, except that in our upscaled equation we have an extra reaction term for the matrix

$$\varepsilon_m(\rho C_p)_m\frac{\partial\langle T_m\rangle^m}{\partial t} = \nabla.\left[\mathbf{K}_{mm}.\nabla\langle T_m\rangle^m + \mathbf{K}_{fm}.\nabla\langle T_f\rangle^f\right] + \mathbf{u}_{mm}.\nabla\langle T_m\rangle^m + \mathbf{u}_{mf}.\nabla\langle T_f\rangle^f - a_V h\left(\langle T_m\rangle^m - \langle T_f\rangle^f\right) + \varepsilon_m A_0 H_{rxn}\exp\left(-E/R\langle T_m\rangle^m\right) \qquad \textbf{(B-38)}$$

Where the transport coefficients are defined by

$$\mathbf{K}_{mm} = k_m\left[\varepsilon_m\mathbf{I} + \frac{1}{V}\int_{A_{mf}}\mathbf{n}_{mf}.\mathbf{b}_{mm}dA_{mf}\right] \qquad \textbf{(B-39)}$$

$$\mathbf{K}_{mf} = k_m\frac{1}{V}\int_{A_{mf}}\mathbf{n}_{mf}.\mathbf{b}_{mf}dA_{mf} \qquad \textbf{(B-40)}$$

$$\mathbf{u}_{mm} = c_{mm} - k_m\frac{1}{V}\int_{A_{mf}}\mathbf{n}_{mf}s_m dA_{mf} \qquad \textbf{(B-41)}$$

$$\mathbf{u}_{mf} = c_{fm} - k_f\frac{1}{V}\int_{A_{mf}}\mathbf{n}_{mf}s_f dA_{mf} \qquad \textbf{(B-42)}$$

In which $a_V h$, c_{mm} and c_{mf} are defined as

$$a_V h = k_m\frac{1}{V}\int_{A_{mf}}\mathbf{n}_{mf\,mf}.\nabla s_m dA_{mf} = k_f\frac{1}{V}\int_{A_{mf}}\mathbf{n}_{mf\,mf}.\nabla s_f dA_{mf} \qquad \textbf{(B-43)}$$

$$c_{mm} = \frac{1}{V}\int_{A_{mf}}\mathbf{n}_{mf\,mf}.k_m\nabla\mathbf{b}_{mm}dA_{mf} \qquad \textbf{(B-44)}$$

And

$$c_{mm} = -c_{fm} \qquad \textbf{(B-45)}$$

For the fracture

$$\varepsilon_f(\rho C_p)_f\frac{\partial\langle T_f\rangle^f}{\partial t} = \nabla.\left[\mathbf{K}_{ff}.\nabla\langle T_f\rangle^f + \mathbf{K}_{fm}.\nabla\langle T_f\rangle^f\right] + \mathbf{u}_{fm}.\nabla\langle T_m\rangle^m + \mathbf{u}_{ff}.\nabla\langle T_f\rangle^f + a_V h\left(\langle T_m\rangle^m - \langle T_f\rangle^f\right) \qquad \textbf{(B-46)}$$

Where the transport coefficients are defined by

$$\mathbf{K}_{ff} = k_f \left[\varepsilon_f \mathbf{I} + \frac{1}{V} \int_{A_{mf}} \mathbf{n}_{mf} . \mathbf{b}_{ff} \, dA_{mf} \right] \quad \textbf{(B-47)}$$

$$\mathbf{K}_{fm} = k_f \frac{1}{V} \int_{A_{mf}} \mathbf{n}_{mf} . \mathbf{b}_{fm} dA_{mf} \quad \textbf{(B-48)}$$

$$\mathbf{u}_{ff} = c_{ff} + k_f \frac{1}{V} \int_{A_{mf}} \mathbf{n}_{mf} s_f \, dA_{mf} \quad \textbf{(B-49)}$$

$$\mathbf{u}_{mf} = c_{fm} - k_f \frac{1}{V} \int_{A_{mf}} \mathbf{n}_{mf} s_f \, dA_{mf} \quad \textbf{(B-50)}$$

In which c_{mm} and c_{mf} are defined as

$$c_{ff} = \frac{1}{V} \int_{A_{mf}} \mathbf{n}_{mf} . k_f \nabla \mathbf{b}_{ff} \, dA_{mf} \quad \textbf{(B-51)}$$

And

$$c_{ff} = -c_{mf} \quad \textbf{(B-52)}$$

References

1. **Ahmadi A., Cherblanc F. & Quintard M., (2007),** Two- domain description of solute transport in heterogeneous porous media: Comparison between theoretical predictions and numerical experiments, *Advances in water resources, 30:1127–1143.*
2. **Ahmadi A., Quintard M. & Whitaker S., (1998),** Transport in chemically and mechanically heterogeneous porous media V. Two-equation model for solute transport with adsorption, *Advances in Water Resources, 22(1):59–86.*
3. **Akin S., Versan Kok M. & Bagci S., (2000),** Oxidation of heavy oil and their SARA fractions: Its role in modeling in situ combustion, *Society of Petroleum Engineers, paper number: 63230.*
4. **Akkutlu Y. & Yortsos Y.C., (2000),** The dynamics of combustion fronts in porous media, *Society of Petroleum Engineers, paper number: 63225.*
5. **Alboudwarej H., (2006),** Highlighting heavy oil, *Oil field review, summer.*
6. **Aldushin A.P. & Matkowsky B.J., (2000)**, Diffusion driven combustion waves in porous media, *Combustion Science and Technology, 156: 221-250.*
7. **Aldushin A.P. & Seplyarskii B.S. (1977),** Theory of filtration combustion of porous metallic specimens, *OIKhF, USSR Academy of Sciences, Chernogolovka.*
8. **Audibert A. & Vossoughi S., (1991)**, Thermo-chemical Alteration of Crude Oils, *Chapter 8 of "Basic Concepts in Enhanced Oil Recovery Processes", edited by Marc Baviere, pp 241-269, Elsevier Science Publishers.*
9. **Awoleke O.G., (2007),** An experimental investigation of in situ combustion in heterogeneous porous media, *Master's thesis, Stanford University, June.*
10. **Aziz K., Sumnu M.D., Brigham W.E. & Castanier L.M., (1994),** Use of simulators in the design of an experiment for steam injection into a fractured system, *Society of Petroleum Engineers, paper number: 27742.*
11. **Aziz K., Sumnu M.D., Brigham W.E. & Castanier L.M., (1996),** An experimental and numerical study on steam injection in fractured systems, *Society of Petroleum Engineers, paper number: 35459.*
12. **Bagci S., Akin S. & Versan Kok M., (2002),** Experimental and numerical analysis of dry forward combustion with diverse well configuration, *Energy & Fuels, 16:892–903.*
13. **Bagci S., (1998),** Estimation of combustion zone thickness during in situ combustion processes, *Energy & Fuels, 12:1153–1160.*
14. **Bagci S. & Shamsul. A., (1999),** A comparison of dry forward combustion with diverse well configurations in a 3D physical model using medium and low gravity crudes, J*ournal of Canadian Petroleum Technology, 38(13).*
15. **Barenblatt G. I., Zheltov Iu.P. & Kochina, I. N., (1960),** Basic concepts in the theory of seepage of homogeneous liquids in fissured rocks (strata), *Journal of Applied Mathematics, 24(5): 1286-1303.*
16. **Berry H.J., (1968),** An Experimental Investigation of Forward Combustion Oil Recovery, *Ph.D. Dissertation, Texas A&M University.*
17. **Bousaid L.S. & Ramey H.J.Jr., (1968),** Oxidation of crude oil in porous media, *Society of Petroleum Engineers*, 8(June):137-148.

18. **Boris V. L'vov., (1997),** Mechanism of thermal decomposition of alkaline-earth carbonates, *Thermochimica Acta, 303:161–170.*

19. **Bourbiaux B. & Granet S., (1999),** Scaling up matrix-fracture transfers in dual-porosity models: theory and application, *Society of Petroleum Engineers, paper number: 56557-MS.*

20. **Brigham W.E., Mamora D.D., Ramey H.J. & Castanier L.M., (1993),** Kinetics of in situ combustion. *Technical report, Stanford university (SUPRI group) Work Performed Under Contract No. DE-FG22-90BC14600, July.*

21. **Burger J., Sourieau P. & Combarnous M., (1984),** Recuperation Assistee du Petrole, les Methodes Thermiques, *Editions Technip, Paris.*

22. **Butler R.G., *(1998),*** Thermal recovery of oil and bitumen, *Prentice-Hall, Englewood Cliffs.*

23. **Carslaw H.S. & Jaeger J.C, (1959),** Conduction of heat in solids, *Oxford science publications, Oxford University press, second edition.*

24. **Castanier L.M. & Brigham W.E., (2003),** Upgrading of crude oil via in situ combustion, *Journal of petroleum science and engineering, 39:125–136.*

25. **Chen. Z.X., (1989),** Transient flow of slightly compressible fluid through double-porosity, double-permeability system- a state of the art review, *Transport in porous media, 4:147–184*.

26. **Cherblanc F., Ahmadi A. & Quintard M., (2007),** Two-domain description of solute transport in heterogeneous porous media: Comparison between theoretical predictions and numerical experiments, *Advances in Water Resources 30 (5): 1127–1143.*

27. **COMSOL Multiphysics Modeling and Simulation, (2007),** *Version 3.4.*

28. **Craig F.F.Jr. & Parrish D.R., (1974),** A multi-pilot evaluation of the COFCAW process, *Journal of Petroleum Technology, June: 659–666.*

29. **Delaplace P., Lacroix S. & Bourbiaux B., (2004),** Simulation of air injection in light oil reservoir: setting-up a predictive dual porosity model, *Society of Petroleum Engineers, paper number: 89931*.

30. **Debenest G. & Quintard M., (2008),** Transport in highly heterogeneous porous media: From direct simulation to macro-scale, *Chemical Product and Process Modeling, 3(1), Article 19.*

31. **Estebenet T., Noetinger B. & Quintard M., (2001),** Upscaling flow in fractured media: Equivalence between the large scale averaging theory and the continuous time random walk method, *Transport in porous media, 43:581–596*.

32. **Fadaei H., Kamp A., Debenest G., Castanier L. & Quintard M., (2009),** Experimental and numerical analysis of in situ combustion in fractured carbonates, *Presented at the 15th European Symposium on Improved Oil Recovery, 27-29 April, Paris.*

33. **Fassihi M.R., Brigham E.W. & Ramey H.J., (1984),** Reaction kinetics of in situ combustion-part 2, *Society of Petroleum Engineers Journal, August, pp. 408–416.*

34. **Farouq Ali S.M., Pooladi Darvish M. & Tortike W.S., (1995),** Behavior of gravity drainage in heavy oil fractured reservoir under steam injection, Sixth *UNITAR International Conference on Heavy Crude and Tar Sands, Houston, TX.*

35. **Freitag N.P & Exelby D.R., (2006),** SARA based model for simulating pyrolysis reactions that occur in high temperature EOR processes, *Journal of Canadian Petroleum technology, 45(3): 38–44.*

36. **Greaves M., Javanmardi J. & Field W., (1991),** In situ combustion in fractured heavy oil reservoir*, Presented in the 6th IOR symposium in Stavanger, Norway, 21 may.*

37. **Greaves M. & Al Shemali O., (1996),** In situ Combustion (ISC) Process using Horizontal Wells, *Journal of Canadian Petroleum technology, 35(2): 464-55.*

38. **Greaves M. & Xia T.X., (2000),** Recent laboratory results of THAI and its comparison with other IOR processes, *Society of Petroleum Engineers, paper number: 59334-MS*.

39. **Greaves M., (2006),** Is THAI heavy oil technology of any use for the North Sea? *Sharp IOR newsletter, 12, Online on: http://ior.senergyltd.com.*

40. **Golfier F., Quintard M., Cherblanc F., Zinn B.A. & Wood, B.D., (2007),** Comparison of theory and experiment for solute transport in highly heterogeneous porous medium, *Advances in Water Resources, 30(11): 2235-2261.*

41. **Hager J., Wimmerstedt R. & Whitaker S., (2000),** Steam drying a bed of porous sphere: Theory and experiment*, Chemical engineering science, 55:1675–1698.*

42. **Hallam R.J., Hajdo L.E. & Vorndran L.D.L., (1985),** Hydrogen generation during in situ combustion, *Society of Petroleum Engineers, paper number: 13661.*

43. **Hassanzadeh H. & Pooladi-Darvish M., (2006),** Effect of fracture boundary conditions on matrix-fracture transfer shape factor*, Transport in porous media, 64(1):51–74.*

44. **Henn N., Quintard M., Bourbiaux B. & Sakthikumar S., (2004),** Modeling of Conductive Faults with a Multiscale Approach, *Oil & Gas Science and Technology - Rev. IFP, 59 (2):197-214.*

45. **Islam M. R., Verma A. Farouq Ali A.M., (1991),** In situ combustion-the essential reaction kinetics in heavy crude and tar sands—hydrocarbons for the 21st century, *5th UNITAR International Conference on Heavy Crude and Tar Sands, Caracas, Venezuela, Aug. 4-9, Vol. 1, page 343– 353.*

46. **Kaviany M., (1995),** Principles of heat transfer in porous media, *Springer, second edition.*

47. **Kfoury M., (2004),** *Changement d'échelle séquentiel pour des milieux fractures hétérogènes, PhD. thesis, Institut Francais du Petrole (IFP) .*

48. **Kharrat R., Vahidreza S. & Razzaghi S., (2007),** Feasibility study of in situ combustion in carbonate reservoir, *Society of Petroleum Engineers, paper number: 105576.*

49. **Kumar M., (1987),** Simulation of laboratory in situ combustion data and effect of process variation, *Society of Petroleum Engineers, paper number: 16027.*

50. **Kumar M. & Garon A.M., (1991),** An experimental investigation of the fire-flooding combustion zone, *Society of Petroleum Engineers, paper number: 17392.*

51. **Landereau P., Noetinger B., Quintard M., (2003),** About the shape factor of complex fractured media: comparison of several approaches, *In proceedings of the 7th Eur. Conf. On the Mathematics of Oil Recovery, Baveno, Italy.*

52. **Le Thiez P., Petit H.J-M. & Lemonnier P., (1990),** History matching of a heavy-oil combustion pilot in Romania, *Society of Petroleum Engineers, paper number: 20249-MS*.

53. **Lide D.R., (2004),** Handbook of chemistry and physics, *48th edition, CRC press.*

54. **Lim K.T. & Aziz K.Z., (1995),** Matrix-fracture transfer shape factors for dual-porosity simulators, *Journal of Petroleum Science and Engineering, 13:169– 178.*

55. **Mailybaev A.A., Bruining J., Chapiro G. and Marchesin D., (2009),** Analytical study of in-situ combustion in a wet porous medium, *15th European Symposium on Improved Oil recovery, Paris, April 27-29.*

56. **Mamora D. D., Ramey H. J. Jr., Brigham W. E. & Castanier L.M., (1993),** Kinetics of in situ combustion, *Report no. DOE/BC/14600-51, July.*

57. **Marle, C. M., Simandoux, P., Pacsirszky, J. & Gaulier, C., (1967),** Etude du de´placement de fluides miscibles en milieu poreux stratifie, *Revue de l'Institut Franc¸ais du Pe´trole, 22:272–294.*

58. **Matowsky, B.J., (2001),** Filtration Combustion in Smoldering and SHS, *Sixth International Microgravity Combustion Workshop, NASA Glenn Research Centre, Cleveland, OH, CP-2001-210826, May 22-24, pp. 281-284*.

59. **Miller J.S. & Jones R., (1983),** Laboratory experiments simulating fire flooding through a fractured reservoir, *United State department of energy report, DE 83009350, April.*

60. **Monin J.C. & Audibert A. (1985) ,** Laboratory simulation of thermal changes of heavy crudes during thermal recovery, *Presented at 3rd Int. UNITAR/UNDP Heavy Crude and Tar Sands Conf. (July), pp. 616–640.*

61. **Moore R. G., Mehta S. A., Ursenbach M. G., & Laureshen C.J., (1998),** Strategies for successful air injection-based IOR processes, *In Proceedings 7th UNITAR International Conference on Heavy Oil and Tar Sands, Beijing, China, 27-30 October.*

62. **Moore R. G., Belgrave J.D.M., Mehta R., Ursenbach, M., Laureshen C.J. & Xi K., (1992),** Some insights into the low-temperature and high-temperature in situ combustion kinetics, *Society of Petroleum Engineers, paper number: 24174.*

63. **Moore R. G., Laureshen C.J., Ursenbach M.G., Mehta S.A. & Belgrave, J.D.M., (1996),** Combustion/Oxidation behavior of Athabasca oil sands bitumen, *Society of Petroleum Engineers, paper number: 35392-MS.*

64. **Ohlemiller T.J., (1985),** Modeling of smoldering combustion propagation, *Progress in Energy and Combustion Science, 11(4): 277-310.*

65. **Oliviera A.A.M. & Kaviani M., (2001),** Non-equilibrium in the transport of heat and reactants in combustion porous media, *Progress in Energy and Combustion Science, 27:623-545.*

66. **Okamoto M. & Bourbiaux B., (2005),** A review of the challenging reservoir engineering aspects of modeling the recovery from a light oil, fractured reservoir by air injection, *Presented at the 26th IEA Annual Workshop & Symposium on Enhanced Oil Recovery, Technology & Research Centre, Japan Oil, Gas and Metals National Corporation, Japan, September 25-29.*

67. **Penuela G., Hughes R.G., Civan F. & Wiggins M.L., (2002),** Time-dependent shape factors for secondary recovery in naturally fractured reservoirs, *Society of Petroleum Engineers, paper number 75234.*

68. **Pooladi Darvish M., (1994),** Steam heating of fractured formation containing heavy oil single block analysis, *Society of Petroleum Engineers, paper number: 28642-MS.*

69. **Prats M., (1982),** Thermal recovery, *SPE Monograph, Society of petroleum engineers of AIME.*

70. **Quintard M., Ahmadi A. & Whitaker S., (1998)**, Transport in chemically and mechanically heterogeneous porous media v: Two-equation model for solute transport with adsorption, *Advances in Water Resources, 22(1):59–86.*

71. **Quintard M. & Whitaker S., (1990),** Two-phase flow in heterogeneous porous media I: the influence of large spatial and temporal gradients, *Transport in porous media, 5:341–379.*

72. **Quintard M. & Whitaker S., (1995),** Local thermal equilibrium for transient heat conduction: theory and comparison with numerical experiment, *Int. J. Heat Mass Transfer, 38 (15):2779–2796.*

73. **Quintard M. & Whitaker S., (1996),** Transport in chemically and mechanically heterogeneous porous media: theoretical development of region averaged equations for slightly compressible single-phase flow, *Advances in water resources, 19(1):29–47.*

74. **Quintard M. & Whitaker S., (1998),** Transport in chemically and mechanically heterogeneous porous media III: Large-scale mechanical equilibrium and the regional form of Darcy's law, *Advances in Water Resources, 21(7):617–629*.

75. **Quintard M. & Whitaker S., (1998),** Transport in chemically and mechanically heterogeneous porous media IV: Large-scale mass equilibrium for solute transport with adsorption. *Advances in Water Resources, 22(1):33–57.*

76. **Quintard M. & Whitaker S., (1998),** Two phase flow in heterogeneous porous media: the method of large-scale averaging, *Transport in porous media, 3:357–413.*

77. **Ramey H.J., Stamp V.V., Pebdani F.N. & Mallinson, J.E., (1992),** Case history of South Belridge, California, in situ combustion oil recovery, *Society of Petroleum Engineers, paper number:* 24200.

78. **Rangel-German E.R. & Kovscek A.R., (2005),** Matrix fractured shape factor and multiphase-flow properties of fractured porous media. *Society of Petroleum Engineers, paper number: 95105-MS.*

79. **Reis J.C., (1990),** Oil recovery mechanisms in fractured reservoirs during, *Society of Petroleum Engineers, paper number: 20204-MS.*

80. **Richardson W.C., Sharpe H.N. & Lolley C.S., (1995),** Representation of steam distillation and in situ upgrading process in a heavy oil simulation, *Society of Petroleum Engineers, paper number 30301.*

81. **Sanders J.P. & Gallagher P.K., (2002),** kinetic analysis using TGA/DSC measurements_part1: decomposition of calcium carbonate in argon, *Thermodinamica Acta, 388:115–128.*

82. **Sarathi P.S., (1999),** In situ combustion handbook-Principles and practices, *Report DOE/PC/91008-0374, OSTI ID 3175, January.*

83. **Sarma P. & Aziz K., (2004),** New transfer functions for simulation of naturally fractured reservoirs with dual porosity models, *Society of Petroleum Engineers, paper number: 90231-MS.*

84. **Sarda S., Jeannin L., Basquet R. & Bourbiaux B., (2002),** Hydraulic characterization of fractured reservoirs: Simulations on discrete fracture network models, *SPE Reservoir Evaluation and Engineering Journal, 5(April): 154-162*.

85. **Schult D. A., Schult D.A., Matkowsky B.J., Volpert V.A. & Fernandez-Pello A.C., (1996),** Propagation and extinction of forced opposed flow smolder waves, *Combustion and Flame, 101(4): 471-490.*

86. **Schulte W.M. & De Vries A.S., (1985),** In situ combustion in naturally fractured heavy oil reservoirs, *Society of Petroleum Engineers Journal, 25(1):67-77.*

87. **STARS User Manual, (2006),** *Computer Modeling Group.*

88. **Shahani G.T., Moosa Jr.R., Kharusi B. & Chilek G., (2006),** The Physics of Steam Injection in Fractured Carbonate Reservoirs: Engineering Development Options That Minimize Risk, *Society of Petroleum Engineers, paper number: 102186.*

89. **Tabasinejad F., Karrat R. & Vossoughi S., (2006),** Feasibility study of in situ combustion in naturally fractured heavy oil reservoirs*, Society of Petroleum Engineers, paper number: 103969-MS.*

90. **Thomas G. W., Buthod A. P. & Allag O., (1979),** An experimental study of the kinetics of dry forward combustion, *Final report, No. BETC-1280-1, DOE, Washington DC.*

91. **Van Golf Racht T.D., (1982),** Fundamentals of fractured reservoir engineering, *Elsevier.*

92. **Vossoughi S., Price D., Razzaghi S., Kharrat R. & Rashtchian D., (2005),** Feasibility study of auto ignition in heavy oil reservoir, *Society of Petroleum Engineers, paper number: 97887*.

93. **Warren J.E. & Root P.J., (1963),** Behavior of naturally fractured reservoirs, *Society of Petroleum Engineers, paper number: 426-PA.*

94. **Whitaker S., (1999),** The method of volume averaging. *Kluwer academic publisher*.

95. **Xia T. & Greaves M., (2001),** 3-D physical model studies of downhole catalytic upgrading of Wolf Lake heavy oil using THAI, *Canadian International Petroleum Conference, Calgary, CIPC, paper No. 2001-17, 12-14, June.*

96. **Xu H.I.H., (2001),** In situ upgrading of heavy oil, *Ph.D thesis, University of Calgary, Alberta, Canada, January.*

97. **Zinn B., Meigs L.C., Harvey C.F., Haggerty R., Peplinski W.J. & Von Schwerin C., (2004),** Experimental visualization of solute transport and mass transfer processes in two-dimensional conductivity fields with connected regions of high conductivity, *Environ. Sci. Technol., 38(14):3916–26.*